ENGINEERING RESEARCH INSTITUTE
UNIVERSITY OF MICHIGAN
ANN ARBOR

AFSWP REP. NO. 352

STRUCTURAL STEEL CONNECTIONS

LEO SCHENKER
CHARLES G. SALMON
BRUCE G. JOHNSTON

Department of Civil Engineering

Project 2065

PREPARED FOR BUREAU OF YARDS AND DOCKS
U.S. NAVY DEPARTMENT
CONTRACT NOY 74521

June, 1954

PREFACE

In determining the load-time-deflection history of a steel structure under shock loading the role of the connections may be of considerable importance. Other factors include the mass and its distribution, the flexibility of the structure in its elastic range, and the strength and ductility of the structure and its components in the inelastic range. If connections are stronger than the adjacent members and adequately rigid, they have little effect on structural behavior, since they transmit load without failure. But if connections are weaker than the adjacent members or too flexible, they may be a determining factor affecting the overall behavior of the structure. If weak connections are "brittle" the structure may fracture and collapse with very little absorption of energy, but if relatively weak connections are ductile the deformation may be concentrated in them without causing yielding in other parts of the structure.

The present work was initiated in June, 1952, as the outgrowth of an earlier project on "Steel Beams, Connections, Columns, and Frames" that was completed for Sandia Corporation by a final report published on March 20, 1952. As stated in its subtitle, the earlier report was a "preliminary review of information on resistance to deflection and collapse". Although the earlier report included comments on the significance of the selected bibliography that was listed, it did not evaluate or summarize available information. The present report covers only one aspect of the problem of structural behavior, but is an attempt to provide a reasonably thorough and usable evaluation and summary of available information in the field of structural connections.

The properties of the actual connectors (rivets, bolts, welds, etc.) are discussed in Chapter I. Chapter II deals with tension connections. In Chapters III and IV the characteristics of rigid and nonrigid connections as used in continuous frames and tier buildings are studied and their effect on the analysis and design procedures for building frames is investigated. The influence of column anchorages on the resistance of buildings to lateral loads is discussed in Chapter V. Very little experimental information on this problem is available so that the discussion here is primarily on a theoretical basis. Chapter VI presents some examples illustrating the procedures that would make use of the information in the previous chapters.

The records of experimental investigations on connections include much information on repeated load and related "fatigue" failure. In recent years a justified emphasis, for design application, has been placed on this aspect rather than on static strength. But fatigue test information is absent from this monograph because the concern here is on the single shock load carrying the structure well into the plastic range. Nevertheless, many fatigue test investigations have included static control tests and these test results have added to the information presented here.

Initial negotiations for the present work were carried out through Sandia Corporation, but the actual contract was negotiated through the Bureau

of Yards and Docks of the U.S. Navy as contract Noy-74521. Commander F. F. Kravath was Officer in Charge of the contract and Mr. A. A. Amirikian furnished technical guidance through his office. Acknowledgment is also made for suggestions received through the Armed Forces Special Weapons Project by way of Lt. Col. Bruce D. Jones.

On July 31, 1952, a preliminary statement of objectives was distributed to all interested parties to make sure that proper direction would be taken during the course of the work. Considerable assistance has been rendered by many members, too numerous to list by name, of the Research Council on Riveted and Bolted Joints and the Structural Steel Committee of Welding Research Council. The help of those who have individually given of their time to review the preliminary drafts of each chapter has been very real and the authors express their appreciation to each and every person who has supplied helpful comment. Acknowledgement is also made again to various firms and individuals who supplied information on unpublished test results during the initial review of research that has formed the basis for this monograph.

TABLE OF CONTENTS

TABLE OF CONTENTS (CONT)

TABLE OF CONTENTS (CONT)

TABLE OF CONTENTS (CONCL.)

NOMENCLATURE

The following is a summary of the most common symbol definitions as used throughout the six chapters. The Roman numerals in parenthesis following the definition indicate the chapter in which that particular symbol is used.

A	cross-sectional area of section
A_g	gross cross-sectional area of plate (II)
A_r	area of tension rivets in beam-to-column connections
A_s	cross-sectional area of stiffener (III)
A_t	area of the anchor bolts in tension
a	minimum distance from edge of hole to end of plate (II)
a	width of concrete compression zone at ultimate moment (V)
B	constant for determining elongation of a bar in tension (I)
B	function of the ratio (bearing stress ÷ tensile stress) in a riveted or bolted joint (II)
b	width of plate
b_{AB}	one-half the width of column at end A of beam AB (IV, VI)
b_{BA}	one-half the width of column at end B of beam AB (IV, VI)
b_e	minimum distance from edge of hole to side of plate (II)
C	constant for determining elongation of bar in tension (I)
C_{AA}, C_{AB}, C_{AC}, C_{BB}	coefficients used in slope-deflection equations for structures with semi-rigid connections (IV, VI)
c	original bearing pressure under base plate (V, VI)
D	diameter of bolt, rivet, or hole
d	depth of section (III, IV)

d horizontal dimension of rectangular base plate (in plane of applied forces) (V)

d_n an equivalent length of plate which is highly stressed in the region of rivet hole (II)

E modulus of elasticity of steel

E_c modulus of elasticity of concrete

E_s secant modulus of anchor-bolt material

e elongation (I)

e distance from anchor bolt to center line of base plate (V, VI)

e' e divided by $d/2$ (V, VI)

F force in flange (III)

F redesign coefficient (IV)

F total reaction between base plate and concrete pier (V)

F_{AA}, F_{BA} coefficients used in slope-deflection equations for structure with semi-rigid connections (IV, VI)

f_c concrete stress

f'_c concrete cylinder strength

G gage, i.e., transverse spacing of connectors (II)

G modulus of rigidity (III)

H force per rivet divided by slip (II)

H shear stiffness of rivet: lbs/in deformation

h ratio of ultimate applied moment to ultimate applied shear

h' h divided by d

I moment of inertia of section

I_f moment of inertia of a rolled section, neglecting web

K moment of inertia divided by span length

k constant pertaining to local deformation of plate (II)

k constant of proportionality for the slip of a bar embedded in concrete (V)

L gage length of bar (I)

L distance between first and last connector, also length of weld (II)

L span length (III, IV)

L' moment arm of applied force in test or connections (III)

L'' value of L' when failure takes place in rolled section and built-up connection simultaneously (III)

L_1 length of anchor bolt above concrete surface (V)

L_2 equivalent free length of embedded portion of anchor bolt (V)

L_e equivalent total length of anchor bolt, $L_1 + L_2$ (V)

L'_e L_e divided by d (V)

L_t terminal length of anchor bolt, i.e., length over which bond stress exists (V)

M moment

$\bar{M}_{AB}$, $\bar{M}_{BA}$ moments at the center of joints A and B respectively (IV)

M' M divided by bd^2 (V)

M_c moment at midspan (IV)

M_f fixed-end moment (IV)

M_h moment at intersection of center lines of beam and column (IV)

M_p plastic moment of a section

M_r moment where straight section is attached to connection (IV)

M_s actual moment under simple support conditions (IV)

M_u ultimate moment of resistance of anchorage (V)

M'_u M_u divided by bd^2

M'_{u1} value of M'_u when half the anchor bolts are within the compression zone (V)

M'_{u2} value of M'_u when all anchor bolts are outside the compression zone (V)

M_y yield moment of a section

M_σ maximum moment as governed by normal stresses (III)

M_τ maximum moment as governed by shear (III)

$\mathbf{m}$ $\dfrac{\text{tensile component of average resultant strength}}{\text{shear component of average resultant strength}}$ (I)

N total number of rivets in a joint (II)

n number of longitudinal spaces between connectors (II)

n_i number of rivets in i-th row (i = 1,2...) (II)

P load applied to or carried by a tension connection (II)

P force applied to a specimen in a connection test (III)

P force in one half the anchor bolts (V)

P equivalent force applied at the story levels (VI)

P_u ultimate force in one half the anchor bolts (V)

p pitch of rows (II)

p percentage rigidity of a connection (IV, VI)

p A_t divided by bd (V)

Q function of method of manufacturing hole (II)

Q equivalent resistance of single degree-of-freedom structure acting at the center of mass (VI)

R radius of circular base plate (V)

R $E\Delta$ divided by height between floors (VI)

R_i the i-th row of connectors (i = 1,2,...), also the load carried by the i-th row

R_y yield load of one row of rivets (II)

r one half the number of rows of rivets (II)

r ratio of ultimate tensile strength of anchor bolt when subject to shear as well as tension to its ultimate tensile strength under tension alone (V)

r_{AB}, r_{BA} carry over factors for member AB with semi-rigid connections (VI)

S section modulus

S_{AB}, S_{BA} stiffness factors for member AB with semi-rigid connections (VI)

S_{res} average resultant load

S_s ultimate load for shear alone (I)

S_t ultimate load for tension alone (I)

s stagger (II)

s length of nonuniform portion of one leg of a rigid knee (III)

s slip of anchor bolt (V)

t thickness of plate

t_f flange thickness

t_h width of horizontal leg of a fillet weld (II)

t_i thickness of inner plate (II)

t_o thickness of outer plate (II)

t_v height of vertical leg of a fillet weld (II)

t_w web thickness (III)

U energy absorbed by a unit volume of material (I)

u_x bond stress developed at a distance x from concrete surface (V)

V shear applied to anchorage (V)

V'_{AB}, V'_{BA} shears at the ends A and B of a simply supported beam AB (IV, VI)

V_F shear absorbed by friction between base plate and concrete (V)

V_s shear resisted by anchor bolts (V)

v width of concrete compression zone at any applied moment (V, VI)

v' v divided by d/2 (V, VI)

W vertical load supported by anchorage (V)

w load per unit length on a beam (IV)

w distance from center of gravity of concrete stress diagram to near edge of base plate (V, VI)

w' w divided by d/2 (V, VI)

X function of material ductility (II)

X parameter which is function of the physical dimensions (IV)

x coordinate distance

x distance of any point of the embedded portion of the anchor bolt from the concrete surface (V)

Y function of material ductility (II)

Y parameter which is a function of the physical dimensions (IV)

y coordinate distance

Z plastic section modulus

z distance of the center of gravity of the ultimate concrete stress diagram from the center of a circular base plate (V)

α fraction of maximum useful force P at which failure of connection occurs (III)

α $2EK \frac{\Theta_A}{M_A}$, a connection parameter (IV, VI)

α factor by which lateral constraint increases the ultimate concrete strength (V)

β $2EK \frac{\Theta_B}{M_B}$, a connection parameter (IV, VI)

γ one-half of the angle extended by the ultimate concrete stress diagram at the center of a circular base plate (V)

γ ratio of rotation to applied moment for a given semi-rigid joint (VI)

Δ total deformation of a tension connection (II)

Δ side-sway deflection (IV,VI)

δ_i relative slip at i-th row (i = 1,2 ...) (II)

ϵ strain in anchor bolt (V)

ϵ_g strain in gross section (II)

ϵ_n strain in net section (II)

ϵ_u strain, corresponding to the maximum stress of the material (II, V)

ϵ_x strain in embedded portion at a distance x from the concrete surface of the anchor bolt (V)

ϵ_{y1} strain in anchor bolt at the beginning and end of yield range maximum
ϵ_{y2} (V)

η predicted ultimate efficiency (II)

η_g gross efficiency of perforated plate (II)

η_n net efficiency of perforated plate (II)

Θ rotation taking place at a connection (III, IV, VI)

θ angle of rotation of base plate (V)

θ_L lower bound for θ at failure (V)

μ $\Theta \div$ rotation in equivalent straight length d/2 (III)

μ coefficient of friction between steel and concrete (V)

ν Poisson's ratio for concrete (V, VI)

σ normal stress

σ_1 normal stress in various directions (II)
σ_2

σ_u normal ultimate strength

σ_{ud} undriven tensile strength (I)

σ_w working stress (IV)

σ_y normal yield strength

τ shear stress

τ_y yield shear stress

τ_d driven shear strength (I)

τ_{ud} undriven shear strength (I)

STRUCTURAL STEEL CONNECTIONS

CHAPTER I

THE CONNECTORS

The elastic and plastic behavior of the fasteners or welds under load must be known as a basis for estimating the behavior of complete connections under shock or static load. Much of the test information on rivets, bolts, and welds gives little data on the deformation of the connectors, but strength data alone are of some interest, since a certain strength may be sufficient to force yielding in adjacent members and thus insure a predictable type of ductile behavior in the structure.

In the following, rivets and bolts are treated together. The number of tests on rivets far exceeds the tests reported on structural bolts, but the results of rivet tests are frequently applicable to bolts. The current trend toward use of high strength bolts to replace rivets is recognized. Pins are connectors in the same sense as rivets or bolts, but are not considered in this chapter because there is too little test information available in which data on the behavior of pins can be separated from that of the complete pin-connected assembly.

The strength and deformation of rivets and bolts under load depend on many factors. The most important of these are:

1. material,
2. prior heat treatment (bolts),
3. heating and driving (rivets),
4. nature of the applied load, i.e., shear, tension or both in combination,
5. grip length,
6. rate of deformation, and
7. effect of test temperature.

The properties of welds are treated in a later section of this chapter, to the extent that these can be divorced from connections as a whole. The strength and deformation properties of a weld are affected by the following variables:

1. composition, size, and history of the metal pieces being joined,
2. composition of the filler metal and weld rod coating,
3. welding procedure, which includes
   a. welding process used,
   b. rate of heat input,
   c. preheat or post-heat treatment, and
   d. mechanical treatment, and
4. test temperature and rate of strain.

THE STRENGTH OF RIVETS

Materials

The majority of steel rivets used for structural purposes are of the low-carbon variety. Manganese, silicon, nickel, and other alloying elements are used for rivet steel to a minor extent. Details of chemical composition vary slightly in different countries. Table 1.a lists some typical rivet-steel specifications, those below the dividing line refer to high strength rivets. Since this monograph deals chiefly with test results, specifications are only of indirect interests. They are quoted here because materials used in test frequently are inadequately described. It would appear from a study of the specifications that there is much similarity between the materials used in various countries. Colloquial names, such as nickel steel or manganese steel, appear to be widely accepted.

Standards for tensile tests are variable in different parts of the world and it is not always indicated whether materials are tested in an annealed or manufactured condition; nevertheless, tensile test results serve a useful purpose in comparing connector materials. This is true in spite of the fact that connectors are often stressed in shear or combined shear and tension rather than in pure tension. There is a wealth of accumulated data on tensile strength tests and the tensile strength can be used as a standard to which the shear strength of connectors is referred. This is particularly true, since the yielding process under any state of stress is fundamentally a phenomenon of shear distortion. It is also possible to estimate other strength properties of a material if the tensile strength is known.

TABLE 1.a

SPECIFICATIONS FOR STRUCTURAL RIVETS
IN VARIOUS COUNTRIES

Country of Origin	Spec. No.	Colloquial name of material	Chemical composition*					Yield point strength ksi	Ultimate strength ksi	Elong. %
			C	Mn	Si	P	S			
U.S.	ASTM A141	Structural Rivet Steel				0.06	0.05	28+	52-62	24+
Germany	ST 34	Structural Mild Steel	0.18	0.55		0.06	0.06	27+	48-59	25
Gr. Britain	8.5.15	Structural Steel	0.20					34+	54-64	
Canada	CESA 5 39							27-33	55-65	
France								27-36	54	28
Spain								36	51	28
Belgium									51	24
Hungary		Mild Steel						34	51-64	22-27
U.S.	ASTM A195	High Strength Structural Rivet Steel	0.30	1.65	0.25	0.06	0.05	38+	68-82	20+
Germany	ST 52	Structural Manganese Steel	0.20	1.60	0.60	0.06	0.06	45+	74-88	20+
Gr. Britain	BS 548	High Tensile Steel	0.25			0.05	0.05	51	67-78	18+
Hungary		Carbon Steel						41	69-82	18-20

*The values quoted for the content of chemical components are maximum values.

The connector material is often of the same or somewhat lesser strength than the steel of the parent structure. In this country rivets made from material with an ultimate strength of 52-62 ksi are normally specified for use with structural steel with a strength of 60-72 ksi. In Germany ST34 rivets are used with St37 structural steel. In England, Brit Stand Spec No. 548 for high-tensile steel specifies the use of rivets with an ultimate coupon strength of 67-78 ksi with steel of a strength of 87-96 ksi.

Installation

The installation of a hot-driven rivet involves many variables, including the initial or "driving" temperature, the soaking time, the driving time and finishing temperature, and the driving method. These will all be considered under two subheadings: (1) Temperature and (2) Driving.

Temperature. There is no evidence that the driving temperature of hot-driven rivets has any effect on the strength of the material after driving. Wilson and Oliver (1.1)* tested rivets that had been driven at temperatures ranging from "dull red" to "badly burned". The ultimate driven strength varied from 75.7 to 66.5 ksi, but no relationship between driving temperature and strength was established. Hechtman (1.9) carried out very extensive tests on the effect of driving temperature on the properties of rivets. The results are expressed in terms of the tension-impact energy absorbed by the as-driven specimens tested to failure in a special impact testing machine. The relative variation of the ultimate strength may be estimated by dividing the energy values by the elongation. This indicates that there was practically no change of ultimate strength with driving temperatures ranging from 1900 to 2300°F. A few tests by Cox (1.7) reveal a very slight increase of static ultimate strength with increased driving temperature. In the same series it was found that an extension of the soaking time from 14 to 28 minutes had a negligible effect on the ultimate strength.

Driving. Strain-hardening in cold-driven rivets produces considerable increase of strength. Wilson and Oliver (1.1) obtained 74.1 ksi as the average strength of six cold-driven rivets (based on the diameter of the hole and a 2 inch grip), which represented a 35 percent increase over the undriven strength. The rivet material is not named, but it would appear to correspond to ASTM A141. In tests carried out by Baron and Larson (1.2) with ASTM A141 rivets, cold-driving increased the strength from 58.1 to 72 ksi on a 2-1/16-inch grip length and to 68.9 ksi on a 3-1/16-inch grip length, an average increase of 22 percent.

Although not pertinent to strength under shock load, cold-driven rivets have relatively poor fatigue characteristics (1.2). In other tests by

*This and subsequent numbers in parentheses refer to the bibliography at the end of this chapter.

Baron and Larson (1.2) hot-driving raised the ultimate strength in some instances by a slightly higher percentage. The driven strength values are all based on an assumed rivet diameter equal to the hole diameter. The improvement of strength cannot be attributed to an underestimate of the rivet area. Other investigators report an increase in strength following hot-driving. Wilson, Bruckner, and McCrackin (1.3) suggest that this increase is due to rapid cooling combined with a sufficiently low finishing temperature to result in work hardening.

Hechtman (1.9) believes that the change in the mechanical properties of hot-driven rivets is the result of a modification of the grain structure above the critical temperature range and then of the cold-working which takes place between the lower critical temperature range and the temperature at which driving ceases. It would appear from Hechtman's work that the actual driving time does not affect the strength except when driving is continued past the lower critical temperature.

The average results of many tests shown in Table 1.b for rivet sizes ranging from 5/8-to 1-1/8-inch diameter and 1 to 5 inch length suggest that machine driving increases the rivet strength by about 20 percent, compared to 10 percent in the case of rivets driven by pneumatic hammer. The increases were of the same order in cases where the driven strength was obtained from complete driven rivets and from specimens machined from driven rivets. A considerable reduction in elongation appears to be associated with the increase in strength.

The Nature of the Stress

Rivets may be required to act in tension, shear, or bending, as well as in any combination of such loads. Tests have shown that there exist certain relationships between the tension and shear strengths of rivets such that the strength of a rivet under any combination of tension and shear can be approximated from a knowledge of its strength in pure tension or pure shear.

Ultimate shear strength and tensile strength. There is no scarcity of information concerning the important relationship between the tensile and shear strengths of a rivet. In this relationship the single or double shear strength, driven or undriven, may be compared with the driven or undriven tensile strength of a rivet and it is important, therefore, to clearly define each term. Let the subscripts ud and d stand for "undriven" and "driven" respectively, so that τ_d/σ_{ud} is the ratio of driven shear strength to undriven tensile strength. Also let the subscript $_2$ stand for double shear. Here σ and τ stand for the average stress components parallel and at right angles to the axis of the rivet.

It is generally found (1.14) that for a bar of circular cross section τ/σ is in the neighborhood of 0.75 and that the shear strength in double shear is about 90-100 percent of the single shear strength. It has already been shown

TABLE 1.b.

THE EFFECT OF DRIVING ON THE TENSILE PROPERTIES OF RIVETS

Ref.	Country	Year	Chemical composition								Before driving				After driving				% Incr.	No. of	Remarks
			C	Si	Mn	P	S	Cu	Ni	Cr	YPS ksi	UTS ksi	Elong %	Red %	YPS ksi	UTS ksi	Elong %	Red %	UTS	Tests	
Machine-Driven Rivets																					
1.4	Canada	1928				Not stated					26.3	51.1	36.8			61.1			20	9	Elong. in 8"
1.1	U.S.	1930				Not stated					36.3	56.0	43.2	69.5		75.8			35	9	Elong. in 2"
1.5	U.S.	1938	.22		1.35	.026	.021	.30			47.9	79.7	31.3	69.4		92.9	18.5	57.1	16	5	do
1.5	U.S.	1938	.13		.45	.02	.033	.26			37.9	57.6	36.1	65.4	43.7	67.1	27.2	65.8	16	5	do
1.3	U.S.	1942	.17	.013	.512	.009	.033	.891	1.84		53.0	74.7	35.7	63.3		88.0	15.2	57.0	18	5	do
1.3	U.S.	1942	.088	.307	.371	.093	.031	.38	.55	.784	49.1	69.1	40.8	74.4		82.9	18.7	63.1	20	5	do
1.3	U.S.	1942	.21	.184	1.47	.013	.031	.25	.52		53.8	81.5	35.7	71.2		99.1	16.6	60.5	21	6	do
1.6	Gr. Brit.	1946	.21		.50	.041	.032				41.6	64.1	37.6	60.0	54.3	71.5*	26.3	57.8	12	6	Elong. in 4"
1.6	Gr. Brit.	1946	.32		.62	.037	.032				47.4	74.7	37.4	56.7	59.1	92.3*	15.5	27.8	23	6	do
1.2	U.S.	1952				ASTM-A-141					31.0	55.6	39.0	65.2		71.5	32.1	64.0	29	9	Elong. in 2"
1.8	U.S.	1926				ASTM-A7-24					30.5	51.0	42.7	74.5	37.4	57.2*	36.8	69.0	12	4	do
1.8	U.S.	1926				"Structural" Rivet Steel					33.8	54.0	42.0	69.0	40.4	60.2*	34.3	64.0	11	4	do
1.8	U.S.	1926				Carbon-Manganese Rivet Steel					60.5	97.6	29.0	69.0	66.4	105.3*	22.8	60.8	8	4	Av. of 77 Tests 19%
Pneumatic-Hammer-Driven Rivets																					
1.4	Canada	1928				Not stated					26.3	51.1	36.8			58.8			15	9	Elong. in 8"
1.1	U.S.	1930				Not stated					36.3	56.0	43.2	69.5		61.5		69.5	10	21	Elong. in 8"
1.5	U.S.	1938	.22		1.35	.026	.021	.30			47.9	79.7	31.3	69.4		91.8	16.6	47.4	15	5	do
1.5	U.S.	1938	.13		.45	.02	.033	.26			37.9	57.6	36.1	65.4	42.3	66.9	23.1	60.0	16	5	do
1.3	U.S.	1942	.17	.013	.512	.009	.033	.89	1.84		53.0	74.7	35.7	63.3		78.7	16.5	63.0	5	6	do
1.3	U.S.	1942	.088	.307	.371	.093	.031	.38	.55	.784	49.1	69.1	40.8	74.4		81.6	19.5	65.6	18	6	do
1.3	U.S.	1942	.21	.184	1.47	.013	.031	.25	.52		53.8	81.5	35.7	71.2		92.0	18.5	65.0	13	6	Elong. in 2"
1.3	U.S.	1926				ASTM-A7-24					30.5	51.0	42.7	74.5	37.5	58.4*	37.0	70.5	14	4	do
1.3	U.S.	1926				"Structural" Rivet Steel					33.8	54.0	42.0	69.0	39.8	60.2*	32.2	59.0	11	4	do
1.8	U.S.	1926				Carbon-Manganese Rivet Steel					60.5	97.6	29.0	69.0	67.0	104.8*	18.8	51.0	7	4	Av. of 70 Tests 11%

Note: "After driving" stresses are based on hole or actual diameter, except where ultimate strength values are marked with an *, and these values were obtained from tensile specimens machined from driven rivets.

that driving improves the tensile strength of rivets by an amount averaging from about 10 to 20 percent and it would seem reasonable to suppose that driving affects the shear strength in the same ratio as the tensile strength. Table 1.c shows the results of a number of shear and tension tests on rivets. The data are presented in ratio form. The results of many tests carried out at different times and localities, as reported in Table 1.c, indicate:

(i) The difference between unit single and double shear strength may be as great as 20 percent, but more often is less than 10 percent.

(ii) The ratio of shear strength to tensile strength varies between 0.66 and 0.83 and the range is approximately the same for driven and undriven values. In any specific case it would seem a reasonable approximation to choose a value of 0.70 and 0.75 for double and single shear respectively.

Strength under combined loading. The primary load on rivets quite commonly is shear, as in the case of gusset plates. In beam-to-column connections combined shear and tension occurs in the top rivets attaching a standard web clip angle or the top angle of a top and seat angle connection to a column. A knowledge of the tensile and shear strengths, independently, will allow an estimate of the strength under combined loading.

The strength of rivets under combined tension and shear was investigated by Young and Dunbar (1.4) and lately by Cox (1.7). The latter series of tests was very extensive, covering variations in grip from 1 to 5 inches, rivet diameters of 3/4, 7/8, and 1 inch, machine and pneumatic driving, hot and cold formed rivets, and some other variables. These other variables produced slight variations in the rivet strength, but Cox (1.7) found good agreement with an empirical expression for the average resultant strength of a rivet under combined tension and shear as follows:

$$S_{res} = \frac{4}{3} S_s \sqrt{\frac{1 + m^2}{\left(\frac{4}{3}\right)^2 + m^2}}$$

or

$$S_{res} = S_t \sqrt{\frac{1 + m^2}{\left(\frac{4^2}{3}\right) + m^2}}$$

where $m = \dfrac{\text{tensile component of } S_{res}}{\text{shear component of } S_{res}}$,

S_s = ultimate strength for shear alone, and
S_t = ultimate strength for tension alone.

These formulas have also been reported by Higgins and Munse (1.8). The results of Young and Dunbar (1.4) on two shear-tension ratios are in good agreement with

TABLE 1.c

VARIOUS SHEAR-TENSION RIVET-STRENGTH RATIOS

Ref.	Country	Year	Material	σ_{ud}	% Red Area	$\frac{\tau_{ud}}{\sigma_{ud}}$	$\frac{\tau_{2ud}}{\sigma_{ud}}$	σ_d	$\frac{\tau_d}{\sigma_d}$	$\frac{\tau_{2d}}{\sigma_d}$	$\frac{\tau_{2ud}}{\tau_{ud}}$	$\frac{\tau_{2d}}{\tau_d}$	$\frac{\tau_d}{\sigma_{ud}}$	$\frac{\tau_{2d}}{\sigma_{ud}}$
1.3	U.S.	1942	Low-Alloy Steel "A"	74.7	63.3	.67	.65	83.8	.68	.67	.97	1.00	.76	.75
1.3	U.S.	1942	Low-Alloy Steel "B"	69.1	74.4	.73	.68	82.2	.70	.66	.94	.95	.83	.78
1.3	U.S.	1942	Low-Alloy Steel "C"	81.5	71.2	.70	.67	95.5	.70	.66	.96	.95	.82.	.78
1.2	U.S.	1952	ASTM A-141	55.6	65.2			71.5		.74				.95
1.10	U.S.	1944	Structural Steel											
1.5	U.S.	1938	Carbon Steel	57.6	65.4	.80	.73	67.0	.68		.91		.79	
1.5	U.S.	1938	Manganese Steel	79.7	69.4	.83	.68	92.3	.67		.82		.77	
1.11	U.S.	1911	Nickel Steel	68.5								.96	.74	.71
1.11	U.S.	1911	Chrome-Nickel Steel	59.0								.93	.82	.77
1.12	U.S.	1925	Open Hearth Struct. Steel	51.2	68.3		.83						.96	
1.12	U.S.	1925	Open Hearth Struct. Steel	50.1	70.7		.82						.95	
1.12	U.S.	1925	Open Hearth Struct. Steel	71.2*	60.0		.56*						.57*	
1.13	Germany	1931	ST 34	63.0			.78							.84
1.13	Germany	1931	ST 52	112.0			.55							.72
1.14	Hungary	1928	Mild Steel	56.7	56.0		.75							.82
1.14	Hungary	1928	Carb-Mang. Steel	75.1	49.0		.73							.85
1.14	Hungary	1918	Silicon Steel	67.5	59.0		.78							.94
1.7	U.S.	1952	ASTMA 141	57.0	67.0			59.5		.76				.79

Note: "After driving" stresses are based on the actual or hole diameter.
σ = tensile strength, τ = shear strength, subscripts ud and d refer to undriven and driven properties respectively; subscript 2 refers to double-shear. * Not included in average.

the above expressions. Their work also included tests in which an eccentric tensile force was applied to the rivets to produce bending. The test rivet was used to hold together two short angles and the line of action of the applied force was 1-1/8 and 2-1/4 inches from the center of the rivet, respectively. The investigators discovered considerable reductions in strength due to eccentric loading, e.g., with 2-1/4 inch eccentricity the average strength was less than half of the concentric strength. However, no attempt was made to link the eccentric strength with the stiffness of the angle, which is clearly an important factor. Consequently, the tests do not allow any general conclusions.

Summary. At this stage it is presumed that the rivet material is known and that an estimate of the driven tensile, shear, and/or combined strengths has been made, but without allowance for the variations caused by grip, different types of rivet head, or the rate of loading.

The Effect of Grip

Practically all investigators report lower driven shear and tensile strengths with rivets of longer grip than for short rivets. The results of a number of tests are shown in Table 1.d and Fig. 1.1. The points in the upper range of Fig. 1.1 correspond to the driven tensile strength. The points in the lower range represent shear strength values, similarly expressed. The abscissa is grip length in inches. The same data were also plotted against the ratio of grip length to rivet hole diameter, but it was found that the method of representation in Fig. 1.1 allows more positive conclusions to be drawn. With regard to the variety of the sources of information, the spread in the case of the tensile values is fair and that of the shear values is good, generally less than 10 percent.

There are three reasons why the strength of a rivet with a short grip length should be greater than that of a longer rivet. First, there is the greater "upsetting effect" due to driving per unit volume of a short rivet. Second, yielding along 45° planes may be restricted by the geometry of very short rivets, resulting in greater ultimate strength. Finally, most driven strength figures are based on the hole diameter, i.e., they are calculated on the assumption that after driving the rivet completely fills the rivet hole. This is most apt to be true in the case of short rivets, hence they have the advantage of having more nearly the cross-sectional area that they are credited with. The fact that the actual cross-sectional area of any driven rivet is rarely known may partly account for the spread of the test results shown in Fig. 1.1.

Summary. If an estimate of the average driven strength has been made, it would appear from a study of Fig. 1.1 that this would most likely correspond to the strength of a rivet with a 3-inch grip. The estimate can

TABLE 1.d

VARIATION OF SHEAR AND TENSILE
STRENGTHS WITH GRIP LENGTH
(in ksi)

Ref.	σ_{tu}	Driven shear strength							Driven tensile strength					
		3/4	1	1-1/2	2	3	4	5	1	1-1/2	2	3	4	5
1.11	68.5	56.9		56.7		54.7								
1.11	59.0	54.9		52.0		48.2								
1.5	57.6											68.0		65.9
1.5	79.8											94.8		89.9
1.3	74.7				58.7	57.1		53.8				86.4		81.3
1.3	69.1				54.2	54.9		53.7				86.8		77.2
1.3	81.5				63.6	63.6		62.0				96.1		95.0
1.1	56.0										69.3	61.7	60.2	55.2
1.2	55.6										74.2	68.7		
1.2	58.1		50.8		50.0	49.5					72.0	68.9		
1.7	57.0		46.8		46.2	45.5		43.5	64.1		61.3	60.1		56.1

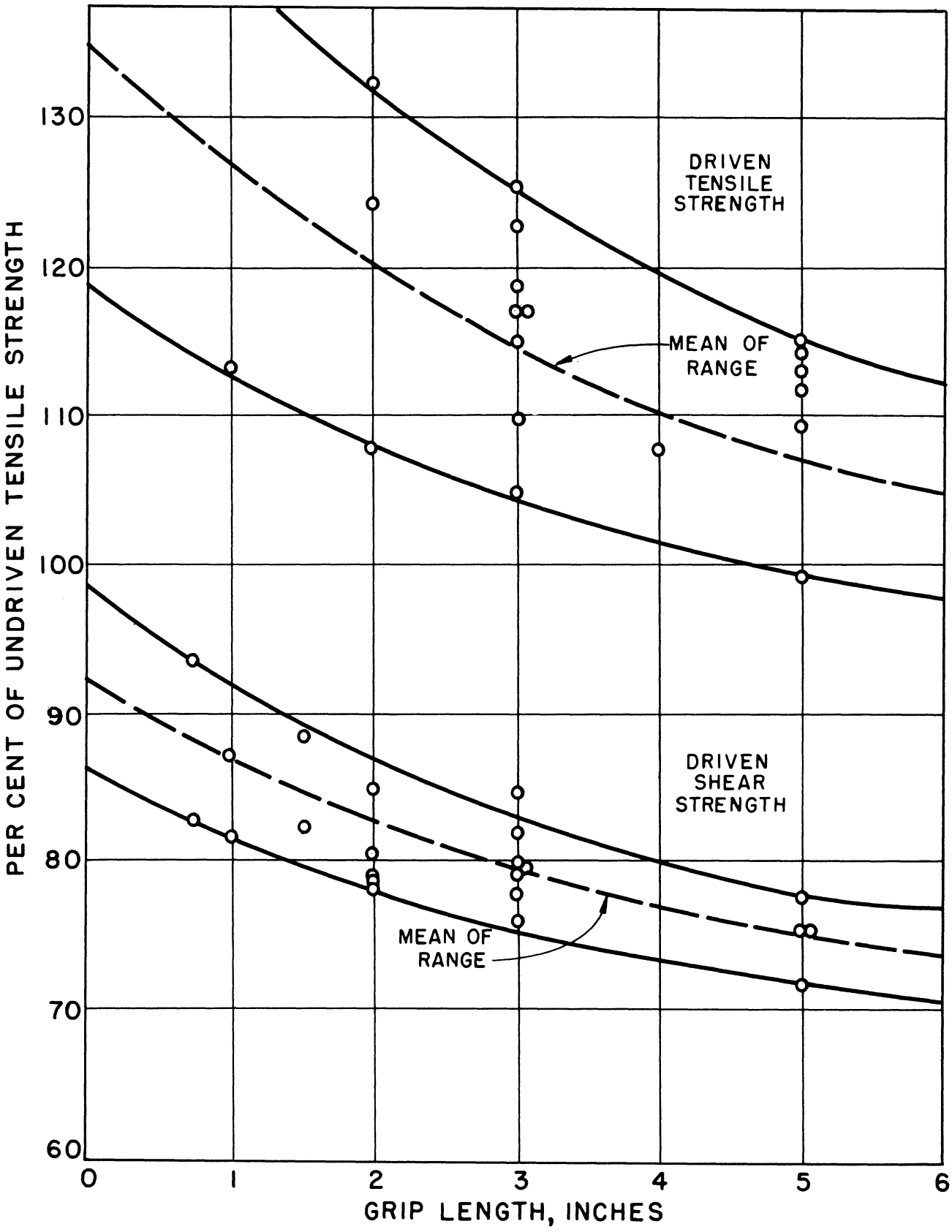

Fig. 1.1
Variation of shear and tensile strengths with grip

now be revised up or down according to the averages of the points shown in the figure to arrive at a new estimate for the actual grip length under consideration.

Rate of Application of Load

A literature search has not revealed tests specifically designed to determine the effect of the rate of loading on the strength of rivets, but a number of investigators have studied the effect of rapid loading on the strength of metals generally. The rate at which most components may be strained as a result of blast loads is estimated to be well below 1.0 inch per inch per second and while such a rate may well increase the yield point stress by 40 to 50 percent the ultimate tensile strength is not so drastically affected (1.45). Thus the strain rate under blast loads is not likely to increase the ultimate strength of components by more than 5 percent of their static strength.

No tests reporting the effect of impact on shear strength are reported here, although some work on a classified basis is in progress at various government and university laboratories.

Although the rate of strain controls the increase of strength, this rate at any particular point depends on the interaction between all parts of a structure and on the rate of load application. There appears to be some need for further research on the effect of impact loads on connectors, connections, and assemblies.

Other Factors

Type of head. Kommers (1.12) carried out fairly extensive tests with the purpose of comparing the properties of joints having rivets with button heads and countersunk heads respectively. According to these tests the ultimate shearing strength of the rivets with the countersunk heads is slightly better, but the strength variation in the tests was such as to render the difference insignificant.

Wilson and Oliver (1.1) investigated the effect of the type of head on the strength of rivets in tension. They compared a button head with a button head flattened to 3/8 inch and with a countersunk head. The flattened head developed only 90 percent of the strength of the rivet shank. The other heads developed the full strength. No conclusions regarding relative fatigue strength should be drawn from the foregoing remarks.

Number of rivets in a joint. All tests concerned with this variable show that the strength of a multirivet joint which fails due to shearing of the

rivets is usually less than the sum of the individual shearing strengths of the component rivets. This is in accord with theoretical considerations. It has been shown by a number of investigators (1.15, 1.16) that the load transmitted by a joint having three or more rivets in the line of load application is not equally shared by all the rivets. Not until plastic deformation has taken place in the most heavily loaded rivets does an equalizing redistribution of load occur. However, if the overall number of rivets is considerable, the slip required to induce ultimate load in the central rivets may cause failure in the end rivets before the full strength of all has been developed. This problem will be analyzed in Chapter II on "Tension Connections". The effect of the ratio of plate strength to rivet strength will also be treated in Chapter II.

Rivet size. There appears in some instances a small tendency for the unit strength of rivets to decrease with increasing diameter. However, Kommers (1.12) as well as Cox (1.7) were unable to establish a definite relationship between strength and diameter. Gallik (1.14), reviewing the work of European investigators, reports a similar uncertainty. It is believed that the rivet unit strength may be considered as independent of size.

Method of rivet manufacture. There is no evidence that the strength of rivets is affected by the method of forming the manufactured head. The driven strength of rivets that have been manufactured by hot-forming is much the same as that of rivets that have been cold-formed, other factors such as driving method being the same.

THE STRENGTH OF BOLTS

Until recently bolts were not normally used in primary structural joints. Bolts were used during erection, in purlin connections, and as temporary replacements for rivets that had become loose. The use of bolts has been avoided when a high degree of resistance against slip was desirable.

There are two reasons why low-carbon steel structural bolts are not effective in preventing slip. (1) To facilitate assembly the holes are usually finished about 1/16 inch larger than the nominal bolt diameter (1.17). Unlike rivets, bolts reduce in diameter during installation. When frictional resistance has been overcome, a slip of up to 1/16 inch may take place with no appreciable change in resistance due to any one bolt (1.18). (2) In the case of low-carbon steel bolts, creep at points of high-stress concentration causes a loss of bolt stress, which in turn reduces the locking action between nut and bolt and eventually results in a reduction of pressure between the faying surfaces. This is

of particular importance in bridges and other structures where joints are subject to frequently changing loads. Under field conditions holes will never be matched exactly and in a joint containing many bolts there will be some increase in load with even a small amount of initial slip. This is discussed in more detail in Chapter II.

Important developments during the past five years have shown that very effective joints can be made by use of high-strength bolts in conjunction with hardened washers and suitable nuts (1.17). With these hard materials an initial tension much higher than the initial tension in rivets can be developed and maintained. The working load is then satisfactorily transmitted by friction without appreciable slip between the faying surfaces.

Part of the information presented here on rivets is also applicable to bolts. Additional information will be presented on aspects not covered in the discussion of rivets. Bolts will also be discussed under the heading of energy absorption.

Tensile and Shear Strength

The tensile strength of bolts per unit of root mean diameter area is invariably greater than the coupon unit strength of the material. Circumferential notches or threads appear to resist the reduction in area that normally takes place in a plain tensile specimen. Notches induce a three-dimensional state of tensile stress, reducing the shear stress that is conducive to ductile behavior. Furthermore, the presence of notches from the geometrical point of view has a tendency to restrict yielding. When coupled with other conditions that also raise the ductile strength, namely low temperature and high rate of loading, an ultimate ductile strength higher than the brittle strength of the material may be produced and brittle failure takes place. Thus, threading raises the strength per unit area of bolts. The increase in tensile strength at the thread root is generally insufficient to offset the area reduction due to the threads and in most cases bolts in tension fail in the threaded portion.

The ratio of the shear to tensile strength for bolts does not differ from the corresponding ratio for rivets by an appreciable amount provided that the bolt tensile strength value used is the coupon strength. For example, for ASTM A325 bolt material Munse, Wright, and Newmark (1.18) report 0.71 and 0.64 as the ratio to the coupon strength of single and double unit shear strength respectively. If the higher full size bolt tensile strength values are used, the above ratios are reduced to 0.64 and 0.58 for single and double shear respectively. Tests on bolts of ASTM A7.39 material carried out by the Lehigh Structural Steel Company (1.10) in 1944 resulted in a ratio of single shear strength to bolt material tensile strength of 0.65.

Failure of bolts will not usually occur by stripping of the threads, but in the case of large bolts the effect of Poisson's ratio in disengaging the threads may be important. This was demonstrated in tests on 3-1/2-inch diameter bolts at Lehigh University (1.46).

Effect on Bolt Strength of Combined Loads

The tightening of a bolt induces in it a tensile stress as well as a shear stress due to the applied torque. When load is applied to the joint the resulting maximum shear stresses are not in general additive to the maximum shears produced by torque. Furthermore, the shear due to torque may be relaxed by the joint loading process. Tests carried out at the University of Illinois (1.18) have shown that bolts having an average ultimate strength of 66.9 kips and tightened to 35.0 kips, their ultimate shear strength is not at all affected by the initial stresses. Similarly H. O. Hill (1.19) reports that the stresses induced in a bolt by the tightening of a nut do not reduce the ultimate tensile strength of the bolt.

It may be concluded that both the ultimate shear and tensile strengths of a bolt are largely independent of the stresses induced by tightening of the nut, unless the tightening process itself is continued to failure.

DEFORMATION AND ENERGY ABSORPTION OF RIVETS AND BOLTS

Under impact loading, the ultimate survival of a structure is dependent on the amount of energy that can be absorbed and hence on the ultimate deformation of the component parts. Energy may be absorbed by the connections, or by the adjacent members, depending on their relative strength. However, in any case, for a group of rivets or bolts to develop full connection strength, some of them must deform plastically.

Tensile Loading

In specifying or describing a structural steel, the yield point strength, the ultimate tensile strength, and the percent elongation and/or the reduction in area are normally quoted.

A comparison of the elongation values of two materials has meaning only if the tests are carried out on specimens that are geometrically similar. Tension test methods and the interpretation of their results have received much attention in the past. The different procedures adopted as standards in various parts of the world are evidence of the fact that no universally accepted method has been developed so far. On this continent the elongation is measured on a

2- or 8-inch gage length and the gage length is not related to the cross-sectional area of the specimen. Barba (1.20), who pointed out that geometrically similar bars deform similarly, suggested the following expression for the percentage elongation of a bar of gage length "L" and cross-sectional area "A".

$$e = \frac{C \sqrt{A}}{L} + B$$

No doubt with this expression in mind, the French use a gauge length of $8.17\sqrt{A}$ and the Germans use $11.3\sqrt{A}$ and $5.65\sqrt{A}$. For round specimens the foregoing gage lengths, in terms of diameter, are 7.2D, 10D, and 5D, respectively. Thus, it is possible to establish values for C and B which will hold good for any gage length and to calculate approximately the elongation for bars of any proportion, e.g., Unwin (1.21) suggests 70 and 18 for the values of C and B for mild steel. This makes it possible to calculate that the elongation of a 0.505-inch diameter specimen of 2-inch gauge length is 34 percent, but it is also possible to calculate that under ideal conditions a 7/8-inch rivet of the same material with 1-1/2-inch grip would elongate 54 percent. The first term is the local or "necking" elongation and the second term the "uniform" elongation that occurs prior to maximum load. Thus this "law" points the way in the direction of a logical method of standardizing elongation measurements.

The percentage length change of a driven rivet tested to failure in tension will be termed "grip elongation". From the foregoing it is clearly an approximation to compare the grip elongation to the percentage elongation value obtained from a standard specimen. However, relative elongation values are of interest in assessing the effect of heat treatment or mechanical processes if they are determined by specimens of the same size.

The effect of driving on the elongation of rivets. The elongation of the undriven rivet material is usually measured on a standard 2-inch gage specimen, but it is the elongation over the total grip length which is a determining factor in overall behavior of a connection. Consequently, the ratio of the grip elongation of driven rivets to the elongation determined from a standard specimen of the undriven rivet material can be used as a relative but not quantitative means of comparison. Since the values of elongation obtained from several specimens of the same material often differ by 25 percent or more, any ratios based on elongation are obviously approximate. Based on grip lengths of 2 to 6 inches, the ratio as defined above is found to vary from 30 to 65 percent. Whereas a systematic variation would be expected according to Barba's Law, many factors combine in determining the active elongation of a driven rivet and the resulting scatter makes exact values of little practical significance.

Unpublished tests by McClintic Marshall Company on standard specimens turned from driven rivets (so that the properties of the undriven and driven material could be divorced from the effect of shape) showed the true ratio of

driven to undriven elongation to be 87 and 72 percent respectively for A7-24 rivets and carbonmanganese steel rivets. In other tests, made in England (1.6) this ratio was 70 and 42 percent respectively for ordinary strength and high tensile rivets. These figures indicate that it is very difficult to predict the elongation of driven rivets. Generally, the loss of ductility is greater for stronger rivets.

The energy absorbed by a material per unit volume is a function of strength and elongation and is a quality factor often quoted in describing the results of tests.

An index of the capacity of a material to absorb energy per unit undeformed volume is the area under the stress-strain diagram. Since this diagram is not usually available, it is suggested that the energy can be approximated by

$$U = \frac{\sigma_y^2}{2E} + \frac{e}{300}\,(\sigma_y + 2\sigma_u) \quad \text{ksi}\,, \tag{1.1}$$

where e = elongation in percent,
σ_y = yield-point stress in ksi,
σ_u = ultimate stress in ksi, and
E = modulus of elasticity in ksi.

This expression assumes that the stress-strain curve above the yield point is a parabola and gives a fairly accurate approximation of the area under the stress-strain diagram. The first part of the expression can be neglected and σ_y taken to be approximately $0.7\sigma_u$, giving

$$U = 9\,\sigma_u\, e \times 10^{-3} \text{ ksi}\,. \tag{1.2}$$

Table 1.e shows the unit energy values for a number of tests on rivets. It may be noted that the energy per unit volume required to break a standard specimen does not vary much for different materials. There is a greater variation after driving because of the different shapes of the driven rivets. If complete test information were available it would be possible to evaluate energy per unit volume more accurately by considering true stress-natural relationships. Incidentally, it is interesting to compare these energy values with the minimum product of ultimate strength and elongation frequently required by A.S.T.M. specifications, i.e., 15 or 16 ksi.

The effect of threads. When the effect of threads and notches on strength was considered earlier in this chapter, it was pointed out that in the extreme case their presence leads to brittle failure. Usually the ductile yield strength is not raised sufficiently by threads to allow brittle failure to take place without any ductile deformation having occurred first. However, the ultimate brittle strength of bolts may be reached before the yielding and necking

process has been completed to the same degree as in a plain specimen. Moreover, in partly threaded bolts the average stress on the plain shank is considerably lower than at the root of the threads. As a result the average percentage elongation of bolts is liable to be less than that of similar plain specimens even though a certain amount of ductile deformation has taken place prior to failure.

TABLE 1.e

ENERGY ABSORBED PER UNIT VOLUME
BY UNDRIVEN AND DRIVEN RIVETS

Ref.	Undriven Tensile Strength ksi	Energy before Driving ksi	Energy after Driving ksi	Remarks
1.6	64.1	21.3	17.3	All from 4 in. standard specimens
1.6	74.7	20.3	12.6	
1.8	51.0	20.3	18.8	
1.8	54.0	19.9	17.7	All from 2 in. standard specimens
1.8	97.6	24.7	19.2	
1.3	74.7	24.2	11.2	
1.3	69.1	25.4	14.0	Undriven elongation from 2 in. standard
1.3	81.5	25.8	13.4	specimens
1.5	57.6	18.4	15.1	Driven elongation from full size rivets
1.5	79.7	21.6	14.7	

The reduced elongation of bolts means, of course, that less average energy per unit volume is required to break a bolt in tension than an otherwise similar plain specimen of the same material. This is illustrated by tests on bolts of five different materials carried out by Whittemore, Nusbaum, and Seaquist (1.24). Attention is given here to two of the materials in the tests that were ferrous. Table 1.f gives the results in terms of energy absorbed per unit volume by standard tensile specimens and by bolts of four sizes made of chromium-nickel steel and cold-rolled steel. The energy values for the bolt specimens were obtained by the investigators from the static stress-strain diagram for the bolts. The energy values for the plain standard specimens were estimated by use of Eq. 1.2,

$$U = 9\ \sigma_u\ e \times 10^{-3}\ \text{ksi} .$$

It is interesting to note that there is practically no variation of average absorbed energy per unit volume between bolts of different sizes. This is to be

TABLE 1.f

ENERGY IN ksi ABSORBED BY BOLTS
PER UNIT VOLUME (REFERENCE 1.24)
(Brittle failures not included)

	Energy* for Stand. Specimen	Energy for Bolts				Average Energy of Bolts	Ratio of Bolt Energy Spec. Energy
		3/8-in.	1/2-in.	5/8-in.	3/4-in.		
Chrom-Nickel Steel.	21.0	6.07	6.10	6.23	6.52	6.23	29.6%
Cold-Rolled Steel.	13.6	4.02	3.92	3.86	3.98	3.95	29.0%

* Calculated from approximate formula $U = 9\sigma_u e \times 10^{-3}$

expected since the test specimens were similar, their effective length being six diameters with a length of one diameter being threaded. All bolt specimens failed in the threads, usually after some necking, with absorbed energy per unit volume of about 29 percent of that of the standard specimens, thus confirming the effect described in the last paragraph.

The effect of impact loads on deformation and energy absorption. A review of literature indicates that elongation is only slightly affected by the rate of application of load, except when the rate is very high (1.23).

The tests on bolts by Whittemore, Nusbaum, and Seaquist resulted in an average increase by a ratio of 1.19 in energy absorbed by chromium-nickel steel bolts under impact as compared with static load. The ratio for cold-rolled bolts was 1.30. The elongation values under impact load also were somewhat greater than those under static load. The impact-static elongation ratio was 1.14 for the chromium-nickel steel bolts and 1.19 for the cold-rolled steel bolts. Application of Eq. 1.2 would indicate that the ultimate strength under impact was about 1.04 times the static for the chromium-nickel steel bolts and 1.09 times the static strength in the case of the cold-rolled steel bolts. Thus, impact does not result in the same degree of improvement of strength for bolts as for plain specimens.

Brittle failure. Brittle failure will occur in rivets or bolts when conditions are such as to raise the stress level for ductile behavior above the brittle strength. For many steels, under any combination of rate of loading and stress concentration, there exists a "transition" temperature below which

brittle rather than ductile failure will take place. With properly manufactured and normally driven steel rivets the transition temperature is rarely above 0°F (1.9). In the bolt tests referred to earlier (1.24) and carried out at ambient temperatures, no brittle failures occurred in the 96 bolts tested statically. Three of 48 bolts tested by impact loading had brittle failures. All three were of cold-rolled steel.

The amount of energy absorbed when brittle failure takes place is only a small fraction of that required to produce ductile failure. Since brittle elongation is even a smaller fraction, it can be concluded that the brittle strength is appreciably higher than the ductile strength.

Hechtman (1.9) found that increasing the initial driving temperature from 1900 to 2300°F would either lower or not affect the transition temperature. The effect of extending the soaking period was similar. Constant driving below 1000°F would raise the transition temperature of rimmed steel rivets to 75°F if driving were continued to a "finishing" temperature of 700°F. Rivets of killed or silico-manganese steel were not affected by the "finishing temperature". When brittle failures did take place, they consistently occurred at the junction of the shank and the manufactured head, rather than at the driven head.

Loading in Shear

It is not clear at present what dimensions and which basic material properties the shear deformation at failure (or shear elongation) should be related to, so that the results of tests on one size of rivet and one kind of material could be used to predict shear elongation for other sizes and conditions.

Unlike the deformation due to tension, the deformation due to shear, as it occurs in a riveted or bolted joint, is independent of the grip length. A relatively small amount of material is affected in the process of failure.

A review of a large number of shear tests on rivets and bolts has revealed only one series of tests in which the shear deformation was measured up to the ultimate shear strength. These tests were carried out by Cox at the University of Illinois (1.7), who found that the ultimate shear deformation of a 7/8-inch diameter rivet was 0.3 inches. This is of the same order as the tensile elongation of a rivet 7/8 inch long.

Further study is required to develop a background of experience concerning the important problem of shear deformation as it occurs in rivets.

THE PROPERTIES OF WELDS IN CONNECTIONS

The following discussion of the effects of welding on structural materials does not include data on the strength and deformation of welded joints.*

Welding is defined by the American Welding Society (1.25) as a "localized coalescence of metals". Of the thirty seven different welding processes listed in the same reference, the designer of structural steel connections is primarily concerned with the metal electrode arc welding process, in which metal from the electrode in the presence of an electric arc is deposited on and united with two metal parts that are being joined.

Reference should be made to the recent monograph by Stout and Doty (1.26) which provides a highly competent evaluation of the current state of knowledge relative to the weldability of steels. These authors define weldability as "the ease with which the required degree of joinability and performance can be obtained with a given welding process and procedure". In connection with weldability, Stout and Doty review both research results and practical considerations and in successive chapters cover the properties of the steel itself, fabrication factors, the effects of carbon content, alloying elements, and thermal and mechanical history of the base metal. Tests for checking weldability are evaluated and an appendix is provided in which sound welding procedures are tabulated for all commonly used steels under a wide variety of practical situations.

The availibility of the monograph by Stout and Doty, which was published during the writing of the present monograph, suggests that it would be rather pointless to provide here any detailed discussion of the metallurgical factors that affect the problem of weldability. Attention will be given primarily to structural behavior as affected by the weld material and the adjacent base metal.

From a structural point of view the primary problem is whether the weld metal will provide a strong ductile union of the material or, crack under service or unusual loading conditions in a way that may lead to structural failure with very little absorption of energy. The matter of transition temperature, previously discussed in connection with bolts and rivets, will also be one of importance.

Although the advent of welding has brought about improvements in the construction of buildings, bridges, ships, and pressure vessels, it has also brought with it certain problems that have been headlined by the failure or

*See Chapters II, III, and IV for the latter.

near-failure of some of the welded ships, particularly those that were fabricated under war-time conditions. The origin of these failures is usually traced to certain points of high-stress concentration, which in combination with low temperature and other factors has brought about a sudden brittle fracture in a ship with occasional disastrous results. Prophetic intimation of such failures in welded structures was given by a number of bridge failures that occurred in Europe during the period of 1930 to 1940 (1.39, 1.40, 1.41, and 1.42). Brittle fractures in ships and in pressure vessels have resulted in extensive research projects at many different institutions under the sponsorship of the Ship Structure Research Committee and the Pressure Vessel Research Council. The work of the Ship Structure Research Committee has been reviewed recently by Wright, Jonassen, and Acker (1.30, 1.49) and in the Third Progress Report of the committee itself (1.48). The problem of brittle fracture as affected by fabrication procedures that are involved in the use of steels used in pressure vessels has been reviewed by H. C. Boardman (1.47). In this review primary attention is given to the investigation of transition temperature as affected by the use of either killed or rimmed steel, welding practice, and straining beyond the yield point. These extensive investigations have been carried out at Lehigh University.

Brittle fracture in a welded structure seems to be caused by a combination of adverse factors that may occur only sporadically in any given type of structural design. These factors include the following:

1. local stress concentrations,
2. poor welding,
3. notch-sensitive steel,
4. shock loading,
5. low temperature,
6. strain aging, and
7. state of stress combination in which all three principal stresses are tensile.

The relation of the problem to plastic analysis in structural design as covered by other Lehigh investigations under the Welding Research Council has also recently been reviewed (1.44).

The effects that welding may have on a structure can be traced in part to the fact that welded joints, unless specially designed for flexibility, are usually more rigid than riveted joints. Riveted joints, by providing some degree of relief for deformation stresses, sometimes help to make up for a lack of notch-toughness of the parent metal. Adequate notch-toughness of material is, therefore, most important in welded construction. In addition, when cracks do start in a riveted structure, they are more likely to stop at some nearby rivet hole, whereas in a continuous welded structure no such relief is possible.

Although residual stresses have been shown to have a detrimental effect on the buckling strength of a metal structure (1.50) within certain limiting proportions, their role as an influencing factor in brittle failure has been a matter of some debate. Residual stresses may produce a biaxial or a triaxial stress distribution, thus tending to raise the yield stress and reduce elongation. This may become critical in extreme cases where other conditions favor brittle failure, but normally the existence of such stresses in structures is not of any apparent consequence. It has been shown (1.32, 1.50) that residual stresses of the order of 20 ksi are present in standard rolled sections. Evidently, residual stresses do not usually produce premature failure of the material.

Notches, cracks, cavities, enclosures, or other geometrical discontinuities, all of which are known to be associated with a relatively large and localized triaxial tensile state of stress, are definitely conducive to brittle failure. Discontinuities may not be critical in one material at a certain temperature, but may produce brittle failure conditions in another more notch-sensitive material. This is an important consideration in weldments, for according to Kloeppel (1.43) minute cracks must always be reckoned with in the transition zone of welds. In fact Kloeppel defines weldability as the ability of the material to resist the spread of such cracks. Thus, poor welds with a great number of enclosures of slag and cracks in the transition zone may result in early failure in conjunction with one parent metal, whereas the progress of cracks may be arrested with a material of greater toughness.

A low yield point and a high degree of ductility in the parent metal adjacent to the weld act as safety valves and limit the stresses which are transmitted to a weld upon cooling. The relatively fast cooling rate after welding tends to increase the strength and reduce the ductility with consequent greater tendencies for cracks to develop in the heat-affected zone during the welding process. It is suggested by Finn Jonassen (1.49) that it may be advisable sometimes to reduce strength requirements by lowering the carbon content, in order to get a more weldable steel.

Procedures developed by Heuschkel (1.29) for the rating of steels in the prewelded and postwelded condition, in comparison with carbon structural steel, have received considerable attention. Using a tee-bend test, he shows that for each composition and temperature of bending, optimum prewelded yield and ultimate strengths and prewelding and postwelding hardness ranges exist. He evaluates the individual influence of each of the common alloying elements on the capacity of the joint to absorb energy under concentrated stresses, both at normal and subzero temperatures. An overall relationship between total analysis and welded performance under both normal and subzero bend test conditions is obtained.

Tests of Welds

It is frequently possible to estimate the strength and deformation properties of structural assemblies from a knowledge of the results of physical tests of the components, e.g., a riveted joint. In the case of a weld information on the physical properties of the filler metal and the parent metal is not sufficient to allow an accurate estimate of the properties of the complete weld or weldment. This is particularly true of the deformation properties. There are mevertheless, several types of tests in connection with welding that help to weed out unsatisfactory materials and methods.

Tensile tests. All-weld-metal tests are carried out to determine basic properties of the weld metal and covering. Since the properties of a welded joint also depend on those of the parent metal, the all-weld-metal test is only of limited interest. Tensile specimens are sometimes machined out of a welded joint so that the welded zone is contained in the specimens. The weld can be situated across or parallel to the line of action of the applied load. The performance of this type of specimen does to some extent depend on the weldability of the parent metal. However, because of the great degree of stress relief and lessened notch effect afforded to the specimen by the machining away of the surrounding material, it is generally tested under more favorable conditions than a full-size welded joint.

A series of tests sponsored by the Steel Structures Research Committee in Great Britain (1.34) gives some insight into the relationship between the tensile strength of an all-weld-metal specimen and that of a specimen involving the parent metal to a greater extent. For 22 different electrodes tested, the strength of butt-welds varied from approximately 90 to 120 percent of the strength of the corresponding all-weld-metal tension specimens. The strength of fillet-welds varied from 43 to 85 percent of the all-weld-metal strength. The chief purpose of the all-weld-metal tension tests was to grade the electrodes so that the scatter of the main tests could be reduced. All electrodes with an all-weld-metal strength of more than 63 ksi and an elongation exceeding 20 percent (over a gage of 3.54 times the diameter of the specimen) were graded as "A", provided also that their notched bar impact value was above 30 foot pounds (Izod test).

The static tensile yield strength of welds increases with lower temperatures in proportion to the corresponding improvement in the properties of the base metal (1.38).

Impact tests. The purpose of an impact test is to evaluate the notch toughness of a material and to determine the degree of likelihood of brittle fracture. Most impact tests on welds are carried out on all-weld-metal specimens or specimens machined from a butt-weld. The usefulness of the impact test is

restricted by the fact that the different standard specimens adopted in different parts of the world do not allow a quantitative comparison of the many test results available in the literature. In addition, impact tests on small specimens do not have, in general, a direct relation to the impact strength of a structure made of the same material.

What significance does an impact test on weld metal have in relation to the shock resistance of a structure or structural member? Spraragen and Claussen (1.37) conclude that the behavior of complete structures under impact cannot be estimated from the behavior of small impact specimens. Impact test results on welds have been reviewed extensively by the same authors (1.36, 1.37). As might be expected, the impact values of welds decrease with increase in carbon content. German tests showed that an increase in the carbon content of the base metal from 0.11 to 0.68 percent reduced the impact value by over 50 percent. Evidently the deposited metal picked up carbon from the parent metal. The impact values decreased at a faster rate up to a carbon content of 0.30 percent than with further increases.

A higher carbon content raises the maximum hardness which the steel can attain and so may result in greater brittleness in the heat-affected zone of a weld. With low-carbon steels the notch toughness of the heat-affected zone is generally no lower than that of the base metal and may even be greater.

The sensitivity of the weld impact test to the presence of impurities is considered important by Spraragen and Claussen. In preventing contamination of welds, coated-welding rods have resulted as early as 1936 in Izod values of 40 foot pounds, whereas in 1920 the corresponding value with bare wire had been about 5 foot pounds.

Cold working can improve the impact value of a weld. This may be due either to stress relief or to strain hardening.

The type and amount of current used is reported to have no important effect on the impact strength of welds (1.37).

Low temperatures reduce the impact values of welds in much the same way as that of the parent metal (1.38) and much of the recent work on impact testing has included evaluation of the transition temperature under a particular set of conditions.

Weldability tests. The failures of welded structures brought the realization that the standard mechanical tests carried out on the filler metal and the parent metal separately were not suitable for predicting the properties of a welded joint. Engineers have, therefore, been striving to develop tests which can be used to determine the degree of weldability resulting from any given combination of materials and welding processes.

Stout and Doty (1.26) devote four chapters of their monograph to a review and summary of the application and development of weldability tests. These include tests for weldability in fabrication, direct tests for service, indirect tests for service, and a "critique" on weldability testing. In final summary, Stout and Doty list the requirements of a satisfactory test as follows:

1. direct correlation with actual fabrication or service,
2. high sensitivity to the effects of welding variables,
3. good reproducibility, and
4. simplicity of preparation and testing.

Quoting directly their conclusions:

> "Of the many direct and indirect tests that have been proposed for the evaluation of weldability, the direct tests offer the most promise of meeting the above requirements. However, there is no all-inclusive direct test which has a high sensitivity to both weldability in fabrication and weldability for performance in service. Only by a group of tests can both phases of weldability be evaluated.
>
> "The most useful test to evaluate the relative susceptibility of steels to underbead cracking is the longitudinal-bead-weld cracking test. The susceptibility of various filler metals to restraint cracking is best evaluated by the Lehigh restraint cracking test.
>
> "Unwelded test specimens cannot provide information on the mechanical properties of welds and of the material in the immediate vicinity of welds. Although it is not possible at present to specify a weldability test which provides the closest approach to correlation with performance in service, it is suggested by the authors that the longitudinal-bead-notch-bend test is the most useful from the standpoint of all other requirements. With respect to the desirable feature of direct correlation with service behavior, the test is potentially as useful as others that have been proposed."

A methodical investigation covering the effect of plastic strain, welding, and heat treatment on killed and rimmed steels has been sponsored by the Pressure Vessel Research Committee of Welding Research Council at Lehigh University. A longitudinal-bead-weld notched bend specimen (1.33, 1.51) similar to the Lehigh and Kinzel bend tests was used and tests were made at various

temperatures to evaluate the transition temperature. The interpretive report (1.47) on the above tests lists the criteria for transition temperature determination as follows:

1. appearance of fracture,
2. percent contraction below notch,
3. energy required to break specimen, and
4. energy absorbed after passing the maximum load.

As had been pointed out by Stout and McGeady (1.33), these criteria do not all determine the same property, since there are two transition temperatures for a notched specimen. The first corresponds to that temperature at which failure will commence ductilely near the notch, but will progress in a brittle fashion due to the more acute notch formed by a crack. This is termed the upper transition temperature. Evidently any failure below this temperature has the appearance of a brittle failure except in the immediate vicinity of the notch. The lower transition temperature is defined as that temperature below which brittle fracture will commence in the notch and progress with no appreciable ductility. Fractures below this temperature are brittle throughout the fracture area. Either the energy absorbed before reaching the maximum load or the contraction in width below the notch can be used to determine the lower or "ductility" transition temperature. The upper or "fracture" transition temperature is determined by the appearance of the fracture surface, i.e., whether it is a shear or cleavage type fracture. For further details on various test specimens and procedures reference should be made to the monograph by Stout and Doty (1.26).

GENERAL SUMMARY AND CONCLUSIONS

The effect of a number of variables on the properties of rivets, bolts, and welds has been reviewed and evaluated. The information which is presented is applicable to problems of analysis and design of structures in which the connections, or, more specifically, the connectors are liable to fail before other components.

The basic properties of the material of which rivets are made are of prime importance in determining the characteristics of the finished rivets. No other single factor can produce such a wide range of ultimate rivet strength values as variation of material. However, in practice, the properties of materials used for structural rivets in most countries vary within relatively narrow limits (Table 1.a).

The installation of a rivet in position involves a mechanical process and, in the case of hot-driven rivets, a heat treatment. The net-result of installation is to increase the tensile strength of rivets by an amount averaging between 10 and 20 percent (Table 1.b). Machine driving produces greater increases than pneumatic hammer driving. The effects of soaking time, driving temperature, and driving time are of a secondary nature.

The increase of shear strength as a result of installation is much the same as the increase in tensile strength. This follows from the shear-tension ratios shown in Table 1.c, which are of the same order for undriven and driven rivet stresses.

The ratio of ultimate shear strength to ultimate tensile strength for rivets does not vary far from 0.75. For rivets under combined stress an empirical formula suggested by Cox, Higgins, and Munse (1.7, 1.8) permits the calculation of the strength under combined load if the ultimate strength in pure shear or pure tension is known.

Rivet strength varies inversely with grip length. This is illustrated in Fig 1.1. Over the practical range of grip lengths the variation in strength is about 15 percent.

A high rate of application of load may increase the ultimate strength of rivets by about 5 percent. Other factors, such as the type of head, rivet size, and method of rivet manufacture, may slightly affect the strength of rivets in individual cases, but no general prediction about their influence can be made.

The relatively new practice of using high-strength steel bolts in connections has stimulated interest in structural bolts. Although the effect of the threads is to increase the unit ductile strength, the reduction of area more than neutralizes this gain and the strength of bolts, based on the shank area, is usually slightly below coupon strength. The ratio of shear strength to tensile coupon strength for bolts is about the same as for rivets. The tightening process, in general, does not affect the ultimate strength of bolts (1.18, 1.19).

The elongation and degree of energy absorption of rivets and bolts cannot be estimated as accurately as their ultimate strength because the data on this aspect of tests are usually less detailed and are scattered over a wide range. The fact that geometrically nonsimilar specimens are often used for tests at different stages of the manufacturing process of the connectors adds difficulties to comparisons. Tests indicate that the elongation, based on grip length of manufactured rivets, may vary from 30 to 65 percent of the standard 2 inch elongation of the material. Table 1.c shows the variation of the energy

absorbed per unit volume of rivets and of the undriven material. The approximate Eq. 1.2 was used to calculate these values. The table shows that in all cases driving results in a reduction of the energy absorbed, but the values are evidently dependent on the shape of the specimens.

While threads have the effect of increasing the stress at yield, the elongation is reduced. Elongation values for bolts are, however, erratic and are not normally quoted. The difference in elongation values compared to plain specimens is greater than the increase in strength, resulting in smaller energy absorption values for bolts (Table 1.f).

Properly installed structural rivets have a very low transition temperature. However, if driving is continued below the critical temperature, the transition temperature is liable to go up (1.9). High strength bolts have given satisfactory service under very unfavorable temperature conditions.

Little information is available on the deformation of rivets and bolts loaded in shear.

The effects of the welding operation in changing the properties of the parent and filler metal are more complex than the effect which the installation process has on rivets. Whereas in the case of rivets only the basic material properties, the method of driving and the grip have a profound effect on the ultimate rivet properties, a greater number of variables have to be controlled within relatively narrow limits to guarantee a good weld. Some of the more important of these requirements are:

1. The parent metal should be notch tough.
2. The welding operation should be carried out so as to minimize distortion.
3. The design and workmanship should be such as to result in the least number of notches, discontinuities, or other stress raisers.
4. The chemical composition of the parent metal should be such that the thermal and mechanical effects of the welding operation do not result in excessive loss of ductility.

In cases where new combinations of materials or methods are involved, weldability tests are available, permitting a comparison of the new procedure with an established one. Two different weldability tests are unlikely to give the same rating to identical weldments; this means that the results of a weldability test have no absolute significance. For example, there is no guarantee that an actual welded joint will not fail in a brittle manner at a higher temperature

than indicated by the corresponding weldability tests. Such discrepancies between standard tests and the performance of weldments under field conditions are normally taken care of by a factor of safety. More precise information can only be obtained from scale or full-size models of the assembly under consideration.

BIBLIOGRAPHY-CHAPTER I

1.1 Wilson, W.M.
Oliver, W.A.
"Tension tests on rivets"
Eng Exp Sta Bul 210, Univ of Ill (1930)

1.2 Baron, F.
Larson, E.W., Jr.
"Comparative behavior of bolted and riveted joints"
Preprint No 50, presented at the Cen Conv of the ASCE, Sept 1952

1.3 Wilson, W.M.
Bruckner, W.H.
McCrackin, T.H., Jr.
"Tests of riveted and welded joints in low-alloy structural steels"
Eng Exp Sta Bul 337, Univ of Ill (1942)

1.4 Young, C.R.
Dunbar, W.B.
"Rivets in combined tension shear and flexure"
School of Eng Res Bul 8:398-418, Univ of Toronto (1928)

1.5 Wilson, W.M.
Thomas, F.P.
"Fatigue tests on riveted joints"
Eng Exp Sta Bull 302, Univ of Ill (1938)

1.6 Henderson, H.M.
"The strength of rivets"
The Engineer 182:416-7 (1946)

1.7 Cox, H.L.
"Static strength of rivets subjected to combined tension and shear"
Master's Thesis, Univ of Ill, (1952)

1.8 Higgins, T.R.
Munse, W.H.
"How much combined stress can a rivet take?"
Eng News Rec 149(23):40-42 (1952)

1.9 Hechtman, R.A.
"A study of the effects of heating and driving conditions on hot-driven structural steel rivets"
Off of Nav Res Project, Univ of Ill (1948)

1.10 Anonymous
"Shear and tension tests for field bolts for Straitsmouth Observation Tower"
Unpublished tests by Lehigh Struc Steel Co, Allentown, Pa, (1944)

1.11 Talbot, A.N.
"Tests on nickel-steel riveted joints"
Eng Exp Sta Bul 49, Univ of Ill (1911)

1.12 Kommers, J.B.
"Comparative tests of button head and countersunk riveted joints"
Eng Series Bul 9:5, Univ of Wis (1925)

1.13 Kayser, H.
"Versuche uber die Abscher- und Lochleibungs Festigkeit von Nietverbindungen"
Stahlbau 4:85-9 (1931)

1.14 Gallik, S.
"Über die Scherfestigkeit und den Lochleibungsdruck von Nieten and Nietverbindungen"
Rep of the 2nd International Congress for Bridge and Struct Eng, Julius Springer, Vienna 1929, 365-84

1.15 Batho, C.
"Experimental and theoretical investigations on riveted and bolted joints with the application of the theory of welded joints"
1st Rep 113-136, Steel Struct Res Comm, Dept Sci Ind Res, London (1934)

1.16 Francis, A.J.
"Investigations on aluminum alloy riveted joints under static loading"
Engineering Structures Academic Press, New York (1949) 187-216

1.17 Higgins, T.R.
Ruble, E. J.
"High-strength bolts--A new concept in structural connections"
Civil Eng 22:176-9 and 255 (Sept 1952)

1.18 Munse, W.H.
Wright, D.T.
Newmark, N.M.
"Laboratory tests on high-tensile bolted structural joints"
Proc ASCE 80: Sep 441 (1954)

1.19 Hill, H.O.
"Does torque weaken bolts"
Fasteners Data Book 104-106, Ind Fasteners Inst, Cleveland (1950)

1.20 Barba
"Resistance à la traction et allongements des meteaux après rupture"
Memoires Soc Ingenieurs Civ, 1st part, 682 (1880)

1.21 Unwin
"Tensile tests of mild steel"
Proc Inst Civ Eng 155:170 (1903-4)

1.22 Clark, D.S.
Duwez, P.E.
"The influence of strain rate on some tensile properties of steel"
Proc ASTM 50:560-75 (1950)

1.23 Clark, D.S.
"The tensile impact properties of some metals and alloys"
Trans AMS 42:45-74 (1950)

1.24 Whittemore, H.L.
Nusbaum, G.W.
Seaquist, E.O.
"Impact and static tensile properties of bolts"
J of Res NBS 14:139-88 (1935)

1.25 American Welding Soc.
Welding Handbook
New York 3rd edition, 1950, 1651 pp

1.26 Stout, R.D.
Doty, W.D.
Weldability of Steels
Welding Research Council 1953, 381 pp

1.27 Kuntze, W.
"Pruftechnische Erfassung der Ursachen zum sproden Bruch des Baustahls"
Stahlbau 14:97-103 (1941)

1.28 Grüning, G.
"Die Schrumpfspannungen beim Schweissen (Versuch einer statischen Berechnung)
Stahlbau 7:110-2 (1934)

1.29 Heuschkel, J.
"Steel properties related to welded performance"
Weld J 28 Res Sup 135s-52s (1949)

1.30 Wright, E.A.
Jonassen, Finn
Acker, H.G.
"Research under the ship structure committee"
Presented at the annual meeting of the Soc of Nav Arch and Marine Engs, New York Nov 1952, reprinted as Weld Res Council Bul 16, Nov 1953

1.31 De Jonge, A.E.R.
Riveted Joints
Res Pub of the ASME, Items 897, 929, 910, (1945)

1.32 Mathar, J.
"Determination of initial stresses by measuring the deformation around drilled holes"
Weld J 13:24-9 (July 1934)

1.33 Stout, R.D.
McGeady, L. J.
"The meaning and measurement of transition temperature"
Weld, J, 38:299s-302s (1948)

1.34 Hankins, G.A.
Brown, A.F.C.
"Mechanical tests and analysis of results" Part 2
Rep of the Weld Panel of the Steel Struct Res Comm, Dept of Sci and Ind Res (1938)

1.35 Wilson, W.W.
"Tests of Welds"
Eng Exp Sta Circular No 21, Univ of Ill (1930)

1.36 Spraragen, W.
Claussen, G.E.
"Impact tests of welded joints"
Weld J 15:2-12 (April 1936)

1.37 Spraragen, W.
Claussen, G.E.
"Impact tests of welded joints"
Weld J 17:8-27 (Sept 1938)

1.38 Spraragen, W.
Cordovi, M.A.
"Behavior of welded joints at low temperatures"
Weld Res Council Rep (June 1943)

1.39 Kommerell, O.
"Augenblicklicher Stand des Schweissens von Stahlbauwerken in Deutschland"
Bautechnik 17:161-3

1.40 Anonymous
"Welded bridge failure in Belgium"
ENR 120:654-5 (1938)

1.41 Bijlaard, P.P.
"Brittle fracture in welded bridges"
Eng News Rec 146: 46-48 (April 1951)

1.42 Schaechterle, K.
"Betrachtungen über geschweisste Brücken"
Bautechnik 17:46-52 (1939)

1.43 Kloeppel, K.
"Schweisstechnik im Stahlbau"
Stahlbau-Handbuch, Walter Dorn (1948)

1.44 Johnston, Bruce G.
Yang, C. H.
Beedle, Lynn S.
"An evaluation of plastic analysis as applied to structural design"
Weld J 32 Res Sup 224s-39s (1953)

1.45 Nadai, A.
Theory of Flow and Fracture of Solids
McGraw-Hill Book Co Inc Vol I, 2nd edition 1950

1.46 Jones, J.
"Strength of large bolts"
Fasteners Data Book 136-37, Ind Fastners Inst, Cleveland (1950)

1.47 Boardman, H.C.
"Interpretive report Fabrication Division, Pressure Vessel Research Committee"
Weld J 39:422s-32s (1950)

1.48 Ship Structure Committee
"Third technical progress report of the ship structure committee"
Reprinted in Weld Res Council Bul 16 (Nov 1953)

1.49 Jonassen, F.
"A resume of the ship fracture problem"
Weld J 31:316s-8s (1952)

1.50 Yang, C.H.
Beedle, L.S.
Johnston, B.G.
"Residual stress and the yield strength of steel beams"
Weld J Res Sup 31:205s-29s (1952)

1.51 Kinzel, A.B.
"Ductility of steels for welded structures"
Trans ASM 40:27-82 (1948)

CHAPTER II

TENSION CONNECTIONS

A tension connection is the arrangement of metal parts and connectors used to join two members carrying tensile loads, as opposed to a connection transmitting bending moments. The objective of this chapter is to examine and present available data pertinent to the estimation of the ultimate strength and the load-deflection characteristics of tension joints used in steel structures. This is recognized as an ideal objective, a goal that cannot be completely realized, particularly so with regard to information on load-deflection characteristics.

RIVETED TENSION CONNECTIONS

Load Deformation Relation

Of the large number of tests which have been carried out on riveted joints, the great majority were conducted to determine strength properties. Where relative movements were measured this was done chiefly to determine the distribution of the load among rivets, although in some cases slip measurements were made to determine the load at which friction between the faying surfaces ceases to be the dominant effect. The total deformation of tension joints is reported in very few instances. Such lack of information can be explained by the fact that in conventional design practice there has been little need for this information. Even when behavior up to ultimate load is considered, the change of length of tension or compression members in trussed structures may be larger than the deformation at the connections. There are, however, instances where a knowledge of the load-deformation relation of tension connections is essential for the prediction of the behavior of a structure under heavy blast loads. One example is the kneebrace used to stiffen the

connection between roof trusses and columns; another is the connection used between girts and columns on the sides of buildings exposed to blast. The catenary action of the girts and the associated resistance is directly related to the movements taking place at the connections.

Whereas there exists sufficient experimental data to predict the ultimate strength of a riveted tension joint within a few percent, a review of the available information shows that no more than an approximate estimate can be made of the deformation of any one joint. An attempt will be made to interpret existing data and to utilize such parts as are applicable outside the range of the conditions of the respective tests.

The interpretation of tension connection tests is greatly facilitated by the graphical representation shown in Fig. 2.1. The joint under consideration is "balanced and symmetrical". This expression is used in this chapter in reference to a symmetrical connection with outer plates of total cross-sectional area equal to that of the inner plate. At first, friction is ignored and the assumption is made that the rivets share the load P equally. The load carried by the inner plate is reduced from P to P/2 by the first row, as shown in Fig. 2.1b. In Fig. 2.1c the ordinates of lines AD and BE, respectively, represent the deformation of points of the inner and outer plates, referred to point O, Fig. 2.1a. The difference between the ordinates of lines AD and BE is the slip between the plates at any point. In this case the slip is constant and equal to the relative movement between the plates at R_1. The total elongation of the joint between R_1 and R_2 is given by ordinate CE, which is composed of the slip AB (= DE) and the stretch in the plates CD. In the elastic range CD = Pp/2btE (effect of rivet holes on stretch is ignored). The total elongation is therefore equal to the slip at the first row of rivets, δ_1, plus the elongation that could take place in a length of plate p under a load P/2.

The elongation of a joint in the elastic range, after slip, cannot be less that $\delta_1 + Pp/2btE$, but it will be greater if the rivets do not fill the holes. For example, let it be assumed that the initial clearances around the rivets in row R_2 (Fig. 2.1) are larger than the clearances around the rivets in row R_1. It is possible, then, for the first row to be loaded before the second row has come into bearing. The total elongation would then be $\delta_1 + Pp/btE$. As P is increased and the second row is also brought into bearing, the total elongation would lie between $\delta_1 + Pp/btE$ and $\delta_1 + Pp/2btE$. If each row has several rivets, the average clearance in the two rows would be about the same and the total deformation would approximate $\delta_1 + Pp/2btE$. The three parts of δ_1 are: the clearance take-up, if any, between the first row of rivets and holes, the deformation of the rivets,

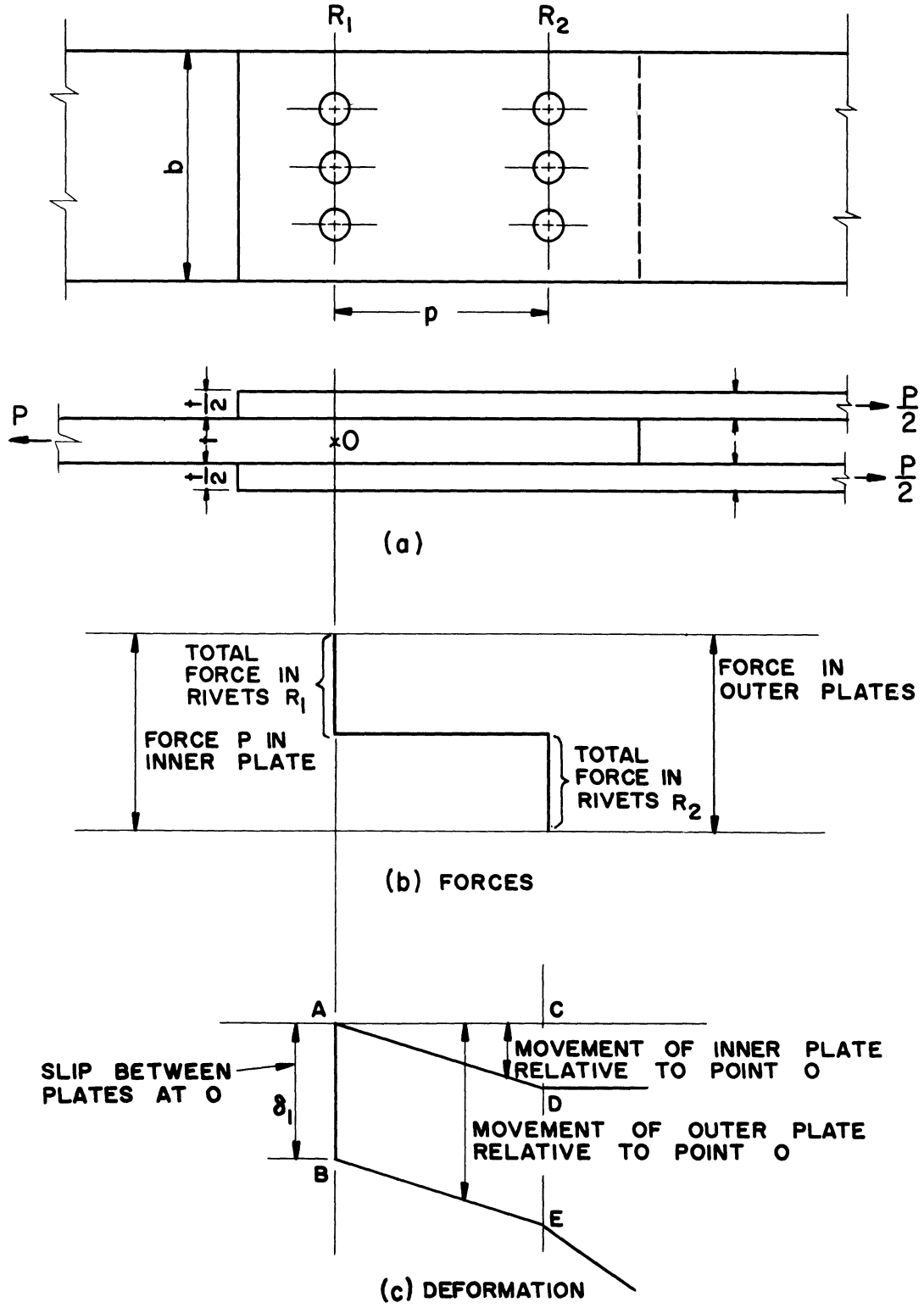
R1
R2
b
p
P
t/2
t
t/2
O
P/2
P/2
(a)
TOTAL FORCE IN RIVETS R1
FORCE P IN INNER PLATE
FORCE IN OUTER PLATES
TOTAL FORCE IN RIVETS R2
(b) FORCES
A
C
SLIP BETWEEN PLATES AT O
δ1
MOVEMENT OF INNER PLATE RELATIVE TO POINT O
D
MOVEMENT OF OUTER PLATE RELATIVE TO POINT O
B
E
(c) DEFORMATION

Fig. 2.1.

and the local deformation of the plate resulting from the bearing-stress concentration produced by the rivets. Since δ_1 must be known in order to calculate the total deformation of multi-row joints, it is an important characteristic of any rivet-plate combination. The distribution of load between the rivets in a two-row joint may be assumed determinate and such a joint may be used to evaluate δ_1. Thus, for any load the values of either AB or DE may be determined (Fig. 2.1c) and their average taken as being δ_1 for the load P/N, where N is the total number of rivets in the joint and P/N is the load per rivet. By plotting P/N against δ_1, curves similar to those shown in Fig. 2.2 are obtained. The curves in Fig. 2.2 are ideal versions and are

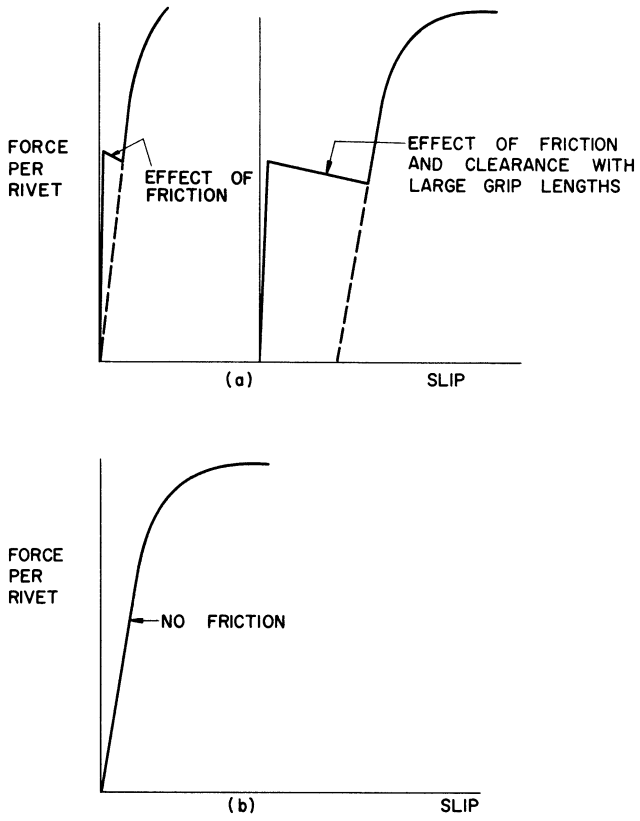

Fig. 2.2. Idealized Force - Slip Curves for Symmetrical Two-Row Tension Joints. (See Ref. 2.1.)

not to scale. Actual curves of this type are reported, for example, in University of Illinois Bulletin No. 302 (2.1). It is possible to obtain from such curves a modulus H, defined here as force per rivet/slip. Typical values for this modulus are given in Table 2.a.

The values of H are approximate since they have been obtained by estimation from a small scale line graph; nevertheless, the values for similar

materials and dimensions are in fair agreement. H is smaller for larger grip/diameter ratios because of the reduced stiffness and the greater clearance normally associated with longer rivets. Although the table below is not sufficient to develop empirical formulas for δ_1, it does allow some significant conclusions to be drawn. A combination of steel rivets and aluminum plates (line 3) results in H values about half of those for a steel-steel combination (line 2), thus confirming that local plate deformation is a major factor, as well as rivet deformation. As might be expected, the effect of grip length on H is pronounced. From the only result for single shear (line 18), H is of a lower order than for double shear.

TABLE 2.a.
EXPERIMENTAL RESULTS FOR THE MODULUS H

	Materials*		Shear	Rivet Dia., in.	Grip in.	H Lbs/in.	Reference
	Rivet	Plate					
1	Carbon St.	Silicon St.	Double	0.875	1.5	12.5×10^6	2.2
2	Carbon St.	Carbon St.	"	0.875	1.5	12.5×10^6	
3	Carbon St.	27 ST	"	0.875	1.5	5.4×10^6	p. 1374
4	17 ST	17 ST	"	0.875	1.5	4.2×10^6	
5	53 SW	53 ST	"	0.875	1.5	4.0×10^6	
6	AW6D	BS/ST AT	Double	0.750	1.5	5.8×10^6	2.3
7	AW6D	BS/ST AT	"	0.500	1.0	3.6×10^6	p. 197
8	ASTM-A141	ASTM-A7	Double	0.750	1.18	12.0×10^6	2.4
9	ASTM-A141	ASTM-A7	"	0.750	2.06	6.0×10^6	Figs.21,22,23
10	ASTM-A141	ASTM-A7	"	0.750	3.06	2.0×10^6	
11	Carbon St.	Carbon St.	Double	1.000	1.5	8.5×10^6	2.5
12	Carbon St.	Carbon St.	"	1.000	3.25	6.6×10^6	p. 34
13	Carbon St.	Silicon St.	"	1.000	3.25	6.1×10^6	
14	Manganese St.	Silicon St.	"	1.000	3.25	3.2×10^6	
15	Carbon St.	Carbon St.	"	1.000	4.75	2.1×10^6	
16	Carbon St.	Silicon St.	"	1.000	4.75	1.7×10^6	
17	Manganese St.	Silicon St.	"	1.000	4.75	1.7×10^6	
18	Struct. St.	Struct. St.	Single	0.562	0.750	0.8×10^6	2.6

* The descriptive names for materials are quoted from various references.

The effect of yielding of the rivets is considered next, assuming that this occurs before yielding of the plate materials. In fact, the practice of designing, multi-row riveted joints for equal distribution of load between the rivets implies some plastic deformation in the outer rivets. Francis (2.3) has shown that for a symmetrical joint containing 2r indentical rows of rivets and assuming an ideal load-deformation curve for the rivets, as in Fig. 2.3, the inelastic deformation in the outer rivets must

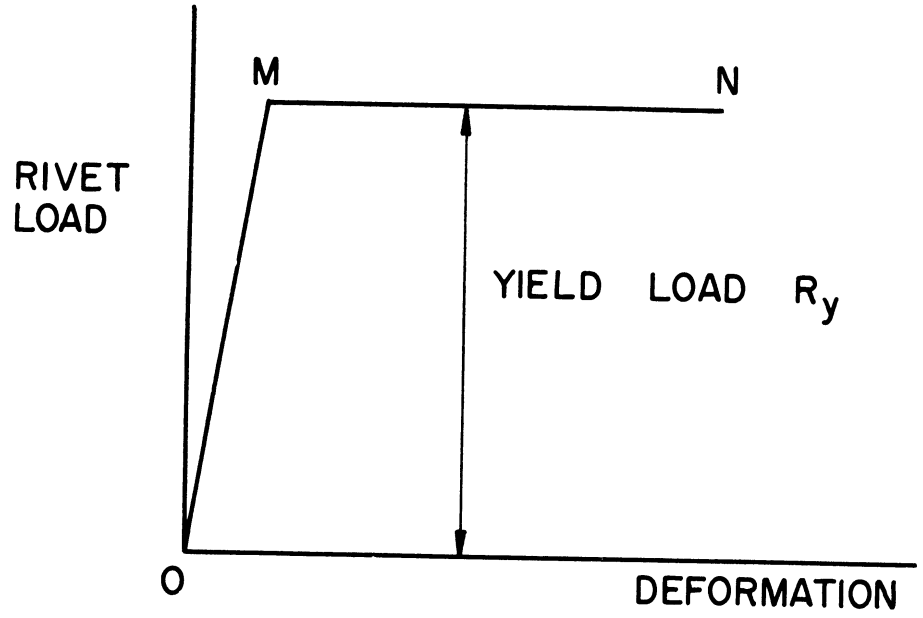

Fig. 2.3.

be $r(r-1)\ R_y p/EA$ before all rivets can be loaded equally to the yield level. In this expression

R_y = yield load of one row of rivets and

p = pitch of rivets.

$R_y p/EA$ is usually of the order of 0.001 inch, but if some of the rivets do not fill holes completely, more than $0.001\ r(r-1)$ inch of inelastic deformation may be required for load equalization. Of course, as the plates begin to yield, E becomes effectively much smaller and $R_y p/EA$ increases rapidly.

It has been shown that in the elastic range the deformation δ_1 at the first rivet or row of rivets in a joint depends on the material and diminsions of the plates, as well as of the rivets. Experimental results were

summarized and the order of magnitiude of H in the elastic range was determined. There is no basis for following a similar procedure in the inelastic range, which generally commences at about 60 percent of the shear-strength. Thus, if the (load)-(end slip) relationship is required for any particular combination of rivets and plates, it must be found experimentally. However, once such a relationship has been determined on a two-row joint it can be used in the computation of the total deformation of larger joints made of plates of the same material and thickness, uniformly matched holes, and rivets of the same material and diameter.

The ultimate value of δ_1 is of interest chiefly in the case of joints designed to fail in the rivets, which is the exception in practice. However, when failure does take place in the rivets most of the deformation δ_1 is due to the detrusion of the rivets, in which case the corresponding local deformation in the plate would be relatively small. Davis, Woodruff, and Davis (2.6) report a maximum detrusion of about 0.3 inch for 7/8-inch-diameter rivets in single shear. Moisseiff, Hartmann and Moore (2.2) report a maximum end slip for two-row specimens of 0.17 to 0.29 inch for 7/8-inch-diameter rivets in double shear with no marked difference between steel and aluminum rivets. Cox (2.7) measured a 0.30 inch detrusion for a 7/8- inch rivet in single shear. This was purely a shear test and the rivet was not in a joint.

The deformation taking place in the plates is now examined in greater detail. Again considering a two row connection, but with friction effective, the load in the inner plate is gradually reduced by the transfer of forces which takes place in the region where friction is caused by the initial tension of the first row of rivets. The force distribution in the inner and outer plates is now as shown in Fig. 2.4b. The ordinates of lines AD and BE in Fig. 2.4c represent the movement of points on the inner and outer plates, respectively, relative to the reference point O. It can be seen from Fig. 2.4c that some slip must take place at the ends of the joint as soon as any load is applied. These slips are represented by AB and DE. Until static friction has been overcome no relative slip takes place at the center of the joint; therefore, lines AD and BE are in contact at the center. The total elongation of the joint (measured over the distance between the two rows of rivets) is again composed of the end slip δ_1 and the elongation that would take place in a length p of the plate under load P/2, i.e., in the elastic range $\Delta = \delta_1 + Pp/2btE$. After static friction has been overcome, there will be relative slip at the center of the joint and line BE will move to B'E' (Fig. 2.4d).

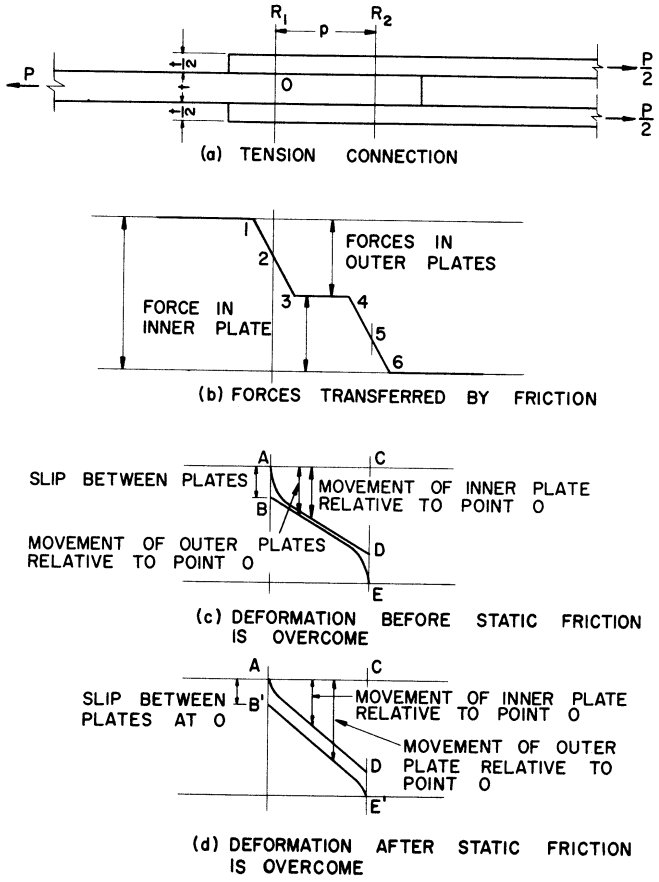

Fig. 2.4.

When sufficient slip has taken place, part of the load is transferred through shear in the rivets and part through friction. The load distribution diagram, line 123456 in Fig. 2.4b, will then have vertical portions at 2 and 5. Then lines AD and BE can be constructed as before.

With joints of more than two rows of rivets the problem of estimating the total elongation is complicated by the statical indeterminateness introduced by the additional rows. With more than two rows or with a nonsymmetrical arrangement, the relative load transferred by the rivets is no longer divided equally, but depends on the relative stiffness of rivets and plates, at least in the elastic range. For example, in a joint such as shown in Fig. 2.5a, if the rivets were infinitely stiff, rows R_1 and R_4 would jointly carry all the load, leaving rows R_2 and R_3 unloaded. If the outer rows are permitted to relax into the shape determined by their actual stiffness, the inner rows will be loaded also, but evidently to a lesser degree. Methods of computing the elastic distribution of loads between rivets in a joint are reviewed by A. J. Francis (2.3), who also extends the analysis into the inelastic range by the use of a semigraphical method. Batho's (2.17) approach to this problem is through the use of energy methods. The distribution of

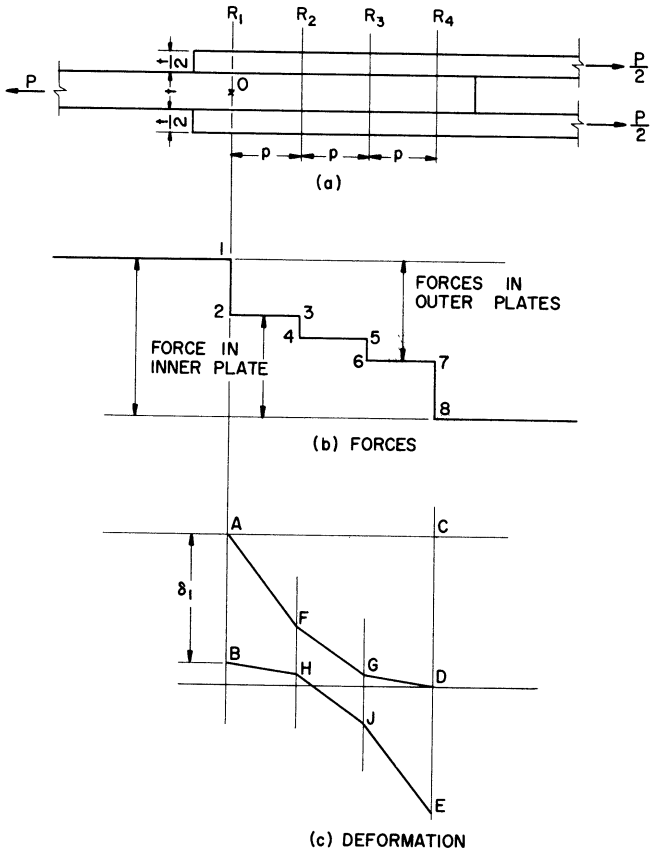

Fig. 2.5.

load in a riveted joint was also studied by Hrennikoff (2.18). Such computations are generally only of academic interest, since it is known that with increasing load the distribution among rivets tends towards uniformity as the more heavily loaded end rivets yield. It can be seen from Figs. 2.5b and 2.5c that the expression for the total elongation of the joint is

$$\Delta = \delta_1 + \frac{nPp}{2btE} \qquad (2.1)$$

in the elastic range, where n is the number of spaces between rows. The second term is again half the elongation that would take place in an equivalent length of the main plate under a load P. That this must be so is evident from the fact that line 1-8 in Fig. 2.5b bisects a rectangle the area of which would represent the elongation of the main plate under a load P. Friction does not affect this conclusion and it does not matter whether the load in all rivets is the same or not. The theoretical correctness of Equation 2.1 is subject only to the two conditions that the joint is balanced and symmetrical and that the stresses in the plates are within the elastic range.

The second item of the expression $\delta_1 + nPp/2EA$ is now compared with experimental information within the elastic range of the plate material. As stated earlier, the measured end slip δ_1 is due not only to the rivet deformation, but also to the strain accompanying the localized stress near the rivet holes. The second term of the above expression does not allow, however, for the fact that A is not the actual area of the plate throughout the length np. It might be assumed that the plates are weakened by the presence of holes, in which case Δ would be somewhat larger than $\delta_1 + nPp/2EA$. However, at low loads the rivet heads share in the transmission of the forces by "bridging" the holes and thus the effective cross section is not neccessarily less than the gross section. In any case Equation 2.1 can be rewritten

$$\Delta = \delta_1 + \frac{knPp}{2EA_g} \qquad (2.2)$$

where k is a factor allowing for the variation in strains in the net section and for the "bridging". To avoid confusion A is now written A_g, the gross area of the section.

In obtaining k from experimental data, the only test programs of use are those in which both Δ and δ_1 are measured. Three such programs have been carried out, (1) the tests of Davis, Woodruff, and Davis (2.6), (2) those of Moisseiff, Hartmann, and Moore (2.2), and (3) the work of A. J. Francis (2.3) in England. The two latter series of tests were on joints in double shear and the values for k which have been computed range from 0.8 to 1.15, both for steel and aluminum plates. The first of the above series of tests was carried out on single shear joints and the computed values of k, as defined by the expression 2.2, range from 1.05 to 3.50, with an average of 1.95 for 33 symmetrical joints. The 33 specimens for which k was computed varied in a number of respects. Although the eccentricity in lap joints will result in relatively greater deformation, no detailed analysis will be attempted at this time to relate k to all of the determining variables.

It is now in order to examine the deformation of the plates in their inelastic range. Davis, Woodruff, and Davis (2.6) define yield efficiency of a joint as the ratio of the load at which the joint begins to yield to the load at which a plain plate with the same gross section would yield. In their tests (2.6) the yield efficiency values were always slightly higher than the ultimate efficiency values. Moisseiff, Hartmann, and Moore (2.2) did not actually calculate the yield efficiency of joints, but from their results it seems that the yield efficiencies were lower than the ultimate efficiencies. Since very reliable information is now available for predicting the ultimate efficiency of many types of joints, it is suggested that these values also be used for the yield efficiency. Therefore, in predicting the deformation of a joint, it is proposed that the expression

$$\Delta = \delta_1 + \frac{knPp}{2EA_g} \qquad (2.2)$$

can be used up to a value for $P = \eta A_g \sigma_y$, where σ_y is the yield strength of the plate material and η the predicted ultimate efficiency.

In considering the yielding of the plate material, it should be recognized that the yield phenomenon is somewhat akin to viscous flow and that the "lower yield level" (usually called "lower yield point") is directly related to the rate of strain in the material. This lower yield level may be multiplied by a dynamic increase factor to provide an approximate correction to values used in the analysis of structures under shock loads. However, if mill-coupon test results for the yield point are used as a basis for analysis, a preliminary downward adjustment must be made before applying the full dynamic increase factor. In order to get a correct evaluation of the "minimum" lower yield level it is necessary to make tests at a rate of strain so slow as to be impracticable for steel mill production where the testing is primarily for quality control. A maximum strain rate of 10^{-3} inch per inch per second is permitted by ASTM Standard Specifications A6-50 covering the acceptance of structural steel. It is presumed that most steels mills will test at a strain rate very near the specified maximum, corresponding to a yield level approximately 10 percent more than that obtained for very slow static test.

To estimate the connection plate deformation after some yielding has taken place is a difficult task. The presence of the holes cannot be neglected. The initial plastic yield level of a perforated plate has been studied carefully by Brady and Drucker (2.11), who, on the basis of the maximum shearing stress yield criterion and the Mises criterion, establish upper and lower bounds for the plastic yield load for thin metal sheets with a variety of configurations of staggered holes. Most of their tests were made with open holes, thus having only an indirect relation to riveted plates in which rivet clamping action and the tightly filled holes cannot help but provide greater continuity of action.

A method for calculating the plate deformation in the inelastic range has been proposed by Koegler and Schnitt (2.8). If a perforated plate is stressed in tension (Fig. 2.6a), the stresses and strains are higher at a section through the hole than at a gross section. Koegler and Schnitt suggest that the deformation of such a plate can be considered equal to the deformation of an equivalent solid plate, part of which is stressed at the gross stress P/Gt and part at the net stress P/(G-D)t. Thus, if the equivalent length of plate at the higher stress is denoted by d_n and the strains corresponding to the gross and net stresses due to

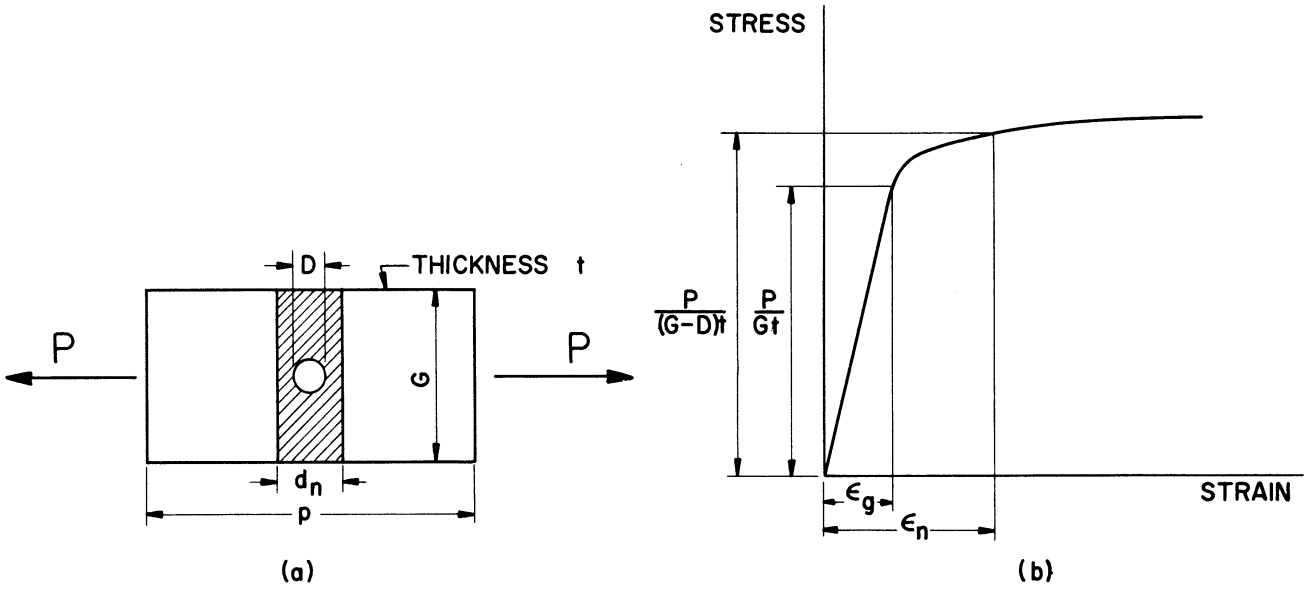

Fig. 2.6.

the load P are denoted by ϵ_g and ϵ_n respectively, the total deformation of the plate under a load P is given by

$$\Delta' = (p-d_n)\epsilon_g + d_n\epsilon_n \quad , \qquad (2.3)$$

or

$$\Delta' = p\epsilon_g + d_n(\epsilon_n-\epsilon_g) \quad ,$$

where Δ' is the deformation in the equivalent plate of length p. Hence, the determination of d_n requires a knowledge of the stress-strain curve for the material and a test on a perforated specimen to find Δ'. It is possible to calculate d_n for many points of the load curve, but the validity of the procedure depends on the result being constant throughout the plastic range. (In the elastic range the values for d_n are liable to fluctuate, since they depend on the quantity $1/(\epsilon_n-\epsilon_g)$, and $\epsilon_n-\epsilon_g$ is small in the elastic range.) Koegler and Schnitt found that for the specimens which they tested d_n remained constant. Therefore, it should be possible to estimate the total deformation for a joint with a G/D ratio for which d_n has been determined from a specimen of the same material. For a joint such as that shown in Fig. 2.5 the total deformation would be

$$\Delta = \delta_1 + P(\epsilon_{g_1} + \epsilon_{g_2} + \epsilon_{g_3}) + d_n [(\epsilon_{n_1} - \epsilon_{g_1}) + (\epsilon_{n_1} - \epsilon_{g_2}) + (\epsilon_{n_3} - \epsilon_{g_3}) + (\epsilon_{n_4} - \epsilon_{g_4})]. \qquad (2.4a)$$

In the above expression ϵ_{g1} ϵ_{n1}, etc. refer to the strains corresponding to the gross and net stresses in the various sections and can be determined from the forces transferred by the rivets and the stress-strain curve for the material. In the inelastic range the forces in all rivets can be assumed to have equalized, so that R_1, R_2, and R_3 are known. If each row has the same number of rivets, $R_1 = R_2 = R_3 = R_4 = P/4$. In the elastic range the last item in expression 2.4a is practically zero and the expression reduces to

$$\Delta = \delta_1 + \frac{3Pp}{2EA} , \qquad (2.4b)$$

since for the joint in Fig. 2.5 $n = 3$.

The method proposed for estimating the deformation of a symmetrical joint in the inelastic range is based on a number of simplifying assumptions and may require modification. No more precise method appears to be available at the present time.

Koegler and Schnitt (2.8) report that the above method gives good results for the ultimate elongation of perforated plates, but their tests were carried out with aluminum specimens. With perforated steel plates the ultimate stress on the net section may be higher than the nominal ultimate strength of the material and thus, outside the range for which elongation values are available. Unfortunately the ultimate elongation of the plates of riveted joints does not appear to have been recorded in any tests reported in the literature.

Early in this chapter a balanced symmetrical joint was defined as one with two outer plates of the same total gross cross-sectional area as the inner plate. If the discussion is generalized to include joints with outer plates of combined thickness t_o and an inner plate of thickness t_i, then all conclusions reached so far will still hold after the loads carried by all rivets have equalized. This is illustrated in Fig. 2.7 for the condition that the plate stresses are still in the elastic range. Let R_1, R_2, R_3, and R_4 denote the rivet rows and also the total load carried by each row. Thus after rivet load equalization $R_1 = R_4 = 1/2\ R_2 = 1/2\ R_3$. Since line 12345678 (Fig. 2.7b) divides the area of rectangle 1-10-8-9 in two equal parts, the elastic extension of the inner plate is given by $3Pp/2bt_iE$ and that of the outer plates is given by $3Pp/2bt_oE$. Hence,

$$\Delta = \delta_1 + \frac{3kPp}{2bt_oE} = \frac{3kPp}{2bt_iE} + \delta_4 .$$

Care must be taken not to confuse δ_1 and δ_4.

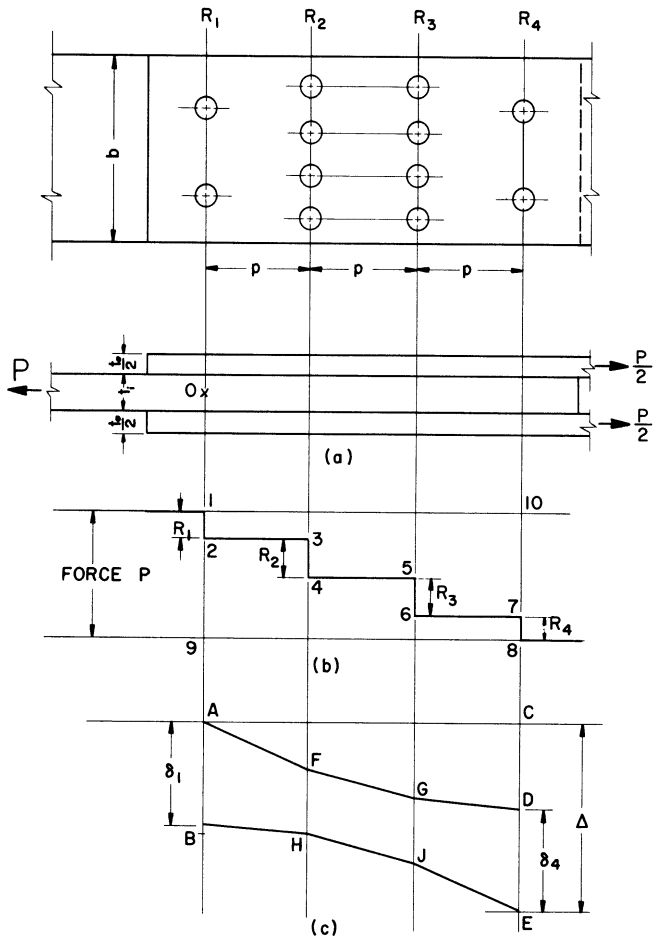

Fig. 2.7.

When the plate stresses are in the inelastic range, the procedure is also similar to that for balanced symmetrical joints, but again the deformation of the rivet row on the extreme left must be added to the deformation of the plates coming from the right or vice versa.

The modifications required to calculate the deformation of nonsymmetrical joints are self-evident, but as for symmetrical joints, the validity of the results is dependent on the accuracy of the available experimental data giving load-deformation curves for the component rivets and plates.

The information on the load-deformation relation of riveted tension joints is summarized at the end of the chapter.

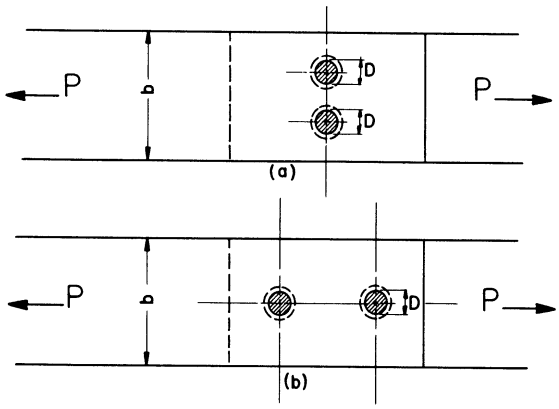

Fig. 2.8.

Effect of Rivet Pattern on Plate Strength

The problem of the choice of rivet pattern to develop the highest efficiency relative to unriveted plate strength has received attention as long as rivets have been used. The weakening effect of rivet holes cannot be avoided, but it has been realized for some time that rivet groups of equal nominal strength might develop the plate strength to a different degree, depending on the size and disposition of the rivets within the group. For example, the two joints shown in Fig. 2.8 are similar,except for the fact that in Fig. 2.8a the two rivets are side by side, whereas in Fig. 2.8b they are in tandem. The average stress at the weakest section in one case is P/(b-2D) and in the other case it is only P/(b-D).

It may seem, then, that the best solution would be to use a single line* of rivets in all joints, since this arrangement is the most efficient from the viewpoint of utilizing the plate cross section to the fullest extent. Although this may be practical for joints containing only a few rivets, a large number of rivets would result in a very long joint and in considerable waste of plate material. Furthermore, for longer joints, greater ductility is required of the rivets if their combined ultimate strength is to be fully realized. The end rivets in a long joint may be deformed so as to pass beyond the point of maximum load, or even fail before the interior rivets reach their ultimate strength.

The development of theoretical plate efficiency is therefore limited by practical considerations and rivet characteristics. Figure 2.9 shows one-half of a butt joint with four rows* of rivets. It is assumed

*"Line" refers to a longitudinal line of rivets; "row" defines a transverse line of rivets.

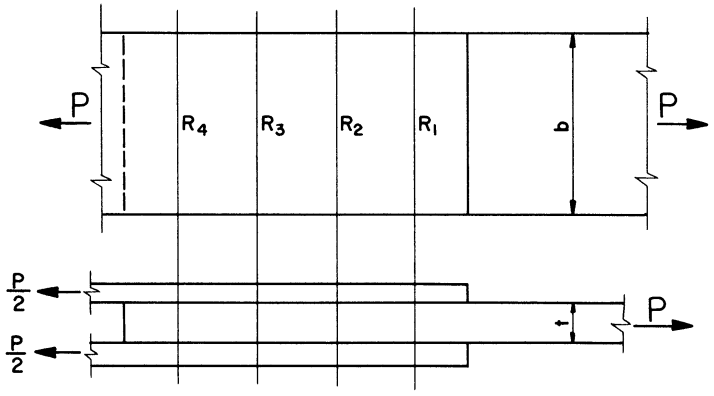

Fig. 2.9.

that the thickness of the central plate does not exceed the sum of the thicknesses of the strap plates. Neglecting secondary stresses, the central plate is evidently free from load to the left of the fourth row of rivets. Between the third and fourth row, the central plate carries the load R_4 transmitted to it by the fourth row and the average stress in the plate at the fourth row is $R_4/t(b-n_4D)$, where n_4 is the number of rivets in the fourth row and D the diameter of each rivet hole. Similarly the average stress at the third row is $(R_4+R_3)/(b-n_3D)t$, at the second row it is $(R_4+R_3+R_2)/(b-n_2D)t$ and at the first row the average stress is $(R_4+R_3+R_2+R_1)/(b-n_1D)t$. If the number of rivets in all rows is the same, the first row is invariably the critical section for the central plate and the fourth row is the critical section for the outer plates. However, the outer plates do not generally present a problem because they are short and their combined thickness can be greater than that of the central plate without any great increase in overall weight or cost.

Theoretically, it is possible for the plate cross section at the second row to be the critical one. For this to occur in the case of the joint shown in Fig. 2.9, $(R_4+R_3+R_2)/(b-n_2D)t$ has to be larger than $(R_4+R_3+R_2+R_1)/(b-n_1D)t$. This would be an extreme case, such as could exist if there were only one rivet in the first row and three rivets in each of the other rows. Let it be assumed first that all rivets will carry the same load and that this is $\tau\pi D^2/4$. Hence, it is required that

$$\frac{9\tau\pi D^2}{4(b-3D)} > \frac{10\ \tau\pi D^2}{4(b-D)}$$

If b = 12d, a typical ratio,

$$\frac{9\tau}{9D} > \frac{10\tau}{11D}$$

and since 1 > 10/11, it would appear that for the joint with one rivet in the first row and three rivets in each of the following three rows failure should occur in the center plate at the second row. However, the end rivets are more heavily loaded than the average, thus causing the left-hand side of the above inequality to be somewhat smaller. Hence, failure might take place at either the first or second rivet row. Another condition which might result in failure at a section other than the first row exists if the end rivet or rivets are already highly strained when the plate enters the inelastic range. The end rivets might shear off and then the second row section would be the most highly stressed. However, the last two examples are exceptions and failure usually occurs at the first rivets. Staggered rivets have not, so far, been considered.

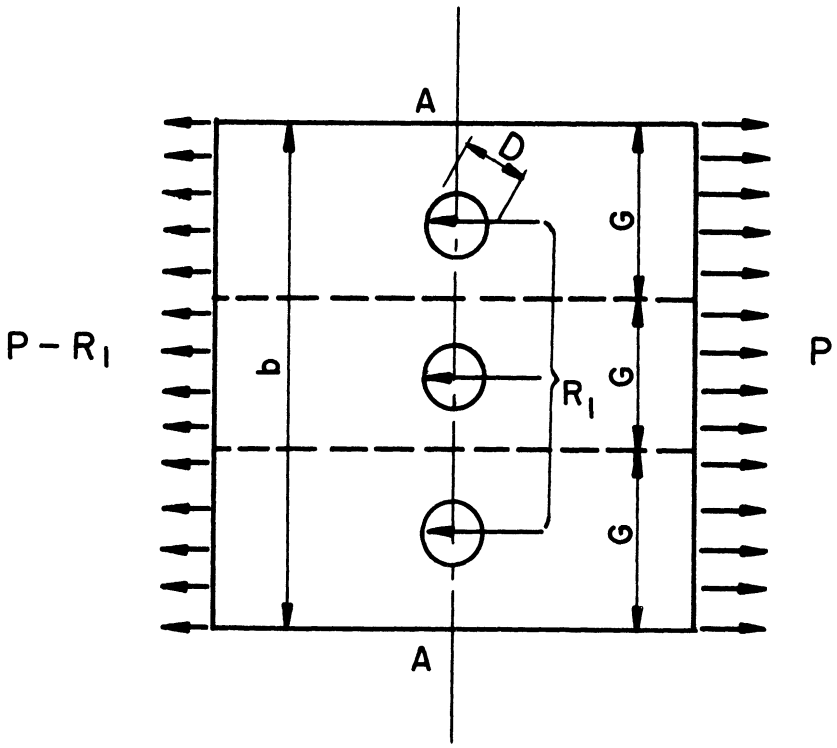

Fig. 2.10.

Figure 2.10 shows the portion of the center plate of a tension joint which contains the first row of rivets. It is assumed that the plate is so dimensioned that it can be divided into a number of strips of equal

width G, each with a hole in the center. If it is further assumed that the strength of the metal is unaffected by the presence of the holes, then the ultimate net strength of the plate is (G-D)/G times the gross strength, i.e., $\eta_g = 1-D/G$, where η_g will be termed the gross efficiency of the perforated plate.

One of the most complete studies of the relation between G/D and η_g for structural connections was made by Schutz (2.9), who not only carried out a large number of tests, but also analyzed similar tests by many earlier investigators, thus giving his conclusions considerable weight.

Work done in the aeronautical field, although less directly applicable to an understanding of heavier joints of structural steel, is nevertheless of interest and will be referred to here (2.10, 2.12).

All investigators agree that the joint plate efficiency η_g is not simply equal to (1-D/G) as might be expected. It has been found that η_g is less than (1-D/G) for large values of G/D, but for small ratios of G/D it is greater than predicted by the expression (1-D/G). Some investigators introduce the concept of net-efficiency, denoted by η_n, and define it as the actual strength of a joint or a perforated plate divided by the nominal ultimate strength of the net section. Then $\eta_n = \eta_g/(1-D/G)$. A net efficiency of 100 percent, i.e., a gross efficiency of (1-D/G) x 100%, will be termed ideal efficiencies, because they are the efficiencies that would result if the ultimate material strength is not affected by the presence of a hole (Fig. 2.11). In the ideal case the net efficiency should therefore

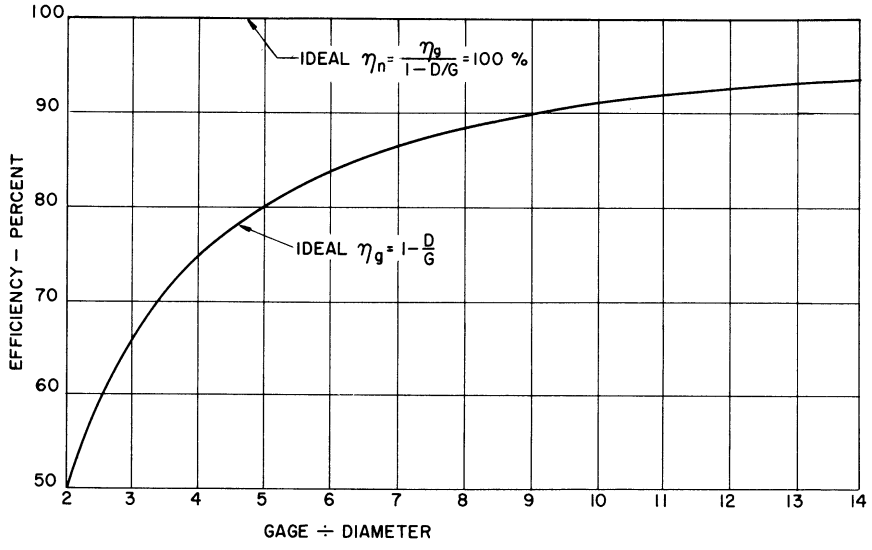

Fig. 2.11.
Efficiency of a Perforated Plate (Gross and Net) if the Ultimate Material Strength is Unaffected by the Pressure of a Hole.

be independent of G/D. Tests show that there is a plus or minus variation from 100 percent of the ideal net efficiency with G/D. This can be explained as follows. The stress distribution in a plate containing a single hole and subject to simple tension (Fig. 2.12) will be examined first. It can be shown that in the elastic range the highest stress in the plate is at least P/3Gt acting in the same direction as the applied pull. The presence of the hole also gives rise to transverse stresses. The approximate distribution of these stresses at the minimum cross section is shown in Fig. 2.12. The maximum value of the transverse stress is at a cross section through the center of the hole and is of the order of P/3Gt. The average value of this stress depends on the G/D ratio, but it is estimated to be of the order of P/10Gt for small G/D ratios. Let the stress at any point of section AA in the direction of the force P be σ_1 and the transverse stress be σ_2, then the octahedral shear-stress yield criterion results in the expression $\sigma_y^2 = \sigma_1^2 + \sigma_2^2 - \sigma_1 \sigma_2$, where σ_y is the yield strength of the material in simple tension. Examination of this expression reveals that for $0 < \sigma_2 < \sigma_1$, σ_1 is larger than σ_y. The maximum value which σ_1 can assume according to this theory is $1.15\ \sigma_y$. For $\sigma_2 = 0.1\ \sigma_1$, σ_1 is about 5 percent greater than the yield strength σ_y. Although it is not possible, quantitatively, to extend this reasoning to ultimate strength values, there is no reason why the same tendency should not exist at failure. This explains why the net efficiency of a perforated plate can be higher than 100 percent.

When the width of the plate is large compared to the hole diameter, another factor effectively reduces the efficiency of the specimens. Tests show that for G/D > (5 to 8) the net efficiency is less than 100 percent. A plausible though qualitative explanation is as follows: Let it be assumed that the stress-strain curve of the material has the idealized shape shown in Fig. 2.13.

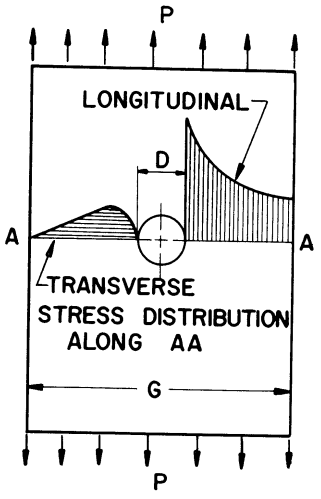

Fig. 2.12.

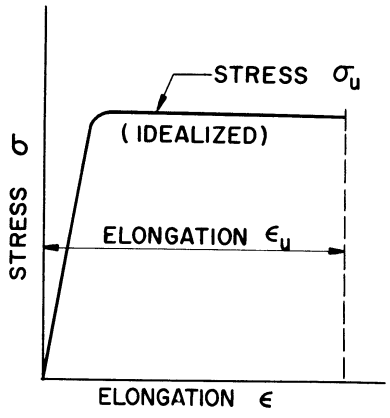

Fig. 2.13.

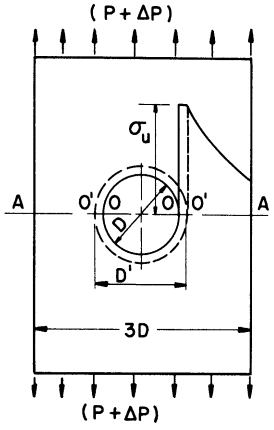

Fig. 2.14.

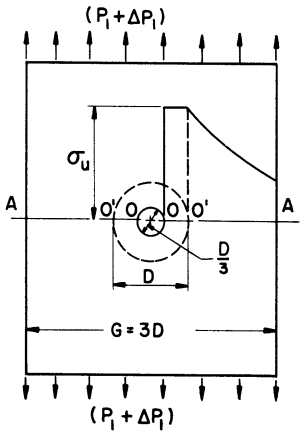

Fig. 2.15.

Consider next a perforated plate of width 3D (Fig. 2.14) loaded in tension. At some critical value of P the stress at the edge of the hole will reach the value σ_u and at some slightly higher load (P + ΔP) the stress distribution will be as shown in Fig. 2.14. Evidently, while the load was being increased from P to (P + ΔP), the portions OO, close to the hole, did not experience an increase in stress because they had already reached σ_u. For any further load increased beyond (P + ΔP) the diameter of the hole can momentarily be considered to be O'O' = D' as an approximation, since the effect on the stress distribution over the remainder of section AA would be at least similar to that corresponding to the presence of a larger hole. As the load P is further increased O' will move across toward A. Although the stress cannot increase above σ_u , the strain between O and O' continues to increase. If the strain at O is still below ϵ_u (= the elongation of the material) when the ultimate stress is reached at A, then the net efficiency of the specimen is 100 percent or more. If the material is not sufficiently ductile, then the specimen may tear at O before the stress σ_u is reached at A. It is interesting to note that as the stress concentration factor decreases to near unity at failure, the strain concentration factor increases. Baron and Larson (2.13) report ultimate strain concentration factors of over 5 (expressed as the ratio of the maximum strains to the strain corresponding to the average stress on the net section) for an ASTM-A7 specimen with a b/D ratio of 3.8. Box (2.10) obtained a strain concentration factor of 9 (expressed as the ratio of the maximum strain to the strain corresponding to the average stress on the gross section) for a 24S-T aluminum alloy specimen with a G/D ratio of 9.

Figure 2.15 shows another perforated specimen under tension. The diameter of the hole is only D/3 so that the G/D ratio is actually 9. At some load (P_1 + ΔP_1) the stress distribution will be as shown in Fig. 2.15. For any further load increases beyond (P_1 + ΔP_1) the diameter of the hole can

momentarily be considered to be O'O' = D as an approximation, since the effect on the stress distribution over the remainder of section AA could be similar to the effect of the presence of a larger hole. The new stresses and strains, after the load $(P_1 + \Delta P_1)$ has been passed, will therefore be similar to the stresses and strains in the previous case after the load P has been passed. The main difference is that in the case shown in Fig.2.15 the strains are added to the already large strains existing at O'O', due to $(P_1 + \Delta P_1)$. The total strains at O are, therefore, much larger and may exceed ϵ_u before the stress at A is σ_u. Thus the specimen with the smaller hole will have a smaller net efficiency.

As a typical example of the kind of data obtained for the efficiency of perforated steel plates, the results of Müller, reported by Matthaes (2.12), are shown in graph form in Fig. 2.16. For easy reference, the results have been plotted in terms of net as well as gross efficiencies. The ideal net and gross efficiencies are shown by dotted lines. It is seen from Fig. 2.16 that below G/D = 10 the actual efficiencies are higher than the ideal and above G/D = 10 they are less.

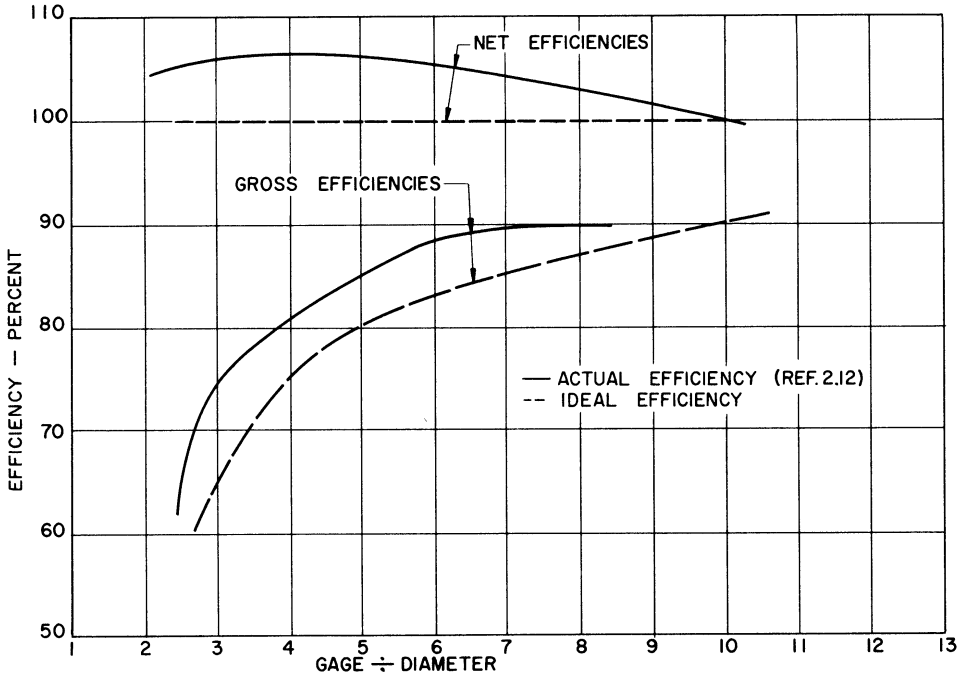

Fig. 2.16.
Typical Actual and Ideal
Efficiency of Perforated Plate

As an intermediate step between tests on perforated plates and on tension joints, Müller (2.12) also carried out tests on perforated plates with rivets inserted in the holes. He found that the curves of efficiency plotted against G/D were similar to those for plates with unfilled holes, but the values of η_n ran about 10 percent higher, probably at the expense of elongation .

A background has now been established against which the very extensive work of Schutz (2.9) can be examined and which provides a basis for a rational interpretation of some of his results. Following the study of a large number of tests and after carrying out a substantial program of tests of his own, Schutz proposes the following empirical expression for the gross-efficiency of a butt joint:

$$\eta_g = (68 + 5\frac{G}{D})\ (1-\frac{D^2}{G^2})\% \quad \text{but} \leq 87\% \quad ,$$

subject to the conditions that:

(1) the reduction in area of a standard control coupon of the plate materials is more than 57 percent.
(2) the (bearing stress) / (tensile stress) ratio is less than 2.0, and
(3) the holes in the plates are drilled.

A more general expression will be quoted later. The above formula is shown in graph form in Fig. 2.17. The results predicted by Wilson's rule (2.14) are also in good agreement with experimental data subject to the above three conditions. However, in its final form the Schutz expression is more generally applicable. Both the Schutz and the Wilson formulae predict results which differ substantially from those calculated from the AREA formula $\eta_g = (1 - D/G)\ 100\%$, which is equivalent to $\eta_n = 100\%$. Figure 2.17 also shows the net efficiency predicted by the Schutz formula; its deviation from 100 percent represents the difference between the results predicted by the Schutz and the AREA rules.

The rapid increase in strains near the boundary of the holes of a perforated plate, as the plate is subjected to tension producing stresses above the yield point, was discussed earlier. The ultimate strength of such a plate depends on the extent to which the average stress at the weakest section can approach the high stress at the boundary of the holes before the strains at that boundary became excessive. It is evident, therefore, that the efficiency of a perforated plate or a tension joint depends on the ductility of the plate material; particularly the ductility near the boundary of the holes.

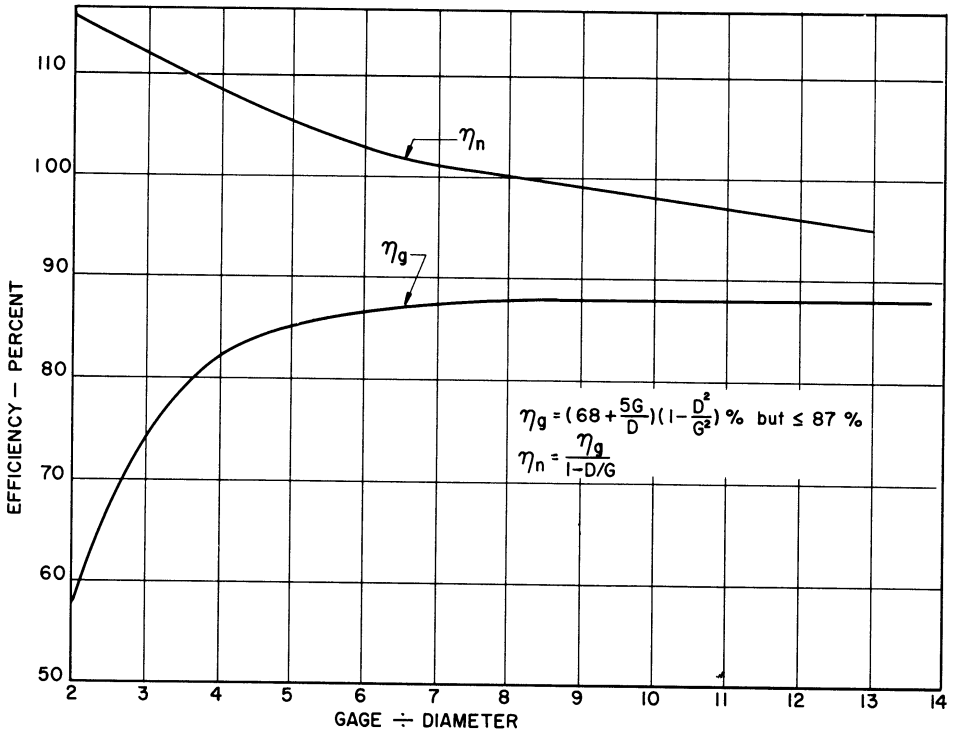

Fig. 2.17.
Efficiency of Riveted Joints as Predicted
By Relative-Gage Method (Ref. 2.9).

Since the method of perforating the plate influences the ductility of the material near the hole, any formula for the efficiency must allow for material ductility as well as for the method of manufacture of the holes. To introduce an allowance for plate material ductility, Schutz multiplies his expression for η_g by a factor X = 0.82 + 0.0032Y, where Y = percent reduction in area of a standard control coupon. It is stipulated that X must not exceed unity. His investigation of the effect of the method of hole manufacture was not extensive, but he proposes the introduction of a factor Q having a value of unity for drilled holes and 0.862 for punched holes. In its final form the Schutz expression for efficiency is

$$\eta_g = (68 + \frac{5G}{D})(1 - \frac{D^2}{G^2}) \text{ X BZ\%} \quad ,$$

where B = 1 if the (bearing stress) / (tensile stress) ratio is less than 2, as it generally is. The exact manner of the variation of B with the (bearing stress) / (tensile stress) ratio was not investigated, but from his study of many test results Schutz concludes that B decreases considerably for values of the ratio greater than 2.

For joints with variable gage Schutz found that the efficiency is better than that predicted on the basis of the smallest gage in the joint. He has developed an empirical method, the "weighted summation method", to predict the efficiency of joints with variable gage. For this purpose, the "half" strips of plate between the outer rivet lines and the edge are considered as being one strip with a gage equal to the sum of their widths. The efficiency of each strip of the variable gage joint is multiplied by the gage of the strip; the results of which are added and the sum divided by the total width of the plate. Thus a "weighted" average efficiency is obtained which is in good agreement with test results.

Stagger may be thought of as the relative displacement in a longitudinal direction of alternate rivets in a row. One of two extreme conditions exists when this displacement is zero. Then the G/D ratio is simply determined and used to find the efficiency. As the relative displacement of alternate rivets in the first row is increased; eventually the displaced rivets will become sufficiently far forward so as to form a new row with failure of the plate then taking place through that row. This is the other extreme condition and the efficiency can again be determined as before, having regard, however, to the larger gage resulting from complete stagger. In between the two extreme conditions Schutz finds that the efficiency varies more or less linearly with s/G, where s is the stagger. He proposes, however, that any joint with a s/G ratio in the first row of less than 2/3 be considered as having no stagger at all. If the s/G ratio is greater than 2/3 the efficiency should be predicted on the basis of a full stagger. The error introduced by this simplification is claimed never to exceed 4 percent.

Schutz implies that his rule for the efficiency of riveted tension joints applies to lap joints as well as butt joints. He makes no specific mention of lap joints, but in his appraisal of past tests he includes the results of tests on lap joints, such as those of Davis, Woodruff, and Davis (2.6), without any qualification. He suggests that the relatively low efficiency values in that series may be due to the method of manufacture of the holes, which was sub-punching and reaming. That additional strains due to bending are induced in lap joints cannot be questioned, but on the other hand the deformation of the joint into an S-shape results in a larger area resisting the principal stresses in the plates.

The information on the effect of rivet pattern on plate strength is summarized at the end of this chapter.

Effect of Rivet Pattern on Rivet Strength

In designing a riveted joint the aim is to make the strength of the joint approach as closely as possible the strength of the main plate. Because of the weakening effect of the rivet holes, a riveted joint can never be quite as strong as the parent plates. There is, however, no problem in providing an adequate number of rivets to transfer the load between plates. The strength of the rivet group therefore requires less attention than the strength of the plates. Hence, the disposition of rivets is usually such as to result in maximum plate efficiency.

Since the design of riveted joints is based on the assumption that the rivets share the load equally, it is necessary that the rivets be capable of some plastic deformation. This has been discussed earlier. Ductility becomes more important in cases where the nominal strength of the rivet group is only slightly higher than the plate strength. In such cases the plastic deformation that takes place in the plates before failure calls for similarly large deformation in the end rivets. If the plastic strain reserve of the rivets is already used up, the rivets may fail before the plates. Francis (2.3) shows that joints designed for equal rivet and plate strength will invariably fail in the rivets at less than the aggregate individual shearing strength of the rivets. Schutz (2.9) found that some joints made with high strength cold-rolled steel rivets failed unexpectedly in the rivets. The failure occurred because the high strength rivets were not sufficiently ductile to permit the equalization of loads among all the rivets.

To insure failure in the plates it is advisable, therefore, to design joints so that the rivet group is stronger than the plates, even at the expense of seemingly uneconomical use of rivets.

BOLTED TENSION CONNECTIONS

Until recently the use of bolts in structural tension joints was not widespread because of the danger that the nuts might loosen in service. As a result of work sponsored by the Research Council for Riveted and Bolted Structural Joints, a combination of high-strength bolt, nut, and hardened steel washer has been developed making possible the maintenance of clamping forces (2.15) to a degree that may even surpass that of the conventional rivet. Insofar as the load-deformation relation and the ultimate strength of bolted joints depend on the properties of the plates, most of the discussion on riveted joints is also valid for bolted joints.

Load-Deformation Relationship

The total deformation of a bolted joint is composed of both the slip taking place at the first row and the elongation of the plates. Again, for a balanced symmetrical joint in the elastic range

$$\Delta = \delta_1 + \frac{PL}{2 A_g E} ,$$

where

δ_1 = slip at the first row,
P = applied force,
L = distance between the first and last row of bolts, and
A_g = gross cross sectional area of center plate.

As long as the static friction is not overcome, Δ is very small. It can be shown that, in theory, δ_1 is about $PL/4 A_g E$. In practice it is slightly larger, not because of any actual slip between the plates, but because of the longitudinal shear deformation that would occur even if the inner and outer plates were one solid piece. It is therefore reasonable to assume that

$$\Delta \simeq \frac{PL}{A_g E} ,$$

i.e., equal to the deformation that would take place in a plate of cross-sectional area A_g and length L under a load P.

As the applied load is increased, a stage will be reached when the friction between the faying surfaces is overcome and substantial slip will take place.

Hechtman and his associates (2.16) report that friction is affected chiefly by the condition of the faying surfaces, by the time duration of the load, and by the tensile stress in the plates. Thus paint or varnish considerably reduces the friction, whereas sand blasting of the faying surfaces appears to improve the coefficient of friction by 20 to 25 percent. In a pair of comparative tests the coefficient of friction under sustained load was 0.22 and 0.29 under short-time loading. It is reported that in general no significant improvement in the resistance to slip of bolted joints can be obtained by increasing bolt tension above a certain critical value. This

value will depend on a number of factors, such as geometry, shear-tension--bearing ratio, etc. However, increasing the bolt tension over the critical value is effective in cases where the stress in the plates is greater than about 60 percent of the yield-point stress of the plate steel.

The plate tension, when it exceeds 50 percent of the yield stress, has the effect of reducing the coefficient of friction.

There is some doubt whether bolted joints with mill-scale faying surfaces are capable of resisting the design loads through friction alone (2.16). However, in field tests under adverse conditions high-tensile bolts have given satisfactory service (2.15). No figure for a safe minimum coefficient of friction has been quoted by the investigators, but present indications are that this may lie between 0.20 and 0.25.

Because of the lack of data the deformation of bolted joints can be discussed in only a qualitative manner. When friction is overcome δ_1 and hence Δ increase rapidly until the bolts come into bearing. In a joint containing only one bolt this sudden movement may vary from zero to double the difference in the diameter of bolt and hole, depending on the original alignment of the holes in the mating plates. In joints containing more than one bolt, some bolts will come into bearing before others, so that the load-slip curve will swerve upward from the horizontal after a small movement. However, the slope will not reach a constant value until all bolts are in full bearing. Before this occurs, the total movement may again be as much as twice the original clearance. This is illustrated in Fig. 2.18. The dotted cage forms a boundary within which the elastic portion of the load-slip curve must remain. For example, if it should happen that all bolts are in full bearing as soon as friction is overcome, then the load-slip curve will be along the inclined line AB. The slope of AB represents the combined elastic stiffness of all the bolts. In the other extreme case, when the alignment of the holes is such that none of the bolts come into bearing until a slip equal to twice the original clearance has taken place, then the load-slip curve will be along ACD. It is possible that some bolts may be stressed to yield even before all bolts are in full bearing, but, in general, the curve will follow some intermediate path, as shown. Assuming that the joint is so proportioned that failure takes place in the bolts, the total slip is the sum of the slip at which the bolt comes into bearing and the deformation of which this bolt is capable. Its numerical value is therefore impossible to predict. It will be at least equal to the detrusion of the bolts, but it may be the sum of this detrusion and twice the original clearance.

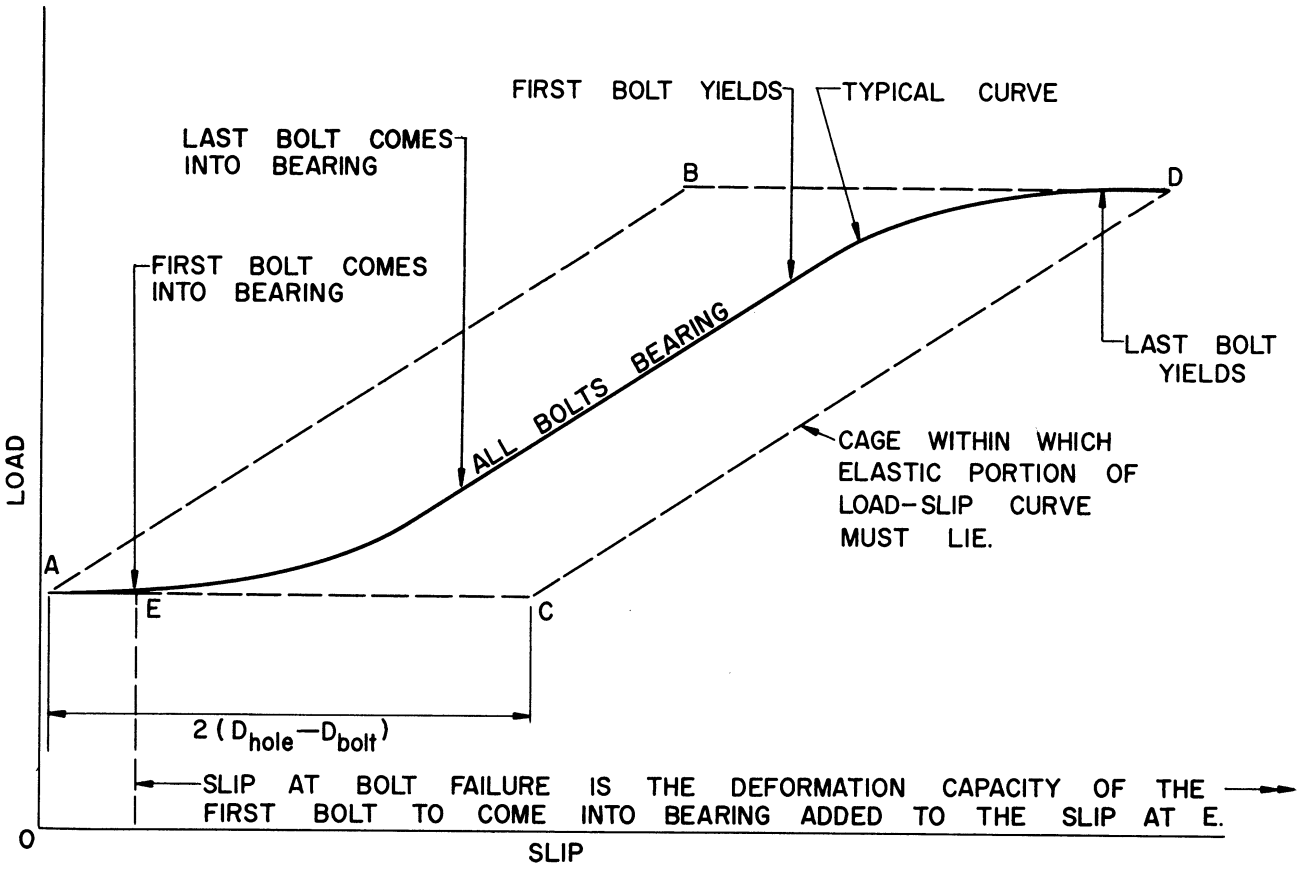

Fig. 2.18.
Theoretical Load-Slip Curve For Bolted Tension Joint, Assuming Eventual Failure of Bolts. (Not to Scale).

The deformation of the plates can best be determined by the method proposed by Koegler and Schnitt (2.8) and discussed for riveted joints. However, the total deformation of a joint cannot be predicted to a greater degree of accuracy than the slip at the first row of bolts and this may vary between wide limits.

It is evident from the above qualitative discussion that much expermental data are still required, together with statistical studies, if the load-deformation relation of bolted joints is to be predictable within reasonable limits.

Ultimate Strength of Bolted Connections

Schutz's rule for the efficiency of structural joints applies also to bolted joints, if failure takes place in the plates. As far as the strength of the bolts is concerned, high-strength bolts are less ductile than mild steel

rivets and hence are unable to attain the same degree of load-equalization. Consequently, it is unlikely that 100 percent of the nominal shear strength of a group of bolts can be realized in a joint, unless all the bolts are in one row. In tests reported by Munse, Wright, and Newmark (2.19) only the nominal tensile strength of the bolts is quoted, but from this the shear stength can be estimated. With joints containing only three bolts in line, no more than 85 percent of the estimated nominal aggregate shear strength of the bolts was reached in cases where failure occurred in the bolts. In some cases this ratio was as low as 65 percent. However, in view of the current practice of designing bolted joints with a bolt shear stress of 0.75 of the plate tensile stress, joints with high-strength bolts and structural steel plates are not likely to fail in the bolts.

PINNED CONNECTIONS

The deformation taking place in pinned connections is small compared to the elongation of the connected members. This is evident from the results of tests carried out Johnston (2.20) in which the difference in the measured elongation of pin-connected plate links and the corresponding elongation that would have occurred in a solid link was equivalent to the stretch that would take place in a length of link of the order of about ten pin diameters. This equivalent length varies somewhat with the dimensions of the components, but is always small compared to the length of the connected member.

The strength of a pinned connection depends on the strength of the pin and that of the link. The computation of the strength of the pin in double shear is a straightforward operation, but more often the pin dimensions are governed by limitations on the bearing stress. Thus, in the case of eye-bars, AREA specifications require the diameter of the pin to be at least 80 percent of the width of the reduced section of the bar. This will ensure a bearing stress of no more than 125 percent of the tensile stress in the body of the eye-bar.

In the consideration of pinned connections, distinction can be made between pin-connected plate links and eye-bars. The former are structural steel plates with pinholes bored near one end. The latter have a body of reduced width and sometimes the thickness of the wide portion around the pinhole is greater than in the body of the bar.

The Strength of Pin-Connected Plate Links

An extensive experimental investigation of the strength of pin-connected plate links was carried out by Johnston (2.20), who defined three modes in which failure could take place and proposed empirical formulae to predict the failure load. The three modes of failure are:

(1) tension failure in the net section at one side of the pin;
(2) crushing and shearing failure below the pin, in some cases followed by tearing fracture in "hoop" tension after considerable deformation; and
(3) dishing failure.

As a result of his tests, Johnston proposed the following expressions for the ultimate load of pin-connected plate links.

At failure in mode (1)

$$P_1 = 2\sigma_u \, t \, b_e$$

At failure in mode (2)

$$P_2 = \sigma_u t \left[1.13a + \frac{0.92 \, b_e}{1 + \frac{b_e}{D}}\right] .$$

At failure in mode (3)

$$P_3 = 20 \, Dt + 315 \, t^2 + \frac{75t^2 b_e}{D} + 20at - 20 \frac{a^2 t}{D} ,$$

where t = thickness of plate,
b_e = minimum distance between side of hole and edge of plate,
a = minimum distance between hole and edge of plate behind the hole,
D = diameter of pinhole, and
σ_u = ultimate tensile strength of plate material.

The least of P_1, P_2 and P_3 is the predicted strength.

Comparing the expression for P_1 with similar expressions for riveted connections, it is seen that a net-efficiency of 100 percent is implied, i.e., that the ultimate strength of the material is not affected by the presence of the hole. From the Schutz expression for efficiency a net efficiency higher than 100 percent is expected for the width-diameter ratios used for pin-connected plates (see Fig.2.17). This was actually evident in Johnston's tests (2.20), so that the expression for P_1 is slightly conservative.

The expression for P_2 gives slightly high results if the plate is rounded off at the perforated end.

The Strength of Eye-Bars

The situation concerning eye-bars was ably summarized by H. D. Hussey, discussing Johnston's paper on pin-connected plate links (2.20). He made three important points: (1) Eye-bars are always designed to fail in the reduced section of the body and not in the region of the eye. This is the very purpose behind the design of eye-bars. The AREA specifies that the net section through a pinhole in an eye-bar should be at least 35 percent greater than the net section of the member. (2)There is, therefore, little information available on tests of eye-bars where failure actually took place near the pinhole. Hussey, however, recalls one occasion where eye-bars varying from standard practice failed near the pinhole when tested. He found that Jchnston's empirical formulae for pin-jointed plates gave good results when predicting the failure loads of these eye-bars. (3) Mr. Hussey's last comment is that eye-bars are sometimes referred to as "forged" eye-bars. Although the head may be produced by upsetting, the body of structural eye-bars is ordinary structural grade steel.

It seems, therefore, that if eye-bars are correctly proportioned, failure will take place in the body of the bar. Typical significant proportions are: (i) net section through pinhole 35 percent greater than net section of body, (ii) diameter of pin at least 80 percent of width of body, (iii) minimum distance from pinhole to edge of eye-bar behind the hole equal to the pin diameter, and (iv) (to prevent dishing) net-width to thickness ratio of not more than 8. When there is doubt about the strength of an eye-bar, Johnston's formulae may be used to insure that P_1, P_2, and P_3 are all greater than the strength at a net section of the body.

WELDED TENSION CONNECTIONS

In the sections on riveted and bolted connections, deformation of the connections was discussed in considerable detail. This was necessary

because the finite deformation resulting from clearances and from the distortion of the connectors and perforated plates can be large in comparison with the deformation taking place in the connected members. It was shown in the last section that eye-bars with upset or forged ends are in a different category; they are invariably designed to fail in the body of the bars so that deformation taking place near the pinhole can be neglected. From the point of view of deformation, welded joints are in the same category as eye-bars for two reasons: (1) welded joints are normally designed to fail outside the weld zone and (2) the welding process does not result in the removal of material from the parent plate as in the case of rivet holes, hence, no significant local deformations take place within the affected zone on the application of load. If failure does take place through a weld, the reduced ductility of the weld zone limits the ultimate elongation of the connection. However, enough is known about the theory and techniques of welding to insure that the welded zone is not weaker than the adjacent members.

In view of the foregoing, the ensuing discussion will be concerned chiefly with the relative strength of welded connections. It will be assumed that the welding has been carried out in accordance with the appropriate codes and specifications, since the discussion of welding procedure is outside the scope of this monograph.

Types of Welds

It is pointed out in the 1931 Report of the Structural Steel Welding Committee of the American Welding Bureau (2.22) that fillet welds are better suited to the types of connection usually required in structural framing than butt welds, mainly because larger tolerances are acceptable when fillet welds are used. However, because of the simplicity of the analysis of stresses much information on welded joints is in the form of test results on butt joints.

When it is desired to express the strength of a weld in terms of stress, there is no difficulty in the case of a butt joint in deciding on the most highly stressed cross section; it is simply the minimum section of the joint.

In computing the stress on a longitudinal fillet weld it is customary to divide the force on the weld by its "throat" area, i.e., by $Lt/\sqrt{2}$, (Fig. 2.19b). (It is assumed that the cross section of the weld is a triangle.) A similar procedure is followed in determining the maximum stress on a transverse fillet weld.

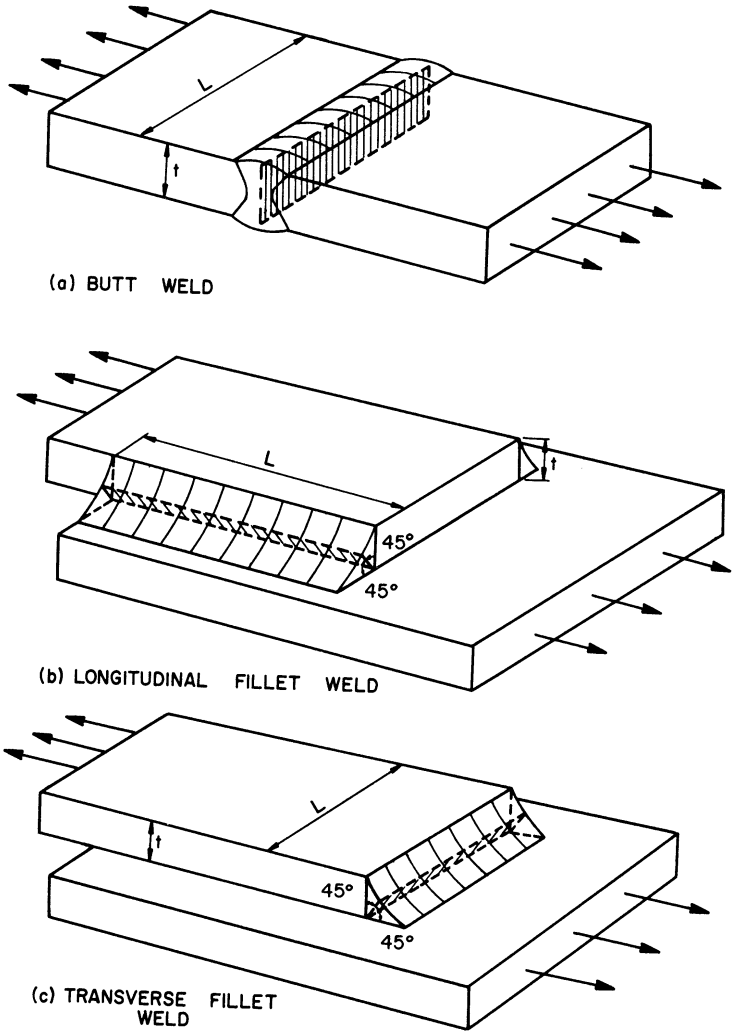

Fig. 2.19.

Based on the above procedure for computing stresses, tests show that on the average the ratios of maximum strength of butt joints, symmetrical transverse fillet joints, and longitudinal fillet joints are about 1.0:0.7:0.5. An examination of the stress distribution in welds illustrates the importance of ductility in the weld metal and makes possible the assessment of the effect of changes in the dimensions of a weld.

Transverse welds are considered first. Let the force transmitted by the weld be P pounds per lineal inch (Fig. 2.20a). It is assumed that the weld is one of a pair of transverse welds so that no eccentricity exists. For equilibrium there must be equal and opposite horizontal forces P acting on

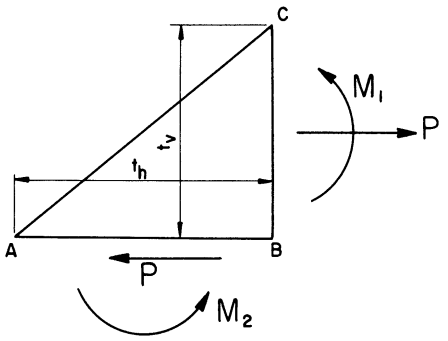

(a)

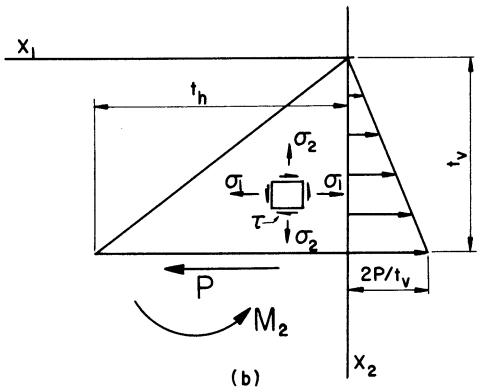

(b)

Fig. 2.20.

the horizontal and vertical surfaces and it is likely that there are some moments acting also. If the exact stress distribution on the boundary were known, then an expression for the stresses anywhere within the weld could be set up. Solakian (2.23) found by means of photo-elastic experiments that the stress on the vertical boundary varies linearly, as shown in Fig. 2.20. It is found that the stress function

$$\Phi = \frac{2P}{t_v^2}\left[\frac{x_2^3}{6} - \frac{t_v^2}{2t_h^2}x_1^2 x_2 + \frac{t_v^3 x_1^3}{3t_h^3}\right]$$

satisfies the boundary conditions on the vertical and inclined sides of the weld and satisfies the equilibrium conditions on the horizontal boundary. From this the stresses anywhere in the weld can be calculated (2.24). Thus,

$$\sigma_1 = \frac{2P}{t_v^2}x_2 , \quad \sigma_2 = \frac{2P}{t_h^3}\left[2t_v x_1 - t_h x_2\right] ,$$

$$\tau = \frac{2P}{t_h^2}x_1 ,$$

and the maximum shear stress is

$$\tau_{max} = \sqrt{\frac{(\sigma_1-\sigma_2)^2}{4} + \tau^2} = P\sqrt{\left(\frac{2t_v x_1}{t_h^3} - \frac{x_2}{t_h^2} - \frac{x_2}{t_v^2}\right)^2 - \frac{4x_1^2}{t_h^4}}$$

for the usual transverse weld $t_v = t_h$, and hence,

$$\tau_{max} = \frac{2P}{t_v^2}\sqrt{x_2^2 - 2x_1x_2 + 2x_1^2} .$$

The largest values of τ_{max} exist at the root of the weld B (Fig. 2.20a) and at the toe A. At these two points $\tau_{max} = 2P/t_v$ but this stress occurs in two very limited areas. When $t_h = t_v\sqrt{3}$ the highest value of τ_{max} is 1.33 P/t_v (Fig. 2.21), but if $t_h = t_v/\sqrt{3}$, the highest value of τ_{max} is $4P/t_v$. This may give some idea of the effect on the elastic stress of a weld being deposited incorrectly.

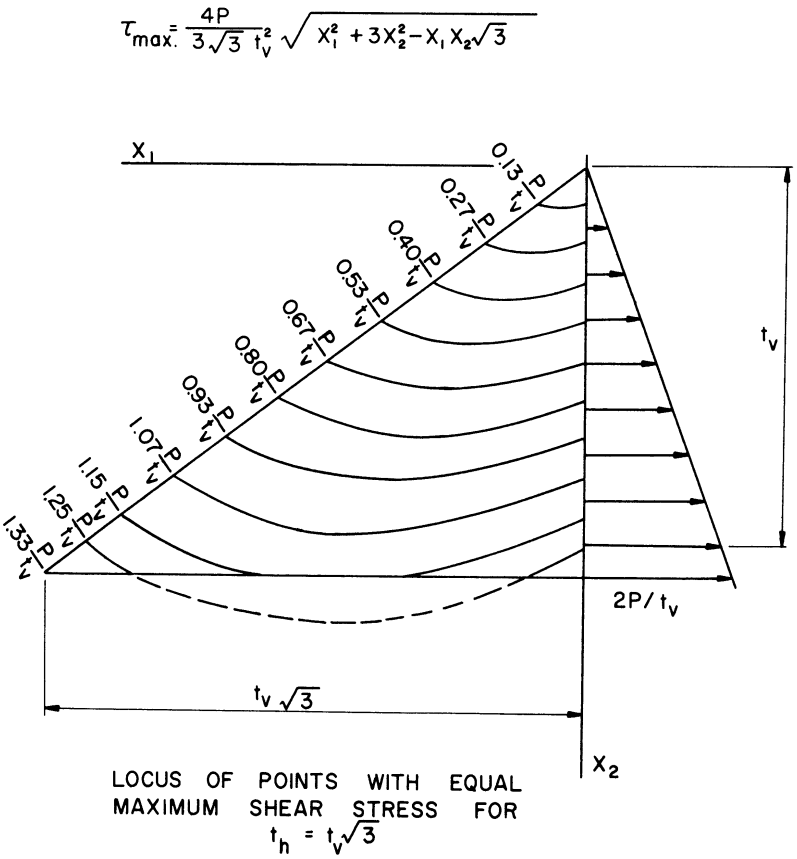

Fig. 2.21

This analysis suffers from certain drawbacks, the chief ones being: (1) residual stresses are neglected and (2) the stresses near the horizontal boundary are correct only if the load there is being transferred from the weld to the lower plate in the manner prescribed by the stress function. The analysis leads to the following conclusions: The highest shear stress in the elastic range in a 45 degree transverse weld is about 50 percent greater than the maximum shear stress predicted by the usual design theory. The highest shear stress is very localized in nature; therefore, a small amount of plastic deformation should be sufficient to relieve it. Lesser peak stresses occur in a weld where $t_h = t_v\sqrt{3}$, but peak stresses are greater when $t_h = t_v/\sqrt{3}$.

This latter type of weld, therefore, makes greater demands on the plastic deformation of the weld metal. The welds with longer horizontal legs would thus provide greater insurance against failure in the weld, particularly under dynamic loads, when the yield point is higher.

Considering next a longitudinal weld, there can be no doubt that at any transverse section the "throat' region is the most highly stressed, but the variation of this stress in a longitudinal direction is far from uniform; consequently, the shear stress calculated from the usual expression

$$\tau = \frac{P\sqrt{2}}{t} ,$$

where P = force per lineal inch of weld, and
t = side of a 45 degree weld,

gives only an average value of the stress. That the shear stress is higher near the ends of the weld than in the middle can be proved by considerations similar to those that were used to show that the end rivets in a riveted joint are more highly stressed than the inner rivets. Experimental evidence is in agreement with this argument (2.25). In theory, the ratio of the high stress at the end of longitudinal fillet welds to the mean stress increases with the length of the weld, but in practice length seems to have only a small effect on strength. Thus, the average strength of longitudinal fillet joints can be considered independent of length over the practical range of dimensions. The foregoing conclusion was reached by Denaro (2.26) after examination of many test results. It is clear that some plastic deformation in the weld metal must take place at the ends of longitudinal fillet welds. Since the strength of longitudinal fillet joints is always less than that of transverse joints, it may be concluded that the longitudinal joints have the greater elastic peak stresses. From this it follows that if the weld metal behaved in an elastic manner right up to failure, the difference in the average strength of transverse and longitudinal welds would be even greater. Since dynamic loading has the tendency to increase yield strength, it is likely that under such loading transverse joints will give the more satisfactory service.

The stress distribution in a longitudinal fillet weld may be unfavorable for another reason. The loads are transferred from one plate to another along two lines parallel to the direction of load. Although the stress distribution across the plate may be uniform at a section some distance from the joint (Section AA, Fig. 2.22), it is characterized by two peaks in the region of the welds (Section BB, Fig. 2.22). Tests on longitudinal fillet joints with relatively wide plates were carried out by Freeman (2.27) and the mode of failure is illustrated in Fig. 2.23. It is apparent that the transfer of load results in a couple on each weld and causes the weld to twist. Then either failure may take place in the weld or the plate may tear.

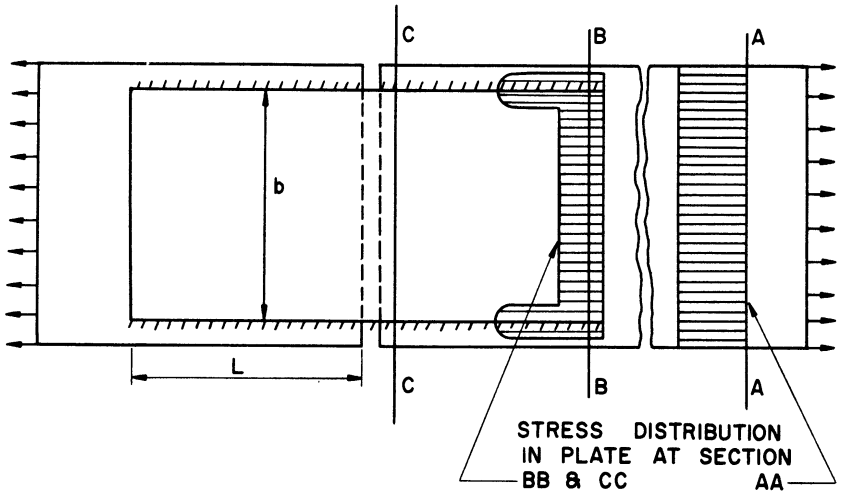

Fig. 2.22.

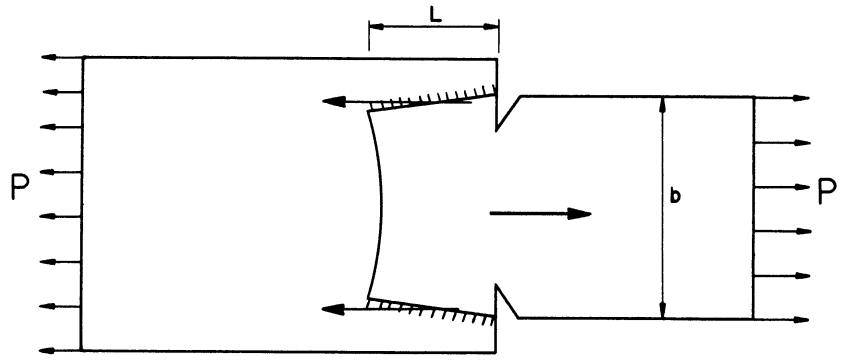

Fig. 2.23.

According to Lobban (2.21) this is not a serious problem when the width of the strap plate b is less than the length of the weld L as is the case in the majority of longtiudinal welds. If $b/L > 1$, Lobban has shown, using Freeman's results, that the strength of the joint decreases rapidly in accordance with the curve in Fig. 2.24. Thus for large b/L ratios longitudinal welds should be reinforced by transverse welds.

In one aspect longitudinal fillet joints are superior to transverse joints, namely, in the ability to resist slightly eccentric loads. This is so because the strength of the welds in a longitudinal joint is concentrated

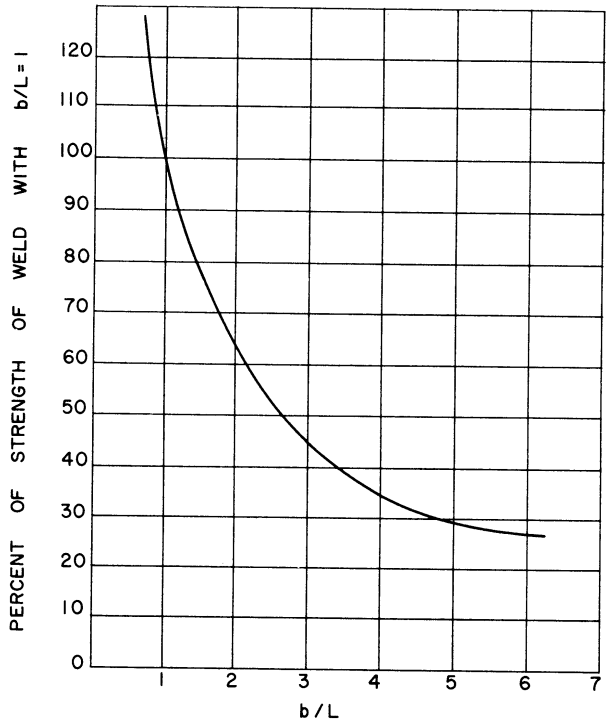

Fig. 2.24.
Variation of Strength of
a Longitudinal Weld

at some distance from the axis. Freeman (2.27) believes that whenever possible transverse welds should be returned along plates to form two short longitudinal welds, each with a length of about 10 percent of that of the transverse weld.

If the construction of the joints is unsymmetrical, the ultimate strength may be seriously affected if there exists a prying effect due to the eccentricity. In the report of the American Welding Bureau (2.22) it is concluded that some unsymmetrical joints, such as shown in Fig. 2.25a, are practically as strong as symmetrical ones. The joints shown in Fig. 2.25b were found to be very much weaker than symmetrical joints. It is doubtful whether the joints in the second group could be made as the strong as the plates which they join, thus their use is not recommended.

The above tests revealed no significant difference in the unit strength of large and small welds. However, small welds tend to be slightly stronger.

Method of Manufacture

In the American Bureau of Welding tests both the electric arc and the oxy-acetylene gas processes were used. The conclusion was reached that there is no important difference in the strength of welds made by the two processes.

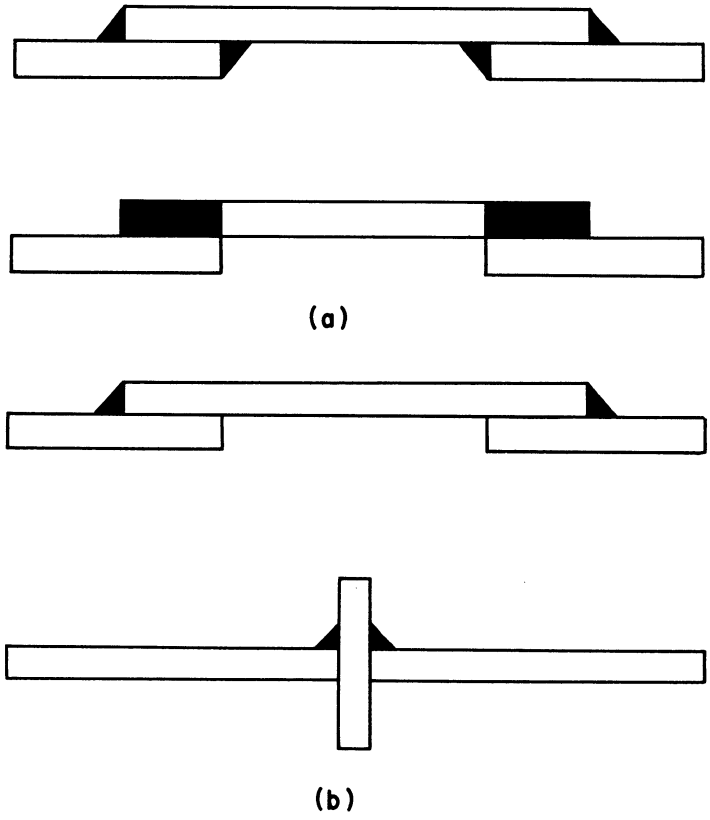

Fig. 2.25.
Nonsymmetrical Welded Joints.

Although the results of these tests on many types of welds are of interest today on a relative basis, there have been some notable advances in technique since the time of the tests. The most important of these is the introduction of the covered electrode which improves the ductility of the deposited weld metal. This results in a more equitable distribution of stresses, and hence, greater ultimate strength of a welded joint for the same unit strength of the deposited weld metal. Absolute values depend on the combination of materials used. In a very limited series of tests on specimens similar to those used in the American Welding Bureau tests (2.22), but made with covered electrodes, Godfrey and Mount (2.28) found that the strength of their specimens was from 20 to 50 percent greater than of those made with bare electrodes.

A welded joint cannot always be made with the component parts in the most convenient position with regard to inclination and situation relative to the welds. In a test program sponsored by Steel Structures Research Committee of Great Britain (2.29), it was found that the effect of the position of the specimen during welding on its ultimate strength is small compared to the effect of other variables.

Recommendations For Practice

Of the many variables affecting the ultimate strength of welds, workmanship and type of electrode are the most important. If it can be assumed that the workmanship is good and that the proper electrode has been used, the range of ultimate strength values of welds on structural steel is:

Type of Weld	Ultimate Strength, ksi
Butt weld (in tension)	65 - 90
Fillet weld	55 - 75
Longitudinal weld or butt weld in longitudinal shear	35-50

Tests indicate that the weld metal behaves elastically up to about 75 percent of the ultimate strength. The above figures do not hold for eccentric welds of the type shown in Fig. 2.25b. Since the strength of eccentric welds varies considerably with the type of weld, no typical strength figures are advanced.

Transverse welds are superior to longitudinal welds in regard to strength, but they are more likely to be affected by eccentric loading. Therefore, a combination of transverse welds and short longitudinal welds is recommended for best results.

The Effect of Welded Joints on Structures

Since welded tension joints can be made stronger than any of the parts which they connect and since their deformation, in general, is negligible, the resultant structure can be considered as one solid piece of material. Consequently, the continuous frame analysis method should give fairly precise results with rigidly welded structures. Although this is true as long as stresses are fairly low, full continuity of a structure brings with it some stress concentrations which are not present to the same degree in more flexible structures and which are not allowed for in the usual methods of analysis. As a result, there have been tests under a particular combination of temperature and loading of welded structures where the material was not sufficiently ductile to absorb local high stresses. To avoid premature failure of welded structures, more care than usual must be given to their geometry in order to avoid local stress concentrations. It is also important to use materials which are ductile over the temperature range in which the structure is expected to give service.

GENERAL SUMMARY AND CONCLUSIONS

In this chapter the data available on the strength and deformation of riveted, bolted, pinned, and welded tension connections are examined.

It is shown that the total deformation of a riveted joint is made up of both the deformation δ_1 taking place at the first rivet or row of rivets and the elongation of the plates. The value of δ_1 depends on the dimensions and properties of the plates as well as on those of the rivets. It is concluded that the variation of δ_1 with applied load, both in the elastic and inelastic range, must be determined experimentally for any rivet-plate combination. Once this has been done for simple two-row joints, the information is equally applicable to multi-row joints made with plates of the same thickness.

The elongation of the plates can be calculated approximately in the elastic range of plate stresses. In the inelastic range this information must also be obtained experimentally, but again certain basic types of experiments may supply the data for a wide range of plates.

A qualitative explanation is presented as to why the plate strength of riveted joints is not always the ultimate material strength multiplied by the area of the most highly stressed section. The results of strength tests are analyzed in some detail and empirical expressions for the efficiency of riveted joints are examined. The effect of rivet pattern on rivet strength is discussed briefly.

The deformation of bolted joints can be treated similarly to that of riveted joints up to the stage when friction is overcome. Thereafter, the slip in bolted joints depends chiefly on the clearance of the bolts in the holes. As far as plate strength is concerned the rules for riveted joints are applicable to bolted joints. If high-tensile bolted joints fail by shear of the bolts, a smaller percentage of the aggregate shear strength of all connectors is more likely to be realized than in the case of riveted joints. To ensure failure of high-tensile bolted joints in the plates it is important to over-design them as far as the strength of the bolts is concerned.

Empirical formulae for the strength of pin-connected plate links are quoted. Eye-bars are not designed to fail in the region of the pinhole.

Welded tension joints should be designed to fail outside the weld zone and this is possible with present-day techniques and materials. Consequently no significant deformation takes place across welded joints, either in the working range or at failure.

The stress distribution in transverse and longitudinal fillet welds is examined and the tentative conclusion is reached that transverse fillet welds are more suitable for connections subject to shock loads. The effect of the rigidity introduced by welding in structures is discussed.

BIBLIOGRAPHY - CHAPTER II

2.1 Wilson, W. M.
Thomas, F. P.
"Fatigue tests of riveted joints"
Eng Exp Sta Bul 302, Univ of Ill (1938)

2.2 Moisseiff, L. S.
Hartmann, E. C.
Moore, R. L.
"Riveted and pin-connected joints of steel and chromium alloy"
Trans ASCE 109:1359-99 (1944)

2.3 Francis, A. J.
"Investigations on aluminum alloy riveted joints under static loading"
Engineering Structures, Academic Press Inc, New York (1949)

2.4 Baron, F.
Larson, E. W., Jr.
"The effect of grip on the fatigue strength of riveted and bolted joints"
AREA Bul 503 (Nov 1952)

2.5 Krefeld, W. J.
"Comparative load-displacement tests on lap joints assembled with Dardelet rivet bolts and hot-driven rivets"
Report, Columbia University (1932)

2.6 Davis, R. E.
Woodruff, G. B.
Davis, H. E.
"Tension tests on large riveted joints"
Trans ASCE 105:1193-1245 (1940)

2.7 Cox, H. L.
"Static strength of rivets subjected to combined tension and shear"
Master's Thesis, Univ of Ill (1952)

2.8 Koegler, R. K.
Schnitt, A.
"Effects of yielding on perforations on a wing tension surface"
J Aero Sc 10:273-84 (1943)

2.9 Schutz, F. W., Jr.
"The efficiency of riveted structural joints"
Doctoral Dissertation, Univ of Ill (1952)

2.10 Box, W. A.
"The effect of plastic strains on stress concentration"
Proc Soc Exp Stress Anal 8:2:99-110 (1951)

2.11 Brady, W. G.
Drucker, D. C.
"An experimental investigation and limit analysis of net area in tension" ASCE Proc, Separate 296 (Oct 1953)

2.12 Matthaes, K.
"The influence of notches under static stress"
NACA TM 862 (1948)

2.13 Baron, F.
Larson, E. W., Jr.
"Static and fatigue properties of carbon, silicon and strength low alloy steel plates having a hole"
Presented at Annual Meeting, ASTM, 1953.

2.14 Wilson, W. M.
Discussion of reference 2.6, Trans ASCE 105:1264-95 (1940)

2.15 Higgins, T. R.
Ruble, E. J.
"High-strength bolts - a new concept in structural connections"
Civil Eng 22:9:176-9, 255 (Sept 1952)

2.16 Hechtman, R. A.
Young, D. R.
Chin, A. G.
Savikko, E. R.
"Slip under static loads of structural steel joints with high-tensile steel bolts"
Presented at Centennial Convocation, ASCE, 1952

2.17 Batho, C.
"Experimental and theoretical investigating on rivet and bolted splices with application of the theory to welded joints"
1st Rep Steel Struct Research Comm Dept Sci and Ind Research, London (1931)

2.18 Hrennikoff — "Work of rivets in riveted joints" Trans ASCE, 99:437-49 (1934)

2.19 Munse, W. H.; Wright, D. T.; Newmark, N. M. — "Laboratory tests on high-tensile bolted structural joints" Centennial Convocation, ASCE, 1952

2.20 Johnston, B. G. — "Pin-connected plate links" Trans. ASCE, 104:314-39 (1939)

2.21 Lobban, C. H. — Discussion of reference 2.27, Proc Inst Civ Eng 231:322-5 (1930-1)

2.22 American Welding Bureau — Report of Structural Steel Welding Committee (1931)

2.23 Solakian, A. C. T. — "Stresses in transverse fillet joints by photo-elastic method" Am Weld Soc J 13:2:2209 (1934)

2.24 Timoshenko, S.; Goodier, J. N. — Theory of Elasticity McGraw-Hill Book Co Inc New York, 2nd edition, 1951

2.25 Weiskopf, W. H.; Male, M. — "Stress-distribution in side-welded joints" Am Weld Soc J, 9:9:23-48 (1930)

2.26 Denaro, L. F. — "Survey of existing published information" Appendix D, Rep of the Weld Panel of the Steel Struct Res Comm, Dept of Sci and Ind Res (1938)

2.27 Freeman, F. R. — "The strength of arc-welded joints" Proc Inst Civ Eng 231:322-5 (1930-1)

2.28 Godfrey, H. J.; Mount, E. H. — "Pilot tests on covered electrode welds" Am Weld Soc J. 19:4:33-6 (1940)

2.29 Hankins G. A.
Brown, A. F. C.

"Mechanical tests and analysis of results"
Rep of the Weld Panel of the Steel Struct Res Comm Dept of Sci and Ind Res (1938)

CHAPTER III

CONTINUOUS FRAME CONNECTIONS

Continuous frame or "rigid" connections are designed to minimize relative rotation between members meeting at a joint. To this end the maximum amount of fastening is provided, whereas in "flexible" connections there are fasteners sufficient only to transmit the vertical reactions. "Semi-rigid" connections are sometimes used in the range intermediate between "flexible" and "rigid". Actually, all connections may be thought of as semi-rigid to a greater or lesser degree. Various types of continuous frame connections are shown in Fig. 3.1.

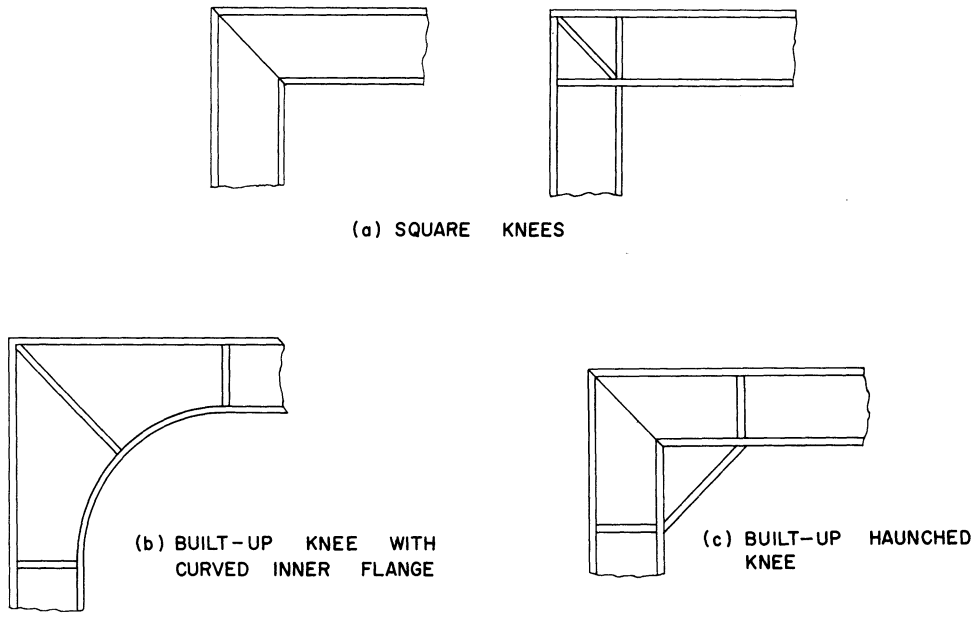

Fig. 3.1

Rigid connections result in greater load capacity for the same maximum stress in the main beams or girders. This makes it possible to employ larger

unsupported spans without having to resort to trusses. In this type of construction more clear working space is available and the resulting structures are pleasing in appearance.

The development of the arc-welding process has promoted the increasingly widespread use of continuous frame connections. Although such connections have been constructed with rivets, these are no longer used extensively. The few tests that have been carried out on riveted continuous frame connections (3.8, 3.9) indicate that they provide full continuity and that the stress distribution in them is similar to that in corresponding welded connections.

Practically all tests on portal frame connections are carried out so as to produce compression in the inner flange. This is the type of stress to which the connections are subjected in practice by vertical loading on beams. If structures are acted on by lateral loads, such as wind, then due to these loads alone the inner flanges of connections on the leeward side would be in compression and on the windward side they would be in tension. Since vertical loads result in compression in the inner flanges on both sides, inner flange tension, if it exists, is likely to be small. Furthermore, failure of connections usually results either from yielding of the flanges or from some type of instability. Connections which are acted on by moments producing tension on the inside are not likely to fail by instability. Hence, tests carried out with the inner flange in compression may be considered to embrace the most probable types of failures.

As far as static design procedure is concerned, it is commonly assumed that the connections of a building frame are either pinned or rigid. Neither of these extreme conditions normally prevails, but the error introduced by the incorrect assumptions is usually small and is taken care of by the factor of safety. When analyzing the dynamic response of building structures, agreement between the assumed and the actual physical properties of the structure becomes more important. The objective of this chapter is to present data, insofar as possible, on the strength and the deformation characteristics of rigid connections in a form that will permit its use in the calculation of the load-deformation curve of a frame joined by a given type of connection.

The term "rigid" is normally applied to the types of connections shown in Fig. 3.1; they will be referred to as square (Fig. 3.1a) and built-up (Figs. 3.1b and 3.1c). Square knees may or may not have diagonal, vertical, and/or horizontal stiffeners. The inner flange of built-up knees may be curved or may consist of one or more straight sections.

The difference between the conditions of stress in a rigid joint and a straight beam can best be appreciated by comparing a straight rolled section with an unstiffened square knee, both acted on by pure moment (Fig. 3.2). In

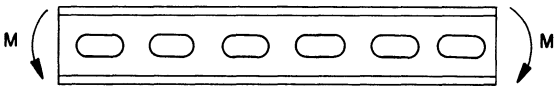

(a) STRAIGHT BEAM SUBJECT TO BENDING WITHOUT SHEAR

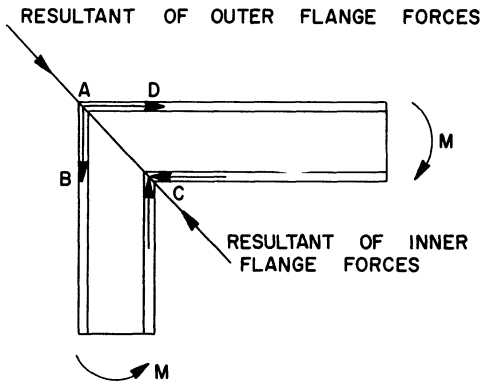

(b) CONNECTION SUBJECT TO BENDING WITHOUT SHEAR

Fig. 3.2

the case of the straight beam (Fig. 3.2a), the web contributes little to the bending resistance and could be completely or partially removed, as shown, since there is no shear acting on the beam. Considering the knee shown in Fig. 3.2b, it is seen that the resultant of the flange stress puts the web in compression along the diagonal AC and removal of the web in this region would result in collapse of the knee, even though it only transmits moment. Evidently, then, the methods of analysis for straight sections cannot be applied to knees without modification.

The web stress in the corner region is one of combined compression and shear, since in this region the actual loading results from the transfer of forces from the flanges, as shown in Fig. 3.3. Thus the web yields either when the shear stress reaches the yield-strength in shear ($0.58\sigma_y$) or, more likely, when buckling takes place due to the compression along diagonal AC. Ultimate collapse may also take place in one of the two modes described above for the yield condition. A third type of ultimate failure may occur in the inner flange in compression, involving local buckling, possibly followed by excessive lateral deflection if the flange is unsupported (3.1).

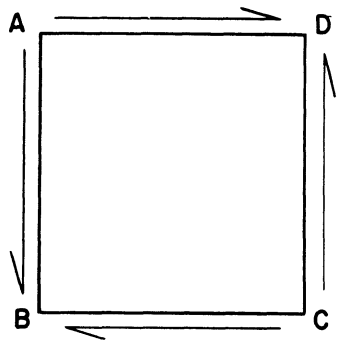

Fig. 3.3

Having discussed the function of a knee and its load-deformation characteristics, the various types of rigid joints will now be examined in greater detail. The discussions of this chapter, as of the others, do not necessarily apply to structures subjected to fatigue loads.

SQUARE KNEES

Before investigating the available experimental data on square knee connections, the assumptions that are usually made in continuous frame analyses will be examined. (i) The spans are measured between the center points of the joints, such as H in Fig. 3.4, and it is assumed that between the joints the

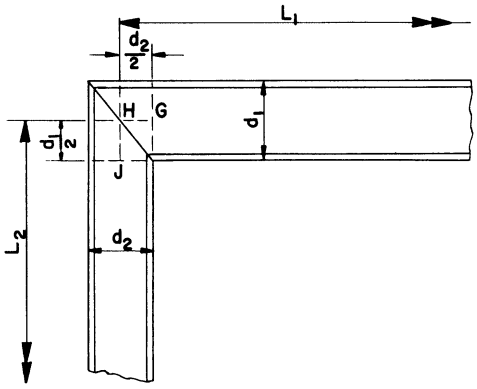

Fig. 3.4

rotation per unit distance is M/EI. This implies that the rotation taking place over the distance HG is 1/2 d_2 M/EI and over HJ is 1/2 d_1 M/EI, where M is the average moment in the region of the joint. Thus, in the length of the joint GHJ a rotation of 1/2 (d_1 + d_2) M/EI is assumed to take place. (ii) It is further assumed that the connection behaves elastically as long as the weaker of the members joined does not yield and that the yield moment of the connection is in fact the yield moment of the weaker section. (iii) If the analysis is based on ultimate strength considerations, it is assumed that a plastic hinge moment will be developed in the weaker section and not in the connection, although a large amount of rotation may take place either in the connection or in the rolled sections.

The extent to which the above assumptions are correct will now be examined in the light of available test results.

Analysis of Results

In Fig. 3.5 are the actual moment-rotation curves for a number of square knees made up of built-up sections. All but one of the connections are unstiffened. Knees without any stiffeners at all are, however, not very common in practice. The results are reviewed here to demonstrate the effect of diagonal stiffeners. Specimens 3 and 5 are identical except that in the case of specimen 5 lateral movement of the lower flanges was prevented. The tests were carried out by Hendry (3.1). The moment is plotted as a percentage of the plastic moment of the straight section. This is calculated by multiplying the material yield strength by the "plastic modulus" which is twice the statical moment of half the section about the center line. As an example, for a rectangular section of width b and depth d. $M_p = \sigma_y Z = \sigma_y \cdot 2 \cdot b\ d/2\ d/4 = 1/4\ \sigma_y\ bd^2$. For the abscissa the results have been reduced so that the rotation shown is that of half the length of the connection (d/2) and does not include any rotation of the straight portion of beam.

According to the assumptions usually made in the analysis of rigid frames the moment-rotation curves would follow the dashed line, which represents the rotation θ = M/EI d/2 that would take place in a length d/2 of a corresponding straight section. It is seen from the figure that the actual moment characteristics of all the unstiffened specimens fall short of the assumptions in three ways: (i) the actual stiffness in the elastic range is less than assumed,

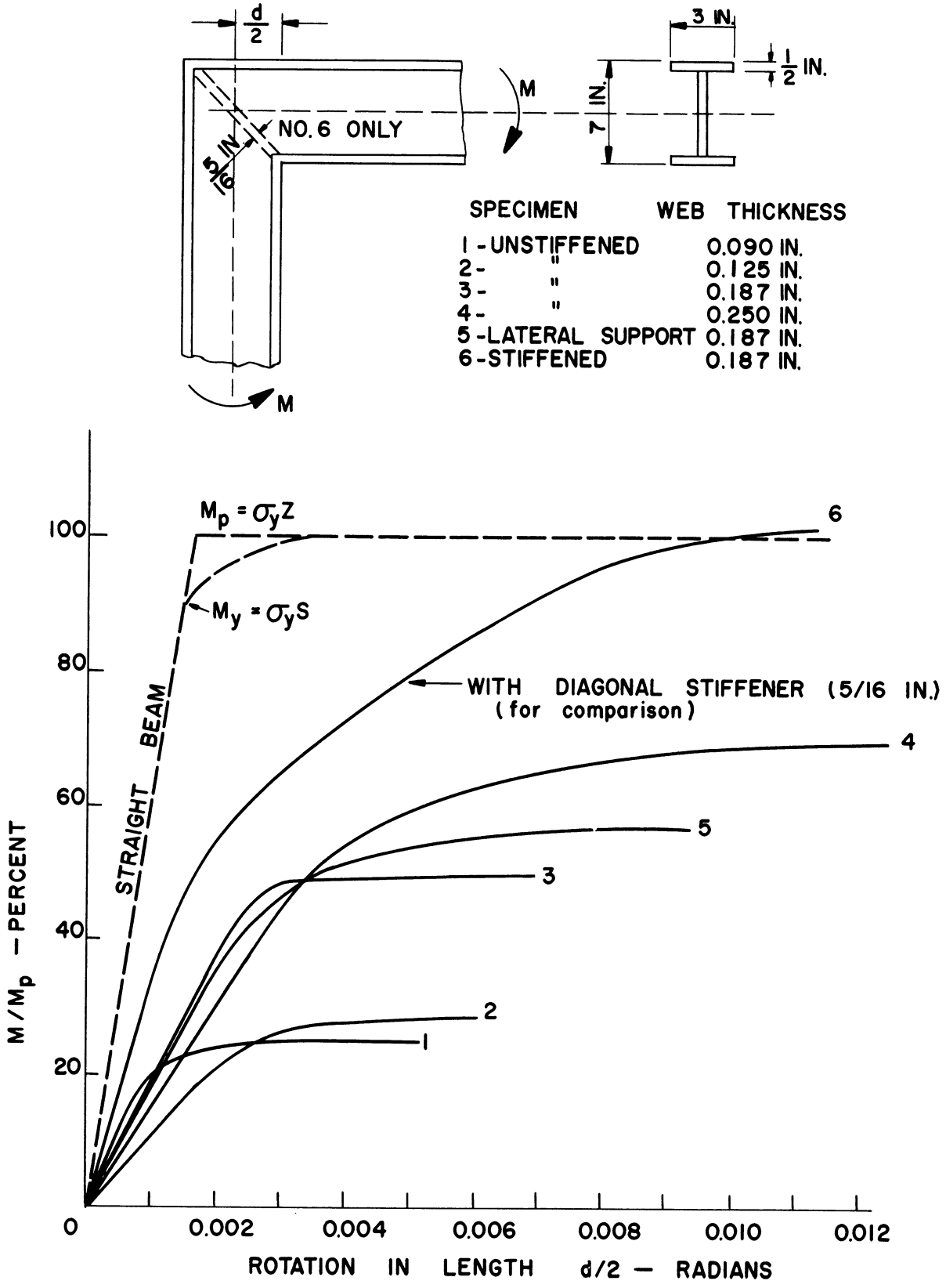

Fig. 3.5 Moment-Rotation Characteristics of Square Knees (All Unstiffened Except One).

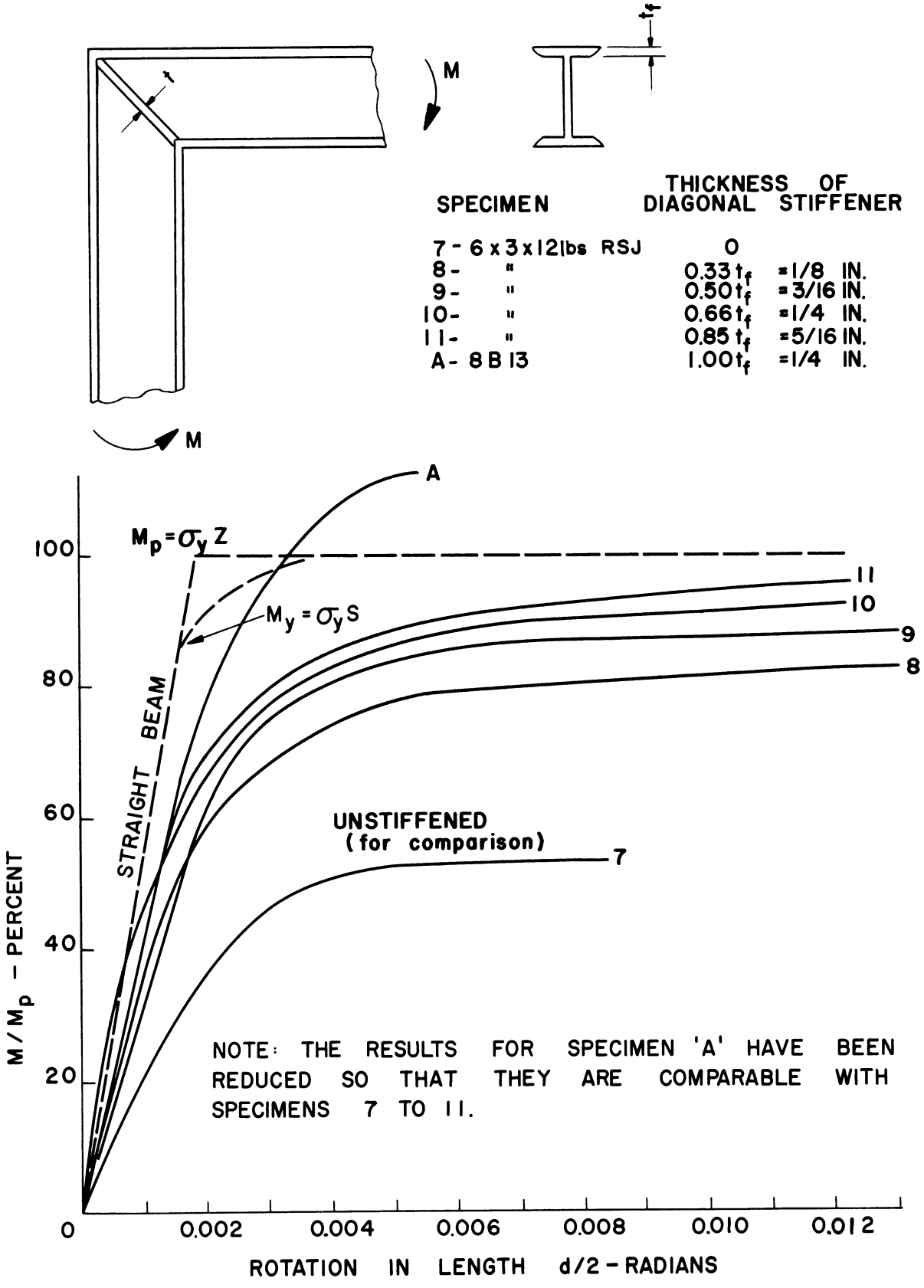

Fig. 3.6 Moment-Rotation Characteristics of Square Knees (All With Diagonal Stiffener Except One).

(ii) the actual yield moment is lower than assumed, and (iii) the actual plastic moment is less than that of the straight section. Specimen 6 (with diagonal stiffener) reached a moment in excess of M_p.

The knees for which moment-rotation curves are shown in Fig. 3.6 differ from those previously considered in two respects; they are made up of rolled sections and all but one have diagonal stiffeners. Curves 7 to 11 represent the results of Hendry's work (3.1) and curve A is the result of one of a series of tests carried out by Topractsoglou, Beedle, and Johnston (3.2). Moments and rotations are plotted as in Fig. 3.5. The thickness of the diagonal stiffener is the parameter whose effect is illustrated in Fig. 3.6. It is seen that the stiffened knees are more rigid and their moment resistance approaches M_p. The differences between curves 8, 9, 10, and 11 are small compared to the difference between them and the curve for the unstiffened specimen 7.

The experiments of Topractsoglou, et al. (3.2) suggest that vertical and horizontal stiffeners have virtually no effect on the stiffness or the strength of square knees composed of structural shapes. In the case of square knees built-up from plates by welding, the ratio of web thickness to depth may be smaller and in that event vertical or horizontal stiffeners would be more effective than with knees of the type tested by Topractsoglou.

The difference between the yield moment of an unstiffened square knee and one with only a thin diagonal stiffener is very pronounced (e.g., curves 7 and 8, Fig. 3.6). The reason is that the unstiffened web in the knee invariably fails at a moment less than the plastic moment of the section. Consider a knee under pure moment, neglecting the change in moment between the center of the joint and the beginning of the straight portion. The force which must be dissipated into the web of the knee between two points such as D and A (Fig. 3.7) is approximately $F = M/d$. This will result in a shear stress $\tau = M/(d^2 t_w)$, where t_w is the thickness of the web. The web will yield in shear when τ reaches its yield value τ_y, then $M_\tau = \tau_y d^2 t_w$. On the other hand, the rolled section yields at a moment $M_\sigma = \sigma_y S$. Hence,

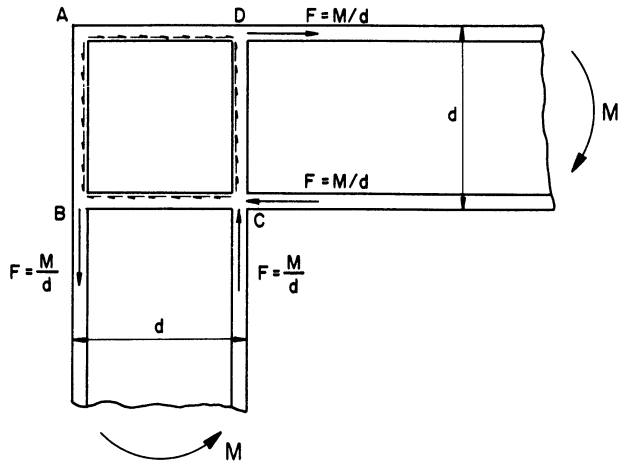

Fig. 3.7

$$\frac{M_\tau}{M_\sigma} = \frac{\tau_y d^2 t_w}{\sigma_y S} ,$$

Taking $\tau_y = (1/2)\sigma_y$,

$$\frac{M_\tau}{M_\sigma} = \frac{d^2 t_w}{2S} .$$

For most standard sections, the value of this ratio is well below unity, indicating that the connection will fail in shear at a moment less than the yield moment of any of the sections of which it is made-up. As an example, for the section of which specimen A in Fig. 3.6 is made (8B13) the above ratio is about 0.75. However, this specimen had a stiffener; thus, it did not fail by shear. For some of the other specimens the calculated value of M_T/M_σ is as low as 0.23. It is evident when considering yield strength alone that an unstiffened square knee is not suitable as a continuous frame connection. Although the yield strength of knees with diagonal stiffeners never quite reaches the yield strength of the straight section, Figs. 3.5 and 3.6 show that the ultimate strength of the stiffened knees can be made to approach or even exceed the ultimate strength of the straight section. With the thinnest diagonal stiffener used in Hendry's tests (3.1)(thickness of stiffener one-third of flange thickness) over 80 percent of M_p was reached. With a stiffener of thickness $0.85t_f$, 96 percent of the plastic section moment was reached. In the tests by Topractosoglou, et al. (3.2), M_p was well exceeded when a diagonal stiffener of thickness equal to the flange thickness was used.

The thickness of the diagonal stiffener also affects the moment-rotation characteristics of a connection (Fig. 3.6). Even with a stiffener of thickness equal to the flange thickness the rotation at any moment exceeds the rotation of an equivalent length of straight section. It is seen, however, from Fig. 3.6 that the difference in rotation is small compared to the difference between an unstiffened knee and the equivalent straight section.

Application in Practice: Analysis

The results of the experimental and theoretical work that has been done on connections can in practice be applied in two ways. First, in the analysis of existing structures the moment-rotation curves of the connections must be known so that the resistance-deflection curves for the structures can be calculated. Second, the connection characteristics should be known when new structures are designed.

In view of the many types of rigid connections and the large number of possible combinations of sizes, it is unlikely that experimental data will always be available for the particular connections of a building being analyzed. In accordance with engineering practice, Beedle, et al. (3.3) have developed theories concerning the stiffness and strength of rigid connections with adequate lateral support. Their formulae give results which agree well with test results from a limited number of specimens.

Because of the many unknowns which affect the characteristics of connections there is no purpose in attempting to predict connection behavior with

a degree if accuracy greater than the errors introduced by the effect of neglecting the unknown variables. Thus it is proposed, for the purpose of analyzing existing connections, to approximate their moment-rotation curves by two straight lines; one an inclined line through the origin, of slope corresponding to the effective stiffness of the connection, and the other a horizontal line at the level of the plastic hinge moment. No account will be taken of changes in the stiffness in the so-called elastic range or of the effect of work hardening.

Square connections can be divided into two categories; those with only vertical and horizontal stiffeners and those with diagonal stiffeners. (It has been demonstrated that diagonal stiffeners have a considerable effect on the properties of square connections.) Square connections without any stiffeners are of little practical interest.

(i) Square connections without diagonal stiffeners: Quoting from reference 3.3 for a connection with a horizontal and vertical stiffener, the elastic relationship between θ and M is

$$\theta = M\left[\frac{1 - \frac{d_1 + d_2}{2L'}}{t_w d_1 d_2 G} + \frac{\left(1 - \frac{d_2}{2L'}\right)d_2}{4EI_{f_1}} - \frac{\left(1 - \frac{d_1}{2L'}\right)d_1}{4EI_{f_2}}\right], \qquad (3.1a)$$

where θ = rotation within the connection,

M = moment at the point of intersection of the center lines of the members being joined,

d_1, d_2 = depth of members being joined,

t_w = thickness of web at connection,

I_{f_1}, I_{f_2} = moment of inertia of the sections minus the moment of inertia of the webs, and

L' = distance from the intersection of the center lines to the point of inflection. (This distance must be estimated, but θ is not very sensitive to variations in L'. If L' is different for the two members, the mean value should be taken.)

When the two members being joined are identical, expression 3.1a reduces to

$$\theta = M\left[\frac{1 - \frac{d}{L'}}{t_w d^2 G} - \frac{\left(1 - \frac{d}{2L'}\right)d}{2EI_f}\right] \qquad (3.1b)$$

The yield moment for the connection under consideration is given by Beedle, et al. (3.3) as

$$M = \frac{t_w d_1 d_2 \sigma_y}{2} \left[\frac{1}{1 - \frac{d_1 + d_2}{2L'}} \right], \qquad (3.2a)$$

with the assumption that yield is taking place due to shear in the web (τ_y has been replaced by $(1/2)\sigma_y$). This is a permissible assumption because, as is shown in reference 3.3, practically all square connections without diagonal stiffeners and made-up of standard sections will yield in this manner. For two identical sections Equation 3.2a reduces to

$$M = \frac{t_w d^2 \sigma_y}{2} \left[\frac{1}{1 - \frac{d}{L'}} \right]. \qquad (3.2b)$$

In case of doubt as to whether the connection may fail due to direct stress a check can be made. The corresponding moment is given by Equation 3.3, but this will nearly always be found to be greater than the moment given by 3.2a.

$$M = \frac{\sigma_y}{\frac{(1 - d/L')}{S} + \frac{1}{AL'}}, \qquad (3.3)$$

where S = section modulus of section and
A = cross-sectional area.

All symbols in 3.3 refer to the weaker section.

(ii) Square connections with diagonal stiffeners, with or without horizontal or vertical stiffeners: Again quoting from Beedle's work (3.3), the elastic M-θ relationship is

$$\theta = M \left[\frac{1}{\frac{t_w d^2}{1 - \frac{d}{L'}} G + \frac{A_s d E}{\sqrt{2}}} + \frac{\left(1 - \frac{d}{2L'}\right) d}{2EI_f} \right], \qquad (3.4a)$$

where A_s = cross-sectional area of stiffener. It will be noted that Equation 3.4a is for a connection joining identical members. Making the adjustments required to generalize it, the equation reads

$$\theta = M \left[\frac{1}{\frac{t_w d_1 d_2 G}{1 - \frac{d_1 + d_2}{2L'}} + \frac{A_s (d_1 + d_2) E}{2\sqrt{2}}} + \frac{(1 - \frac{d_2}{2L'}) d_2}{4EI_{f_1}} + \frac{(1 - \frac{d_1}{2L'}) d_1}{4EI_{f_2}} \right]. \qquad (3.4b)$$

Finally, an expression is required for the yield moment of a square connection with diagonal stiffener. Such an expression was not given by Beedle, et al. (3.3). This may be because a diagonal stiffener will generally allow a square connection to develop the full or very nearly full plastic moment of the sections joined and the yield moment of the connection proper is of reduced interest. Referring to Fig. 3.6, it is seen that in the British tests the thinnest practical stiffener raised the plastic strength of the connection to over 80 percent of the straight section plastic strength. For practical purposes it is proposed to assume that a somewhat similar ratio applies to the yield strengths. It may be assumed, then, that the yield moment of a square connection with any diagonal stiffener is at least 75 percent of the yield moment of the straight section. A more accurate estimate can possibly be made in individual instances by considering the actual thickness of the stiffener relative to the flange thickness and the degree of lateral support.

As numerical examples of the use of the expressions quoted above, Equation 3.4a (M-θ relation for square connection with diagonal stiffener, joining two equal sections) has been applied to three specimens that were actually tested and the results are shown compared to the experimental curves in Fig. 3.8. It should be noted that because of the nonlinearity of the moment-rotation curves, Equation 3.4a results in higher stiffness values than prevail over any reasonable working range. It is suggested that in practice the stiffness values given by Equations 3.1a, 3.1b, 3.4a, and 3.4b be halved to bring them into line with test data.

The first step in analyzing a structure with square connections is to determine the moment-rotation curve by use of modified Equations 3.1 to 3.4. In isolated instances an experimental curve may actually be available. Thereafter any method suitable for the analysis of structures with semi-rigid connections can be used, e.g., the method developed by Pippard and Baker, also presented with minor modifications and experimental verification by Johnston and Mount (3.4). Numerical examples of the application of this method are given in Chapter VI.

Application in Practice: Design

The AISC recommends certain rules for the design of rigid connections (3.5). Because of their importance not only in the case of square connections, but also when built-up connections are involved, these rules are quoted in full in the appendix to this chapter. The AISC rules are based on strength considerations. From the point of view of design it is desirable also to determine readily any errors introduced by assuming a connection as completely rigid. If the moment-rotation curve is known, this can be done by use of Equation 3.1 or 3.4 as follows: Consider a beam with both ends attached to rigid supports

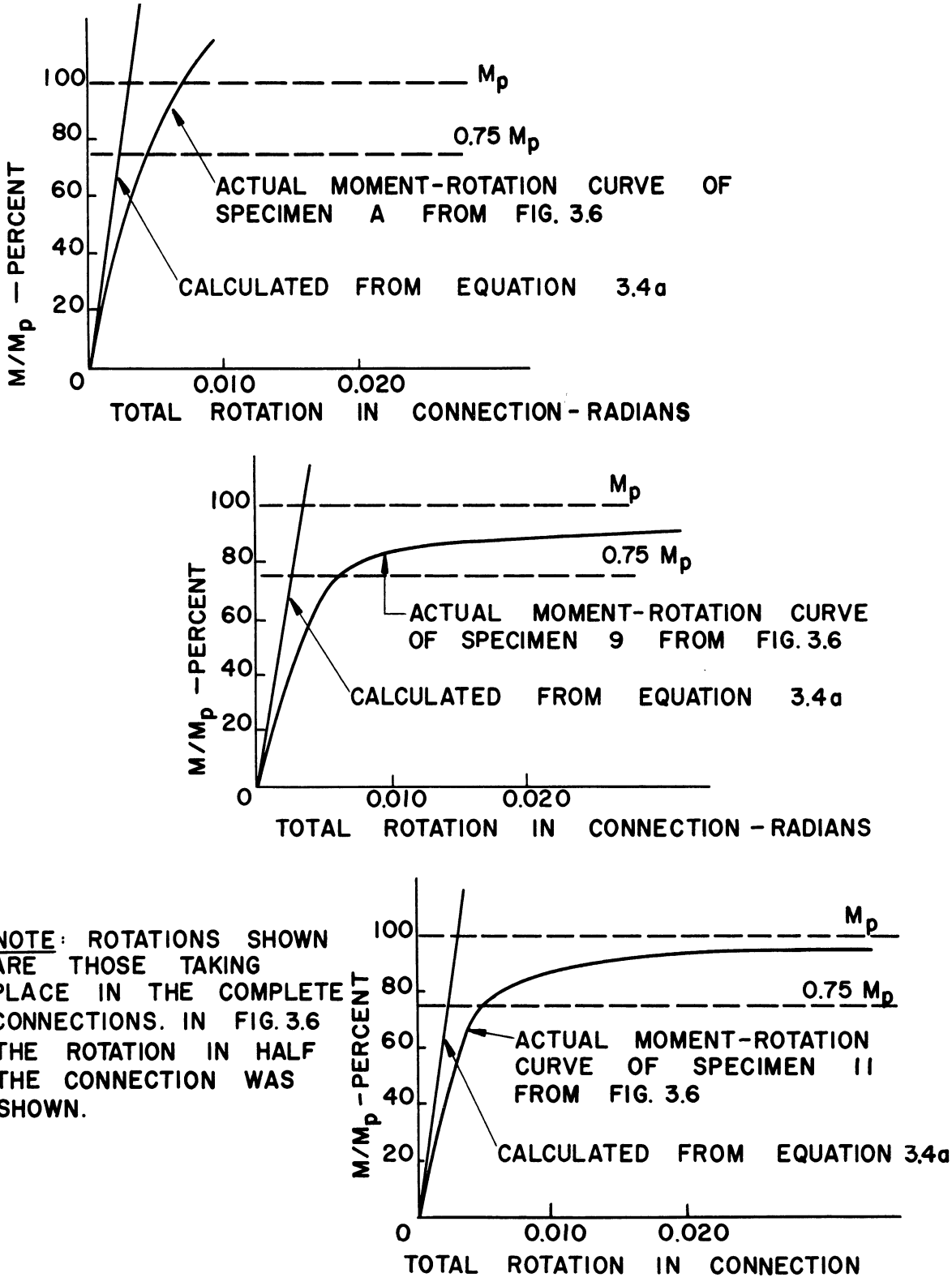

Fig. 3.8 Comparison of Equation 3.4a with Actual M - ϕ Curves.

through identical square knees. Since only the beam is being considered (not the columns), only half the total rotation of the connection affects the rotation of the ends relative to the fixed supports. Hence, the problem is somewhat hypothetical (Fig. 3.9), but it will serve to assess the effect of the connection flexibility.

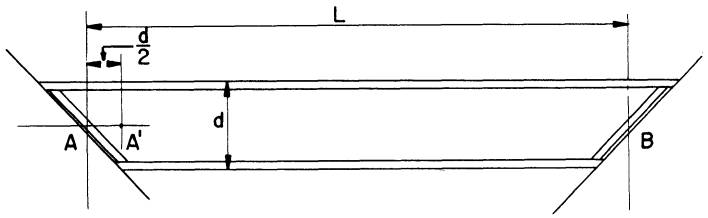

Fig. 3.9

It is assumed that the load on the beam is symmetrical and such that it would result in fixed-end moments M_f and $-M_f$ at A and B, respectively. If the beam were rigidly attached to the supports those would in fact be the moments at A and B. Since the connections are not entirely rigid, there will be a lesser moment at A and B. Let the moment at A be M_a ($M_a < M_f$). If the connection at A were rigid, then the customary method of analysis implies that a rotation $M_a/EI\ d/2$ takes place in the length AA'. (The difference between the moments at A and A' is neglected here.) The rotation $M_a/EI\ d/2$ corresponds to PQ (Fig. 3.10) for a moment M_a. However, the actual rotation taking place in the length AA' is PR. The additional rotation due to the connection flexibility, PR-PQ = QR can be considered as taking place at the very end of the beam. Let $QR = \theta_a$ and, furthermore, let

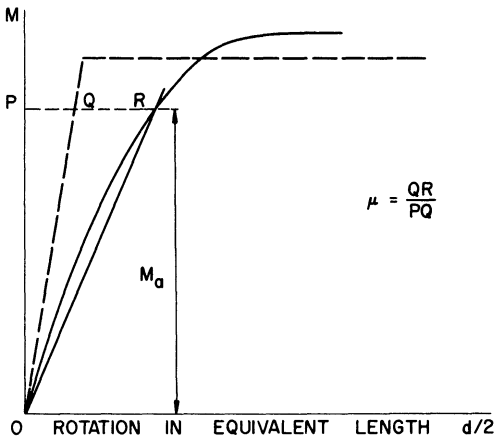

Fig. 3.10

$$\theta_a = QR = \mu PQ = \mu \frac{M_a}{EI} \frac{d}{2},$$

hence,

$$\theta_a = \mu \frac{M_a}{2EK} \frac{d}{L}, \qquad (3.5)$$

where I = moment of inertia of section
L = span, i.e., AB
K = I/L
$\mu = \theta_a \div$ rotation in equivalent straight length d/2. Thus for an entirely rigid connection, $\mu = 0$. The slope deflection equation for the symmetrically loaded beam is

$$M_a = M_f - 2EK\,\theta_a . \qquad (3.6)$$

Equations 3.5 and 3.6 between M_a and θ_a can be represented graphically, as in Fig. 3.11. It can be concluded from Fig. 3.11 that if the slope OT is large, M_a

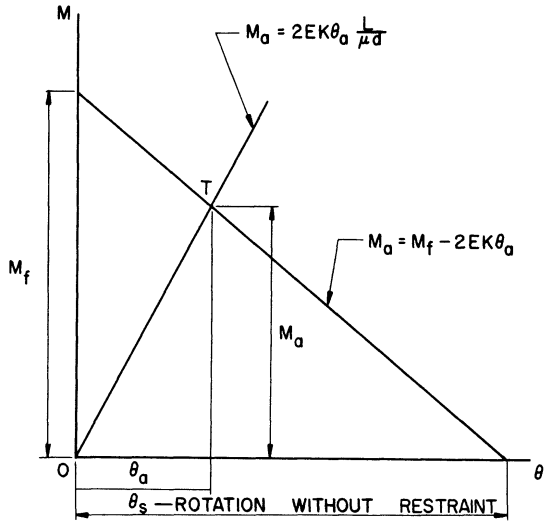

Fig. 3.11

is not much less than M_f. If the slope is ∞, i.e., if $\mu = 0$, then $M_a = M_f$. It is natural now to examine the experimental results to determine approximately the values of μ.

From experimental curves, μ can be determined as shown in Figs. 3.5 and 3.6, or from a theoretical M-Θ curve. At any particular moment μ is found by subtracting from the total rotation the corresponding rotation that would occur in a straight section (abscissa of dashed line in Figs. 3.5 and 3.6) and dividing this difference by the rotation in a straight section. Since the experimental moment-rotation curves are not straight, μ may be different for every moment. From Fig. 3.6 at $M = (2/3) M_p$, μ ranges from about 0.25 for specimen A to 1.1 for specimen 8. In general $\mu < 1$ at $M = (2/3) M_p$. From Equations 3.5 and 3.6, by eliminating Θ_a

$$M_a = \frac{M_f}{1 + \mu \frac{d}{L}} \quad . \tag{3.7}$$

Choosing a typical ratio for d/L, say 1/20, and $\mu = 1$

$$M_a = \frac{M_f}{1 + 1/20} = 0.95\ M_f \ ,$$

i.e., the error introduced by treating the connection as rigid is only 5 percent.

For completely unstiffened knees μ is very much larger. For specimen 2 in the elastic range μ is 6, hence, for $d/L = 1/20$, $M_a = M_f/(1 + 6/20) = 0.77\ M_f$ and the error introduced by assuming the connection to be rigid is 23 percent.

In view of the foregoing the following practical rules in addition to the AISC rules, are proposed for initial design purposes on new structures.

(a) Use connections with diagonal stiffeners of thickness equal to at least the flange thickness.

(b) If the moment at the knee is estimated to be less than $(2/3)\ M_p$, the knee may be treated as rigid. The error involved is small.

(c) If the moment at the knee is greater than $(2/3)\ M_p$, analyze structure twice. First, assume the knee to be rigid; next, assume a

value of $\mu = 6$ and design for the most critical stress condition.

(d) Assume that the stiffened knee can resist the plastic moment of the weaker section; but that after this moment is exceeded, unrestricted deformation takes place in the weaker straight member where it joins the connection.

BUILT-UP CONNECTIONS

The practice of using built-up connections (see Fig. 3.1), haunched or curved, has arisen from the need in design to make the most effective elastic use of the beam and column material. However, the savings made in the total amount of material may be offset or even outweighed by the increased cost of labor for the fabrication of built-up connections. The decision to use built-up connections must, therefore, be made after considering the cost of materials as well as labor, but in some cases technical or architectural considerations may override purely economic factors.

To illustrate the effect of built-up connections, a beam with ordinary rigid connections under a uniformly distributed vertical load and fixed between relatively stiff columns will be considered. According to elastic design procedure the greatest bending moments exist at the beam ends. When these moments reach the value of the yield moment of the beam section, the carrying capacity of the beam has been reached, even though the remainder of the beam is not stressed to the same extent. To increase efficiency in the elastic use of material an extreme solution would be to remove from the beam all excess metal so as to make the modulus of each section exactly proportional to the bending moment. A more practical step is to reinforce the beam over some distance from the ends; effectively reducing the span and shifting the critical section towards the center.

A beam may be a part of a portal frame under lateral load. Here again, the greatest moments occur at the beam ends so that reinforcement of the connections will result in increased strength as well as elastic efficiency for the whole frame.

For a built-up connection to be able to carry out its function, adequate bending strength in the strong direction is only one of several important requirements. There is a greater tendency towards "kicking out" or "buckling" of the compression flange than with square connections. The reason for this is that in square connections a relatively small portion of the compression flange (near the re-entrant corner) is highly stressed, whereas in a curved or haunched

connection the stress distribution along the inner flange is more uniform. Hence, a larger amount of energy can be released by buckling.

Lateral buckling may also occur when the average flange stresses are still in the elastic range. This is frequently the result of local buckling of the compression flange. Local buckling is usually associated with stress concentrations and appears to occur more frequently in haunched connections than in connections with a uniformly curved inside flange. If lateral buckling has not taken place in the elastic range, instability nearly always arises soon after the stress in the compression flange has passed the yield point. If lateral instability is taken care of by adequate supports, failure of built-up connections can take place as a result of buckling of the web, as with square knees. This type of failure becomes more unlikely as the depth of throat of the connection is increased, causing the flange forces to be transferred to the web more gradually.

Analysis of Results

Since in square connections the length of the connection is small in comparison with other linear dimensions, it can be neglected in analyzing results without introducing appreciable error. Such is not the case with a built-up connection whose very function is to effectively move a critical section away from the joint.

An understanding of the relationship between the moment at the intersection of beam and column and at the extremities of the built-up connection is required for an interpretation of test results. Figure 3.12 shows a built-up connection and a typical bending-moment diagram. The bending moment may vary linearly, as shown, or in some other manner. The calculation of the bending resistance of a section is much more certain than the determination of the moment under which connection instability would occur resulting from lateral deformation or web buckling. Consequently, it is desirable to have connections fail by yielding rather than instability.

Assume that in a test, such as depicted in Fig. 3.12, failure in bending takes place at B, where the straight section is joined to the connection. This would imply that the yield moment of the straight section M_{ry} had been reached, but that the yield moment of connection had not been reached at any point. Since in this example the moment at B is critical, it is possible to change the applied loading to make the moment increase more rapidly between B and A. Tests could actually be carried out in which the moment arm is progressively reduced until failure takes place in the connection and the straight section at the same time. Let it be assumed that this occurs when the moment arm is L" (Fig. 3.12b). It would then be established that under the particular

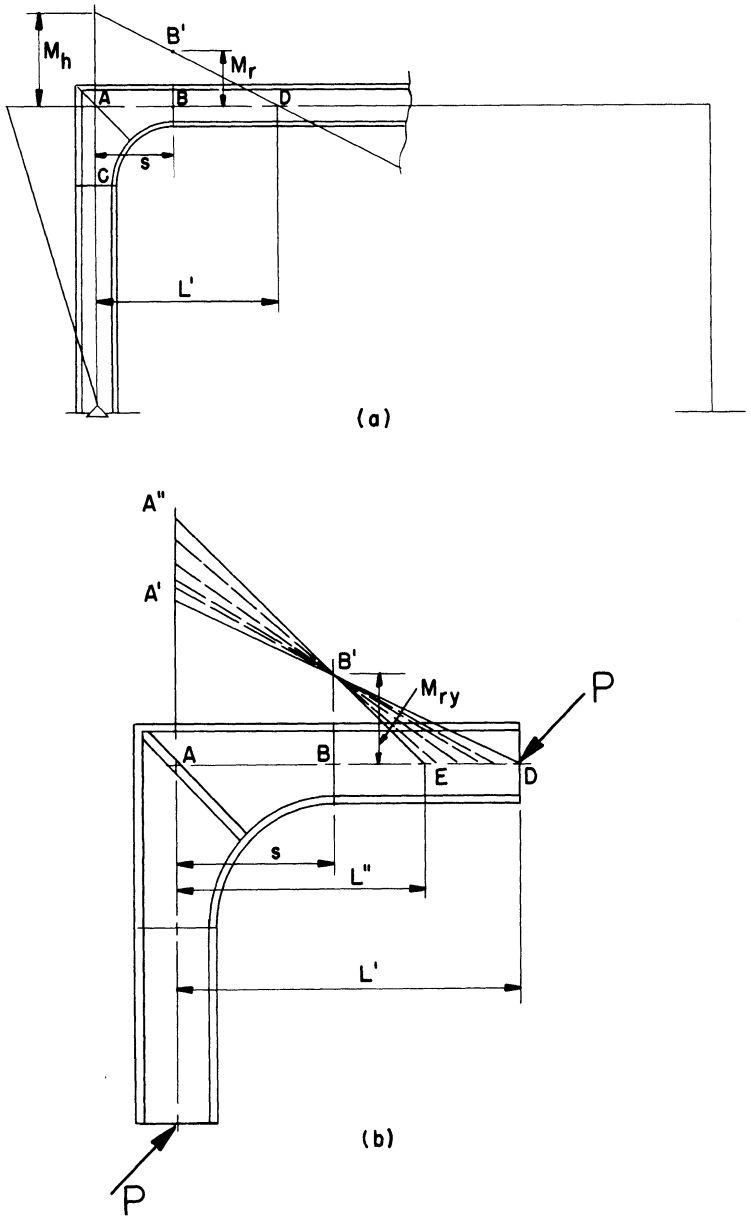

Fig. 3.12

condition of lateral support and for a straight-line variation of the moment diagram, the connection would not fail sooner than the straight section, provided the distance from the corner A to the point of inflection is L" or greater. Although the moment diagram is a straight line in special cases only, a test such as the one described above, in which failure occurs in the connection proper, can conveniently be used as a standard.

To illustrate the purpose of this discussion, the results of actual experiments will be examined. In Fig. 3.13 results are shown of tests by

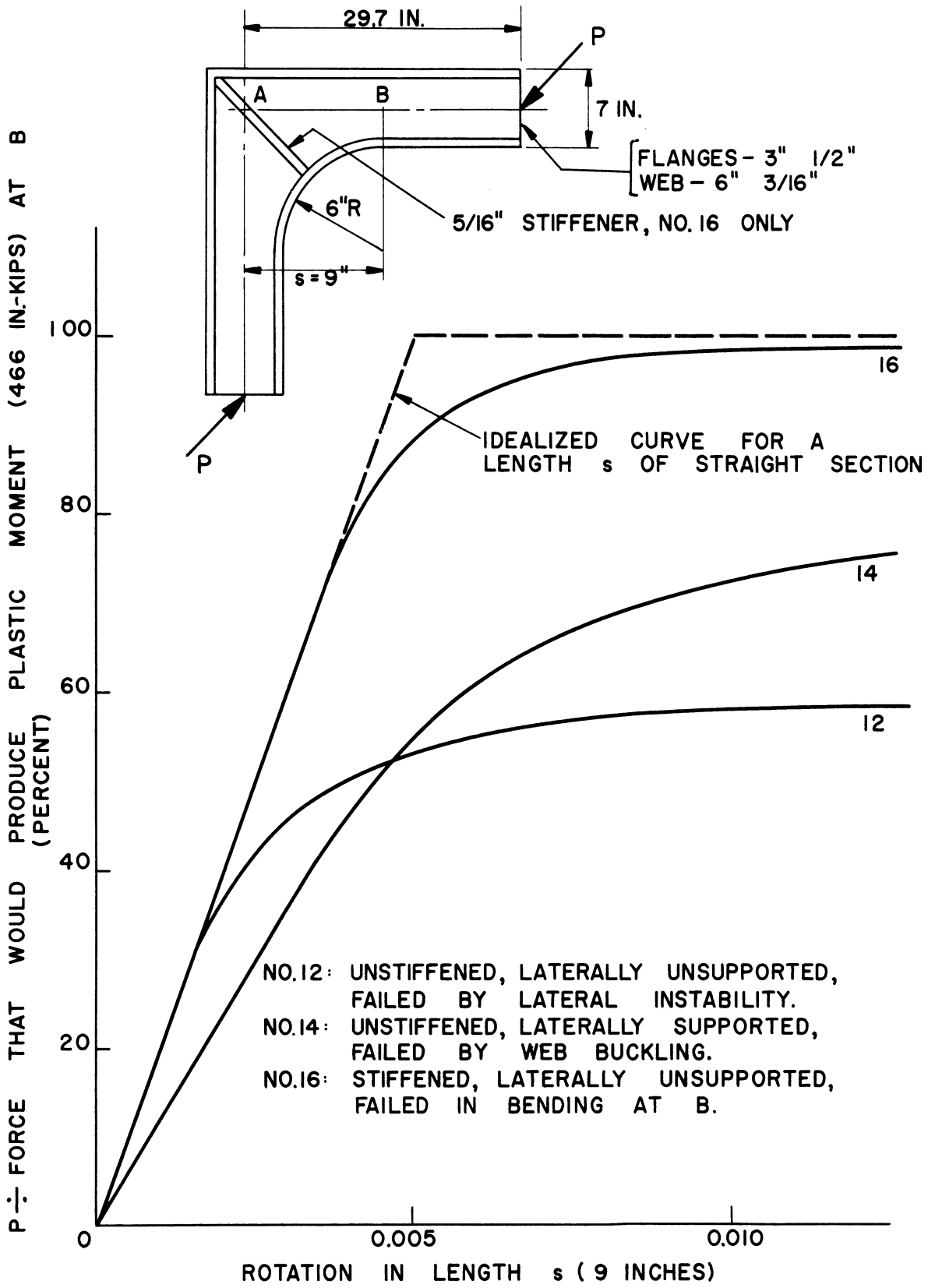

Fig. 3.13 Moment Rotation Characteristics of Curved Knees. (Radius of Inner Flange Approximately "d").

Hendry (3.1) on curved connections. In one series three connections were tested, all having a radius of curvature at the inner flange about equal to d, the depth of the section. Specimen 12 was unstiffened and laterally unsupported. Specimen 14 was unstiffened, but lateral deflection was restrained. Specimen 16 had a diagonal stiffener, but no lateral support. The graphs represent moment-rotation curves, although the ordinates are actually expressed as a percentage of the force required to produce the plastic moment at the joint between the straight section and the connection. One hundred percent of this is the maximum useful force which the connection should resist for the particular moment arm (29.7 in.). If it could resist more than 100 percent, failure would take place in the straight section anyway. The idealized curve (dashed), of course, reaches the 100 percent level. It is seen from Fig. 3.13 that with an inner flange radius d, an unstiffened, unsupported curved connection is quite unsatisfactory, since it only allows about 60 percent of the resistance available in the straight section to be developed. Denoting L' as the moment arm in the test, L" as the arm which should be used to result in failure of the connection and the straight section at the same load, and s as the length of one leg of the connection (see Fig. 3.12); then if α is the fraction of the maximum useful force $P = M_{ry}/(L' - s)$ at which the connection failed. The moment at the center of the connection is given by $\alpha PL' = \alpha L' M_{ry}/(L' - s)$. By definition of L", α is unity when the moment arm is L". It follows that

$$\frac{\alpha L' M_{ry}}{L' - s} = \frac{L'' M_{ry}}{L'' - s}$$

or

$$L'' = \frac{\alpha s L'}{\alpha L' + s - L'} \qquad (3.8)$$

For connection 12, L" turns out to be negative, indicating that there is in fact no moment-arm L" at which the connection could develop the strength of the member. Specimen 14, with some lateral support, is 75 percent effective at the moment arm used (29.7 in.). For the connection to be 100 percent effective, expression 3.8 requires that L" be 130 inches or more. In the case of specimen 16 a diagonal stiffener, somewhat thicker than the web, permits the connection to be practically 100 percent effective with a moment arm of 29.7 inches.

The test results recorded in Fig. 3.14 were on specimens similar to the ones described above, but with the radius of curvature of the inner flange approximately 2d. Specimen 13 failed in a manner similar to 12, while specimen 15 failed in the same manner as 14. However, connection 17, which was unsupported but stiffened, failed in bending within the connection, indicating that the moment-arm of 29.7 inches was somewhat too short to produce simultaneous failure in connection and straight section. From Equation 3.8, L" = 44 inches.

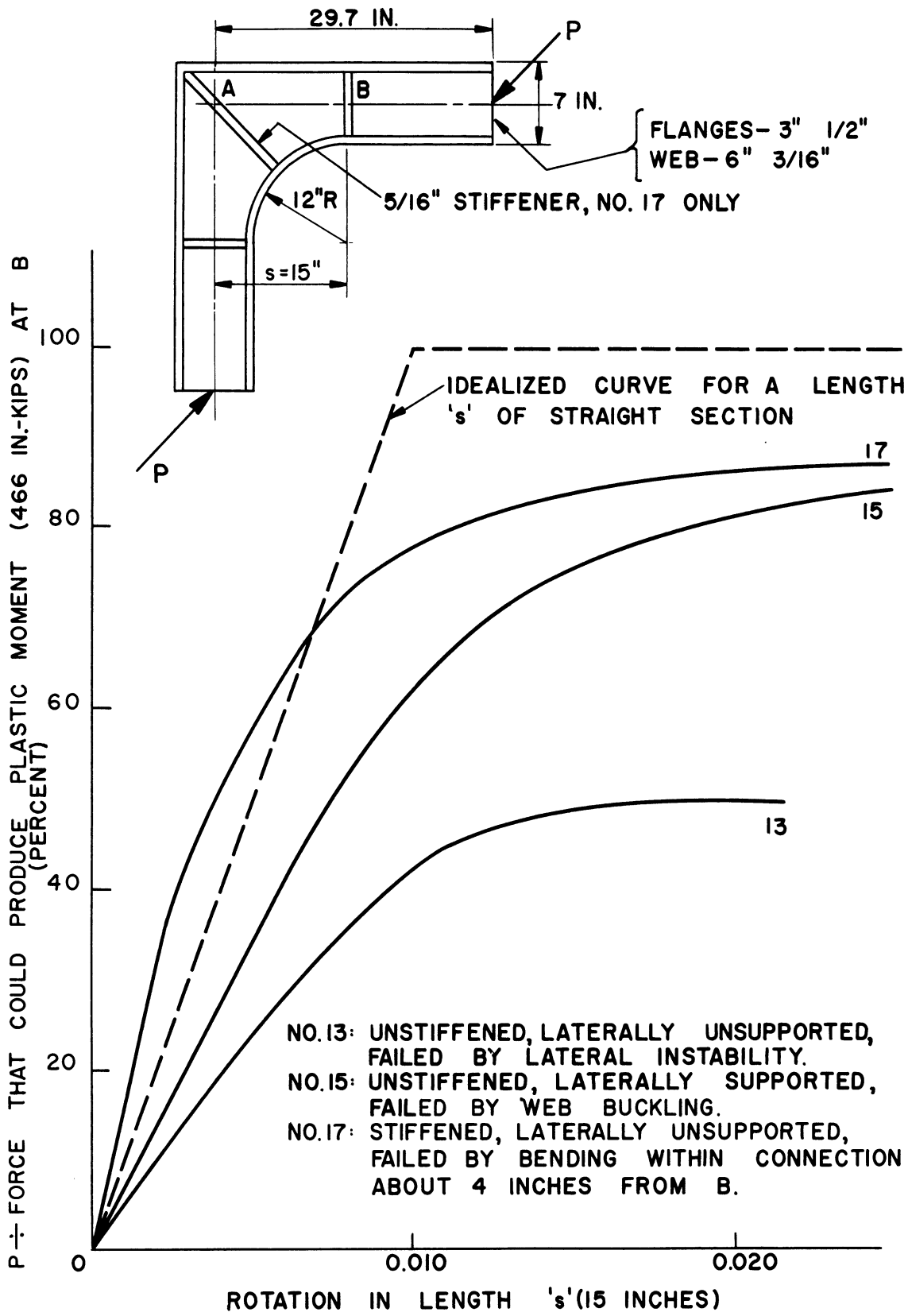

Fig. 3.14 Moment-Rotation Characteristics of Curved Knees. (Radius of Inner Flange Approximately 2d.)

In the tests of Topractsoglou, et al. (3.2) referred to earlier, a number of built-up connections were investigated. From their experience these investigators were able to select the proper moment arms to make the connections and rolled sections fail at about the same load. According to the terminology used in this series, the built-up connections that were tested can roughly be divided into three groups: curved, tapered, and haunched, as shown in Fig. 3.15. All connections were supported laterally and were stiffened.

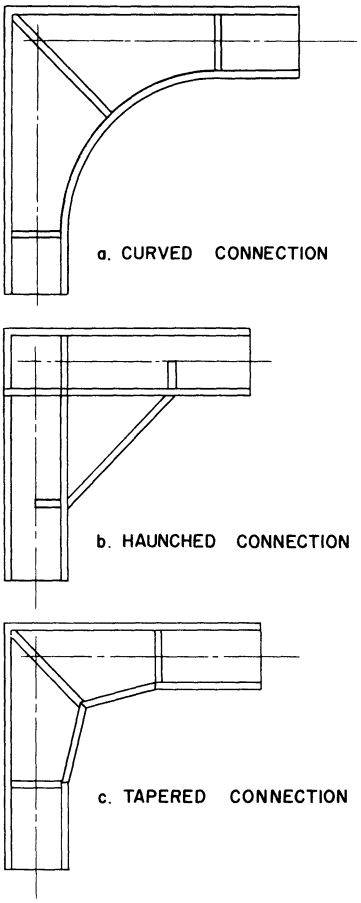

Fig. 3.15 Types of Built-Up Connections Tested by Topractsoglou, Beedle, and Johnston.

The curved connections were designed in accordance with AISC recommendations (Ref 3.5 and Appendix 3.1). Apart from confirming that the connections were of balanced design, as mentioned earlier, the AISC recommendations indicate that the same maximum haunch moment can be attained with connections of various curvatures. This gives a designer some latitude in the choice of members and dimensions, since $M_h/M_r = L''/(L''-s)$ (Fig. 3.12). For example, if a connection is available with a maximum resistance of 1000 inch-kips and the straight member has a maximum moment resistance of 500 inch-kips, then $L'' = 2s$. Thus a suitable radius of curvature can be chosen to result in the most convenient value of L". Figure 3.16 shows the moment-rotation curves for three curved connections tested by Topractsoglou, et al. The ordinates are plotted in the same form as in Figs. 3.13 and 3.14, but the abscissae are rotation per unit length to accomodate the results of different specimens on the same graph.

In these tests the haunched connections were also proportioned so that they would fail at about the same load as the adjoining rolled section. For comparative purposes a curved connection was tested which had a depth of throat equal to one of the haunched connections. Because of the geometry this implies that the curved connection had a larger effective length s. As a result the curved connection was not able to develop the full plastic moment of the

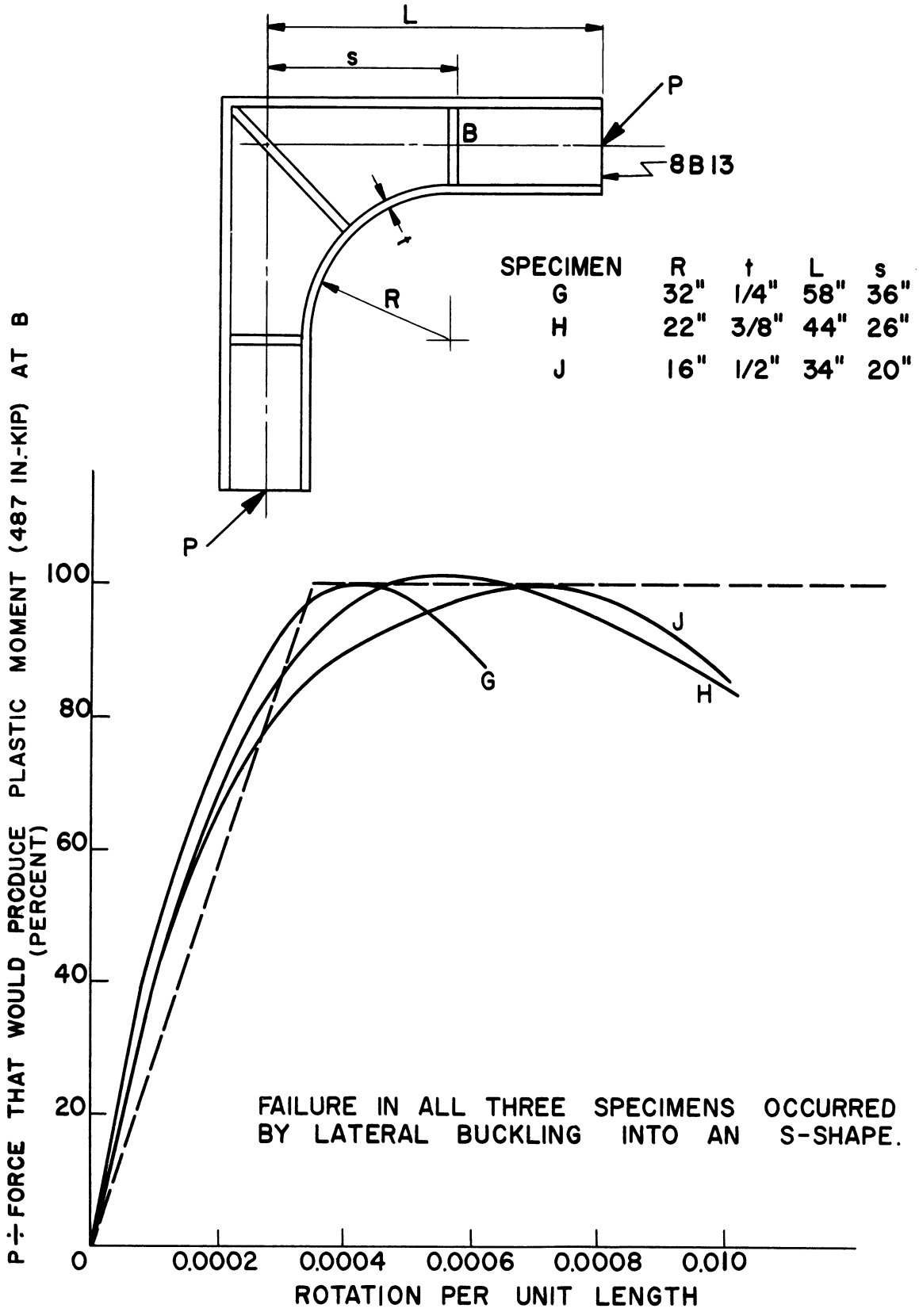

Fig. 3.16 Moment-Rotation Characteristics of Curved Knees.

rolled section. even though a larger absolute haunch moment was reached than in the case of the haunched knee.

Application to Practice

In the discussion of tests of square connections, emphasis was laid on the connection stiffness compared to the stiffness of an equivalent length of straight beam. From Figs. 3.13, 3.14, and particularly from Fig. 3.16 it will be seen that a connection which is sufficiently strong to develop the full moment of the adjoining beam is invariably quite rigid. It follows, therefore, that rigid frame analysis is justified in dealing with structures that have built-up connections and in actual design it remains only to estimate correctly the maximum moment resistance of the connections.

The task of estimating the moment resistance of built-up connections is difficult. Not only can such connections fail in at least three distinct modes, but the ultimate moment of resistance in each of these modes is affected by the connection type and the absolute and relative proportions. In the case of square connections it was possible to point out types of connections which would develop the full plastic moment of the straight section. Most built-up connections will do this, but their efficiency depends on the development of a substantially larger moment (see Fig. 3.12). Attempts to analyze the strength of built-up connections have been made by Bleich and Olander (3.6, 3.7), but their analyses are limited to the elastic range and are too complex for practical purposes. Furthermore, they have not been developed in sufficient detail to be applicable to all types of built-up connections. In determining the moment resistance of a built-up connection, the best course at present is to refer to existing experimental information. In general, however, it would be desirable to use the tests carried out by Topractsoglou, et al. (3.2) at Lehigh University as pilot tests designed to select certain types of connections as standards. With the variables thus narrowed down, further tests should be carried out on various sizes of those selected standard connections. Some such tests are now in progress at Lehigh University.

In the meantime the rules of design for connections as prepared by the AISC are available. Although these rules do not give any indication about the actual strength of connections, they represent an "envelope" of practices that have been followed successfully in the past. Thus the designer is in a somewhat better position than the analyst as far as the use of built-up connections is concerned. The AISC rules are quoted in the Appendix to this chapter. They should be read in conjunction with the AISC "Specification for the Design, Fabrication and Erection of Structural Steel for Buildings", contained in the AISC Steel Construction Manual.

GENERAL SUMMARY AND CONCLUSIONS

This study of continuous frame connections is divided into two parts: one dealing with straight connections (Fig. 3.1a) and the other with built-up connections (Fig. 3.1b and c). For both types, existing experimental and analytical information is reviewed first; then, the practical significance of the data in analysis and design work is examined.

Experimental results indicate that diagonal stiffeners have a profound influence on the stiffness and strength of square connections. The conclusion is drawn here that all square connections should have diagonal stiffeners of thickness equal to the flange thickness of the straight member whose plastic moment is to be developed. Analytical methods for calculating the stiffness and strength of square connections, in the absence of experimental data, are given. A quick check to determine whether a connection with known characteristics should be treated as rigid or semi-rigid is also described. Some practical design rules for square connections are recommended.

With built-up connections the line between satisfactory and unsatisfactory connections is not so sharply defined. A built-up connection which in one case develops the plastic moment where it is joined to the straight section may not do so under conditions which move the point of inflection closer to the corner. It is concluded that most built-up connections which have satisfactory strength properties are sufficiently stiff to be treated as 100 percent rigid in an analysis. It is not considered feasible to analyze particular connections, but for design purposes the AISC rules will give satisfactory results. Further systematic tests are desirable.

BIBLIOGRAPHY - CHAPTER III

3.1 Hendry, A.W.
"An investigation of the strength of welded portal frame connections"
Struct Eng 28:265-80 (1950)

3.2 Topractsoglou, A.A.
Beedle, L.S.
Johnston, B.G.
"Connections for welded continuous portal frames"
Prog Rep No. 4 Pt I, Weld J Res Supp 30: 359s-384s (1951)

3.3 Beedle, L.S.
Topractsoglou, A.A.
Johnston, B.G.
"Connections for welded continuous portal frames"
Prog Rep No. 4 Pt II, Weld J Res Supp 30:397s-405s (1951)

3.4 Johnston, B.G.
Mount, E.H.
"Analysis of building frames with semi-rigid connections"
Trans ASCE 107:993-1038 (1942)

3.5 Griffiths, J.D.
"Single span rigid frames in steel"
AISC (Oct 1948)

3.6 Bleich, F.
"Design of rigid frame knees"
AISC (July 1943)

3.7 Olander, H.C.
"A method for calculating stresses in rigid frame corners"
Proc ASCE V79 Separate 249 (Aug 1953)

3.8 Stang, A.H.
Greenspan, M.
Osgood, W.R.
"Strength of riveted steel rigid frame having straight flanges"
J of Res NBS 21:269-313 (1938)

3.9 Stang, A.H.
Greenspan, M.
Osgood, W.R.
"Strength of riveted steel rigid frame having a curved inner flange"
J of Res NBS 21:853-71 (1938)

APPENDIX 3.1

ASIC RULES FOR THE DESIGN OF RIGID CONNECTIONS

The stress distribution within the knee section has been the subject of considerable research, both in this country and in Europe. Data obtained from large scale model tests conducted at the National Bureau of Standards and at Lehigh University, together with a development and summary of theory by Dr. Friedrich Bleich, constitute valuable sources of information in regard to this problem.

These data indicate that, if certain precautions are observed regarding its shape, the knee section may be safely designed in accordance with conventional practices with little if any sacrifice in economy. It is therefore recommended that the knee section be proportioned and designed on the following basis:

Rule 1. That the critical design sections be taken
- (a) at the inside face of column and bottom of girder for a straight knee,
- (b) at the points of tangency for a circular haunched knee, and
- (c) at the extremities and common intersection point for haunches made up of tapered or trapezoidal segments.

Rule 2. That the allowable bending stress at these critical sections be limited to 20,000 psi, modified where necessary according to the formula

$$F_b = \frac{12 \times 10^6}{Ld/bt}$$

The allowable direct compressive stress be limited to $F_a = 17{,}000 - 0.485\ L^2/r^2$ and that the maximum combined stress be limited by the provisions of Section 12(a) of the AISC Specification.

Rule 3. That the maximum combined stress be determined by the conventional formula $f = P/A + Mc/I$.

Rule 4. That positive lateral support be provided for the compression (inner) flange in the region of the knee.

Rule 5. That the average shear stress on the web, computed at the critical design sections referred to in Rule No. 1, be limited to 13,000 psi.

Rule 6. That, in the case of a curved haunch, the ratio R/d be not less than that determined by the curve in Fig. A.1.

Rule 7. That, in the case of a curved haunch, the relationship b^2/Rt be not more than 2, where b is the width, t is the thickness, and R is the radius of curvature of the inner flange, all in inches.*

Rule 8. That stiffeners be provided at the midpoint, and at or near the extremities, of a curved knee; in line with the lower flange of the girder and the inner flange of the column, in the case of a straight knee.

---

* Note: If it is desired to maintain the smallest radius of curvature consistent with Rule No. 6 it may sometimes be found necessary to increase somewhat the thickness, t, of the curved inner flange over that of the flanges of the prismatic sections. The following table of radii will satisfy the conditions $b^2/Rt<2$, with curved flanges no thicker than those of the wide flange shapes required for the columns and girders.

Depth of Wide Flange Shape	R	
12"	5'0"	
14"	5'0"	
16"	5'0"	(except for heaviest series)
18"	5'0"	(except for heaviest series)
21"	5'0"	(except for heaviest series)
24"	7'6"	
27"	8'6"	
30"	8'6"	
33"	9'0"	
36"	9'0"	

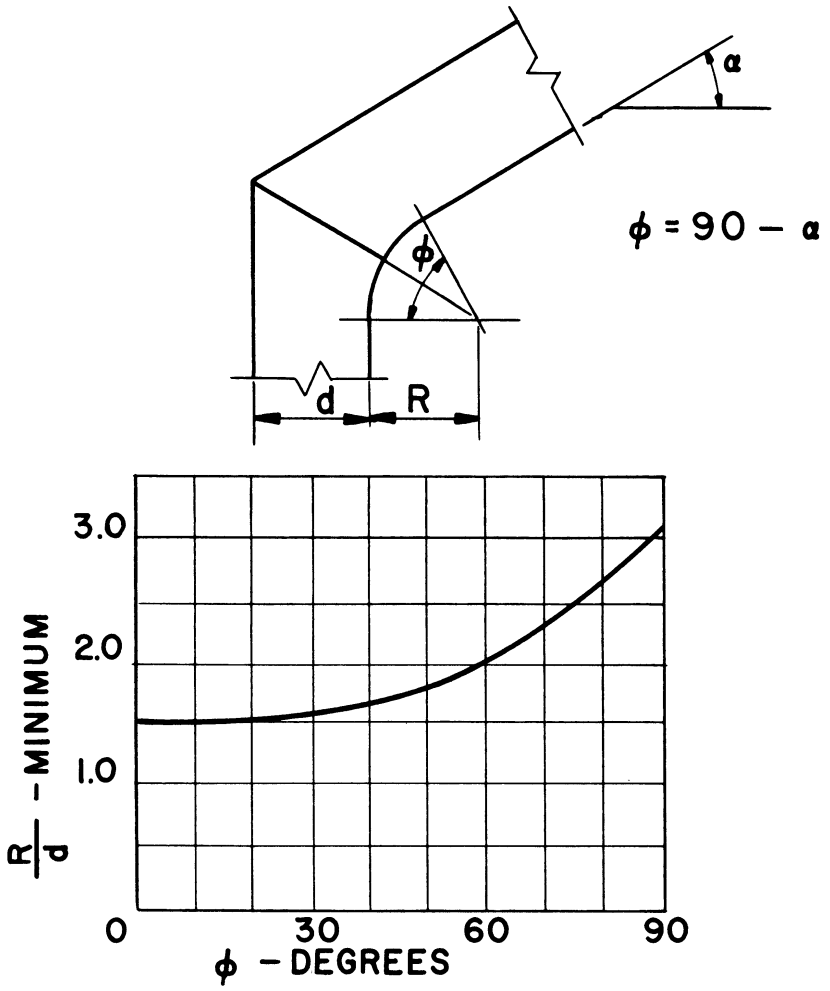

Fig. A.1

CHAPTER IV

FLEXIBLE AND SEMI-RIGID BEAM-TO-COLUMN CONNECTIONS

It was stated in Chapter III that very few beam-to-column connections are truly rigid. Neither are such connections entirely flexible, but it is accepted practice, nevertheless, to assume connections to be either rigid or pinned. This assumption introduces inconsistencies in the actual factors of safety of various parts of a structure. Such inconsistencies are acceptable in practice because the additional labor of carrying out a "semi-rigid" analysis is not usually justified by the saving of material that might be made. However, simiplified design procedures are available which allow consideration of a dependable and easily determined portion of the restraint in connections which might otherwise be considered as flexible. A background of information covering the experimental data and the rigorous analytical procedures is of advantage even when simplified design procedures are used. Furthermore, in the analysis of building behavior under atomic blast, it may be important to include the effect of connection behavior in determining the load-deflection characteristics of the structure.

The types of connections to be considered are those in which angles, tees, or flat plates are used as intermediate components between beams and columns. They can be grouped as follows:

(i) seat and top angle, Fig. 4.1a;
(ii) as (i), but with structural tees instead of angles;
(iii) web angles, Fig. 4.1b, and
(iv) seat angle and top plate, Fig. 4.1c.

All the connection types can be attached either to the column flange or to the web. In this report the types of connections described above are referred to simply as "nonrigid" connections, to distinguish them from the connections discussed in Chapter III.

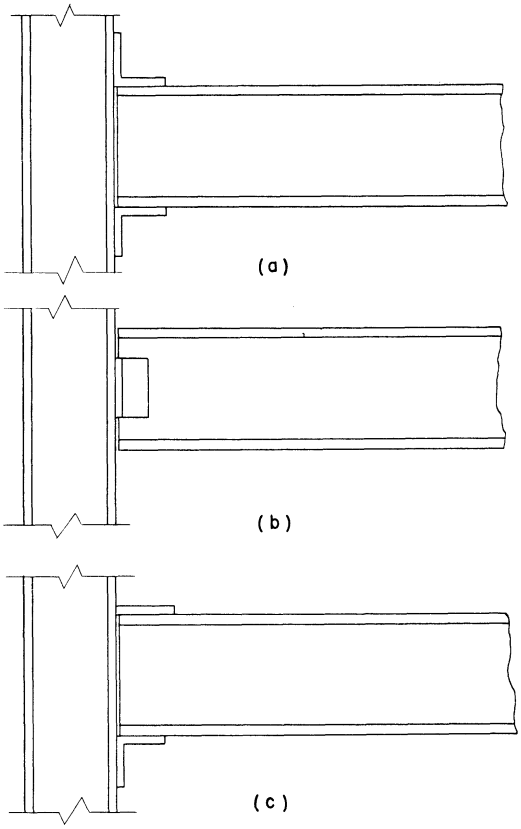

Fig. 4.1.
Types of Nonrigid Connections

The moment from a column to a beam must be transmitted from the column flange or web through fasteners to the intermediate members (angles, tee, or plates) and then through further fasteners to the beam flange or web. In transmitting force, the various components act as links of a chain; the weakest component controls the strength of the connection and the deformation of each of the parts is additive insofar as the effect on the rotation between the center lines of beam and column is concerned. Since the characteristics of nonrigid connections are dependent on the properties of all the component parts, they are subject to much variation. In analyzing expermental results it is desirable to be able to "interpolate" the data, making it useful over as wide a range as possible. It is necessary, therefore, to have available a procedure which will permit the classification of connections in order of their rigidity.

CONNECTION RIGIDITY AND ROTATION CAPACITY

The most common way of testing nonrigid connections is to attach two beam stubs to opposite sides of a column stub by means of the connections to be tested. Moment is applied to the connections by supporting the beam stubs and loading the column in a standard testing machine (e.g., reference 4.1). The relative rotation between the center lines of the column and each beam is determined by mirrors or level bars. The resulting moment-rotation curve, such as OA, Fig. 4.2, yields necessary but insufficient information to classify the degree of rigidity of a connection. This can be illustrated by Batho's "beam line" construction (4.2), which has already been briefly mentioned in Chapter III. Using the slope deflection equations, the moment at the end of a symmetrically loaded beam is given by

$$M = M_f - 2EK\theta \quad , \qquad (4.1)$$

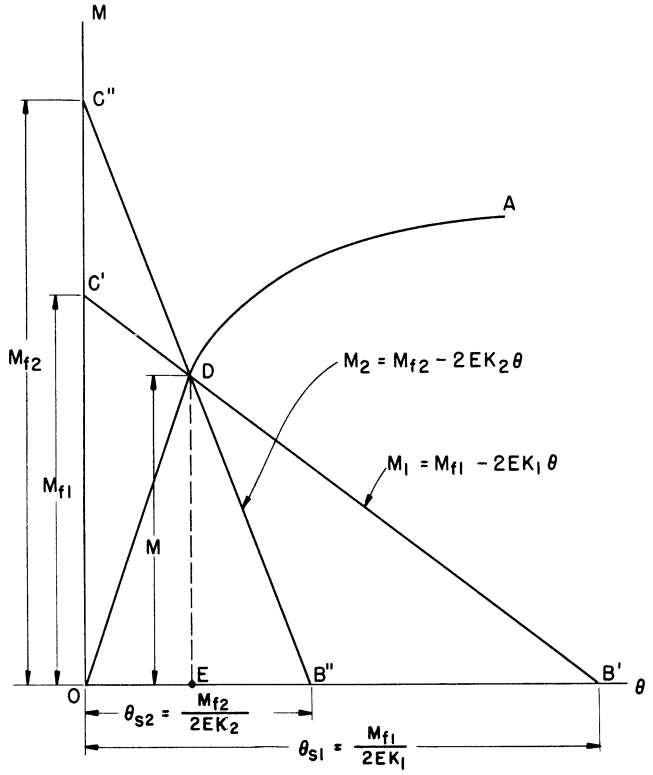

Fig. 4.2.
Connection Moment-Rotation
Curve and "Beam Line"

where M_f is the fixed-end moment corresponding to the applied load and θ is the slope at the end of the beam. K is the stiffness (I/ℓ) of the beam. The relation between M and θ for fixed values of M_f and K can be represented by a straight line such as C'B', termed the "beam line". If the beam is attached to rigid supports (Fig. 4.2), the end rotation θ can be due only to the flexibility of the connection. Since OA is the moment-rotation relationship for the connection, the point of intersection D represents the only condition for which M and θ have compatible values for both beam and connection. It is now possible to consider a second beam with a larger K and, for purposes of illustration, carrying a load which would result in a fixed-end moment OC" (Fig. 4.2). Defining the percentage rigidity p as one hundred times the ratio of the actual end moment to the fixed-end moment, it is seen that for the flexible beam p is DE/OC' x 100% and for the stiffer beam it is DE/OC" x 100%. This shows that the same connection can have a different percentage rigidity when associated with beams of different stiffness.

A satisfactory connection must not only have good strength properties, but also adequate rotation capacity. This is illustrated by a somewhat extreme example in Fig. 4.3. Supposing OADE is the moment-rotation curve of the connections used at either end of a beam carrying a uniformly

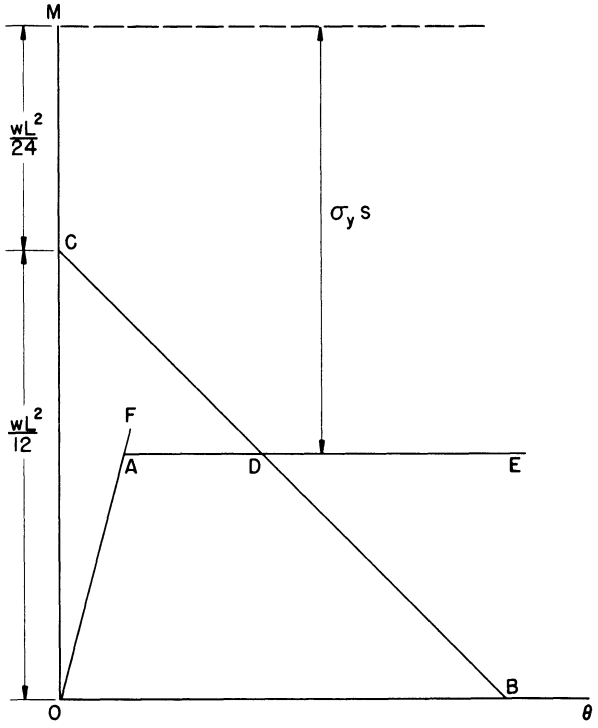

Fig. 4.3.
Hypothetical Connection
Moment-Rotation Curve
and Beam Line

distributed load. Since nonrigid connections often cause the highest stresses to exist at the center of the beam, a beam line BC can be determined which will correspond to a load producing the yield moment $\sigma_y S$ at the center. If the connection is not sufficiently ductile, then its moment-rotation curve might never intersect BC. This would be the case if the moment-rotation curve for the connection were given by OAF, implying brittle fracture of the connection before the beam were fully loaded.

Good rotation capacity is particularly important whenever a joint is assumed to be entirely flexible. If a "flexible" joint does not possess this property, it may fail before the rotation corresponding to the end rotation of a simply supported beam has taken place. This emphasizes the necessity of checking the moment-rotation characteristics of a connection, even if it is assumed that the connection has no moment resistance. Failure due to lack of rotation capacity may impair the ability of the connection to take a vertical reaction. This may come about when web clip angles are used without the supporting seat angles. Sufficient rotation capacity is usually available with riveted and bolted joints because of the flexibility of the connectors. Because of their greater rigidity, welded connections are not so often used when semirigidity or flexibility is desired. However, several series of tests have been conducted as part of an effort is to develop flexible and semi-rigid welded connections. The results are discussed in the next section of this chapter.

In this general discussion of nonrigid connections, the example of a beam carrying a symmetrical vertical load has been used to assess the behavior of the connections. In practice such simple conditions of loading are not common. Methods are available, and will be described, whereby the moment distribution and slope deflection procedures of analysis can be modified to take account of the actual rigidity of connections under any condition of loading. This requires that the moment-rotation characteristics of the connections be

known. For design purposes, simplified procedures have been developed. The remainder of the chapter is, therefore, readily subdivided into (1) a discussion of the moment-rotation characteristics of nonrigid connections and (2) the application of the information to analysis and design.

EXPERIMENTAL INFORMATION ON NONRIGID CONNECTIONS

Because of the many factors which contribute to the characteristics of nonrigid connections it is not possible to make a purely analytical approach to the problem of relating connection details to their moment-rotation characteristics. An alternative would be to reproduce here the relevant moment-rotation curves which are on record, enabling the reader to make use of the characteristics for the specimen which most closely resembles the connection that he has under consideration. This would not be too satisfactory for two reasons: (i) About one hundred curves might have to be reproduced and to present so much undigested information would result in confusion. (ii) In spite of the many tests which have been carried out on nonrigid connections, the information is in most cases incomplete in a statistical sense, because usually only one double-specimen of each kind was tested. Thus, in examining the results of one test alone, doubt must arise whether the information is typical of what would be obtained if a number of identical specimens were tested in the same way. The data can be given a broader basis by comparing the test curves of specimens which, though not identical, vary only in one aspect, say the beam depth. It should be possible in this way to spot specimens whose behavior is not in line with the trend of the group.

Another difficulty then arises in deciding what identifying properties of the experimental curves can be expressed numerically for comparison? Clearly it would be desirable to find expressions which, in graph form, would closely fit the experimental curves. Then the parameters of these expressions could be considered the characteristics of the specimens. Fortunately, examination of the experimental moment-rotation curves reveals that most lend themselves very well to "curve-fitting". The type of expression that appears to give the best results is

$$M = X \log^*(Y\theta + 1) \quad , \qquad (4.2)$$

where X and Y are to be considered as the characteristic parameters. Study of expression 4.2 shows that variation of X results in a family of curves, all essentially similar shapes, whereas variation of Y affects the shape,

* Common or base 10 logarithms.

i.e., the greater the value of Y the greater the curvature. To illustrate how well an equation of the above type fits the experimental curve, Fig. 4.4.

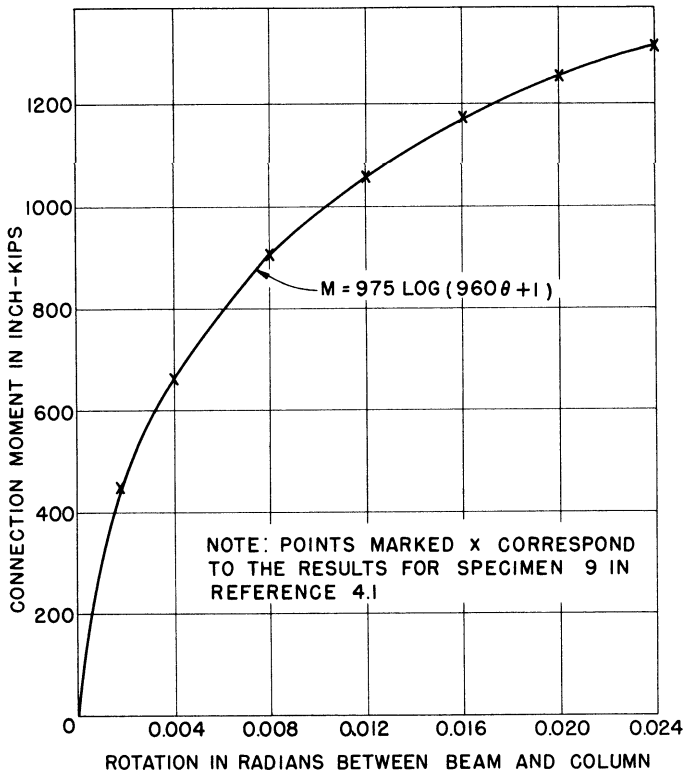

Fig. 4.4.

Comparison of Typical Experimental
Results With a Suitable Analytical Expression

shows a plot of the expression

$$M = 975 \log (960\theta + 1) \quad , \qquad (4.3)$$

together with points taken off the curve for specimen 9 in the tests of Hechtman and Johnston (4.1).

The curve representing the expression 4.2 passes through the origin. Parameters X and Y are determined from the coordinates of any two experimental points. Conversely, any two experimental points can be used to find a set of values for X and Y and unless the logarithmic expression completely represents the experimental curve, no two sets of values for the parameters will be the same. Since a number of the logarithmic

equations might come equally close to the experimental curve, it is not usually possible to single out only one of them as being the correctly fitted curve for a particular specimen. Moreover, as was stated earlier, it is not certain whether the experimental curve itself is typical of the specimen group or whether it is a freak. It was decided, therefore, to determine the values of the parameters X and Y by trial and error so that when these parameters are plotted against the variable under investigation in a group of specimens the resulting graph would have some regular shape. This procedure and the underlying logic will be discussed again later in the chapter.

Riveted Top and Seat Angle Connections

The moment-rotation curve of a top and seat angle connection depends mostly on

(i) the depth of the beam,
(ii) the stiffness of the top angle,
(iii) the stiffness of the rivets connecting the top angle to the column, and
(iv) the stiffness of the face of the column to which the top angle is connected.

Other factors, such as the stiffness of the shear rivets between the top angle and the beam, the thickness of the beam flange, and the proportions of the seat angle also affect the moment-rotation curve, but to a lesser extent.

Fig. 4.5 and 4.6 show the variation with beam depth and top angle thickness of the parameters X and Y in the expression $M = X \log (Y\theta + 1)$. This information was extracted from the tests of Hechtman and Johnston (4.1) in the manner described in the preceding section. The empirical expressions resulting from the use of these parameters, as given in Figs. 4.5 and 4.6, obtain curves which are in good agreement with the available experimental curves. It is to be expected, therefore, that the empirical procedure will give good results for all the beam depths and top angle thicknesses shown in Figs. 4.5 and 4.6. These values just about cover the practical range.

It will be noted that the top angle stiffness is represented by its thickness. This was done because there is no information on the effect produced by variation in the other top angle dimensions, but it is likely that these are sufficiently related to the other dimensions of the connections so as not to require specific consideration.

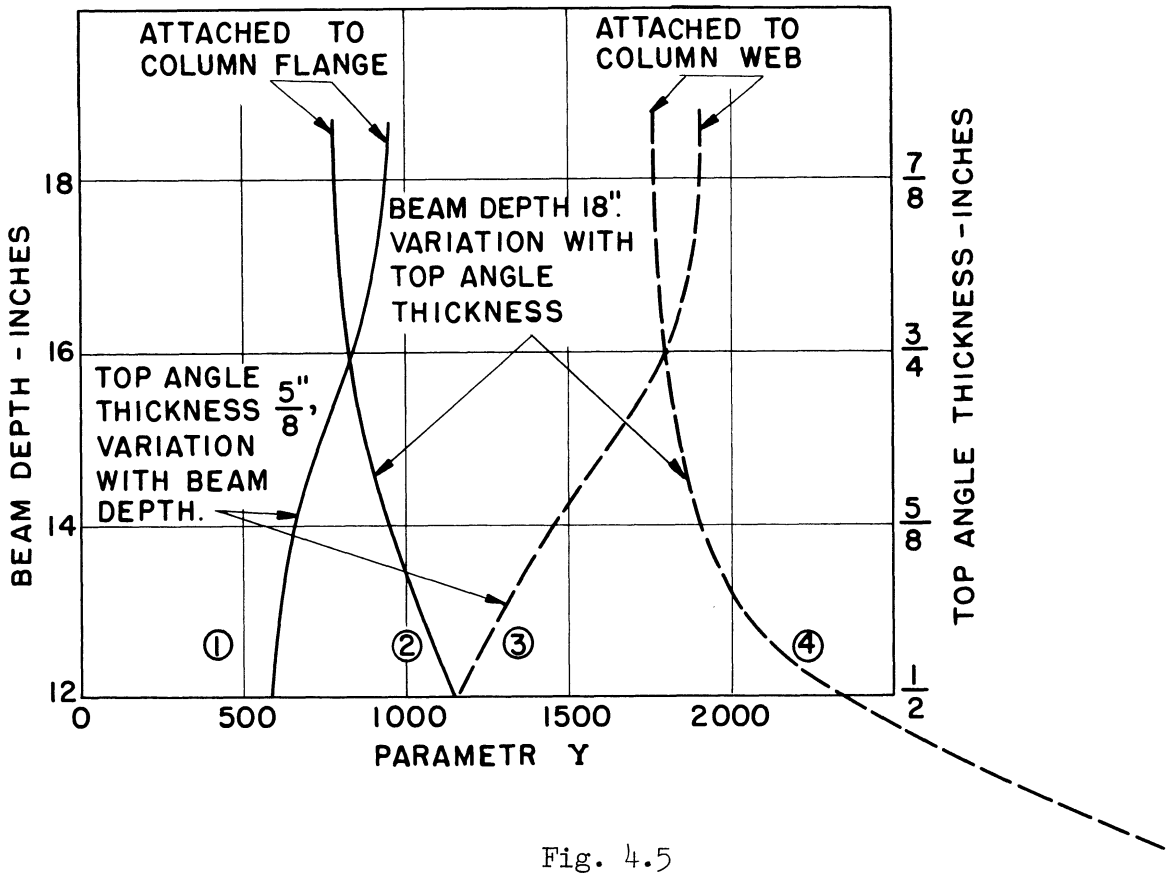

Fig. 4.5
Variation of Y in Expression
$M = X \log (Y\theta + 1)$
for Top and Seat-Angle Connections

Note: Solid curves based on 12WF65 column size. Dashed curves based on 14WF58 column size. All curves based on 6" x 4" top angles, 10"-12" long, and 4-3/4-inch diameter rivets in each horizontal and vertical leg.

The effect of the stiffness of the column face can be estimated by comparing the parametric curves for the cases when the connection is attached to the column flange and the column web respectively. When connections are made to the column web, the maximum stiffness is obtained because two identical connections are made to the two sides of the web. The curves associated with the column flange connections are not as generally applicable as the column web curves, because column flanges of different dimensions might result in different curves. However, the two sets of curves in the figures provide sufficient information to permit interpolation and extrapolation for occasions when the column flanges are more or less stiff than those of a 12WF65 section.

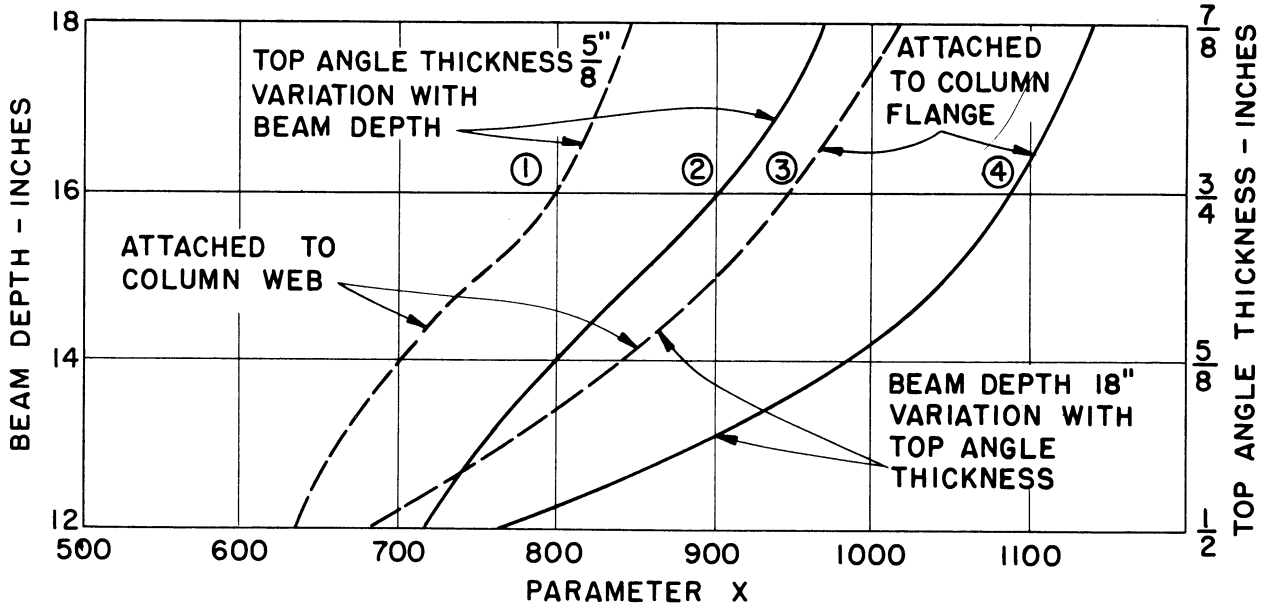

Fig. 4.6.
Variation of X in Expression
$M = X \log (Y\theta + 1)$
for Top and Seat-Angle Connections

Note: Solid curves based on 12WF65 column size. Dashed curves based on 14WF50 column size. All curves based on 6" x 4" top angles 10"-12" long and 4-3/4"$^{\Phi}$ rivets in each horizontal and vertical leg.

The curves in Figs. 4.5 and 4.6 give no information on the variation of the parameters with the area of the tension rivets of the vertical leg of the top angle. The curves shown are all for the case of 4-3/4-inch diameter rivets, i.e., a rivet area of 1.77 square inches. From this experimental data the conlcusion has been reached that over the range considered the parameter Y is not affected by any variation in the tension rivet area. The parameter X should be multiplied by a factor

$$\sqrt{\frac{A_r}{1.77}} \quad ,$$

if the tension rivet area differs from 1.77 square inches A_r is the area of all the tension rivets.

The test data indicate that the thickness of the beam flange may influence the moment-rotation curves. However, the effect does not seem sufficient to be significantly disassociated from the probable errors in the experimental curves caused by scatter.

An example will be given to show how the above procedure can be applied to obtain the moment-rotation curve of a top and seat angle connection. By considering a 12-inch deep beam joined to a column web, the flexibility of the column flange does not enter into the picture. Let it be assumed that the tension rivet area is 1.77 square inches and that the top angle thickness is 3/8 inch. From Fig. 4.6 X can be found, but the curves were not carried on below an angle thickness of 1/2 inch. Extrapolating the appropriate curve (3) down to 3/8 inch, X is found to be 440. However, curve (3) is for an 18-inch deep beam; from curve (1) it is seen that for a 12-inch deep beam X is 635/845 = 75% of what it is for an 18-inch deep beam. Hence the correct value for X for the connection under consideration is 0.75 x 440 = 330. Similarly, from Fig. 4.5, Y is found to be 2000. Hence the equation for the moment-rotation curve is

$$M = 330 \log (2000\,\theta + 1). \qquad (4.4)$$

This is the solid line in Fig. 4.7b.

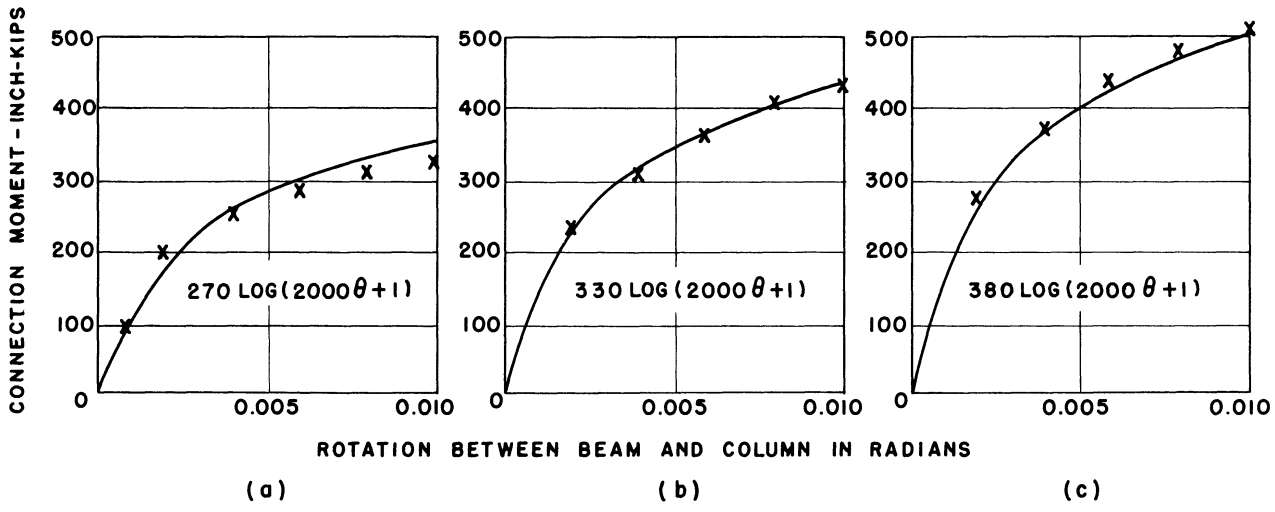

Fig. 4.7.
Empirical Moment-Rotation Curves Compared
With Appropriate Experimental Results.
(Ref. 4.3, Specimens 8, 9, 10).

A connection such as the one for which the above empirical expression has been computed was tested by Rathbun (4.3, specimen 9) and the experimental points are marked on the graph, Fig. 4.7. Two other similar connections were also tested, one having two 7/8-inch diameter tension rivets (A_r = 1.20 sq. in.) and the other having four such rivets (A_r = 2.40 sq. in.). The corresponding values for the parameter X are computed to be $330\sqrt{1.20/1.77}$ = 270 and $330\sqrt{2.40/1.77}$ = 380 , respectively; Y is unchanged. The empirical curves and experimental points for these two connections are shown in Figs. 4.7a and 4.7c. In view of the variation to be expected as a result of differences in material yield point and fabrication practice, such good agreement must be considered somewhat coincidental, but nevertheless it does support the proposed formulas.

Riveted Web Clip Angle Connections

Web clip-angle connections are much more flexible than top- and seat-angle conections; therefore, they cannot be counted on to result in any substantial reduction in the moment at the center of beams. Tests have shown that web-angle connections have very good rotation capacity. Thus, their small resistance to moment can be safely neglected and the connections can be treated as entirely flexible except in the case of very deep girders. Some web-angle connections were included in the major test programs on riveted semi-rigid connections (4.1, 4.3).

While the results confirm the above statement in a qualitative manner, insufficient tests on web-angle connections have been carried out to make a distinction between the effects of the variables and the scatter. The results also indicate that the moment-rotation characterisitcs of web-angle connections depend more on the connection itself than is the case with top- and seat-angle connections. The depth of beam and the column face to which the connection is attached are of less importance than the thickness of the web angle and the area and disposition of the rivets holding the connection to the column. A typical moment-rotation relationship for this kind of connection expressed in the logarithmic form is

$$M = 173 \log (580\,\theta + 1). \qquad (4.5)$$

Using the "beam line" construction shown in Fig. 4.2, it can be confirmed that for the flexible beam carrying its appropriate design load, a connection with the above characteristic results in less than 25 percent of the full fixed-end moment. For a stiffer beam, the percentage rigidity of the connection is even less. For example, in conjunction with a 12WF31 beam of 30-

foot span the connection with the characteristic given by Equation 4.5 is 24.6 percent rigid. The beam in this case is supporting a uniformly distributed load which causes a stress of 20 ksi at the center. For a greater stress at the center the percentage rigidity is still less. For a somewhat stiffer beam, a 12WF58 section spanning 20 feet, the percentage rigidity under similar conditions is 12 percent.

Web angles are sometimes added to other types of connections as, for example, a top-, seat-, and web-angle connection. Such combinations result in greater stiffness (4.1, 4.2, 4.3).

Riveted Connections With Structural Tees

Structural tees used in a manner similar to top and seat angles (Fig. 4.8) result in the most rigid connections of the simple types that do not include knee braces or brackets. The reason for this is clear. Whereas the top angle of a top- and seat-angle connection is loaded eccentrically, the load on the top tee is along the center line and causes relatively small deformation. Consequently, the stiffness of such connections, as measured by the slope of the M-θ curve, is five to ten times greater than that of top- and seat-angle connections.

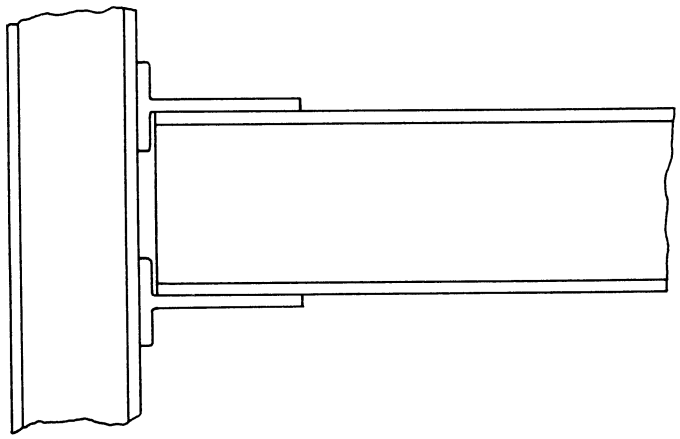

Fig. 4.8
Semi-Rigid Connection With Structural Tees.

Test information on connections employing structural tees is not plentiful and deals in some cases with sections which were never used in this country (4.2) or are now obsolete (4.3).

However, experimental data of the type that has so far been presented in this section are the essential basis for the analysis and design procedures which are discussed later in the chapter. Only very tentative general rules concerning the variation of parameters X and Y in the logarithmic formula can be suggested. To lead up to these rules, expressions corresponding to specific experimental curves will be given and discussed in a qualitative manner.

The following relationships correspond to moment-rotation curves from reference 4.1. All refer to connections made to the column web, thus, details of the column are unimportant. All rivets have 7/8-inch diameters. The seat details are suitably stiffened angles or tees.

Beam Size	Top Detail	No. of Rivets in Hor. Leg	No. of Rivets in Vert. Leg	M-θ Relationship
12WF25	ST 10WF41 x 7-1/2	4	4	$M = 413 \log (300\,\theta + 1)$
18WF47	ST 10WF41 x 7-1/2	4	4	$M = 900 \log (300\,\theta + 1)$
16WF78	ST 12WF37 x 11-1/2	6	8	$M = 1470 \log (300\,\theta + 1)$

It will be noted that there is no variation in the parameter Y, but that X varies over a much larger range than for top- and seat-angle connections. With regard to beam depth, the third connection would be expected to have a value of X lying between those for the first and second connection. In fact X for the third connection is much higher, which must be due to its having twice as many tension rivets. Because of the comparative rigidity of the structural tee, any variation in the stiffness of the rivets is likely to be reflected much more heavily in the shape of the moment-rotation curve than would be the case of top- and seat-angle connections. In fact it is very likely that within the range of practical structural tee connections, the effect of all variables other than beam depth and combined rivet area can be neglected. Proceeding on this basis it is possible to review the results of Rathbun's tests (4.3), which otherwise would have to be ignored because of the outdated sections. It is found that a fair approximation to the actual curves can be achieved by using Y = 300 and using values of X in proportion to beam depth and tension rivet area. (It will be recalled that in the case of the top- and seat-angle connections, the evidence indicated that X varies in proportion to the square root of the tension-rivet area.) This is sufficiently simple so that it is not necessary to produce a graph showing the variation of X and Y with beam depth. The expression representing the moment-rotation curves of Rathbun's connections with structural tees attached to column webs is

$$M = X \log (300\,\theta + 1), \qquad (4.6a)$$

where

$$X = -1315 + 309\,A_r + 82d \qquad (4.6b)$$

and M = moment in in.-lb,
θ = rotation in radians,
A_r = area of tension rivets in top detail in sq in.,
d = depth of beam in inches.

It should be pointed out again that Equation 4.6 does not have a very firm basis, but appears to give quite good results for values of d between 12 a and 18 inches and A_r between 2.4 and 6.3 square inches.

There is no indication as to how X and Y might vary if the connection is made to the column flange, but in the absence of other data, the corresponding information for top- and seat-angle connections indicates the trend.

Welded Nonrigid Connections

Welded nonrigid connections are not used extensively because the requirements for flexibility conflict with those for strength. Whereas riveted joints have an inherent flexibility, welded joints must have this flexibility provided by design if it is required. Flexibility cannot be incorporated in the weld proper, and hence, it must be introduced by a suitable choice of connecting members.

The following three studies are representative of the present status of knowledge on welded nonrigid connections:

"Flexible Welded Angle Connections" by B. G. Johnston and L. F. Green (4.4).

"Tests on Miscellaneous Welded Building Connections" by B. G. Johnston and G. R. Deits (4.5).

"Reports of Tests of Welded Top Plate and Seat Building Connections" by J. L. Brandes and R. M. Mains (4.6).

Johnston and Green (4.4) found that by using very thin top and and seat angles, or web angles, connections can be made which in combination with beams of appropriate dimensions will develop less than 10 percent of the fixed-end moment. The authors list a number of beam-dimension limitations for this type of connection. Considering these limitations and the not too satisfactory behavior of the connections under a relatively small number of repeated loadings, there is little to recommend the use of welded flexible connections over riveted connections.

Of the miscellaneous connections tested by Johnston and Deits (4.5) only those with top plates and seat angles show promise of possessing the characteristics required of semi-rigid connections. The tests of Brandes and Mains (4.6) were carried out solely on top-plate seat-angle connections. They found that the shape and dimensions of the top plate and of the weld

between top plate and beam provide very good control of the moment-rotation characteristics of the connection. The results, in graph form, cover a fairly wide range of beams, columns, and connection details, thus lending themselves readily to interpolation where required. Since all this information is available in one reference (4.6) it is not repeated here.

APPLICATION TO ANALYSIS

Methods for analyzing structures with semi-rigid connections were developed by J. F. Baker (4.7) and were confirmed and extended by Johnston and Mount (4.8), who tested a nearly full scale frame having two stories and three bays under a variety of loading conditions.

Considering a beam AB which forms part of a building frame with rigid connections, the slope-deflection equations read

$$M_{AB} = 2EK\left(2\theta_A + \theta_B - 3\frac{\Delta}{L}\right) - M_{RAB} \quad , \qquad (4.7a)$$

and

$$M_{BA} = 2EK\left(2\theta_B + \theta_A - 3\frac{\Delta}{L}\right) + M_{RBA} \quad , \qquad (4.7b)$$

where the symbols have the customary meaning. In the case of a frame with semi-rigid connections, let it be assumed that the moment at the end A of the beam under is M_a. From the connection moment-rotation characteristic (Fig. 4.9) this would be associated with a rotation θ_a at the connection itself. Let $\alpha = 2EK\,\theta_a/M_a$ and let β be defined in a corresponding manner for the end B. It can be shown (4.8) that for a frame with semi-rigid connections, taking account also of the width of members, Equations 4.7a and 4.7b must be modified to

$$M_{AB} = \frac{1}{1 + 2\alpha + 2\beta + 3\alpha\beta}\left[2EK\left(C_{AA}\,\theta_A + C_{AB}\,\theta_B - C_{AC}\frac{\Delta}{L}\right)\right.$$

$$\left. -F_{AA}M_{RAB} - F_{BA}M_{RBA}\right] + V'_{AB}\,b_{AB} \quad , \qquad (4.8a)$$

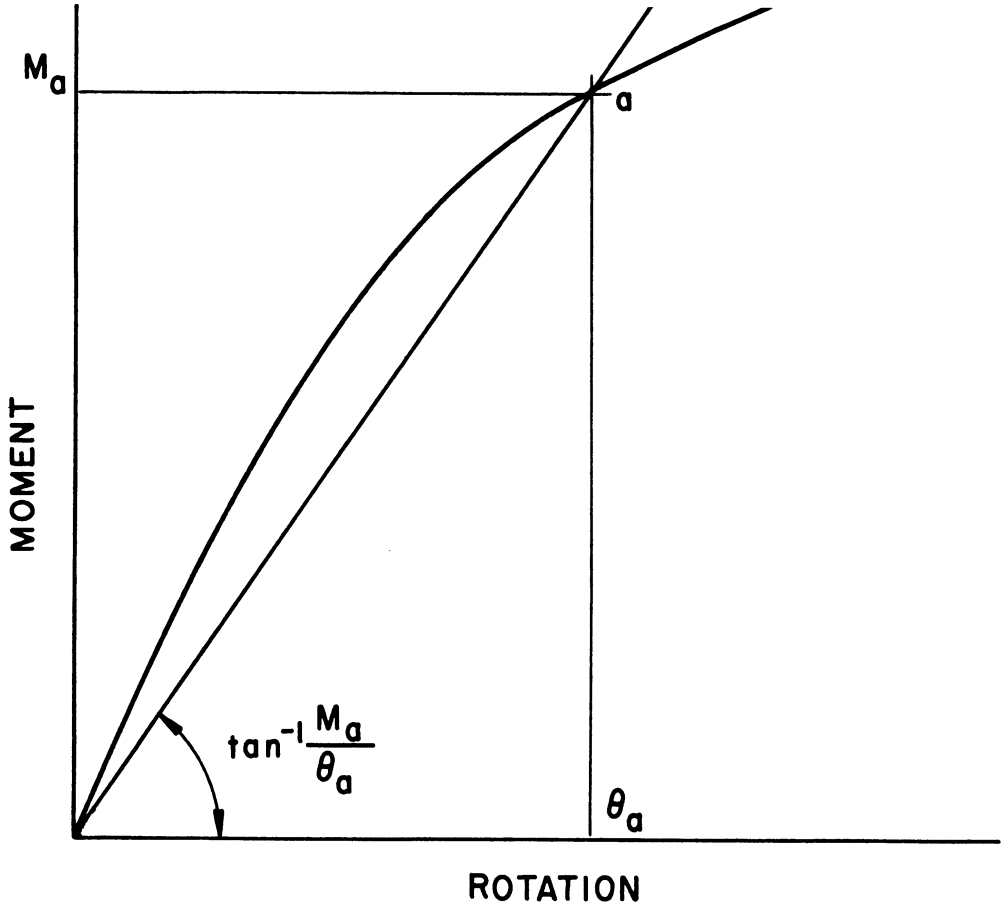

Fig. 4.9
Connection Moment-Rotation Curve.

and

$$M_{BA} = \frac{1}{1 + 2\alpha + 2\beta + 3\alpha\beta}\left[2EK\left(C_{BB}\theta_B + C_{BA}\theta_A - C_{BC}\frac{\Delta}{L}\right) + F_{BB}M_{RBA} + F_{BA}M_{RAB}\right] + V'_{BA}\,b_{BA}\,, \qquad (4.8b)$$

where

M_{AB} and M_{BA} are the moments at the center of joint A and B respectively;

θ_A and θ_B are the total rotations of the member at A and B respectively, i.e., the sum of the rotation of the whole joint and that in the connection;

V'_{AB} and V'_{BA} are the shears that would exist at the ends A and B if the member were simply supported;

b_{AB} and b_{BA} are one-half of the widths of the columns at A and B respectively;

C_{AA}, C_{AB}, C_{AC}, C_{BA}, C_{BB}, and C_{BC} are coefficients whose values are shown in Fig. 4.10.

Figure 4.11 shows a type of member to which Equations 4.8a and 4.8b apply.

Equations 4.8a and 4.8b are not as complex as they appear because the various coefficients are easily computed; thereafter, the equations are used in exactly the same manner as Equations 4.7a and 4.7b. Furthermore, if the connections at the two ends are symmetrical or if the width of the columns can be neglected, the expression for the coefficients are relatively simple.

The chief difficulty in using Equations 4.8a and 4.8b is that the values of α and β depend on an assumed linear relationship between moment and connection rotation. Thus, if the results obtained from Equations 4.8a and 4.8b are widely different from the moments on which α and β are based, the calculation must be repeated.

From the slope-deflection Equations 4.8a and 4.8b the carry-over factors, relative stiffness factors, etc. can be calculated for the moment-distribution method. This has been done in reference (4.8) where the factors are listed in table form.

Also in reference (4.8) the results of the actual tests on a two-story three-bay steel-frame with semi-rigid connections are compared with the moments calculated by the analytical procedure. The agreement is excellent.

THE EFFECT OF NONRIGID CONNECTIONS ON DESIGN PROCEDURE

The primary requirement for all connections, rigid or nonrigid, is capacity to transmit vertical reaction. The design of connections for end reaction is adequately covered by codes, such as that of the American Institute of Steel Construction.

Design Procedure for Vertical Loading

It is evident that the procedure of the last section for analysis is too involved for direct design application. A practical design method developed by Hechtman and Johnston (4.1) gives good results and is very

Coefficient	Nonsymmetrical Semi-Rigid Connections Taking Account of Width of Members	Nonsymmetrical Rigid Width of Members Considered	Nonsymmetrical Semi-Rigid Connections Width of Members = 0	Rigid Connection Width of Members Ignored.
C_{AA}	$2 + 3\beta + 6(1+\beta)\frac{b_{AB}}{\ell} + 3(2+\alpha+\beta)\frac{b_{AB}^2}{\ell^2}$	$2 + \frac{6b_{AB}}{\ell} + \frac{6b_{AB}^2}{\ell^2}$	$2 + 3\beta$	2
$C_{AB} = C_{BA}$	$1 + 3(1+a)\frac{b_{AB}}{\ell} + 3(1+\beta)\frac{b_{BA}}{\ell} + 3(2+\alpha+\beta)\frac{b_{AB}b_{BA}}{\ell^2}$	$1 + \frac{3b_{AB}}{\ell} + \frac{3b_{BA}}{\ell} + \frac{6b_{AB}b_{BA}}{\ell^2}$	1	1
C_{BB}	$2 + 3\alpha + 6(1+\alpha)\frac{b_{BA}}{\ell} + 3(2+\alpha+\beta)\frac{b_{BA}^2}{\ell^2}$	$2 + \frac{6b_{BA}}{\ell} + \frac{6b_{BA}^2}{\ell^2}$	$2 + 3\alpha$	2
C_{AC}	$3(1+\beta) + 3(2+\alpha+\beta)\frac{b_{AB}}{\ell}$	$3 + \frac{6b_{AB}}{\ell}$	$3(1+\beta)$	3
C_{BC}	$3(1+\alpha) + 3(2+\alpha+\beta)\frac{b_{BA}}{\ell}$	$3 + \frac{6b_{BA}}{\ell}$	$3(1+\alpha)$	3
F_{AA}	$1 + 2\beta + (1 - \alpha + 2\beta)\frac{b_{AB}}{\ell}$	$1 + \frac{b_{AB}}{\ell}$	$1 + 2\beta$	1
F_{AB}	$\beta + (\beta - 2\alpha - 1)\frac{b_{AB}}{\ell}$	$-\frac{b_{AB}}{\ell}$	β	0
F_{BB}	$1 + 2\alpha + (1 - \beta + 2\alpha)\frac{b_{BA}}{\ell}$	$1 + \frac{b_{BA}}{\ell}$	$1 + 2\alpha$	1
F_{BA}	$\alpha + (\alpha - 2\beta - 1)\frac{b_{BA}}{\ell}$	$-\frac{b_{BA}}{\ell}$	α	0

Fig. 4.10.
Slope-Deflection Coefficients For Equations 4.8a and 4.8b.

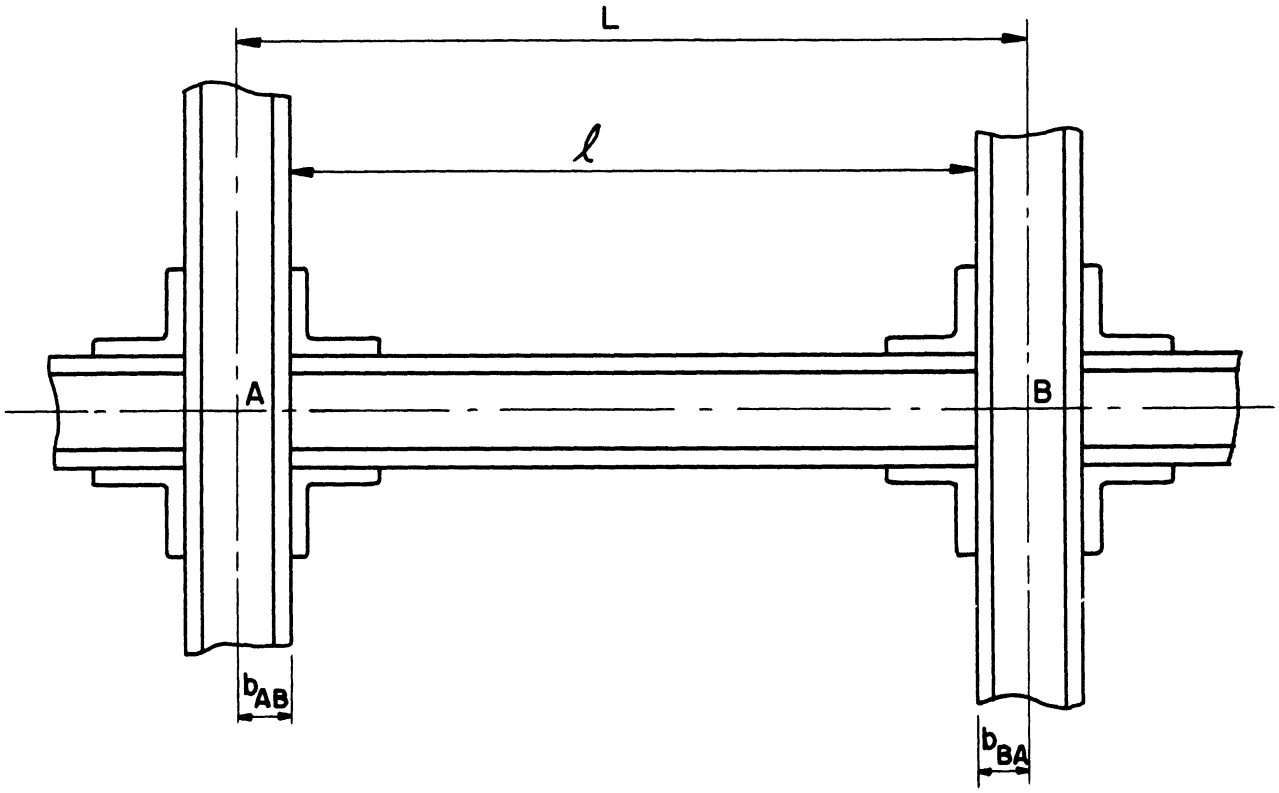

Fig. 4.11.
Beam Attached Through Semi-Rigid
Connections to Columns of Finite Width

simple in application. Using this method, a beam is designed first on the assumption that it is simply supported. A "redesign coefficient" is then determined by which the section modulus of the simply supported beam is multiplied to arrive at a new section modulus. This new modulus is less than the original section modulus, thus taking some advantage of end restraint. However, the results are always on the safe side compared to those obtained by the rigorous analytical method. This design procedure is described in a progress report published by the American Institute of Steel Construction and is readily available (4.1). The various tables and graphs which are required for the use of the method are, therefore, not reproduced here.

The underlying theory of the design procedure will be described briefly. It is assumed that the maximum bending moment in a beam with semi-rigid connections occurs at the center. For uniformly distributed loads this is true if the connections are less than 75 percent rigid, as is the case for most connections classed as semi-rigid. For a central concentrated load the assumption is valid for any percentage of rigidity. Thus, in order to be on the safe side it is necessary to underestimate the rigidity of a connection, rather than to overestimate it.

The minimum dependable rigidty of a connection is computed as follows: from Equation 4.1 the bending moment at the connection is given by

$$M = M_f - 2EK\theta \quad , \qquad (4.1)$$

where M_f is the fixed-end moment for the particular type of loading and θ is the angle through which the end of the beam rotates. It has been shown that by solving Equation 4.1 simultaneously with the M-θ relationship for the connection, the actual values of M and θ may be determined. This is a "cut-and-try" method, since after the values of M and the central moment have been determined, it will normally be found that the beam has not been stressed to its working stress σ_w . If the stress at midspan is a lower or higher than σ_w the procedure is repeated for a new load and M_f. To permit the direct computation of the load which will result in the stress σ_w at the center, Hechtman and Johnston (4.1) propose the use of the "constant stress line" in place of the "beam line" of Fig. 4.2. For example, in the case of a uniformly loaded beam

$$M_f = \frac{wL^2}{12} = \frac{2}{3}(M + \sigma_w S) \quad . \qquad (4.9)$$

Substituting Equation 4.9 in 4.1, results in

$$M = 2\sigma_w S - 6EK\theta \quad , \qquad (4.10a)$$

which can be rewritten

$$M = 2\sigma_w S - \frac{3ES\theta}{L/d} \quad . \qquad (4.10b)$$

Hence, for any value of L/d a number of constant stress lines can be drawn for various values of σ_w . Figure 4.12 is reproduced from reference (4.1). It shows a typical M-θ curve and two constant stress lines for σ_w = 20 ksi and for σ_w = 33 ksi, under the condition of a uniformly distributed design load. The point at which the connection moment-rotation curve intersects the 20 ksi line denotes the end-moment value corresponding to a stress at the

center of the beam of 20 ksi. This value is denoted by M'. If the moment-rotation curve of the connection were a straight line, such as the dash line OD , it would intersect the 33 ksi stress line at 1.65 times the design load; making the safety factor 1.65. Since the connection curve bends over, the maximum stress under 1.65 design load is greater than 33 ksi. Thus, to insure a safety factor of 1.65, it is necessary to make a "limit design" approach to the problem; the 33 ksi stress line is intersected by the connection curve at a value M". This is the end moment corresponding to a stress of 33 ksi at the center of the beam. The corresponding load is divided by 1.65 to arrive at the working load, then the actual end moment is M"/1.65 (point B). It is seen in Fig. 4.12 that this is about 40 percent of the fixed-end moment for the 20 ksi stress line. This is termed the "dependable" percentage of rigidity.

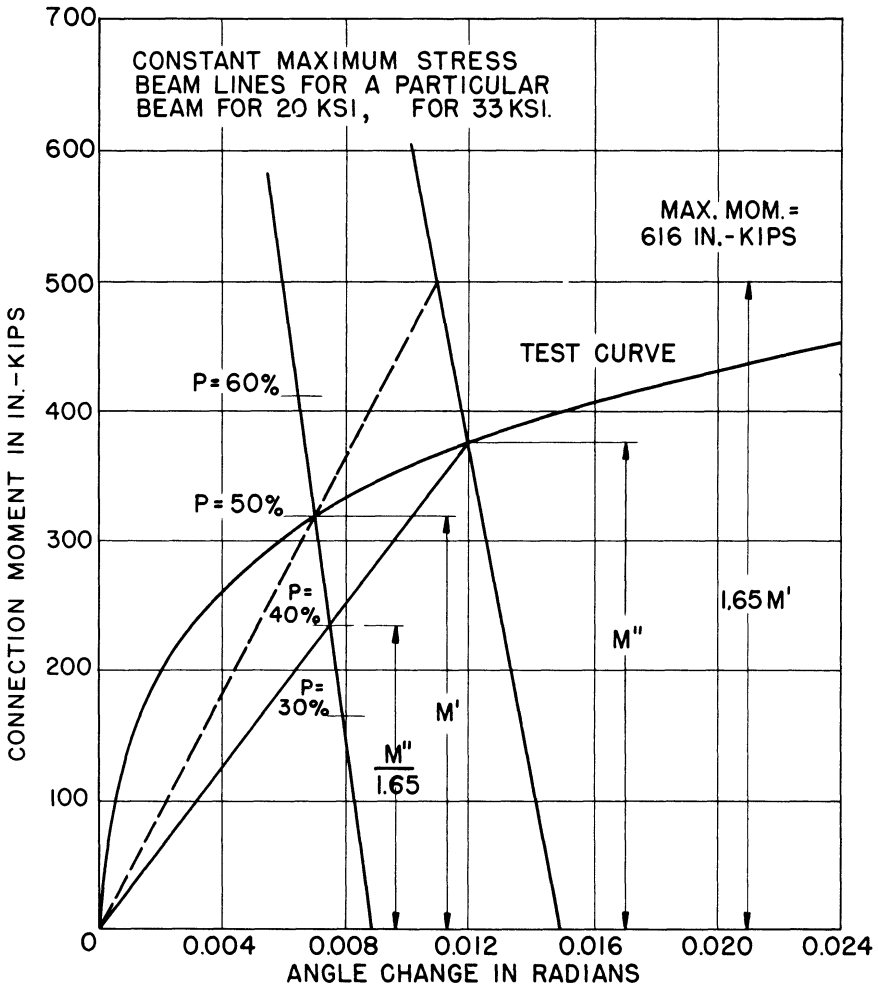

Fig. 4.12.
Typical M-θ Curve For a Connection
Showing Two Constant-Stress Lines

Reference (4.1) contains a table listing the dependable percentage rigidity for a number of semi-rigid connections in combination with various beams within the practical range. Using the logic of moment distribution, Hechtman and Johnston show that for the most severe condition of loading, namely that of alternate spans on alternate floors, the moment at the ends of the beam under consideration must be at least

$$M_f = \left(\frac{1}{\frac{100}{p} + \frac{K_b}{\sum K_c}} \right) \quad ,$$

where K_b = stiffness of the beam, i.e., I/L; and
$\sum K_c$ = sum of the stiffnesses of the columns at one end of the beam.
If the columns at the two ends of the beam are not the same, the smaller value of $\sum K_c$ should be chosen. Let M_s stand for the positive moment at midspan under simple support conditions. The end restraint then causes the actual moment to be $F_L M_s$, where the "redesign coefficient" is given by

$$F_L = 1 - \frac{M_f}{M_s} \left(\frac{1}{\frac{100}{p} + \frac{K_b}{\sum K_c}} \right) \quad , \qquad (4.11)$$

where M_f/M_s is a function of the type of loading and is readily computed. The determination of p , the dependable percentage of rigidity, has previously been discussed in some detail. K_b and $\sum K_c$ must be estimated.

The determination of F_L is facilitated by a number of graphs in reference (4.1), in which F_L is plotted against $K_b/\sum K_c$ for various values of p ranging from 10 to 60 percent. The graphs have been prepared for various types of loading.

The loading on which the coefficient F_L in Equation 4.11 is based results in the most severe stresses at midspan. It is interesting also to consider the load condition which would cause the least possible stresses at the center of a beam. This exists when all spans are loaded in the same manner allowing no rotation at the joints. Under such loading the end moments are $pM_f/100$ and the central moment $M_c = M_s - pM_f/100$. The dead-load redesign coefficient is therefore

$$F_D = 1 - \frac{M_f}{M_s} \left(\frac{1}{\frac{100}{p}} \right) \quad . \qquad (4.12)$$

In most cases at least a third of the loads are of dead-load nature; therefore Hechtman and Johnston propose the use of weighted redesign coefficient

$$F = 1/3\ F_D + 2/3\ F_L \qquad (4.13a)$$

so that

$$F = 1 - \frac{M_f}{M_s}\left[\frac{1 + \frac{pK_b}{300\sum K_c}}{\frac{100}{p} + \frac{K_b}{\sum K_c}}\right], \qquad (4.13b)$$

Values of F are also shown in graph form in reference (4.1). The proposed method of design is summarized as follows:

1. Design the beam for maximum bending moment, assuming simple supports.

2. Calculate K_b for the next lighter beam and $\sum K_c$ for the less stiff of the two supporting columns and then compute $K_b/\sum K_c$.

3. From the table in reference (4.1) find the value of p appropriate to the type of connection and size and span of beam. (If using a combination for which p is not listed in this table, it can be computed by the procedure outlined earlier; provided the moment-rotation characteristic for the connection is known.)

4. Choose the curves appropriate to the type of loading; enter Figs. 14, 15, or 16 of reference (4.1) with the computed value of $K_b/\sum K_c$ and the value of p determined from (3) above, then read off the redesign coefficient F. For interior spans of frames having nearly equal bay widths, the dotted curves giving the weighted coefficients may be used; otherwise, use the solid curves to obtain F_L. If the bending is produced by a combination of uniform loading and concentrated loads, a suitably weighted F coefficient may be derived from the graphs. A single concentrated load may be assumed to be located at midspan, regardless of its actual location, for the purpose of obtaining the F coefficient.

5. Multiply the section modulus from (1) by the F coefficient from (4) and select the lightest beam which will provide a section modulus equal to the product of this multiplication.

6. Repeat the procedure, if economically warranted.

No mention is made in reference (4.1) to any design procedure for the columns in a frame containing semi-rigid connections. The reason may be this; to estimate the highest moments in a beam it is necessary to underestimate the end moments, but for the sake of computing the largest moments that are likely to occur in columns, the end restraints must be overestimated. Consequently, thought must be given to the possible effect of concrete encasement. To be on the safe side it must be assumed that the connections are perfectly rigid. Thus, the connection characteristics are not permitted to play any part in the design of the columns. The design of columns in rigid structures is not within the scope of this study. A procedure proposed by Baker and Williams (4.7) has found little acceptance. A more rapid method, using nomograms, was suggested recently by Wood (4.10).

Design Procedure for Lateral Loading

The discussion is aided by consideration of the diagrams in Fig. 4.13. This figure shows the bending moment diagram in the columns of a tier

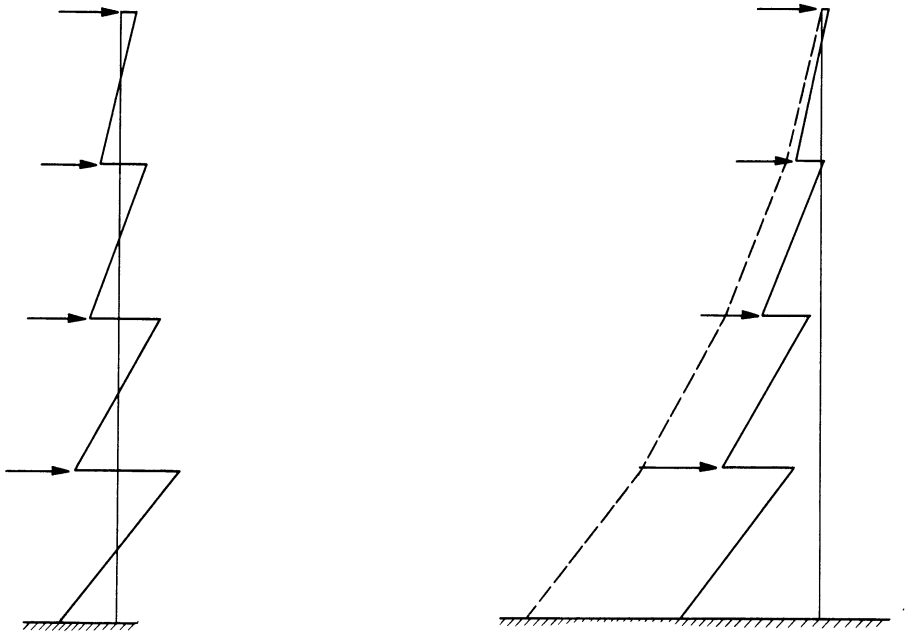

(a) Girders and Connections are Infinitely Rigid.

(b) Girder and/or Connections Are Not Rigid. If Connections Were Pinned, the Bending Moment Diagram is the Dashed Line.

Fig. 4.13.
Diagram of Bending Moment in Column of a Tier Building Under Lateral Load

building which has infinitely rigid girders and connections, this is a hypothetical case. Since the columns are then fully fixed, any moments due to lateral loads are the side-sway fixed-end moments. The points of inflection are at the midheight of each column. The rigidity of the girders thus prevents the accumulation of increments of column moment in excess of the side-sway fixed-end moment. If either the girder connections or the girders are not rigid, then joint rotation will take place with a resulting readjustment of column moments. The lateral loads are then resisted not so much by "shear beam" action of the building as a whole as by "bending beam" action of the columns individually. The more flexible the connections, the greater are the column moments for any given loading. In the extreme case where the connections are pinned, the columns must individually resist all the moment in a cantilever fashion. This is true because the girders cannot transfer the shear between the columns which is essential for integral action of the building as a unit. The condition described is represented by the dashed moment line in Fig. 4.13b.

Consideration of Fig. 4.13 leads to the conclusion that for lateral loads the largest moments in beams occur if the connections are fully rigid. Hence, as in the case of columns under vertical loading, it is conservative in designing the beams to assume that the connections are fully rigid. Any method used for designing beams in a rigid frame structure may, therefore, be used.

The largest stresses in the columns occur when all connections are pinned. To assume such a condition would clearly result in a very uneconomical as well as impractical design, since great flexibility would also be introduced. It is customary, therefore, to include some rigid "wind-bracing" connections in a tall tier building in which mostly semi-rigid connections are used. If wind-bracing connections are omitted in a structure expected to resist lateral loads, it may be necessary to carry out a complete analysis using slope-deflection or moment-distribution.

GENERAL SUMMARY AND CONCLUSIONS

The early part of the chapter presents a statement of problems that arise in structures with nonrigid connections. The importance of rotation capacity, particularly in the case of flexible connections is pointed out. Next, the experimental data on semi-rigid connections are discussed. Whenever possible, analytical expressions are developed to fit the experimental results so that interpolation is made easier.

The analysis of structures with semi-rigid connections is straightforward, though laborious, if the moment-rotation characteristics of the connections are known.

Not too much thought appears to have been given to all aspects of the design procedure for structures with semi-rigid connections. There are four problems; the design of beams and columns for vertical loading and the design of beams and columns for lateral loading. For the design of beams in structures with semi-rigid connections under vertical loading there is a relatively simple and rapid method available that has actually been applied in building design. Because of uncertainties regarding the physical properties of structures the remaining three problems usually reduce to the corresponding rigid frame problems.

BIBLIOGRAPHY-CHAPTER IV

4.1 Hechtman, R. A.
Johnston, B. G.
"Riveted semi-rigid beam-to-column building connections"
Prog Rep No. 1, AISC (Nov 1947)

4.2 Batho, C.
Rowan, H. C.
"The analysis of the moments in the members of a frame having rigid or semi-rigid connections, under vertical loads"
Sec Rep Steel Struct Res Comm 177-97, Dept Sci Ind Res, London (1934)

4.3 Rathbun, J. C.
"Elastic properties of riveted connections"
Trans ASCE 101: 524-96 (1936)

4.4 Johnston, B. G.
Green, L. F.
"Flexible welded angle connections"
Weld J 19: 402s-8s (1940)

4.5 Johnston, B. G.
Deits, G. R.
"Tests of miscellaneous welded building connections"
Weld J 21: 5s-27s (1942)

4.6 Brandes, J. L.
Mains, R. M.
"Report of tests of welded top plate and seat building connections"
Weld J 23: 146s-65s (1944)

4.7 Baker, J. F.
Williams, E. L.
"The stress analysis of steel building frames"
Sec Rep Steel Struct Res Comm 200-40
Dept Sci Ind Res, London (1934)

4.8 Johnston, B. G.
Mount, E. H.
"Analysis of building frames with semi-rigid connections"
Trans ASCE (107): 993-1038 (1942)

4.9 Williams, E. L.
Badland, P. A.
"The effect of lateral load on steel-framed buildings"
J Inst Civ Eng 31: 117-55 (1948)

4.10 Wood, R. H.

"A derivation of maximum stanchion moments in multi-story frames by means of nomograms"
Struct Eng 31: 316-28 (1953)

CHAPTER V

COLUMN ANCHORAGES

To permit the analysis of a complete structure the knowledge of the ultimate strength of the column anchorages must be supplemented by an estimate of their moment-rotation characteristics, particularly so in the case of structures subjected to lateral blast loads.

Analytical and test information on the ultimate behavior of column anchorages is largely lacking and this chapter will present a theoretical analysis of the problem applicable to simple types of anchorages.

The degree to which anchorages affect the capacity of structures to resist lateral loads, such as could occur as a result of a bomb blast, varies with the type of structure. This follows from consideration of the three ways in which a column anchorage can fail:

(1) failure in shear resistance,
(2) failure in moment resistance, and
(3) failure in tensile resistance.

Shear failure of an anchorage might take place in a low, wide building. This failure could take the form of cracking of the concrete pier to which the anchorage is secured or shearing off of the anchor bolts. The latter type of failure might occur due to shear alone or in combination with the applied moment, causing combined tension and shear failure of individual bolts. Anchorages of multistory buildings are unlikely to fail in shear in view of their high degreee of rigidity and the great amount of friction due to vertical loads. While each design should be examined individually, in general the anchorages of tall buildings, being heavily embedded in concrete, can be considered fully fixed; hence, deformation and failure would be governed by the properties of the columns.

A related problem outside the scope of this monograph is the possibility of overall footing failure. Between the two extreme cases of fixed and flexible anchorages is the group encountered in most light industrial buildings. These anchorages consist of plates attached to the bottom of columns and held down by anchor bolts embedded in a concrete pier (Fig. 5.1). The moment-rotation relationship of this type of anchorage will now be investigated, omitting consideration of any relative movement between the concrete foundation and the surrounding soil.

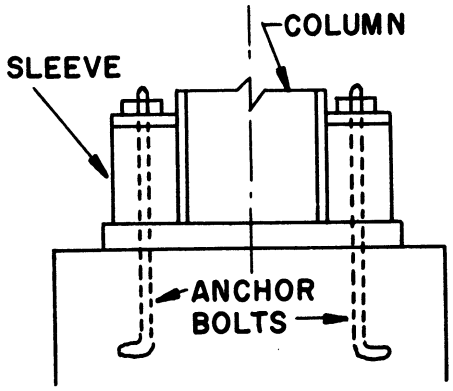

Fig. 5.1.

A number of technical articles have appeared on the subject of the design of simple anchorages (5.6), but a review of literature has not revealed any experimental or analytical investigation of such anchorages. Empirical procedures have been used for design purposes with the knowledge that a large factor of safety is available to absorb discrepancies between the assumptions and the actual behavior of anchorages. The assumptions made in this chapter are more realistic and readily adjustable to results of tests as they become available.

UPPER BOUND* OF MOMENT

Rectangular Base Plate

The most important variables that enter into the moment-rotation relationship of column anchorages are:

(i) dimensions of base plate;
(ii) dimensions, location, and stress-strain characteristics of anchor bolts;
(iii) dimensions and stress-strain characteristics of concrete pier; and
(iv) vertical loading.

*"Upper bound" means an approximate evaluation of a resisting moment below which the actual resting moment must lie.

As a first step in determining the manner in which changes in these variables affect the moment-rotation relationship of the anchorage, the upper bound of the moment and the corresponding minimum rotation will be estimated.

In this chapter symbols are defined when they are used for the first time and a summary of the notation appears at the end of the monograph. Since it is convenient to express many variables in terms of the dimensions of the base plate, all primed symbols signify such a manner of expression. For example, e is defined as the distance of an anchor bolt from the center line of the base plate and $e' = e/(1/2\ d) = 2e/d$. The only exceptions to this use of primed symbols is f'_c, which has the conventional meaning of ultimate concrete (cylinder) compressive strength.

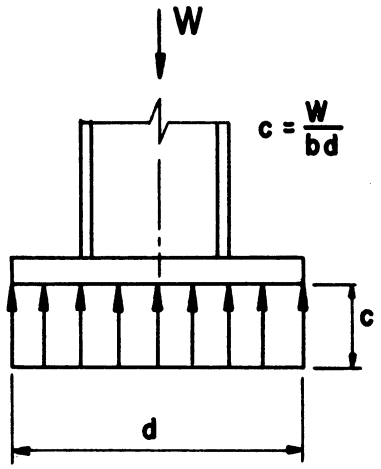

Fig. 5.2.

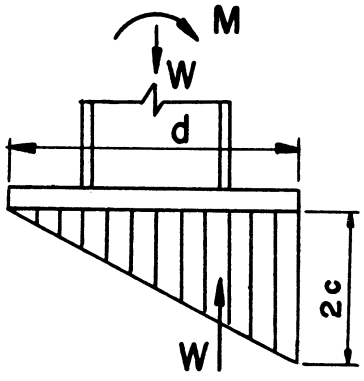

Fig. 5.3.

Upper bound for moment. Consider a column anchorage without anchor bolts as shown in Fig. 5.2. The unit bearing pressure "c" due to a concentric vertical load W is assumed to be uniform. On a concrete foundation the maximum value for c permitted by most codes is 600 or 800 psi. If a moment is now applied by the column, the stress distribution at some stage will be assumed to be approximately as shown in Fig. 5.3. Evidently, the resisting moment is W d/6 , where d is the length of the base plate. If, hypothetically, the concrete had infinite strength and the bearing plate were infinitely rigid, then equilibrium considerations alone would determine the maximum moment that could be resisted. Just before the column toppled over, as shown in Fig. 5.4, the resultant base pressure would be at the edge of the plate and the "upper bound" moment would be

$$M_u = \frac{1}{2} Wd \quad . \qquad (5.1)$$

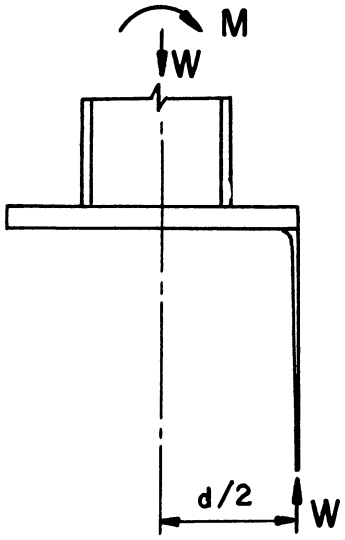

Fig. 5.4.

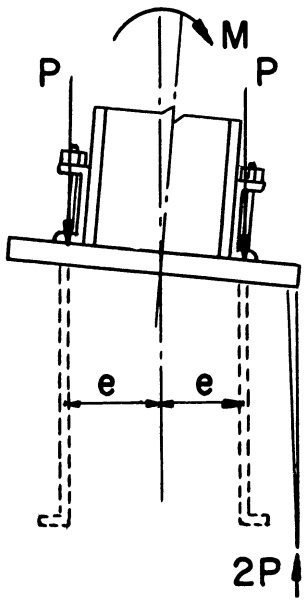

Fig. 5.5.

Next, condsider the same column and base plate arrangement supporting no weight at all, but this time held down by anchor bolts. The plate and the concrete are again assumed as infinitely rigid. The degree to which the bolts have been tightened is immaterial. Let the ultimate strength of the bolt or bolts on either side of the center line of the base plate be P_u. Also, let the distance from the anchor bolts to the center line be e, as shown in Fig. 5.5. In this case the upper bound for the resisting moment is

$$M_u = P_u \left(\frac{d}{2} + e\right) + P_u \left(\frac{d}{2} - e\right)$$

$$= 2P_u \frac{d}{2} \qquad (5.2)$$

Adding the upper bound moments for the two cases (Equations 5.1 and 5.2), The upper bound for moment for an anchorage supporting a weight W and held down by anchor bolts of ultimate strength $2P_u$ is

$$M_u = (W + 2P_u)\frac{d}{2} \qquad (5.3)$$

If interested only in the moment which without any doubt would cause complete structural failure of an anchorage of the type under consideration, Equation 5.3 would provide sufficient information.

The symbol p is now introduced for A_t/bd, where A_t is the cross-sectional area of half the anchor bolts and b is the width of the base plate. Thus p has a meaning similar to that in the reinforced concrete theory.*

* In reinforced concrete theory "d" is the distance from the extreme compression fibers to the reinforcing steel.

$$M_u = (c\ bd + 2p\ \sigma_u\ bd)\frac{d}{2} \quad ,$$

where σ_u = ultimate steel strength.
Thus, $M_u = (c + 2p\ \sigma_u)\frac{bd^2}{2}$.

Writing

$$\frac{M_u}{bd^2} = M_u'$$

$$M_u' = \frac{1}{2}(c + 2p\ \sigma_u) \quad .$$

Hence, the upper bound moment divided by bd^2 is the same for similar anchorages of different size, provided that the original uniform bearing stress and the ratio of anchor bolt area to base plate area remains the same.

Next, a more realistic assumption is made with regard to the concrete strength. The actual ultimate concrete strength depends to some degree on the relative size of the base plate and the concrete footing. It is known that the compressive strength of concrete confined in one or more directions is greater than the value of f_c' determined from standard cylinder tests. It will be assumed, therefore, that the concrete strength is $\alpha f_c'$, where $\alpha \geqq 1$ and must be either estimated or determined by suitable tests.

Theoretical considerations based on elastic theory (5.1) suggest that α might be between 1 and about 1.5. Tests carried out by the Hydro-Electric Power Commission of Ontario (unpublished) on concrete cubes loaded over a small central square indicate that α may be proportional to the cube root of the ratio of total area to loaded area. Values for α as high as 10 have been obtained in tests at the Commission's laboratories.

From the viewpoint of determining the moment resistance of anchorages, the effect of loading a rectangular strip is of more interest than that of loading a small square. Graf (5.2) reports on tests performed on concrete cubes in which ultimate strength under a loading on a strip covering only a third of the top surface was 1.6 times as high as the ultimate strength of a cube loaded uniformly over all its cross section. Loading on a strip one-seventh of the width of the cube resulted in values for α varying from 2.5 to 2.8. Moving the loaded strip toward the edge of the cube resulted in a reduction of α to 1.2 to 1.5. Fortunately, as is shown later, the values

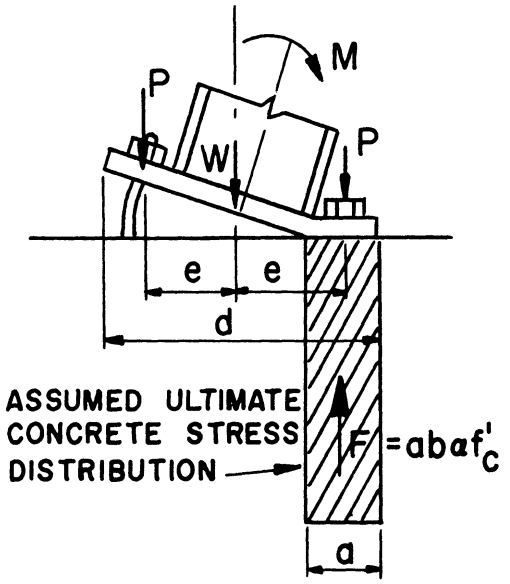

Fig. 5.6.

M_u are relatively insensitive to changes in α. The concrete stress distribution just before failure is likely to be nearly trapezoidal, but it is considered that in view of the large strains involved, no great error is introduced by assuming the stress distribution to be uniform, as shown in Fig. 5.6. Let the width of the strip of concrete in touch with the base plate be a. Then let

$$\alpha f'_c\, ab = W + P_u, \text{ for } \left(\frac{d}{2} - e\right) < a \qquad (5.4a)$$

or

$$\alpha f'_c\, ab = W + 2P_u, \text{for } \left(\frac{d}{2} - e\right) > a \ . \qquad (5.4b)$$

Analyzing first the case when $(d/2 - e) < a$, i.e., the bolts near the compression zone are not effective, and defining a_1 as the width of concrete bearing area in this particular case,

$$a_1 = \frac{W + P_u}{\alpha f'_c\, b} = \frac{(c + p\,\sigma_u)d}{\alpha f'_c}$$

$$M_{u1} = W\left(\frac{d}{2} - \frac{a_1}{2}\right) + P_u\left(\frac{d}{2} + e - \frac{a_1}{2}\right)$$

Writing

$$e' = \frac{e}{(1/2)\,d} = \frac{2e}{d}$$

$$M_{u1} = \frac{cbd^2}{2}\left[1 - \frac{c + p\,\sigma_u}{\alpha f'_c}\right] + \frac{p\,\sigma_u\, bd^2}{2}\left[1 + e' - \frac{c + p\,\sigma_u}{\alpha f'_c}\right],$$

$$M'_{u1} = \frac{M_{u1}}{bd^2} = \frac{1}{2}(c + p\,\sigma_u)\left(1 - \frac{c + p\,\sigma_u}{\alpha f'_c}\right) + \frac{1}{2} p\,\sigma_u\, e' \quad . \qquad (5.5a)$$

For the second case, when

$$\left(\frac{d}{2} - e\right) > a$$

$$a_2 = \frac{W + 2P_u}{\alpha f'_c\, b} = \frac{(c + 2p\,\sigma_u)d}{\alpha f'_c} \quad ,$$

then

$$M_{u2} = W\left(\frac{d}{2} - \frac{a_2}{2}\right) + P_u\left(\frac{d}{2} + e - \frac{a_2}{2}\right) + P_u\left(\frac{d}{2} - e - \frac{a_2}{2}\right)$$

$$= W\left(\frac{d}{2} - \frac{a_2}{2}\right) + 2P_u\left(\frac{d}{2} - \frac{a_2}{2}\right)$$

$$M'_{u2} = \frac{1}{2}(c + 2p\,\sigma_u)\left(1 - \frac{c + 2p\,\sigma_u}{\alpha f'_c}\right) \quad , \qquad (5.5b)$$

which is seen to be independent of e.

M'_{u1} and M'_{u2} are shown in Fig. 5.7, plotted against e' for specific values of c, p, $\alpha f'_c$, and σ_u . The larger one of the two is the upper bound.

In most cases the value of e' does not differ much from 0.8 and the effective value of the upper bound will be in the range where M'_{u1} is greater than M'_{u2} . In the following, the expression for M'_{u1} will be used for M'_u with rectangular base plates.

A study of Equations 5.5a and 5.5b reveals that in any practical case all variables except $\alpha f'_c$ are known. To illustrate the effect on M'_{u1} of any error in estimating $\alpha f'_c$ the graph in Fig. 5.8 was prepared, again using specific typical values of c, p, e', and σ_u. M'_{u1} is greater than M'_{u2} up to values of $\alpha f'_c$ of about 11000 psi which is near the limit of practicality. Hence, M'_{u1} is the effective upper bound all the way. The change in M'_{u1} for a change in $\alpha f'_c$ from 4000 to 8000 psi is only 7 percent. Even if a considerable error is made in estimating $\alpha f'_c$, a fairly accurate estimate of M_u should be possible.

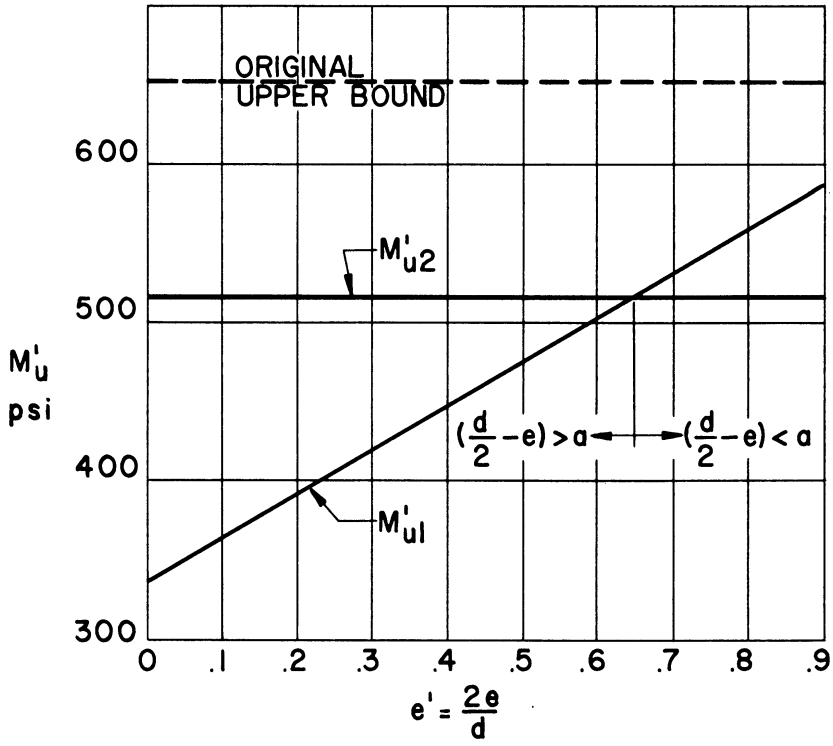

Fig. 5.7.
Upper Bound for Moment: Variation With Eccentricity Using the Following Typical Values; $\alpha f'_c$ = 6000 psi, c = W/bd = 300 psi, $p\sigma_u$ = P/bd = 500 psi.

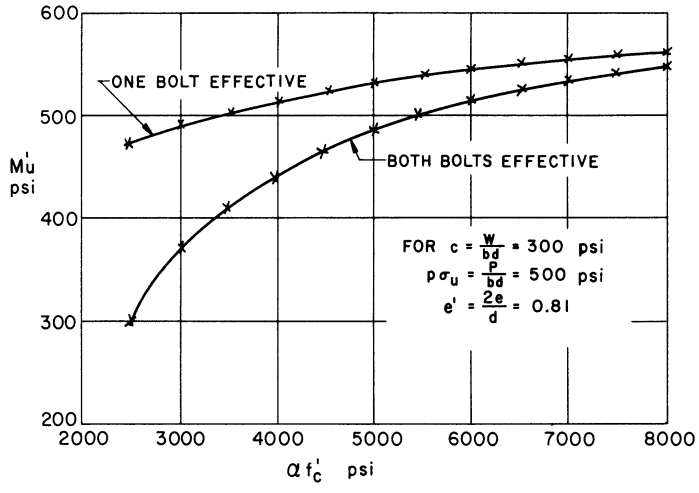

$$M'_{u_1} = \frac{M_{u_1}}{bd^2} = \frac{1}{2}(c+p\sigma_u)\left(1-\frac{c+p\sigma_u}{\alpha f'_c}\right)+\frac{1}{2}e'p\sigma_u \quad \text{.....(5.5a)}$$

$$M'_{u_2} = \frac{M_{u_2}}{bd^2} = \frac{1}{2}(c+2p\sigma_u)\left(1-\frac{c+2p\sigma_u}{\alpha f'_c}\right) \quad \text{.....(5.5b)}$$

Fig. 5.8.
Upper Bound for Moment: Variation With Ultimate Concrete Strength.

No assumption has been made in the above as to the manner of application of the moment because such an assumption is not required. The moment which is considered here is the total external moment and in the case of large lateral displacements of the structure, vertical loads may be responsible for a considerable fraction of the total moment.

Lower bound for rotation. The amount of rotation associated with the ultimate moment cannot be estimated with any degree of accuracy, since it depends to a large extent on the elongation of the anchor bolts. It was pointed out in Chapter I that the bolt elongation is more variable than that of plain rods and although the elongation of a tensile specimen made of the same material may be 20 to 30 percent, the bolt may elongate no more than 5 percent at failure. However, it is possible to estimate a minimum value for the rotation based on the extension of the bolt at the maximum stress.

From Fig. 5.9 the lower bound for the rotation is

$$\theta_L = \frac{\epsilon_u (L_1 + L_2)}{(\frac{d}{2} + e - a)} ,$$

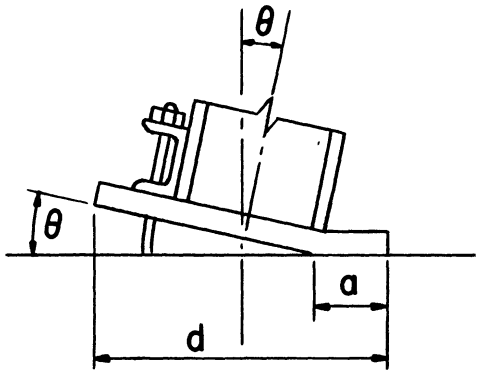

Fig. 5.9.

where ϵ_u = strain, corresponding to the maximum stress for the material of the anchor bolts (from stress-strain diagram); L_1 = length of bolt above the surface of the concrete; and L_2 = equivalent free length of embedded portion of the bolt (see Appendix 5.1). L_2 can be taken at least 8 times the diameter of the plain portion of the bolt (see Appendix 5.1).

Circular Base Plate

Pipe columns, such as those used to support water towers, rest on circular base plates and these can be treated similarly to rectangular plates. The case with two diametrically opposed anchor bolts is considered here, but other types of anchorages can be analyzed in a similar manner to find the upper bound moment.

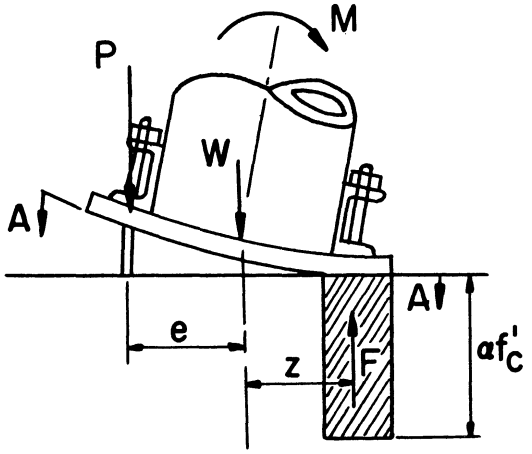

As in the case of rectangular plates, it is assumed that at the ultimate moment only part of the base plate is in contact with the concrete (Fig. 5.10) and that the bearing pressure there is uniform and equal to $\alpha f'_c$. The distance to the center of gravity of the compression area from the center of the base plate is

$$z = \frac{d \sin^3 \gamma}{3 (\gamma - \sin \gamma \cos \gamma)} .$$

With one bolt ineffective because it is in the compression zone,

$$M_{u1} = Wz+P_u(z+e) = Wz+A_s\sigma_u(z+e) .$$

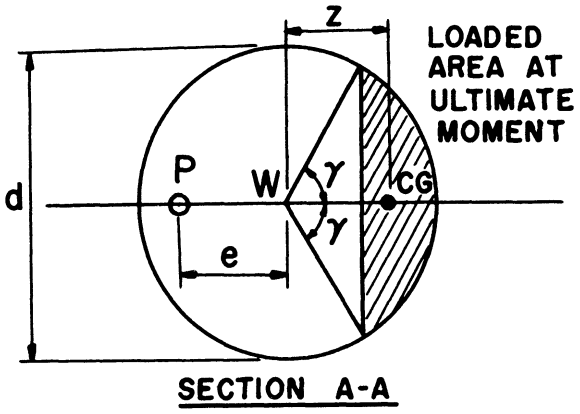

Fig. 5.10.

Let, $M_{u1} = \frac{M_{u1}}{\frac{\pi}{4} d^3}$

$$c = \frac{W}{\frac{\pi}{4} d^2}$$

$$p = \frac{A_t}{\frac{\pi}{4} d^2},$$

$$e' = \frac{e}{\frac{1}{2} d}$$

$$M'_{u1} = \frac{(c + p\ \sigma_u) \sin^3 \gamma}{3(\gamma - \sin \gamma \cos \gamma)} + \frac{p\ \sigma_u\ e'}{2} , \qquad (5.6)$$

which can also be written

$$M'_{u1} = \frac{\alpha f'_c \sin^3 \gamma}{3} + \frac{P\ \sigma_u\ e'}{2} .$$

Furthermore, since at the stage considered the compression force in the concrete must equal the ultimate strength of one bolt plus the load W,

$$\left(\frac{d^2}{4}\gamma - \frac{d^2}{4}\sin\gamma\cos\gamma\right)\alpha f_c' = p\pi\frac{d^2}{4}\sigma_u + c\pi\frac{d^2}{4}$$

$$\alpha f_c' = \frac{\pi\,(p\,\sigma_u + c)}{\gamma - \sin\gamma\cos\gamma} \quad . \qquad (5.7)$$

It is difficult to eliminate γ from Equations 5.6 and 5.7, but they can be used together with γ as a parameter in the same way as Equation 5.5 is used alone. For example, a curve relating M_{u1}' to $\alpha f_c'$ can be plotted (Fig. 5.11). Comparing Figs. 5.11 and 5.8 it is seen that for the same values of $\alpha f_c'$, M_{u1}' is slightly smaller for a circular base plate. It should be recalled, however, that the factor by which M_{u1}' is multiplied in the two cases to obtain the upper bound moment is not the same.

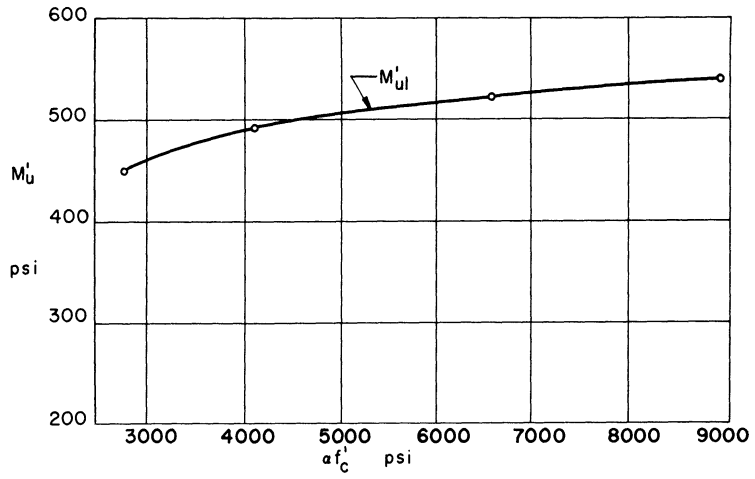

FOR A CIRCULAR BASE PLATE WITH TWO ANCHOR BOLTS

$$M_{ul}' = \frac{\sin^3\gamma}{3(\gamma - \sin\gamma\cos\gamma)}(c + p\sigma_u) + \frac{p\sigma_u e'}{2} \qquad \ldots(5.6)$$

$$\alpha f' = \frac{\pi(p\sigma_u + c)}{\gamma - \sin\gamma\cos\gamma} \qquad \ldots(5.7)$$

WHERE γ IS THE ANGLE SHOWN IN FIG. 5.10

Fig. 5.11.

Variation of Upper Bound Moment With Ultimate Concrete Strength For a Circular Base Plate

EFFECT OF SHEAR

Horizontal shear on a simple anchorage is resisted by the anchor bolts and by friction. The resistance of the anchor bolts is, of course, the shear strength multiplied by the cross-sectional area.

The horizontal resistance due to friction is μW. When the base plate has rotated so as to cause its toe to dig into the concrete, larger horizontal forces might be transmitted.

In analyzing the effect of the friction forces alone (assuming uniform bearing pressure) it is found that they produce compression in a horizontal direction under one-half of the base plate and tension under the other half. The variation of these stresses is shown in Fig. 5.12 and, theoretically, infinite stresses exist near the edges. Actually, plastic deformation reduces the peaks and, furthermore, when cracks on the tension side reduce the rigidity of the concrete on that side most or all the resistance is provided on the compression side. When the toe of the base plate digs into the concrete, all the resistance is concentrated along one line. Tracing further the path of the horizontal forces it is found that unless the footing is completely embedded in fairly rigid material, the forces have to be transmitted to lower parts of the footing through shear along sections such as AA in Fig. 5.13. When the horizontal load is concentrated at the toe of the base plate, the distance AA is quite short and the high diagonal tension may result in the corner of the footing spalling off. Failure due to excessive compression could, however, be evidenced by smilar symptoms and the two should not be confused. The conclusion to be drawn from this discussion is that not all the horizontal resistance which appears to be available as a result of friction between base plate and concrete may be effective, owing to the possibility of premature failure in another mode.

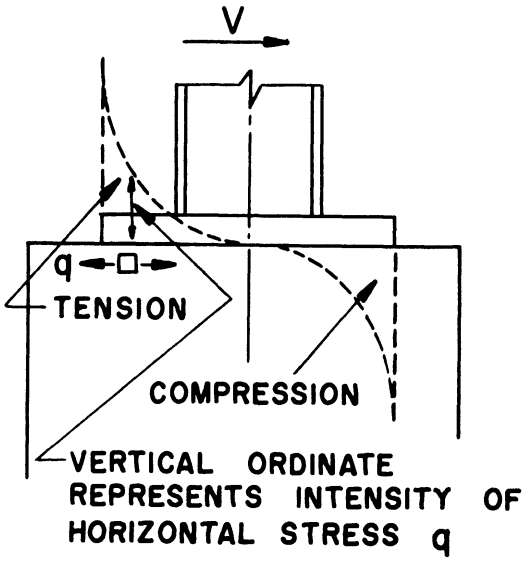

Fig. 5.12.

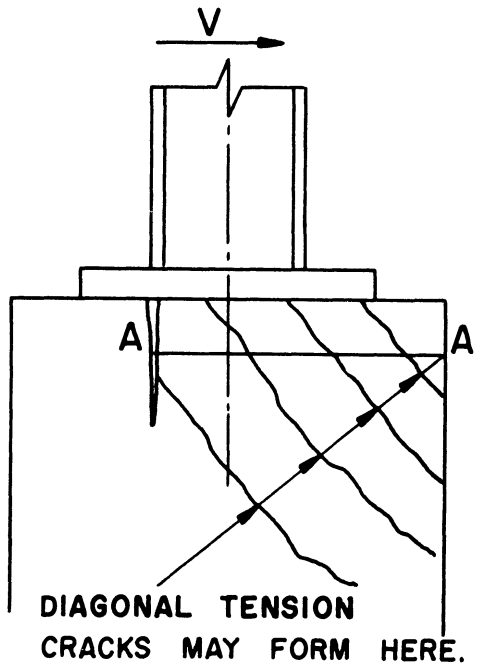

Fig. 5.13.

The Effect of Shear On the Ultimate Moment

The effect of combined tension and shear on the strength of a rivet was discussed in Chapter I. It was shown by Cox (1.7) that the relation between the tensile and shear components and their resultant at failure can be represented by a quarter ellipse, as shown in Fig. 5.14. It is proposed to assume that a similar relationship holds good for the unthreaded portion of an anchor bolt.

The question arises, what fraction of the ultimate tensile strength of the anchor bolts is available to resist moment if shear forces are also acting on the bolts. If $r\sigma_u$ is this fraction when the shear stress on the anchor bolts is τ, then from Fig. 5.14 the relation between τ, r, σ_u is

$$\tau = \frac{3\sigma_u}{4}\sqrt{1 - r^2}$$

Let the shear force causing this shear stress be V_s. Since this force is resisted by all the anchor bolts,

$$V_s = 2A_t\tau = 2p\ bd\ \tau \quad .$$

Furthermore, let the additional shear force due to friction between the base plate and the concrete be $V_F = \mu F = \mu(W + P)$.* Hence, the total applied shear $V = V_s + V_F$. Set the ratio $M_u/V = h = h'd$, i.e., the distance from the base plate at which the shear V would have to be applied to result in a moment M_u.

* The full frictional force is used here for illustration, but its complete omission does not greatly affect the numerical results.

Now

$$\tau = \frac{V_s}{2pbd} = \frac{V - V_F}{2pbd} = \frac{\frac{M_u}{h'd} - \mu(W + P_u)}{2pbd} \quad .$$

Dividing numerator and denominator by bd,

$$\tau = \frac{M_u'}{2ph'} - \frac{\mu\,(c + pr\sigma_u)}{2p} \quad .$$

Equating the two expressions for τ ,

$$\frac{3\sigma_u}{4}\sqrt{1 - r^2} = \frac{M_u'}{2ph'} - \frac{\mu c}{2p} - \frac{\mu r \sigma_u}{2} \quad ,$$

and hence

$$h' = \frac{(c + pr\sigma_u)\left(1 - \frac{c + pr\sigma_u}{\alpha f_c'}\right) + pr\sigma_u e'}{3p\sigma_u\sqrt{1 - r^2} + 2\mu(c + pr\sigma_u)} \quad . \qquad (5.8)$$

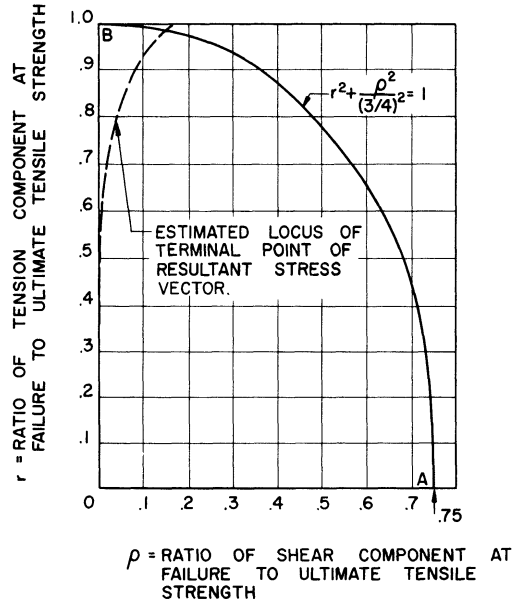

Fig. 5.14.
Effect of Combined Shear and Tension on Ultimate Strength of Round Steel Bar.

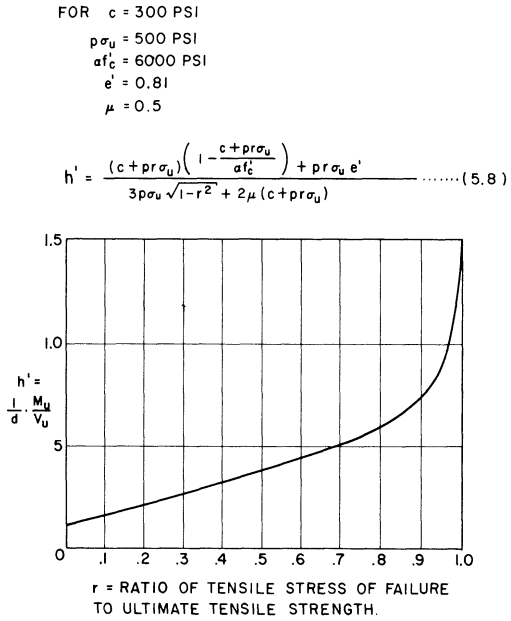

Fig. 5.15.
Effect of Moment-Shear Ratio On Ultimate Anchor Bolt Strength.

Equation 5.8 establishes a relationship between h' and the fraction r of the ultimate tensile strength that can be counted on at failure. The relationship is shown in graph form in Fig. 5.15 for some typical values of c, p, σ_u, $\alpha f'_c$, e', and μ . This shows that for values of $h > 1.38\ d$, $r = 1$, i.e., no shear stress exists in the anchor bolts, implying that all the shear is resisted by friction.

Although the shape of the graph would change with different values of the various parameters, it is evident that only for very small values of h would the ultimate tensile strength be seriously reduced by the action of shear. As the anchorage yields and rotates, the value of h decreases and h will approach zero as the plastic hinge forms. This could change the relative magnitude of the shear and tensile components in a manner illustrated by the dotted line CC in Fig. 5.14. The point C determines the stress components at failure. Although free rotation may eventually take place it is unlikely that C will be below $r = 0.9$. In general, it is suggested that, in regard to the degree of accuracy to which the ultimate strength is known, the effect of shear on the ultimate strength can be neglected.

THE GENERAL MOMENT-ROTATION RELATIONSHIP

The method described earlier of calculating the upper bound for the resisting moment of an anchorage, apart from being of interest in itself, helps to visualize the relation between the variables at all stages.

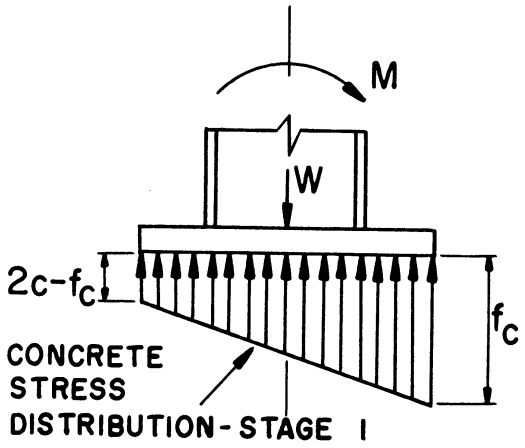

Fig. 5.16.

Let it be assumed that during the first stage of application of moment the concrete stress distribution is as shown in Fig. 5.16. If the highest stress is f_c, then the least stress must be $2c - f_c$, since the average stress is $W/bd = c$. At the end of stage 1, $2c - f_c = 0$, i.e., $f_c = 2c$.

During the stage 2 the point of zero stress moves across from the edge of the plate toward the first anchor bolt. Stage 2 ends as the point of zero concrete stress passes the anchor bolt, i.e., when tensile stress is induced in the bolt.

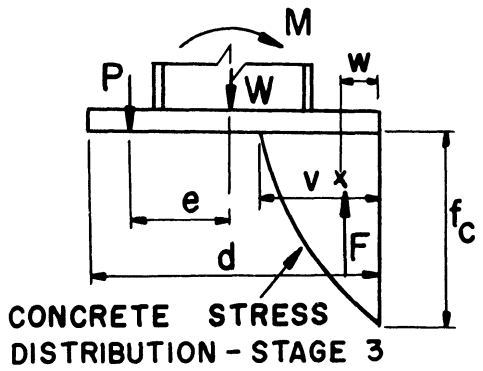

Fig. 5.17.

Stage 3 is considered to end when yield point stress is first reached in the anchor bolts. The forces on the anchorage during stage 3 are shown in Fig. 5.17. Equilibrium considerations yield only one equation, namely

$$P + W = F ,$$

but this is not sufficient to permit the calculation of the concrete stress distribution diagram. Specifically, the distance w, shown in Fig. 5.17, is required to calculate values of M at any stage,

$$M = W\left(\frac{d}{2} - w\right) + P\left(\frac{d}{2} + e - w\right) ,$$

or if

$$w' = \frac{w}{\frac{d}{2}} = \frac{2w}{d}$$

$$M' = \frac{1}{2}\,(c + p\sigma)\,(1 - w') + \frac{1}{2}\,p\sigma\,e'. \qquad (5.9)$$

Stage 4 is considered to terminate when the anchor bolt strain reaches the strain hardening range. Expression 5.9 for M' still applies, but the value of w' is now different from that in stage 3. The remaining stage, up to failure, is called stage 5.

In a previous section of this chapter the ultimate value of M' was estimated by assuming that the concrete stress just before failure would be uniformly distributed and equal to the ultimate concrete strength as modified by the prevailing conditions of restraint.

To estimate the value of θ, the angle of rotation of the column base, corresponding to a moment M and a steel stress σ the strains at the end of stage 1 are considered, i.e., when the concrete stress is zero under one edge

of the base plate and 2c under the other edge. The difference in the displacement at the two edges can be approximately calculated in two ways. Assuming that the depth to which the stresses are transmitted is equal to width d and ignoring the effect of the concrete all around the base plate, the differential movement is $2cd/E_c$ and $\theta = 2c/E_c$. Alternatively, Timoshenko (5.1) gives an expression for the average deflection under a rectangular plate subject to a load F, namely,

$$F \frac{(1 - \nu^2)}{E_c \sqrt{bd}} \qquad \text{approximately, } (\nu = \text{Poisson's ratio})$$

$$= \frac{(c + p\sigma)\, bd\, (1 - \nu^2)}{E_c \sqrt{bd}} = \frac{(c + p\sigma) \sqrt{bd}\, (1 - \nu^2)}{E_c} .$$

Assuming that the maximum deflection is twice the average deflection,

$$\theta = \frac{2 \sqrt{bd}\, (1 - \nu^2)}{E_c\, d}$$

and when numerical values are substituted, the result is practically the same as obtained from the first expression for θ.

The second stage is only of brief duration and can be treated similarly to stage 1. In the third, fourth, and fifth stages rotation is due to three causes: (i) extension of the anchor bolts; (ii) compression of the concrete; and (iii) flexure of part of the base plate. A knowledge of the anchor bolt extension and the distance v (see Fig. 5.17) would permit the calculation of θ for any value of σ and for any value of M', if w were also known. In this stage

$$\theta = \frac{\sigma\, L_e}{E_s \left(\frac{d}{2} + e - v \right)} \qquad (5.10)$$

where $E_s = \sigma/\epsilon$ = stress/strain, for any point on the stress-strain diagram of the anchor bolt material in the elastic or plastic ranges, and L_e is the equivalent total length of the anchor bolts. By L_e is meant the length of a similar bolt, not embedded but fixed at the end only, that would have the same extension under a stress σ.

The above considerations on the M-θ relationship can be summarized as follows: If M' were plotted against θ, then the first part of the graph would be a straight line of approximate slope, $(c/6) \div (2c/E_c) = E_c/12$. From there on the Equations 5.9 and 5.10 with σ as parameter determine the shape of the curve.

It was pointed out earlier that the values v' and w', the equivalent anchor bolt length Le, as well as the stress-strain relationship of the anchor bolts, must be known before the M'-θ curve can be drawn. Sufficient basic test information exists to make possible a fairly accurate estimate of the stress-strain relationship of the anchor bolts. An idealized curve is shown in Fig. 5.18, drawn as far as the maximum stress value. Alternatively, it would be relatively easy to actually test anchor bolts of a type proposed in any new design.

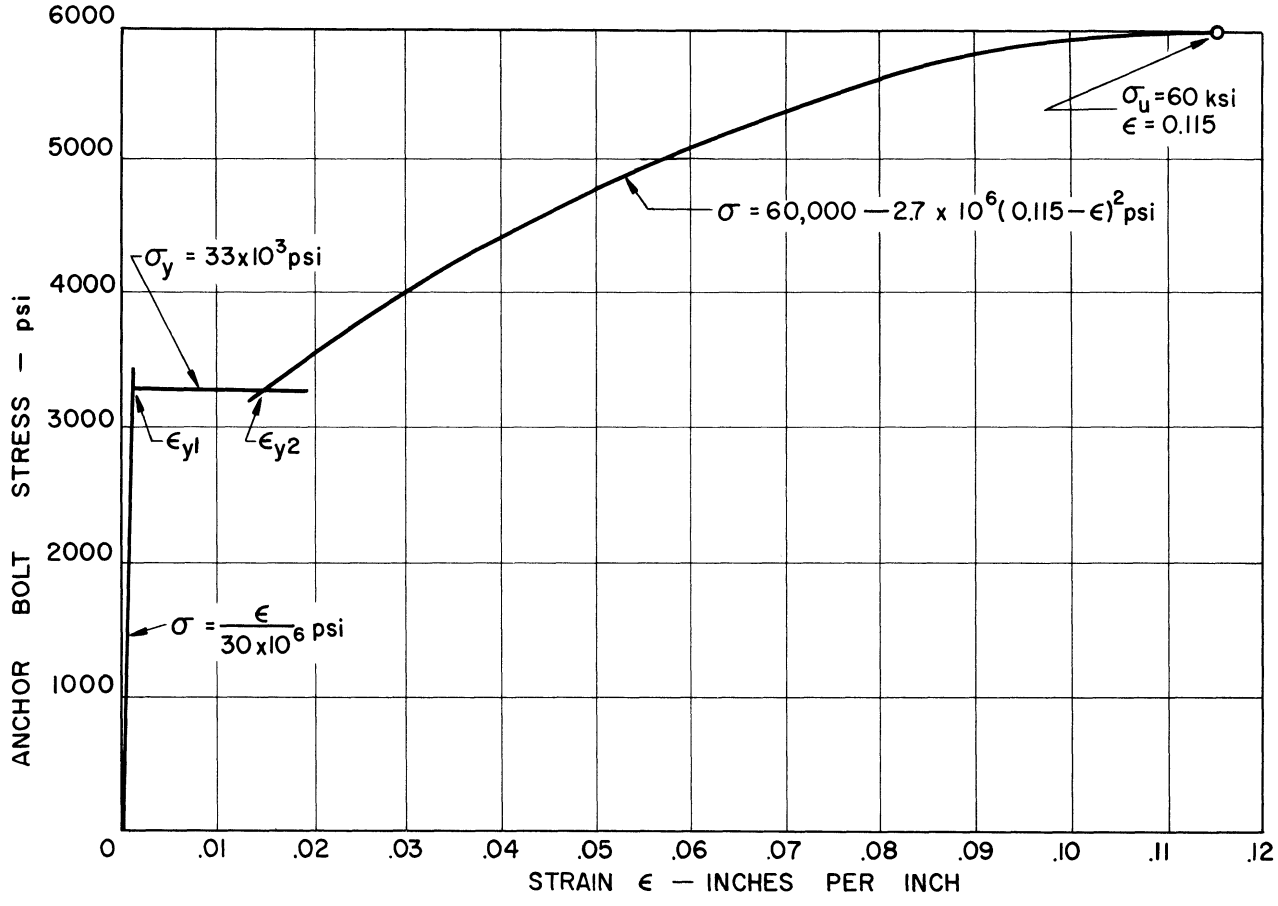

Fig. 5.18.
Idealized Stress-Strain Curve
For Anchor Bolts.

The estimate of L_e , the sum of L_1 and L_2 , is somewhat more difficult. However, it is possible to proceed as follows: Gilkey (5.4) suggests that for a long embedded steel bar being pulled out of concrete bond is not effective over the whole length of the bar, but that it is effective only over a length of about 24 diameters. Assuming that this is so, the tensile stress in the bar decreases from σ at the point where it emerges from the concrete to zero at 24D (D = diameter of bar). It is shown in Appendix 5.1 that the length of bar L_2 , which under a stress σ would strain by an amount equal to the slip s of the embedded bar, is equal to the distance of the center of gravity of the bond stress diagram from the concrete edge at the loaded end. Hence, to be able to estimate L_2 the bond stress distribution must be assumed. Assuming a linear decrease of bond stress from a value u_o at the loaded end to zero at 24 D ,

$$L_2 = 1/3 \times 24D = 8D$$

and

$$L_e = L_1 + 8D \quad .$$

The length L_1 of anchor bolt above the concrete surface is known and so is D.

If v and w (Fig. 5.17) are known at the various stages, the M'-θ diagram can be drawn. When this is done an M'-θ curve such as the one in Fig. 5.19 would result for a particular combination of values of p, c, $\alpha f'_c$, e, L, and a given anchor bolt stress-strain diagram. The initial slope of the curve has been estimated to be $E_c/12$. The ultimate values of M' and θ estimated earlier in this chapter were based on the assumption of rectangular bearing stress distribution. Hence, the coordinates of the terminal point of the curve can be estimated and the slope of the curve at that point would be zero. To fill in the rest of the curve, the bearing stress distribution must be estimated at intermediate stages, i.e., the values of v and w must be estimated. For this purpose it is considered justifiable to make use of the reinforced concrete theory for the stresses at the end of stage 3 (yield point reached) and a modified theory for the stresses at the end of stage 4 (strain-hardening range reached). (The modification consists of assuming trapezoidal stress distribution at the end of stage 4, with the maximum bearing stress limited to $\alpha f'_c$.)

Details of typical computations to obtain the M-θ curve in the manner outlined above are shown in Appendix 5.2 and the results are plotted in Fig. 5.19. In Fig. 5.19 there are two points marked A and B which give an idea of the sensitivity of the method to variations in assumptions. Point A corresponds to point (3), but a modular ratio of 10 was used for (3), whereas 15 was used for A. Point B corresponds to point (4), but rectangular stress distribution was assumed for B (similar to the distribution at failure), whereas trapezoidal distribution was assumed for (4).

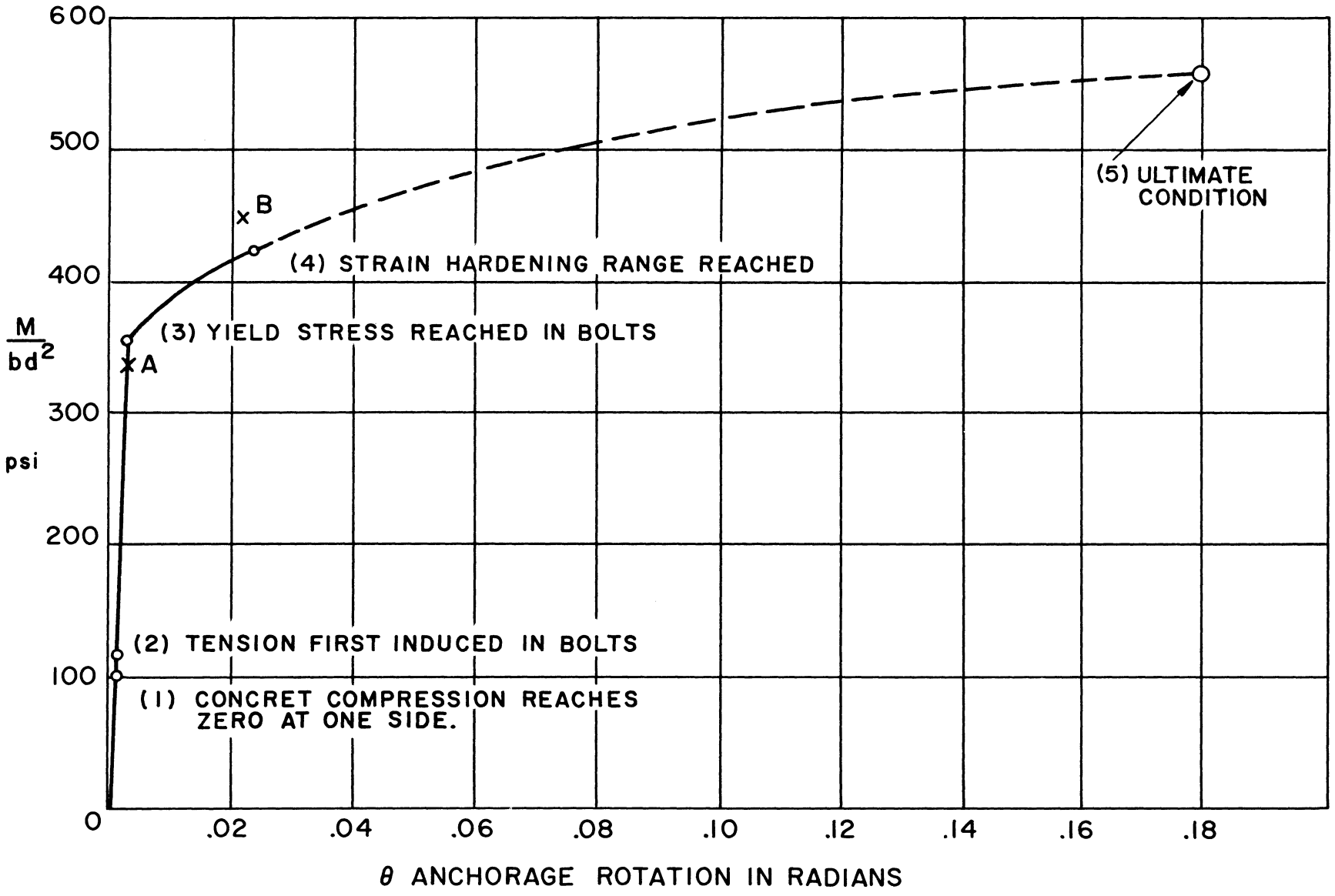

Fig. 5.19 Typical Theoretical Moment-Rotation Curve For Simple Column Anchorage
p = 0.6%; c = 600 psi; σ_y = 33000 psi; σ_u = 60000 psi;
$\alpha f'_c$ = 6000 psi; e = .4d; L_1 = 2d/3.

Figures 5.20 to 5.23 further illustrate the effect on the M-θ curve of the variation of c, $\alpha f'_c$, e, and L_1. The effect of increasing p would be similar to that produced by increasing c, i.e., it would result in more rigidity and a higher ultimate resistance moment. The effect of changes in the concrete strength is not very pronounced. The result of reducing e to zero is interesting because such a procedure could be followed for estimating the M-θ curve for anchorages with only two bolts about an axis joining the bolts, i.e., about the axis of least resistance.

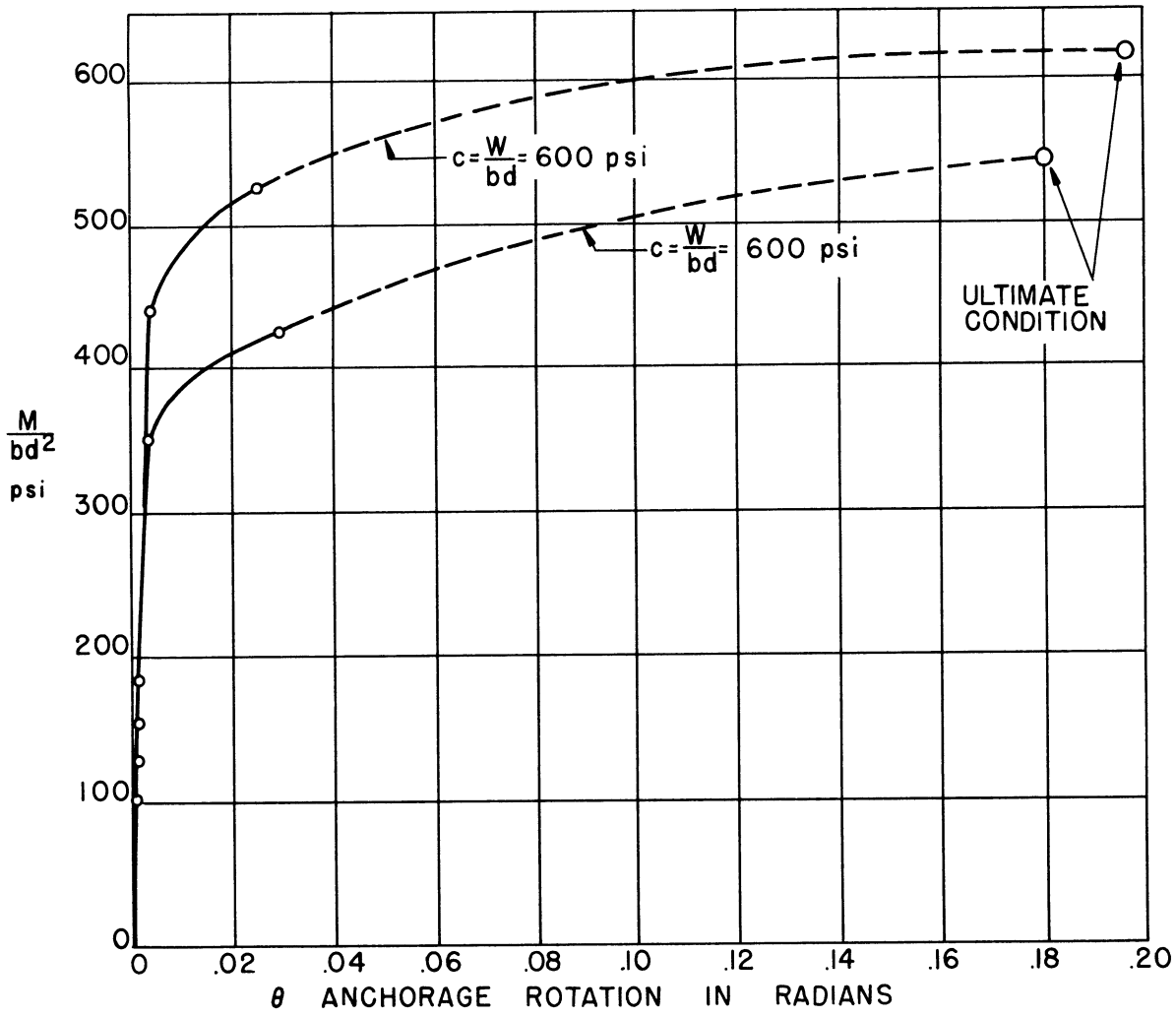

Fig. 5.20 The Effect of Different Initial Bearing Stresses, For p = 0.6%; σ_y = 33000 psi; σ_u = 60000 psi; $\alpha f'_c$ = 6000 psi; e = .4d; L_1 = 2d/3.

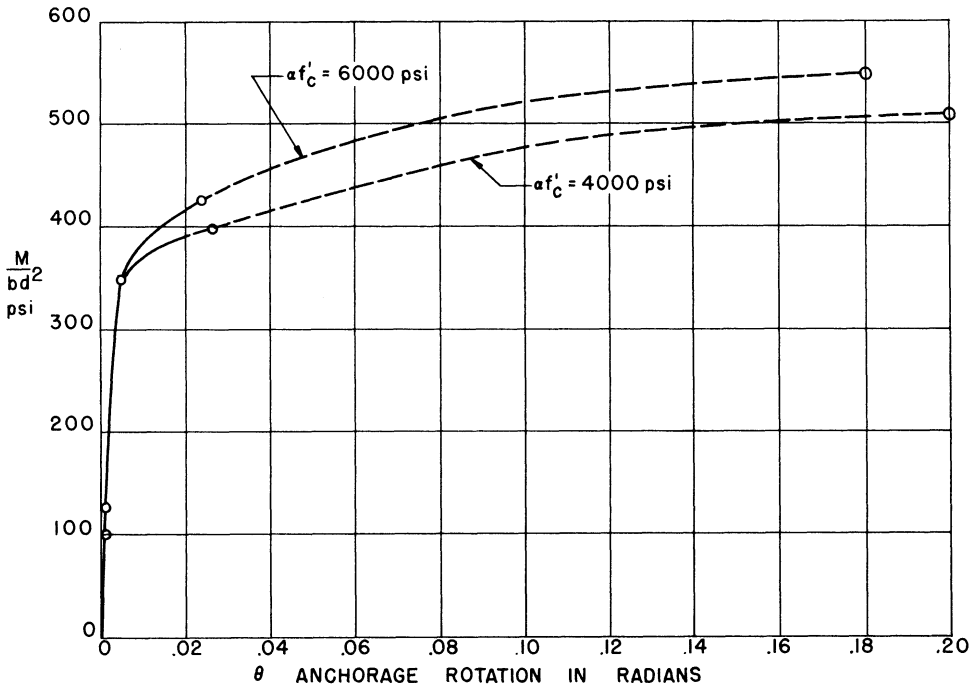

Fig. 5.21 The Effect of Variations in the Concrete Strength.
p = 0.6%; c = 600 psi; σ_y = 33000 psi; σ_u = 60000 psi; e = .4d; L_1 = 2d/3.

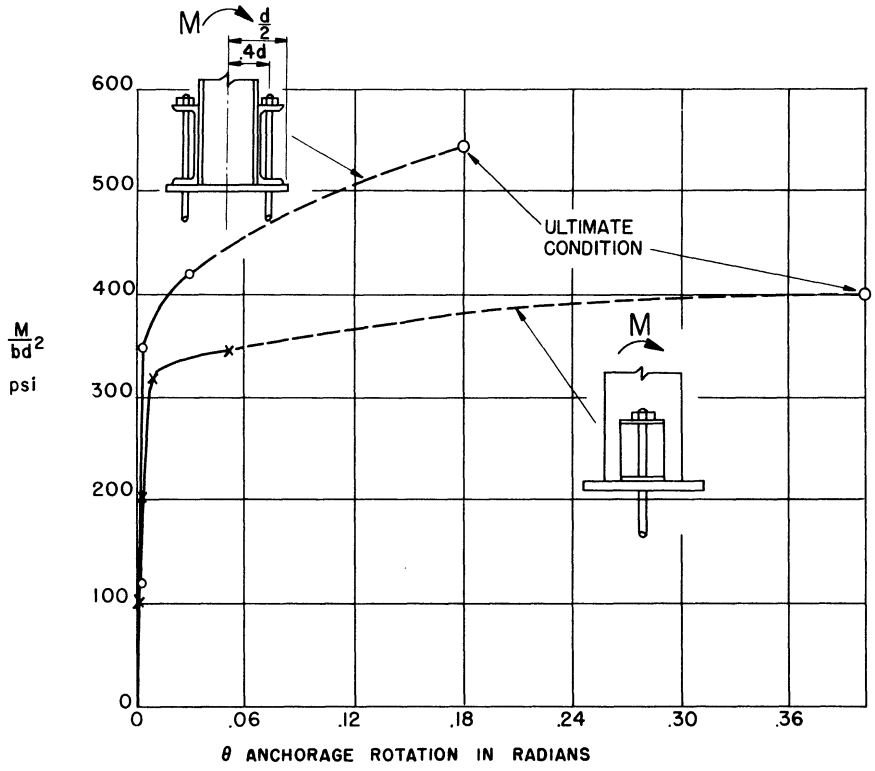

Fig. 5.22 The Effect of Varying the Eccentricity of the Anchor Bolts.
p = 0.6%; c = 600 psi; σ_y = 33000 psi; σ_u = 60000 psi; $\alpha f'_c$ = 6000 psi; L_1 = 2d/3.

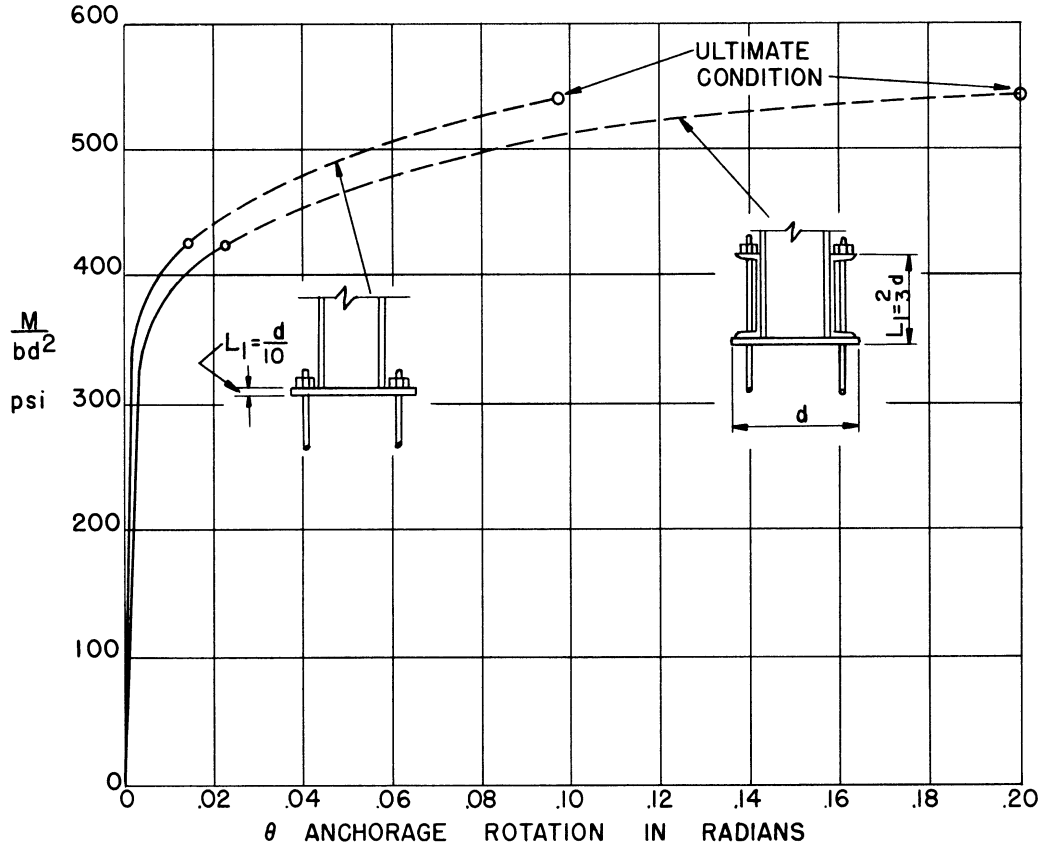

Fig. 5.23 The Effect of Varying the Free Anchor Bolt Length L_1. p = 0.6%; c = 600 psi; σ_y = 33000 psi; σ_u = 60000 psi; $\alpha f'_c$ = 6000 psi; e = 0.4d.

While the above procedure for estimating the moment-rotation characteristics of a simple column anchorage may be satisfactory as a first approximation, it can hardly be accepted without experimental verification and subsequent correction of the assumptions that were made. Such a correction of the assumptions, after an initial series of tests on anchorages, may result in a refinement of the method permitting the estimate of the M-θ curve for any similar anchorage without further tests, or it may be necessary at times to carry out small supplementary tests in the nature of combined pull-out and tension tests on anchor bolts.

The following considerations are of interest from the viewpoint of giving a limited number of tests the widest significance. Defined as the total equivalent anchor bolt length, L_e consists of two parts, L_1 and L_2, where L_1 is the actual length of the bolt above the concrete surface and L_2 is the equivalent free length corresponding to the embedded portion of the anchor bolt.

Considering two anchorages which are similar in all respects except size, all linear dimensions will be proportional to d. Evidently then $L_1 \propto d$. Furthermore, it is shown in Appendix 5.1 that for two similar anchorages L_2 is also likely to be proportional to d. Set $L_e = L'_e d$, where L'_e should be constant

for similar anchorages, thus, L'_e is independent of d and dependent only on the proportions chosen. Then

$$\theta = \frac{2 \sigma L'_e}{E_s (1 + e' - v')} \quad , \qquad (5.11)$$

where

$$v' = \frac{v}{\frac{d}{2}} = \frac{2v}{d} \quad ,$$

v' and w' (Equation 5.9) are constants for similar anchorages because the shapes of the concrete stress diagrams are evidently similar.

Equations 5.9 and 5.11 for M' and θ are thus independent of the actual dimensions of any part of the anchorage. This is an important conclusion as it means that a model test for one anchorage should hold true for a similar larger anchorage. The experimental verification of this conclusion would be a part of any test program.

SUMMARY

In the absence of tests on column anchorages an analytical procedure is developed in this chapter to calculate an upper bound for the moment resistance of typical anchorages. This upper bound for moment does not seem to be greatly affected by shear.

A step-by-step procedure for the calculation of the moment-rotation characteristics of anchorages is also developed. Experimental confirmation of these procedures would be desirable.

BIBLIOGRAPHY - CHAPTER V

5.1 Timoshenko, S.
Goodier, J. N.
"Theory of Elasticity"
McGraw-Hill Book Co Inc, New York
1951.

5.2 Graf, O.
"Die Eigenschaften des Betons"
Springer Verlag, Berlin (1950)

5.3 AISC
"Steel construction"
AISC, New York (1948)

5.4 Gilkey, H. J.
Chamberlin, S. J.
Beal, R. W.
"Bond between concrete and steel"
Iowa Eng Exp Sta Bul 147 (1940)

5.5 Newmark, N. M.
"Analysis and design of structures subjected to dynamic loading"
Proceedings, MIT Conference on "Building in the atomic age" (June 1952)

5.6 Brown, A. A.
"Analysis of anchor bolts and concrete piers for large stills and kettles" Civ Eng 22:7:491-2 (July 1952)

APPENDIX 5.1

EQUIVALENT FREE LENGTH OF EMBEDDED BAR

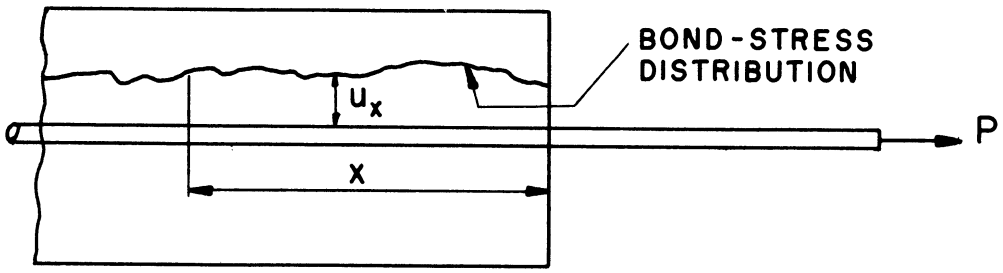

Fig. 5.24.

It is necessary to investigate whether the equivalent free length of an embedded bar is proportional to d, the length of the base plate, for bars of various sizes provided that p and σ is the same.

If p is the same,

$$\frac{A_t}{bd} = \frac{\pi D^2}{4bd} = \text{constant},$$

where D = diameter of bar. Also, if the ratio of b to d is kept the same,

$$b = kd$$

$$\therefore \frac{D^2}{d^2} = \text{constant}$$

and it remains to be proven that the equivalent length is proportional to D.

The equivalent length L_2 is defined as follows: if the slip is s, then $s = P L_2/E_s A_t = \sigma L_2/E_s$ or $L_2 = sE_s/\sigma$. Since we are comparing various cases at a stage when θ and therefore σ are the same, σ can be considered a constant. Further, for L_2 to be proportional to D, s must be proportional to D.

From Fig. 5.24

$$P_x = P - \int_0^x u_x \pi D \, dx$$

$$\sigma_x = \sigma - \int_0^x \frac{4u_x}{D} \, dx \quad .$$

Hence, σ_x decreases as x increases and eventually becomes zero at L_t. The part of the bolt at a distance greater than L_t is of no importance.

$$0 = \sigma - \int_0^{L_t} \frac{4u_x}{D} \, dx, \text{ or } \sigma = \int_0^{L_t} \frac{4u_x}{D} \, dx.$$

The strain $\epsilon_x = \frac{1}{E_s} \sigma_x$

$$\therefore E_s \epsilon_x = \int_0^{L_t} \frac{4u_x}{D} \, dx - \int_0^x \frac{4u_x}{D} \, dx = \int_x^{L_t} \frac{4u_x}{D} \, dx$$

$$\therefore s = \int_0^{L_t} \epsilon_x \, dx = \frac{4}{DE_s} \int_0^{L_t} \int_x^{L_t} u_x \, dx^2 \quad .$$

(i) If u_x is constant and independent of x

$$s = \frac{2uL_t^2}{DE_s} \quad .$$

It has been shown by Gilkey (5.4) and others that the effective length L_t is about 24D. But in any case L_t can at least be assumed to be proportional to D. Hence,

$$u = \frac{\sigma D}{4 L_t} = \frac{\sigma}{4K} \quad ,$$

where K is a constant and

$$s = \frac{2uL_t^2}{DE_s} = \frac{2\sigma K^2 D^2}{4K DE_s} = \frac{\sigma KD}{2E_s} \quad ,$$

i.e., for any one σ, the slip is proportional to the diameter. Furthermore, the equivalent length L_2 is found to be

$$\frac{E_s}{\sigma} = \frac{KD}{2} = \frac{L_t}{2} \quad .$$

This means that the equivalent free length L_2 is half the effective length L_t, i.e., the amount of slip at the loaded end is the same as the extension of a nonembedded bar fixed at the center of gravity of the bond-stress distribution diagram.

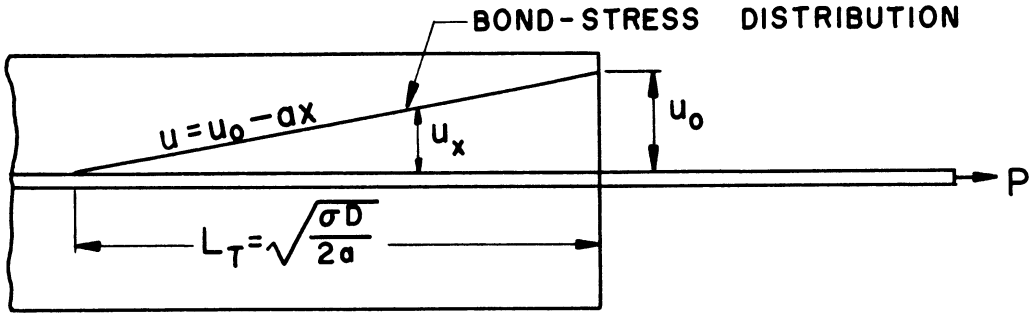

Fig. 5.25.

(ii) If the bond stress varies linearly, as shown in Fig. 5.25, then

$$s = \frac{2u_o L_t^2}{3\,DE_s} \quad \text{and} \quad \sigma = \frac{2u_o L_t}{D} = 2u_o K$$

$$= \frac{\sigma\, KD}{3\, E_s}, \text{ i.e., s is proportional to D}$$

and

$$L_2 = \frac{1}{3} L_t \quad .$$

It would appear to be generally true that $s \propto D \propto d$ for the same p and σ.

APPENDIX 5.2.

TYPICAL COMPUTATIONS FOR MOMENT-ROTATION CURVE

Data: c = 600 psi; p = 0.6%; $\alpha f'_c$ = 6000 psi; e = 0.4d;

L_1 = 2d/3; stress-strain curve for anchor bolt material as in Fig. 5.18; n for concrete is 10.

By definition

$$e' = \frac{2e}{d} = 0.8; \qquad L'_1 = \frac{L_1}{d} = \frac{2}{3} .$$

Also

$$p = \frac{A_t}{bd} = 0.006, \text{ therefore, } \frac{\pi}{4}D^2 = 0.006bd .$$

Assuming

$$b \simeq d, \quad D = d\sqrt{\frac{0.012}{\pi}} = 0.062d .$$

Further assuming a bond-stress distribution as in Fig. 5.25 (Appendix 5.1) and a total effective length of embedment of 24D, the equivalent length L_2 of the embedded portion of the bolt is 8D. Thus, L_2 = 8D = 0 496d. The total equivalent length of the anchor bolt $L_e = L_1 + L_2 = (0.667 + 0.496)d = 1.163d$. By definition

$$L'_e = \frac{L_e}{d} = 1.163 .$$

a. Stage 1

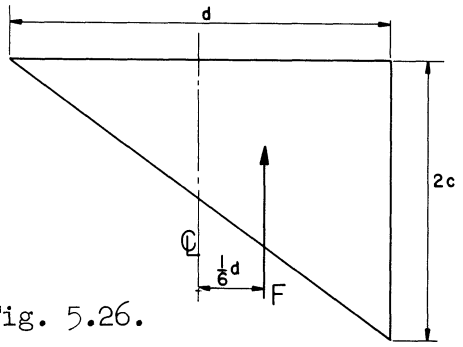

Fig. 5.26.

At the end of stage 1, as defined on page 15, the stress distribution under the plate is as shown in Fig. 5.26. The moment of resistance is

$$M = \frac{1}{6}dF = \frac{bd^2c}{6} .$$

By definition

$$M' = \frac{M}{bd^2} = \frac{c}{6} ,$$

Therefore

$$\underline{M_1' = 100 \text{ psi}} .$$

Similarly the rotation at the end of stage 1 is given by

$$\theta_1 = \frac{2c}{E_c} \qquad \underline{\theta_1 = 4 \times 10^{-4} \text{ rad}} .$$

b. Stage 2

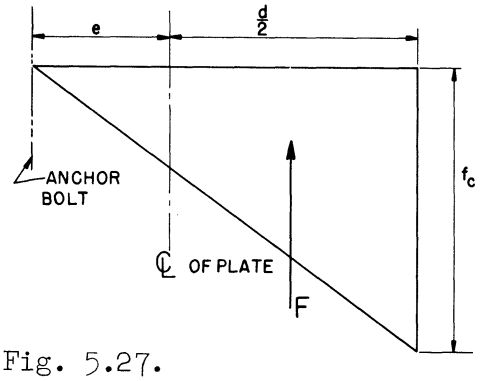

Fig. 5.27.

At the end of the second stage, tensile stress is just being induced in the anchor bolt on one side. The stress distribution under the plate is as shown in Fig. 5.27. The reaction is

$$F = \frac{1}{2} f_c b \left(\frac{d}{2} + e\right) = \frac{f_c bd}{4} (1 + e').$$

But since there has been no additional stress induced in the anchor bolt as yet, F must also equal the original reaction bdc. Thus,

$$bdc = \frac{f_c bd}{4}(1 + e')$$

and

$$f_c = \frac{4c}{1 + e'} \quad .$$

The moment of resistance is given by

$$M_2 = bdc\left[\frac{d}{2} - \frac{1}{3}\left(\frac{d}{2} + e\right)\right] = \frac{bd^2c}{2}\left[1 - \frac{1}{3}(1 + e')\right]$$

and

$$M_2' = \frac{c}{6}(2 - e') = 100\,(2 - 0.8); \qquad \underline{M_2' = 120 \text{ psi}} \; .$$

The strain in the concrete due to a stress f_c is given by

$$\frac{f_c}{E_c} = \frac{4c}{(1+e')E_c} \quad .$$

Assuming, as indicated in the text, that an effective depth d strains this amount

$$\theta_2 = \frac{4cd}{(1+e')\,E_c} \cdot \frac{1}{e+\frac{d}{2}} = \frac{8c}{(1+e')^2 E_c} \; ; \qquad \underline{\theta_2 = 5\text{x}10^{-4} \text{ rad.}}$$

c. Stage 3

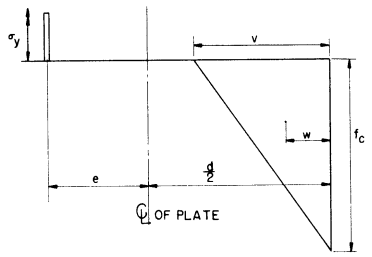

Fig. 5.28.

During this stage, the anchor plate is tilted sufficiently so that it is in contact with the concrete over a strip of width v. At the end of the stage (by definition) the stress in the anchor bolt has reached the yield point (Fig. 5.28).

To determine v and w, the following two equations can be written and solved. By geometry

$$\frac{\sigma_y}{f_c} = \frac{n(\frac{d}{2} + e - v)}{v} = \frac{n(1 + e' - v')}{v'} \quad .$$

From equilibrium $pbd\sigma_y + bdc = \frac{vbf_c}{2}$.

Thus,

$$\frac{\sigma_y v'^2}{4n(p\sigma_y + c)} + v' + (1 + e') = 0$$

from which

$$v' = 0.92; \quad w' = \frac{1}{3}v' = 0.307 \quad .$$

From Equation 5.9,

$$M' = \frac{1}{2} \times 798\ (1\text{-}0.307) = \frac{1}{2} \times 198 \times 0.8 \ ,$$

therefore, $\underline{M_3 = 354 \text{ psi}}$.

Using Equation 5.11,

$$\theta_3 = \theta_2 + \frac{2 \times 33 \times 1.163}{30 \times 10^3\ (1.8\text{-}0.92)} \ ; \quad \underline{\theta_3 = 34 \times 10^{-4} \text{ rad.}}$$

d. Stage 4

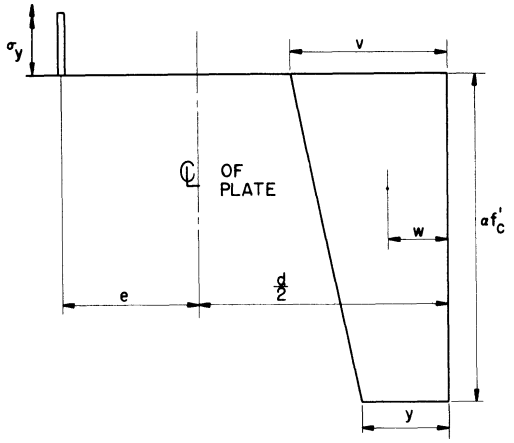

Fig. 5.29.

This stage ends when the strain in the anchor bolts reaches the value ϵ_{y2} (Fig. 5.18). At this time the concrete stress distribution is nonlinear and may be approximated by a trapezoid (Fig. 5.29). To determine v and y two equations can be written and solved. By geometry

$$\frac{\epsilon_{y2}}{\alpha f'_c/E_c} = \frac{\frac{d}{2} + e - v}{v-y}$$

From equilibrium $pbd\sigma_y + bdc = \frac{1}{2}\ \alpha f'_c\ (v + y)b$

from which

$$v' = \frac{2v}{d} = 0.353 \qquad \text{and } y' = \frac{2y}{d} = 0.178\ .$$

Also,

$$w' = \frac{v'^2 + v'y' + y'^2}{3(v' + y')} = 0.137\ .$$

As in stage 3, $M' = \frac{1}{2} \times 798\ (1-0.137) + \frac{1}{2} \times 0.198 \times 0.8$

$$\underline{M'_4 = 423 \text{ psi}}\ .$$

Using Equation 5.11, but replacing σ_y/E_s by ϵ_{y2} ,

$$\theta_4 = \theta_2 + \frac{2\epsilon_{y2} L'_e}{1+e' - v'} \quad ; \quad \underline{\theta_4 = 246\text{x}10^{-4} \text{ rad.}}$$

e. Stage 5

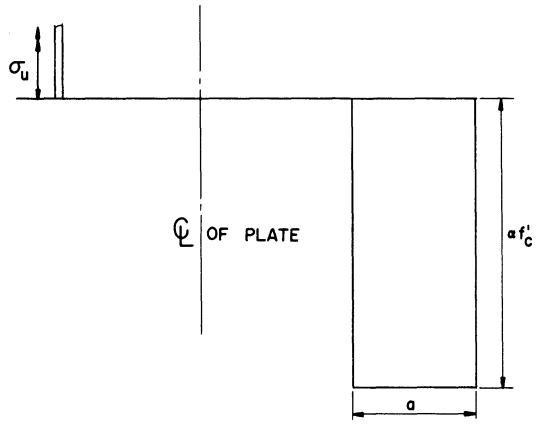

Fig. 5.30.

This stage represents the condition of ultimate moment. From Equation 5.5a

$$a = \frac{(c + p\sigma_u)d}{\alpha f'_c} = 0.16d$$

$$M'_u = \frac{1}{2} \times 960(1-0.16) + \frac{1}{2} \times 360 \times 0.8$$

$$\underline{M'_u = 547 \text{ psi}}$$

$$\theta_5 = \theta_2 + \frac{\epsilon_u L_e}{\frac{d}{2}+e-a} = \theta_2 + \frac{2\epsilon_u L'_e}{1+e'-a'}$$

$$\underline{\theta_5 = 0.18 \text{ rad.}}$$

The above values of M' and θ are shown in graph form in Fig. 5.19.

CHAPTER VI

THE ROLE OF CONNECTIONS IN THE DYNAMIC BEHAVIOR OF BUILDINGS

In the preceding five chapters the properties of various types of structural connections have been reviewed. Information based on tests was mostly from tests of a static nature; hence the results of experimental, as well as analytical investigations, were presented in the form of static load-deformation curves.

In static problems the deformations of the various parts of a structure are dependent on the instantaneous loads only, while in dynamic problems the deformations and strains are functions of the instantaneous values of the loads as well as of the values they had earlier. In other words, the deflections depend on two parameters: the load system and the time.

It would be unfortunate, indeed, if all the information available on the static properties of structures were of no use in dynamic analyses and if it were necessary to obtain new experimental results for the behavior of a structure for every different time varying force system. The aim of the dynamic analysis method is, therefore, to define the properties of structures which govern their dynamic behavior, irrespective of the nature of the applied force system. Once these independent structural properties have been calculated or found experimentally, the dynamic analysis can be carried out for any external time-dependent system of forces.

For a single-degree-of-freedom system, such as a one story building, the structural property referred to in the last paragraph is the "resistance" curve, defined as the relation between a force applied to the point where the mass is considered concentrated and the resulting displacement of the mass, exclusive of inertial and damping resistance. If this curve is known, the response of the structure to any external time-dependent force system can be calculated. Figure 6.1 shows a typical resistance-deflection curve for lateral loads for a single story building and force-time curve.

For a multi-degree-of-freedom system, such as a building with several stories, the characteristic information on the building can no longer be reduced

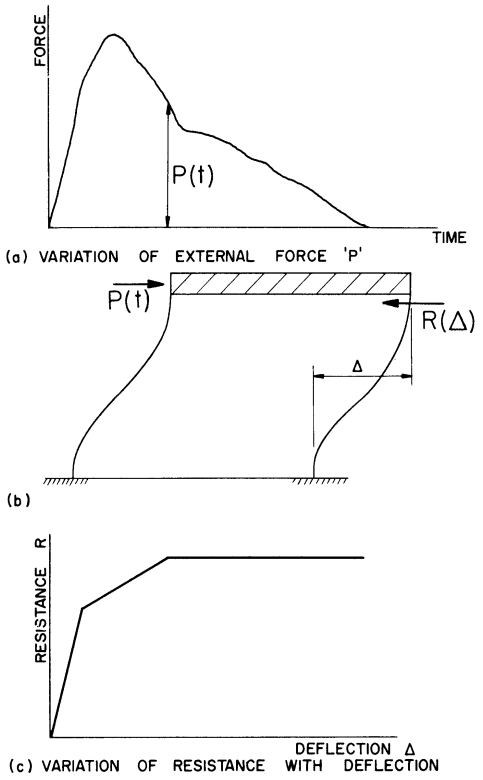

Fig. 6.1

to one resistance curve. The data has to be transformed into one or more stiffness matrices (6.1). The lateral stiffness matrix of a five story building is a square array of 25 numbers:

$$[S] = \begin{bmatrix} S_{11} & S_{12} & S_{13} & S_{14} & S_{15} \\ S_{21} & S_{22} & S_{23} & S_{24} & S_{25} \\ S_{31} & S_{32} & S_{33} & S_{34} & S_{35} \\ S_{41} & S_{42} & S_{43} & S_{44} & S_{45} \\ S_{51} & S_{52} & S_{53} & S_{54} & S_{55} \end{bmatrix}$$

of which the r-th row represents the forces that have to be applied at the various levels to produce a unit deflection at the r-th level and zero deflection at all other levels. Figure 6.2 is a schematic representation of a five story structure acted on by forces that form the third row of the stiffness matrix. Once the stiffness matrix, as defined above, has been determined, the equations of motion can be written immediately as

$$M_r\ddot{x}_r + S_{r1}\,x_1 + S_{r2}\,x_2 - - - - - + S_{rn}\,x_n = F_r(t) \qquad (r = 1,2 - - - n), \qquad (6.1)$$

where $F_r(t)$ are the external forces acting at the various levels.

The accuracy with which the response of the structure can be computed by solving Equation 6.1 is dependent on what factors are taken into account in the determination of [S]. An approximation results from assuming that girders and connections are infinitely rigid so that the relative deflections between stories takes place without rotation of the joints. Better values would be obtained if joint rotation, as governed by the relative stiffness of beams and columns, were taken into account. A still better estimate could be made if the semi-rigid characteristics of the connections themselves were accounted for, as discussed in Chapter IV. In addition it is possible, without great difficulty, to take care of the effects produced by flexibility of the foundation or the lengthening and shortening of the columns. More difficult is the problem of assessing the effect of walls, partitions, and floor slabs in their influence both on frame stiffness and dynamic damping. In brief, whatever the nature of the external forces the corresponding response of a structure can be computed to the same degree of accuracy to which the lateral stiffness matrix is known (6.1).

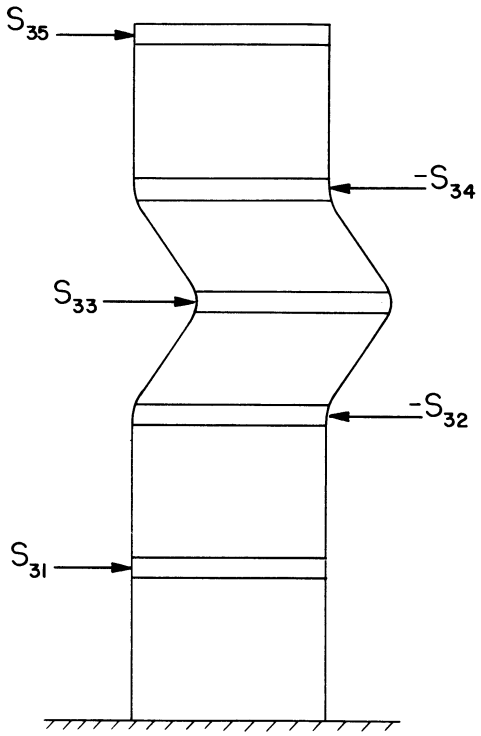

Fig. 6.2 Forces Producing Unit Displacement at the Third Story

The significance of the above statement is that it is possible to assess the effect of any structural variations on the dynamic behavior of a building by comparing static properties as evaluated in the stiffness matrices.

A building with semi-rigid connections has a lateral stiffness matrix in the same sense as a building with rigid connections. However, the slope of the M - θ curve for connections is not constant and at best these curves can be approximated by a series of straight lines. Thus, whenever the stiffness of a connection changes, a new stiffness matrix must be computed. In practice two or three stiffness matrices are sufficient to cover the range of deformations that is relevant.

For any framed structure composed of members and connections of known characteristics the stiffness matrix can be computed by the modified moment-distribution or slope-deflection methods discussed in Chapter IV. However, as mentioned, the neglect of walls and partitions will, in the case of certain buildings, introduce considerable error. It may be possible to determine the stiffness matrix experimentally and a dynamic analysis based on such static tests should give quite accurate results. Static tests for the determination of a stiffness matrix may require much preparation, though they are more easily arranged than dynamic tests. The results of such static tests would in a sense have a greater significance because they would be applicable to the response analysis of the structure to any set of dynamic forces instead of just one.

It is the purpose of this study to determine what effect connection characteristics have on the dynamic response of structures. This is readily achieved in the case of single story buildings by computing the resistance curves. For multistory buildings the stiffness matrix incorporates the effect of the connection characteristics. There is no difficulty in calculating the stiffness matrix for a typical multistory structure, but for the purpose of illustrating the effect of semi-rigid connections it was decided to simply compute the relation between lateral loads and the displacement at the top of a structure.

SINGLE STORY BUILDINGS

In Appendix 6.1 the lateral resistance curve for a single story bent is computed under three assumptions:

(1) The bases are pinned and the joints are fully rigid.
(2) The bases and joints are semi-rigid.
(3) The bases and joints are fully rigid.

For the semi-rigid case, the fixed-end moments, distribution factors, and carry-over factors were calculated using the procedure outlined by Johnston and Mount (6.2). Thereafter, moment-distribution was used in the same manner as for the rigid frames. Of course, the calculation of the above factors requires a knowledge of the moment-rotation characteristics of the connections used. For joints B and C these properties were obtained by interpolation from the results of the work of Hechtman and Johnston (6.3). The moment-rotation curve for the anchorages was computed analytically, as outlined in Chapter V of this monograph.

The resistance curves for the three cases are shown in Fig. 6.7 in Appendix 6.1, which gives some idea of the error introduced if a structure with standard connections and anchorages is categorized as fully rigid and having either pinned or rigid bases. Although it may not always be considered practicable to compute the resistance curve of a single story bent on the basis of case 2, a number of comparative analyses of the type carried out in Appendix 6.1 may lead to rules for estimating the position of the resistance curve of a single story bent with good accuracy.

MULTISTORY BUILDINGS

In Appendix 6.2 two numerical examples are worked out. Case 1 is a three story two-bay rigid frame subjected to three concentrated lateral forces at the story levels. The procedure is similar to that used in Appendix 6.1, except that the slope-deflection method is used, then the resulting nine simultaneous equations are solved by successive approximation. Referring to Fig. 6.8 in Appendix 6.2, plastic hinges form in the following order: in the column at H; in the columns at D and L; at G (in the lower story); and finally at C and K (in the lower story). Thus the final mode of collapse is by failure at both ends of all the columns in the first story. Knowing the mode of collapse, it is possible to check the value of the loads at collapse by the method proposed by Greenberg and Prager (6.4).

The second numerical example in Appendix 6.2 deals with the same frame and loading, except that it is assumed that the beam-to-column connections and the column anchorages are semi-rigid. In theory a greater number of phases would have to be considered than in the rigid case because new equations have to be set-up, not only when a plastic hinge forms, but also when a significant change of slope occurs in the moment-rotation curve of any of the connections. In practice it is usually possible, without great sacrifice in accuracy, to make adjustments so that several conditions which require a change in the equations occur at the same time. The order of the error introduced by such a manipulation can be gaged by comparing the value of the collapse load obtained by adding the loads for each phase with the collapse load calculated by the Greenberg-Prager method. In this example the difference is 3.8 percent.

It is interesting to note that the mode of collapse of the semi-rigid frame is quite different from the mode in which the rigid frame collapses. In the semi-rigid case, failure occurs by yielding at the column bases and at the ends of all girders.

CONCLUSION

This study shows that considerable errors will result both in stiffness and ultimate strength if a structure with semi-rigid connections is analyzed as if it had rigid connections.

Structures that have partitions and members that are encased with concrete will initially be very stiff, but as deformations continue to increase the brittle masonry is apt to crack so that its resistance is no longer available when the maximum strength of the steel frame is reached. In view of this the collapse loads calculated by the procedures illustrated in this chapter are very likely to be closer to the actual collapse loads than might first be suspected.

BIBILIOGRAPHY

6.1 Schenker, L. "The dynamic analysis of tall structures in the elastic and inelastic ranges" Doctoral Dissertation Univ of Mich (1954)

6.2 Johnston, B.G. Mount, E.H. "Analysis of building frames with semi-rigid connections" ASCE Trans 107:993-1033 (1942)

6.3 Hechtman, R.A. Johnston, B.G. "Riveted semi-rigid beam-to-column building connections" Prog Rep No.1, AISC (Nov 1947)

6.4 Greenberg, H.J. Prager, W. "Limit design of beams and frames" Trans ASCE 117:447-58 (1952)

6.5 Maugh, L.C. Statically Inderterminate Structures John Wiley and Sons New York, 1946

6.6 Johnston, B.G. Yang, C.H. Beedle, L.S. "An evaluation of plastic analysis as applied to structural design" Weld J Res Supp 32:224s-31s (1953)

6.7 Ketter, R.L. Beedle, L.S. Johnston, B.G. "Column strength under combined bending and thrust" Weld J Res Supp 31:543s-60s (1952)

APPENDIX 6.1

RESISTANCE CURVES FOR A SINGLE STORY SINGLE-BAY FRAME

The proportions of the frame (Fig. 6.3) were chosen so as to be compatible with the following loadings:

30 psf dead load
40 psf snow load
20 psf lateral load due to wind
span between frames, 20 feet.

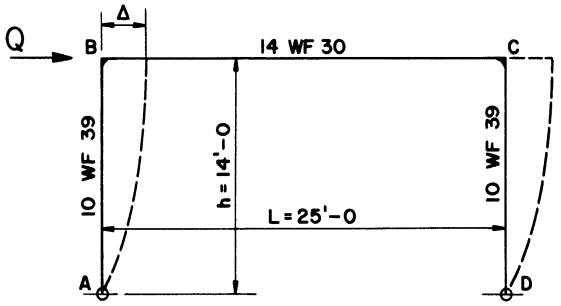

Fig. 6.3

In the presentation of these illustrative examples, it is assumed that the reader is already familiar with the moment-distribution procedure of frame analysis; see, e.g., L. C. Maugh (6.5). Likewise, some familiarity with plastic analysis is also essential to the understanding of these examples (6.6).

CASE I - JOINTS RIGID, BASES PINNED

a. Moment Distribution for Unit Horizontal Side-Sway

Stiffness values	$K_{BA} = 1.25$ in.^{3}; $K_{BC} = 0.97$ in.^{3}
Distribution factors	$r_{BA} = 0.394$; $r_{BC} = 0.606$
Fixed-end moment for $\Delta_B = 1$ in.	-670 in.-kips

After moment distribution, M_{BA} corresponding to Δ_B = 1 in. is 406 in.-kips. Therefore Q for Δ_B = 1 in. is given by

$$\frac{Q}{\Delta} = 2\left(\frac{406}{168}\right) = 4.83 \text{ kips/in.}$$

This is the slope of the first part of resistance curve 1 (Fig. 6.7).

b. Plastic Hinge Moments

Let the "plastic modulus" Z equal twice the statical moment of one-half cross-sectional area to one side of and about the axis of zero bending stress. For many sections this can be obtained directly from the structural properties of tee sections which are manufactured by splitting a WF shape along the center line. Also σ_y equals the yield strength of structural steel under dynamic load (assumed 45 ksi). Then the plastic moment M_p of a symmetrical section is given by $M_p = Z\sigma_y$. Z (column) = 2 x 5.74 (4.97 - 0.88) = 46.95 $in.^3$, Z (beam) = 2 x 4.41 (6.93 - 1.59) = 47.10 $in.^3$, thus, M_p (column) = 2110 in.-kips, M_p (beam) = 2120 in.-kips, and therefore, the strength of the columns controls the strength of the joint.

When the columns yield, the deflection at B is

$$\Delta_B = \frac{2110}{406} = 5.2 \text{ in.}$$

The value of Q when the columns yield is

$$Q = 2 \times \frac{2110}{168} = 25.1 \text{ kips.}$$

The complete resistance curve is curve 1 in Fig. 6.7.

In the foregoing it has been assumed that the load carried by the columns has no effect on plastic bending strength. This will be approximately true for relatively small column loads.

CASE 2 - SEMI-RIGID JOINTS AND BASES

It was assumed that the connections at joints B and C are of type V as defined in reference (6.3). The anchorage was designed in accordance with the

AISC specifications and the details are shown in Fig. 6.4.

The first step in determining the resistance curve of the semi-rigid frame is to obtain the moment-rotation curve for each joint, including the anchorages.

a. Moment-Rotation Curve for the Anchorage

This moment-rotation curve was determined in accordance with the procedure illustrated in Appendix 5.2.

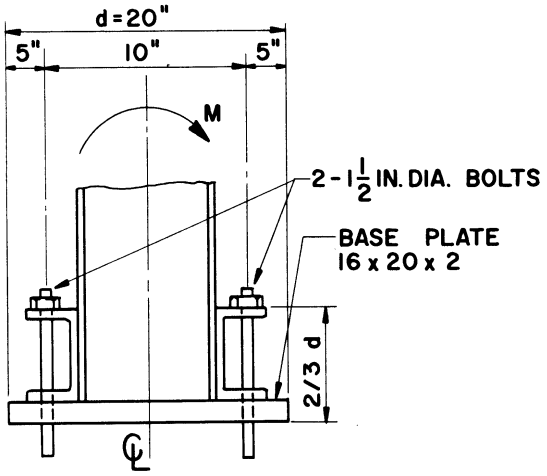

Fig. 6.4

Assumed bearing pressure c = 600 psi, $E_c = 3 \times 10^6$ psi, n = 10, b = 16 in., and d = 20 in. Other details are shown in Fig. 6.4. The area of a 1-1/2-inch diameter bolt is 1.77 square inches. Hence, p = 1.77/320 = 0.0055; assumed $\alpha f'_c$ = 6000 psi; e = 5 in., ∴ e' = 0.5; $L_1 = 2d/3 = 13.33$ in.; σ_y = 45 ksi; $\epsilon_{y1} = 0.0015$; and $\epsilon_{y2} = 0.15$.

Stage 1

$$M'_1 = c/6 = 100 \text{ psi},$$

$$\therefore M_1 = 640 \text{ in.-kips}$$

$$\theta_1 = 2c/E_c = 4 \times 10^{-4} \text{ rad}$$

Stage 2

$$M'_2 = \frac{c}{6}(2 - e') = 150 \text{ psi}, \therefore M_2 = 960 \text{ in.-kips}$$

$$\theta_2 = \frac{8c}{(1 + e')^2 E_c} = 7 \times 10^{-4} \text{ rad}$$

Stage 3

$$\frac{\sigma_y v'^2}{4n(p\sigma_y + c)} + v' - (1 + e') = 0$$

$$1.323\, v'^2 + v' - 1.5 = 0$$

$$\therefore v' = 0.75; \quad w' = \frac{1}{3} v' = 0.25$$

$$M'_3 = \frac{1}{2}(c + p\sigma_y)(1 - w') + \frac{1}{2} p\sigma_y e' = 380 \text{ psi}$$

$$M_3 = 2430 \text{ in.-kips}$$

$$L_e = L_1 + L_2 = 13.33 + 8(1.5) = 25.33 \text{ in.}$$

$$L_e' = L_e/d = 1.266$$

$$\theta_3 = \theta_2 + \frac{2\epsilon_{y_1} L_e'}{E_s(1 + e' - v')} = (7 + 50.5) \times 10^{-4} \text{ rad}$$

$$\theta_3 = 57.5 \times 10^{-4} \text{ rad}$$

Stage 4, by the procedure of Chapter V

$$v' = 0.291 \quad ; \quad w' = 0.142$$

As stage 3

$$M_4' = \frac{1}{2} (c + p\sigma_y)(1 - w') + \frac{1}{2} p\sigma_y e' = 427 \text{ psi}$$

$$M_4 = 2735 \text{ in.-kips}$$

$$\theta_4 = \theta_2 + \frac{2\epsilon_{y_2} L_e'}{1 + e' - v'} = (7 + 314) \times 10^{-4} \text{ rad} = 321 \times 10^{-4} \text{ rad}$$

The moment-rotation curve for the anchorage is shown in Fig. 6.5. For the purpose of subsequent computations this will be approximated by two straight lines, as shown.

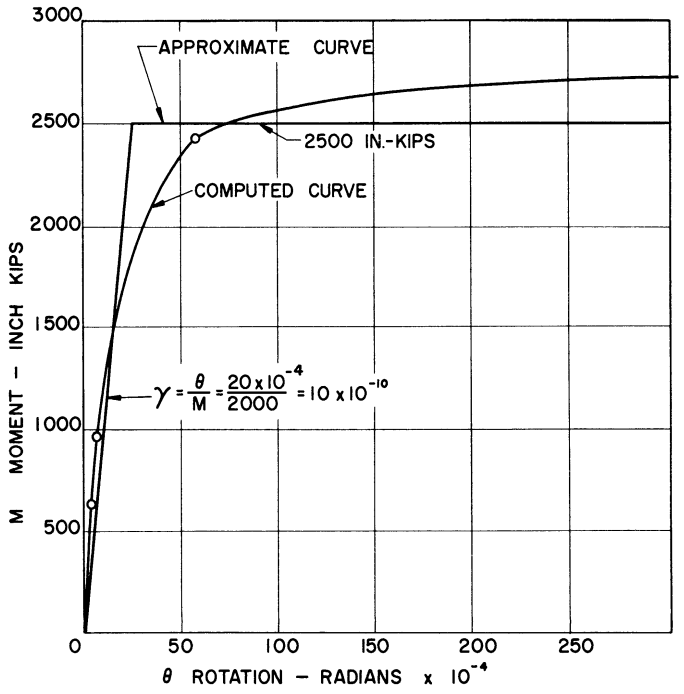

Fig. 6.5 Moment-Rotation Curve for the Anchorage

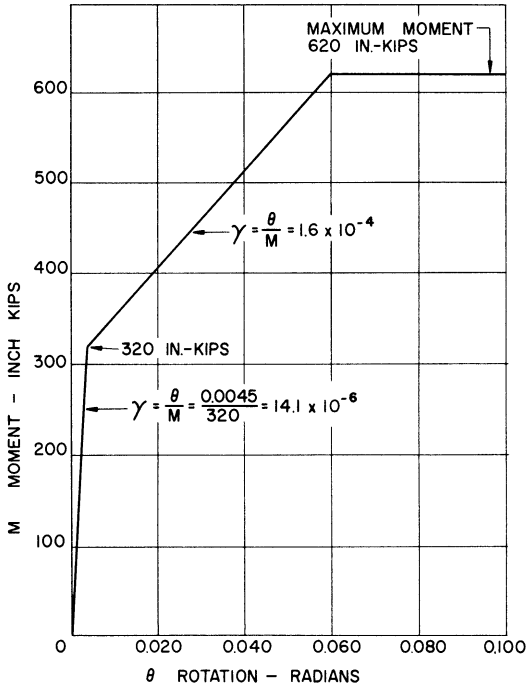

Fig. 6.6 Approximate M-θ Relationship for Joints B and C.

b. Moment-Rotation Curve for Joints B and C

The moment-rotation curve for these joints was estimated by referring to the results of tests on similar connections (6.3). The curve was then approximated by two straight lines, as shown in Fig. 6.6.

c. Stiffness and Carry-Over Factors

From reference (6.2), the stiffness factor is given by

$$S = \frac{2EK\,(2 + 3\beta)}{1 + 2\alpha + 2\beta + 3\alpha\beta}$$

and the carry-over factor by

$$r = \frac{1}{2 + 3\beta} \quad .$$

In the above expressions $\alpha = 2EK\gamma$ for the near end of the member considered and $\beta = 2EK\gamma$ for the far end. For member AB

$$\alpha_{AB} = \beta_{AB} = 0.075$$

$$\beta_{BA} = \alpha_{BA} = 0 \quad .$$

Hence,

$$S_{AB} = 3.475E \quad ,$$

$$S_{BA} = 3.870E \quad ,$$

$$r_{AB} = 0.50 \quad ,$$

$$r_{BA} = 0.45 \quad .$$

For BC, for the initial slope,

$$\alpha_{BC} = \alpha_{CB} = \beta_{BC} = \beta_{CB} = 0.82 \quad ,$$

$$\therefore \; S_{BC} = S_{CB} = 1.368E$$

$$r_{BC} = r_{CB} = 0.224 \quad .$$

For BC, for the second slope,

$$\alpha_{BC} = \alpha_{CB} = \beta_{BC} = \beta_{CB} = 9.25$$

$$S_{BC} = S_{CB} = 0.194E$$

$$r_{BC} = r_{CB} = 0.0336.$$

d. Semi-Rigid Fixed-End Moments Due to Unit Side-Sway

From reference (6.2),

$$M_{RAB} = \frac{-6EK_{AB}}{L}\left[\frac{1+\beta}{1+2\alpha+2\beta+3\alpha\beta}\right] = -1167 \text{ in.-kips}$$

$$M_{BA} = -1251 \text{ in.-kips.}$$

e. Moment-Distribution for Semi-Rigid Frame to Determine Initial Slope of Resistance Curve - Phase I

Using the distribution factors 0.74 (B to A) and 0.26 (B to C), the carry-over factors 0.45 (B to A) and 0.224 (B to C), and the fixed-end moments, the distribution is carried out and the results are

$$M_{AB} = 767 \text{ in.-kips}; \quad M_{BA} = -376 \text{ in.-kips}; \quad M_{BC} = 376 \text{ in.-kips.}$$

Thus, the shear Q in the columns compatible with a unit displacement is given by

$$Q = 2\left[\frac{767 + 376}{168}\right] = 13.6 \text{ kips per in.}$$

This is the initial slope of the resistance curve.

Since the moment-rotation curve for the connection at B changes slope at 320 in.-kips, the initial slope of the resistance curve continues only until this value is reached. Thus at the end of phase I,

$$Q_1 = 13.6\left[\frac{320}{376}\right] = 11.6 \text{ kips}$$

$$\Delta_1 = \frac{320}{376} = 0.85 \text{ in.}$$

f. Moment-Distribution for Semi-Rigid Frame - Phase II

During the second phase the distribution factors are 0.952 (B to A) and 0.048 (B to C) and the carry-over factors are 0.45 (B to A) and 0.0336 (B to C). Distribution of the fixed-end moments for unit side-sway results in

$$M_{AB} = -629 \text{ in.-kips}, \quad M_{BA} = -56 \text{ in.-kips}, \quad M_{BC} = 56 \text{ in.-kips}.$$

The slope of the resistance curve during phase II is given by

$$\left(\frac{Q}{\Delta}\right)_2 = 2\left(\frac{629 + 56}{168}\right) = 8.15 \text{ kips/in.}$$

The resistance curve continues at this slope until the column limit moment of 2110 in.-kips is reached at A and D, or until the connection limit moment of 620 in.-kips is reached at B and C. Computations show that the limit moment at A and D is reached first. At the end of phase II

$$\Delta_2 = 3.17 \text{ in.}, \quad Q_2 = 30.5 \text{ kips}, \quad M_{AB} = -2110 \text{ in.-kips}, \quad M_{BA} = -450 \text{ in.-kips}.$$

g. Moment-Distribution for Semi-Rigid Frame - Phase III

The distribution during phase III is carried out considering joints A and D hinged. Recalling that the value of K = I/L for the column AB is 1.25, then the stiffness, allowing for the hinge at the far end, is 3 x 1.25 = 3.75. On this basis the distribution factors at B are 0.95 (B to A) and 0.05 (B to C). The carry-over factors are 0 (B to A) and 0.0336 (B to C). The fixed-end moment for unit side-sway is now calculated as it would be if the connection at B were rigid,

$$M_{RBA} = \frac{-3EK}{L} = -670 \text{ in.-kips}$$

$$M_{RAB} = 0.$$

After moment distribution,

$$M_{BA} = -36 \text{ in.-kips} \quad .$$

The slope of the resistance curve during this phase is given by

$$\left(\frac{Q}{\Delta}\right)_3 = 2\left(\frac{36}{168}\right) = 0.43 \text{ kips/in.}$$

It is found that for a value of Q = 2.03 kips during this phase, there is an additional moment at B of -170 in.-kips, making the total value of M_{BA} = -620 in.-kips, corresponding to the limit moment of the connection. Any further increase in Q results in uncontrolled displacement. The additional deflection during this stage is 4.72 inches.

The following table can now be prepared, showing the values of deflection Δ, shear Q, and the moments at the various stages.

End of Phase	Q(kips)	Δ(inches)	M_{AB}(in.-kips)	M_{BA} (in.-kips)
I	11.6	0.85	-652	-320
II	30.5	3.17	-2110	-450
III	32.53	7.89	-2110	-620

The complete resistance curve for this case is curve 2 in Fig. 6.7.

CASE 3 - JOINTS AND BASES RIGID

a. Moment-Distribution to Determine Initial Slope of Resistance Curve - Phase I

Stiffness values $K_{BA} = 1.25 \text{ in.}^3$, $K_{BC} = 0.97 \text{ in.}^3$

$$M_{RAB} = M_{RBA} = -\frac{6EK_{BA}}{L} = -1340 \text{ in.-kips}$$

After moment-distribution,

$$M_{AB} = -1031 \text{ in.-kips}, \quad M_{BA} = -721 \text{ in.-kips}, \quad M_{BC} = 721 \text{ in.-kips}.$$

The shear Q in the columns compatible with a unit displacement is given by

$$\frac{Q}{\Delta} = 2\left(\frac{1031 + 721}{168}\right) = 20.9 \text{ kips/in.}$$

At a deflection at the top of column of 2.05 in., (Q = 42.8 kips), the yield moment of 2110 in.-kips is reached at A and D. Thereafter, the frame must be analyzed considering joints A and D hinged.

b. Moment-Distribution - Phase II

Distribution of the fixed-end moment M_{RBA} = .670 in.-kips results in M_{BA} = -407 in.-kips. The corresponding value of Q/Δ is

$$\frac{Q}{\Delta} = 2\left(\frac{407}{168}\right) = 4.8 \text{ kips/in.}$$

After the application of a further Q = 7.6 kips, a plastic hinge exists at B. The following table can now be prepared.

End of Phase	Q (kips)	Δ (inches)	M_{AB} (in.-kips)	M_{BA} (in.-kips)
I	42.8	2.05	-2110	-1476
II	50.4	3.63	-2110	-2120

The complete resistance curve for this case is curve 3 in Fig. 6.7. The very marked differences between these resistance curves illustrates the importance of the role of connection behavior in the computation of the lateral strength characteristics of a simple framed bent.

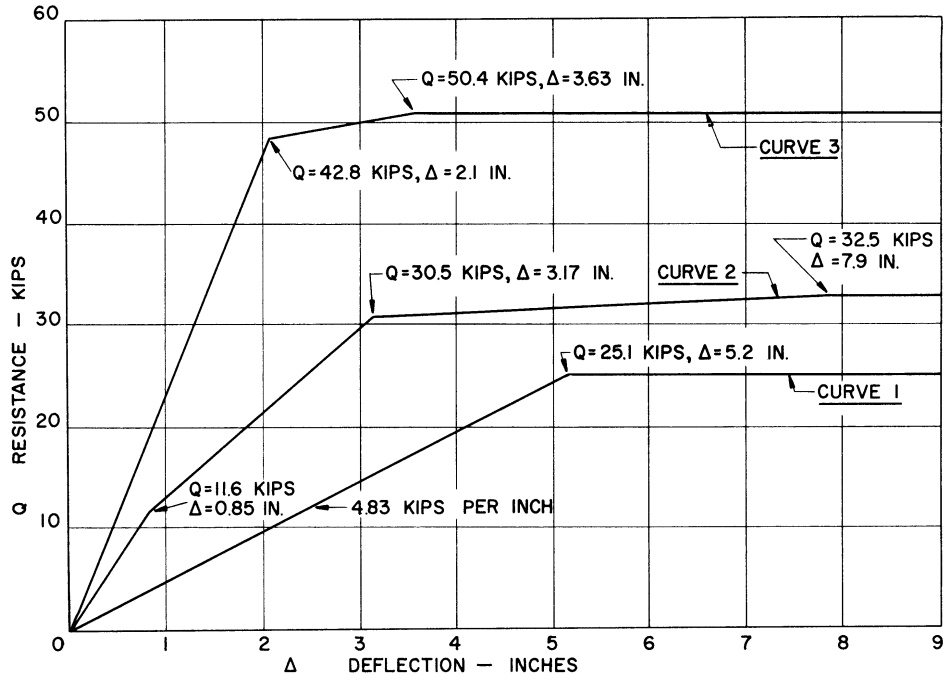

Fig. 6.7 Resistance-Deflection Curve for Three Frames: (1) Joints Rigid, Bases Pinned; (2) Joints and Bases Semi-Rigid; (3) all Joints Rigid, Bases Fixed.

APPENDIX 6.2

QUASI-RESISTANCE CURVES FOR
THREE STORY TWO-BAY FRAME

As discussed in Chapter VI, the term "resistance function" should perhaps be applied only to a single degree of freedom structures. Nevertheless, an estimate of the effect of connection characteristic may be made for a multidegree of freedom structure by means of the following illustrative example.

The dimensions and sizes of members of the frame to be analyzed are shown in Fig. 6.8.

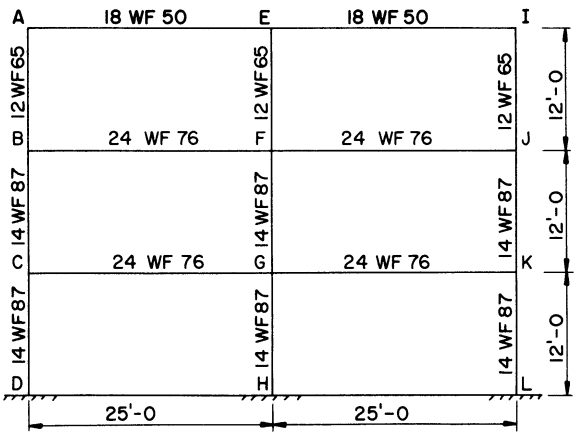

Fig. 6.8

$K = \frac{I}{L}$ factors:

18WF50	K = 2.69
24WF76	K = 7.0
14WF87	K = 6.7
12WF65	K = 3.7

The same members and K factors will be used for both the rigid and semi-rigid analysis.

The "resistance function" is to be determined for a uniformly distributed static lateral load over the full height of the building. This loading will be divided into three equivalent concentrated forces at the floor levels as shown in Fig. 6.9. The analysis for both rigid and semi-rigid cases is carried out using the slope-deflection method and it is expected that the reader is familiar with this procedure.

The general statical equations to be used for all phases of both rigid and semi-rigid frame analyses are:

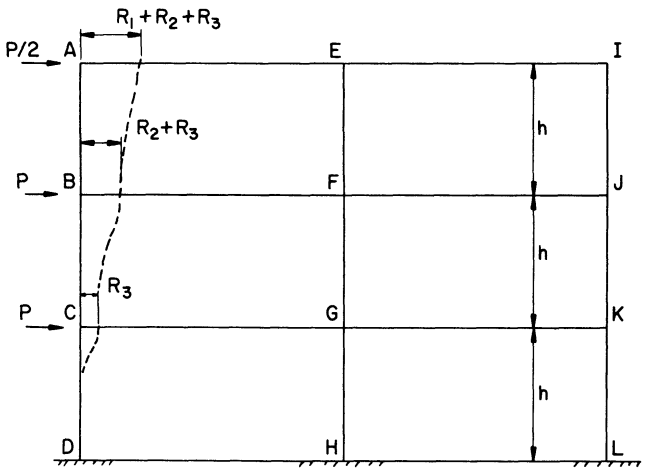

Fig. 6.9

$$
\left.
\begin{aligned}
M_{CD} + M_{CG} + M_{CB} &= 0 \\
M_{BC} + M_{BF} + M_{BA} &= 0 \\
M_{AB} + M_{AE} &= 0 \\
2\,M_{EA} + M_{EF} &= 0 \\
M_{FE} + M_{FG} + 2\,M_{FB} &= 0 \\
M_{GF} + M_{GH} + 2\,M_{GC} &= 0 \\
2\,M_{AB} + 2\,M_{BA} + M_{EF} + M_{FE} &= -\frac{Ph}{2} \\
2\,M_{BC} + 2\,M_{CB} + M_{FG} + M_{GF} &= -\frac{3Ph}{2} \\
2\,M_{CD} + 2\,M_{DC} + M_{GH} + M_{HG} &= -\frac{5Ph}{2}
\end{aligned}
\right\} \quad (6.2)
$$

Full advantage of symmetry is to be taken throughout this analysis.

The letters A, B, C, D, E, and F denote slopes at the various joints, i.e., θ_A = A etc. The letters R_1, R_2, and R_3 refer to the relative Δ/L between the floors, as shown in Fig. 6.9.

CASE 1. FULLY RIGID FRAME

The general slope-deflection equations from which the end-moment equations are obtained are as follows:

$$M_{AB} = E_s K\,(4\theta_A + 2\theta_B - 6R) - M_{RAB}$$

$$M_{BA} = E_s K\,(4\theta_B + 2\theta_A - 6R) - M_{RBA}$$

a. Phase I: Initial Slope of Resistance Curve

$$
\begin{aligned}
M_{AB} &= 14.8A + 7.4B - 22.2R_1 \\
M_{BA} &= 7.4A + 14.8B - 22.2R_1 \\
M_{AE} &= 10.76A + 5.38E \\
M_{EA} &= 5.38A + 10.76E
\end{aligned}
\quad (6.3)
$$

$$
\begin{aligned}
M_{EF} &= 14.8E + 7.4F - 22.2R_1 \\
M_{FE} &= 7.4E + 14.8F - 22.2R_1 \\
M_{BF} &= 28.0B + 14.0F \\
M_{FB} &= 14.0B + 28.0F \\
M_{BC} &= 26.8B + 13.4C - 40.2R_2 \\
M_{CB} &= 13.4B + 26.8C - 40.2R_2 \\
M_{FG} &= 26.8F + 13.4G - 40.2R_2 \\
M_{GF} &= 13.4F + 26.8G - 40.2R_2 \\
M_{CG} &= 28.0C + 14.0G \\
M_{GC} &= 14.0C + 28.0G \\
M_{CD} &= 26.8C - 40.2R_3 \\
M_{DC} &= 13.4C - 40.2R_3 \\
M_{GH} &= 26.8G - 40.2R_3 \\
M_{HG} &= 13.4G - 40.2R_3
\end{aligned}
\qquad (6.3)
$$

Note: All values for angles and deflections contain E_s, the modulus of elasticity of steel.

The end-moment equations for Phase I are then substituted in the general statical Equations 6.2, which are then solved by a method of successive approximations. The results in Phase I are:

$$
\begin{aligned}
A &= 0.00528 \\
B &= 0.00774 \\
C &= 0.01265 \\
D &= 0 \text{ (fixed end)} \\
E &= 0.00321 \\
F &= 0.00486 \\
G &= 0.00752 \\
H &= 0 \text{ (fixed end)} \\
R_1 &= 0.00943 \\
R_2 &= 0.01508 \\
R_3 &= 0.01583
\end{aligned}
\qquad \text{in terms of Ph}
$$

The end moments are computed substituting the above values in the Equations 6.3. The moments are multiplied by 144 inches (the height between floors) to get the moments in terms of inch kips for P = 1 kip. Any unbalanced moment at a joint is distributed in proportion to the end moments about the joint. Figure 6.10 shows the moments in Phase I after balancing, for P = 1 kip. Calculations of deflections in Phase I for P = 1 kip:

$$A = \frac{(R_1 + R_2 + R_3)\, Ph^2}{E_s} = \frac{0.04034 \times P \times 20736}{30\,000} = 0.0278 \text{ in.}$$

$$B = \frac{(R_2 + R_3)\, Ph^2}{E_s} = \frac{0.03091 \times P \times 20736}{30\,000} = 0.02135 \text{ in.}$$

$$C = \frac{R_3\, Ph^2}{E_s} = \frac{0.01583 \times P \times 20736}{30\,000} = 0.0110 \text{ in.}$$

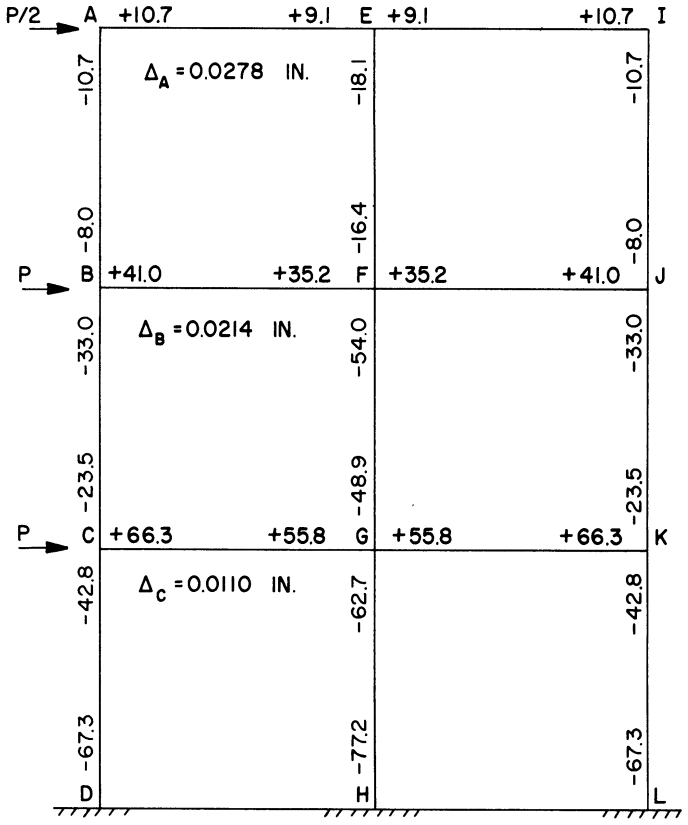

Fig. 6.10 Moments for Phase I (P = 1 kip)

Calculation of plastic hinge moments:

$$M_p = Z\, \sigma_y$$

where σ_y = 45 ksi = yield point under dynamic load and Z = the "plastic modulus", as defined in Appendix 6.1. For members AE and EI (18WF50),

M_p = 45 x 2 x 7.35(9.00 - 2.14) = 4538 in.-kips.

For members AB, EF, and IJ (12WF65),

M_p = 45 x 2 x 9.55 (6.06 - 0.98) = 4366 in.-kips.

For members BF, CG, FJ, and GK (24WF76),

M_p = 45 x 2 x 11.18 (11.95 - 3.00) = 9005 in.-kips.

For members BC, FG, JK, CD, GH, and KL (14WF87),

$$M_p = 45 \times 2 \times 12.78\ (7.00 - 1.65) = 6153 \text{ in.-kips.}$$

By taking ratios of $\frac{(M \text{ for } P = 1)}{M_p}$, the location of the first plastic hinge can be found.

$$\frac{M_{AE}}{M_p} = \frac{10.7}{4538} = 0.0023$$

$$\frac{M_{EF}}{M_p} = \frac{18.1}{4366} = 0.0041$$

$$\frac{M_{CG}}{M_p} = \frac{66.3}{9005} = 0.0074$$

$$\frac{M_{HG}}{M_p} = \frac{77.2}{6153} = 0.0125$$

$$\frac{M_{DC}}{M_p} = \frac{67.3}{6153} = 0.0109$$

Thus, P = 80 kips causes a hinge to form at H.

As in the case of the one story frame it has been assumed that the plastic moment is unaffected by direct stress in the column. This is more questionable in the present case and, in fact, there would be a probable reduction of between 10 and 20 percent due to this effect. Nevertheless, for comparative purposes, the reduction in plastic resistance due to direct force in the columns has been neglected. It may be introduced, if desired, by use of interaction curves (6.7).

The actual moments and deflections developed during Phase I are tabulated in Fig. 6.11. Subtracting the moments shown in Fig. 6.11 from the plastic moments at the end of every member leaves the elastic moments available at all such locations. These are shown in Fig. 6.12.

b. Phase II: Member GH Pinned at Bottom, All Other Joints Rigid

Rewriting the end-moment equations gives

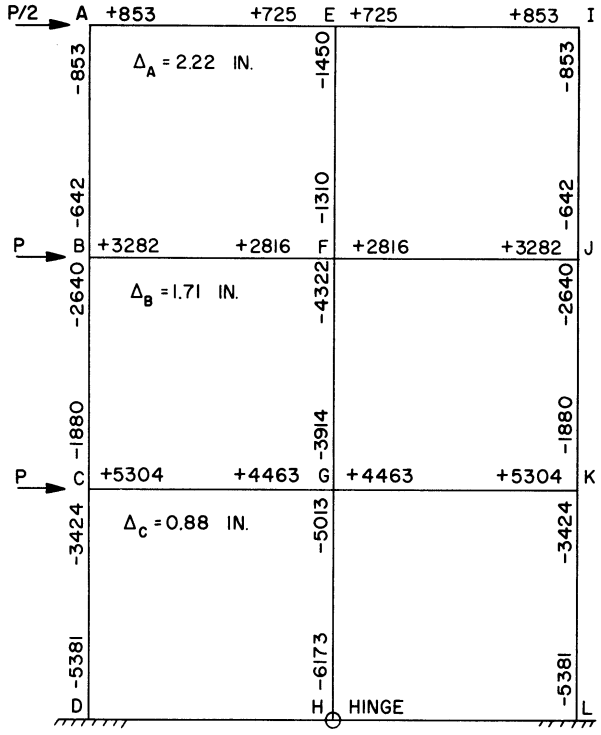

Fig. 6.11 Moments for Phase I (P = 80 kips).

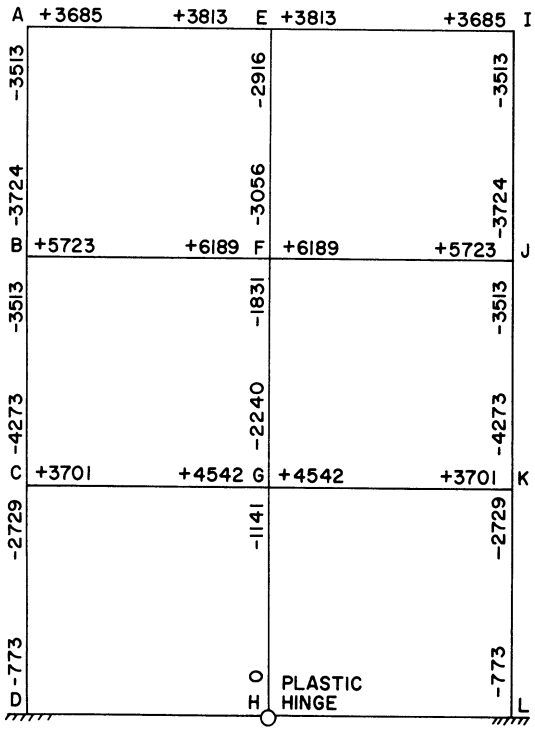

Fig. 6.12 Moments Remaining at Beginning of Phase II ($M_p - \sum M$)

$$M_{AB} = 14.8A + 7.4B - 22.2R_1$$

$$M_{BA} = 7.4A + 14.8B - 22.2R_1$$

$$M_{AE} = 10.76.A + 5.38E$$

$$M_{EA} = 5.38A + 10.76E$$

$$M_{EF} = 14.8E + 7.4F - 22.2R_1$$

$$M_{FE} = 7.4E + 14.8F - 22.2R_1$$

$$M_{BF} = 28.0B + 14.0F$$

$$M_{FB} = 14.0B + 28.0F$$

$$M_{BC} = 26.8B + 13.4C - 40.2R_2$$

$$M_{CB} = 13.4B + 26.8C - 40.2R_2$$

$$M_{FG} = 26.8F + 13.4G - 40.2R_2$$

$$M_{GF} = 13.4F + 26.8G - 40.2R_2$$

$$M_{CG} = 28.0C + 14.0G$$

$$M_{GC} = 14.0C + 28.0G$$

$$M_{CD} = 26.8C - 40.2R_3$$

$$M_{DC} = 13.4C - 40.2R_3$$

$$M_{GH} = 20.1G - 20.1R_3$$

$$M_{HG} = 0 .$$

Then, substituting into the general Equations 6.2 and solving, the following results are

obtained for the rotation of the joints under the conditions of Phase II.

$$\left.\begin{aligned} A &= 0.00547 \\ B &= 0.00736 \\ C &= 0.01644 \\ E &= 0.00301 \\ F &= 0.00567 \\ G &= 0.00527 \\ R_1 &= 0.00947 \\ R_2 &= 0.01597 \\ R_3 &= 0.02172 \end{aligned}\right\} \text{ in terms of Ph}$$

End moments are calculated, balanced, and converted to in.-kips for P = 1 kip in the same manner as Phase I. Figure 6.13 shows these moments after balancing.

By the end of Phase II, the next hinges form at the bottom of members CD and KL.

Let

$$\frac{M_R}{M} = \frac{\text{moment remaining at end of Phase I}}{\text{moment for P = 1 in Phase II}} = \frac{773}{94} = 8.22$$

The moments and deflections resulting from the application of P = 8.22 kips under the conditions of Phase II are shown in Fig. 6.14. Figure 6.15 shows the elastic moments remaining at the ends of every member after Phase II.

c. Phase III: Members CD, GH, and KL all Pinned at Bottom With All Other Joints Rigid

Rewriting the end moment equations gives

$$M_{AB} = 14.8A + 7.4B - 22.2R_1$$

$$M_{BA} = 7.4A + 14.8B - 22.2R_1$$

$$M_{AE} = 10.76A + 5.38E$$

$$M_{EA} = 5.38A + 10.76E$$

$$M_{EF} = 14.8E + 7.4F - 22.2R_1$$

$$M_{FE} = 7.4E + 14.8F - 22.2R_1$$

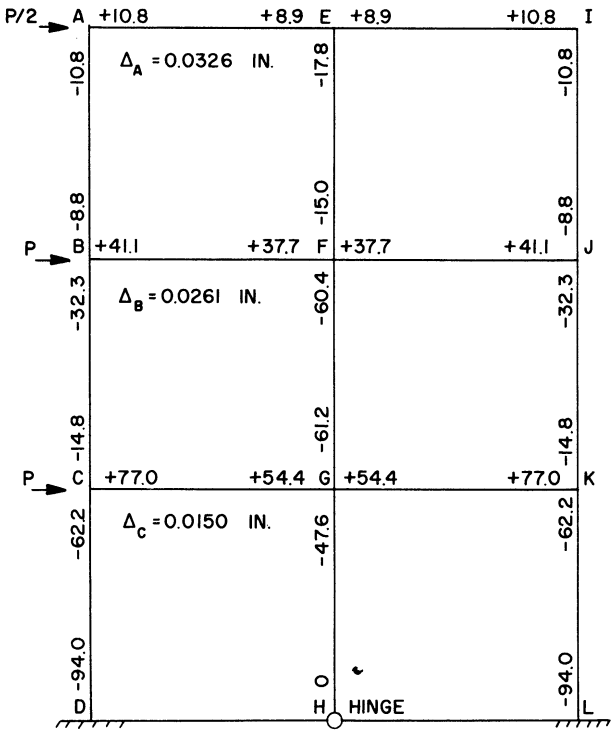

Fig. 6.13 Moments for Phase II (P = 1 kip).

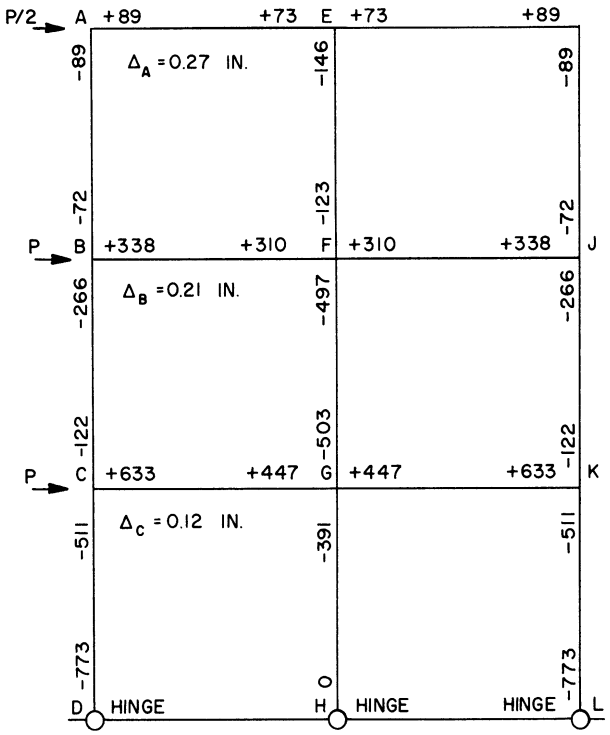

Fig. 6.14 Moments for Phase II (P = 8.22 kips).

$$M_{BF} = 28.0B + 14.0F$$

$$M_{FB} = 14.0B + 28.0F$$

$$M_{BC} = 26.8B + 13.4C - 40.2R_2$$

$$M_{CB} = 13.4B + 26.8C - 40.2R_2$$

$$M_{FG} = 26.8F + 13.4G - 40.2R_2$$

$$M_{GF} = 13.4F + 26.8G - 40.2R_2$$

$$M_{CG} = 28.0C + 14.0G$$

$$M_{GC} = 14.0C + 28.0G$$

$$M_{CD} = 20.1C - 20.1R_3$$

$$M_{DC} = 0$$

$$M_{GH} = 20.1G - 20.1R_3$$

$$M_{HG} = 0$$

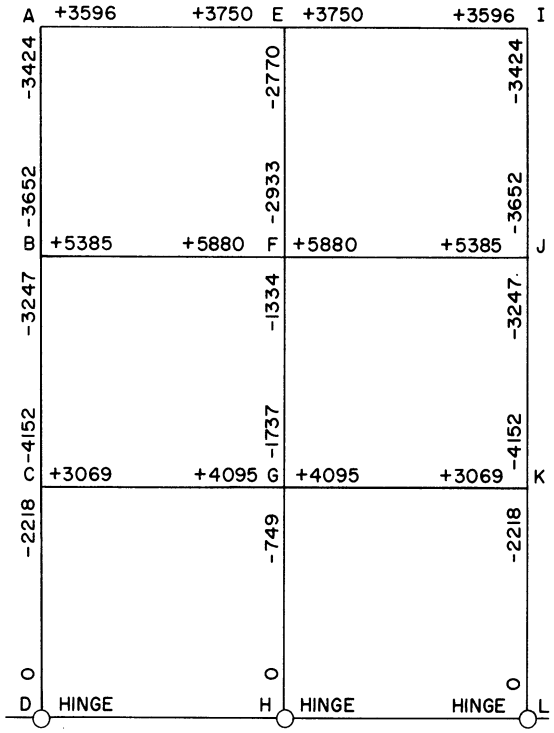

Fig. 6.15 Moments Remaining at Beginning of Phase III ($M_p - \sum M$).

Substituting as before, and solving, the results are as follows.

A	= 0.00553	in terms of Ph
B	= 0.00834	
C	= 0.02318	
E	= 0.00318	
F	= 0.00606	
G	= 0.01258	
R_1	= 0.00991	
R_2	= 0.01983	
R_3	= 0.06111	

End moments are calculated, balanced, and converted to in.-kips for P = 1 kip as before. Figure 6.16 shows the balanced moments and the corresponding values of Δ_A, Δ_B, and Δ_C.

The next hinge forms at the top of member GH.

$$\frac{M_R}{M} = \frac{749}{140.5} = 5.33$$

This hinge will form when P has increased 5.33 kips during Phase III. The moments resulting from the application of P = 5.33 kips under the conditions of Phase III are shown in Fig. 6.17. Figure 6.18 shows the moments still available at the ends of all members at the end of Phase III.

d. Phase IV: Members CD, GH, and KL All Pinned at Bottom, Member GH Pinned at Top and all Other Joints Rigid

Rewriting the end moment equations gives

$$M_{AB} = 14.8A + 7.4B - 22.2R_1$$

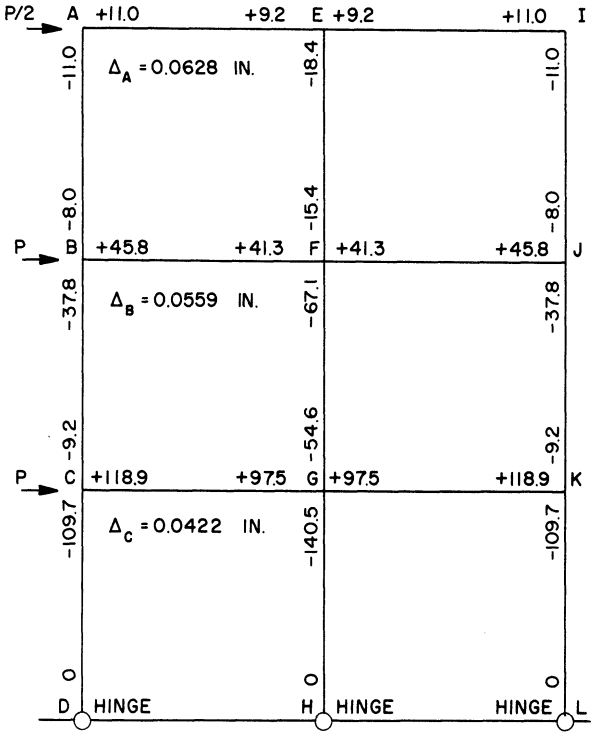

Fig. 6.16 Moments for Phase III (P = 1 kip).

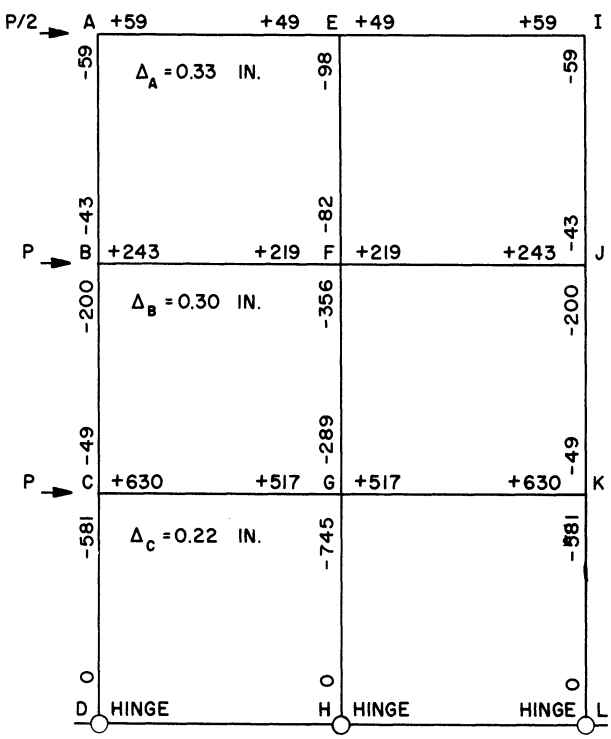

Fig. 6.17 Moments for Phase III (P = 5.33 kips).

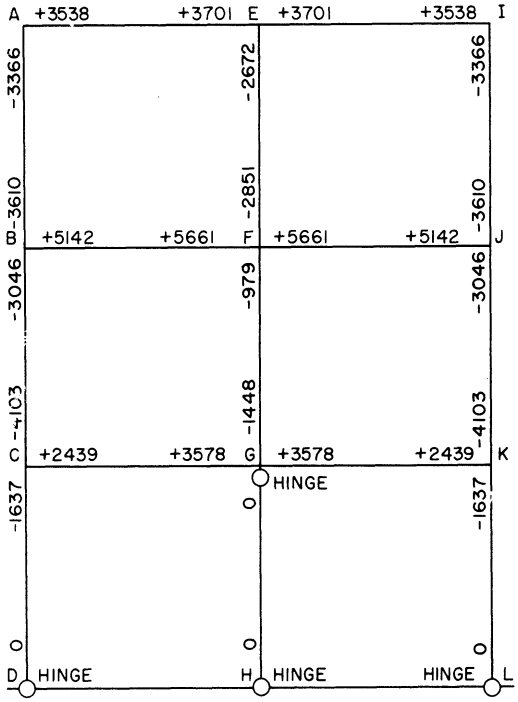

Fig. 6.18 Moments Remaining at Beginning of Phase IV ($M_p - \sum M$).

$$M_{BA} = 7.4A + 14.8B - 22.2R_1$$

$$M_{AE} = 10.76A + 5.38E$$

$$M_{EA} = 5.38A + 10.76E$$

$$M_{EF} = 14.8E + 7.4F - 22.2R_1$$

$$M_{FE} = 7.4E + 14.8F - 22.2R_1$$

$$M_{BF} = 28.0B + 14.0F$$

$$M_{FB} = 14.0B + 28.0F$$

$$M_{BC} = 26.8B + 13.4C - 40.2R_2$$

$$M_{CB} = 13.4B + 26.8C - 40.2R_2$$

$$M_{FG} = 26.8F + 13.4G - 40.2R_2$$

$$M_{GF} = 13.4F + 26.8G - 40.2R_2$$

$$M_{CG} = 28.0C + 14.0G$$

$$M_{GC} = 14.0C + 28.0G$$

$$M_{CD} = 20.1C - 20.1R_3$$

$$M_{DC} = 0$$

$$M_{GH} = 0$$

$$M_{HG} = 0$$

Substituting in Equations 6.2 and solving, the results are as follows.

$$\left.\begin{aligned} A &= 0.00644 \\ B &= 0.00568 \\ C &= 0.03853 \\ E &= 0.00203 \\ F &= 0.01003 \\ G &= 0.00398 \\ R_1 &= 0.00980 \\ R_2 &= 0.02195 \\ R_3 &= 0.10072 \end{aligned}\right\} \text{ in terms of Ph}$$

End moments are calculated, balanced, and converted to in.-kips for P = 1 kip as before. Figure 6.19 shows the balanced moments and the corresponding values of Δ_A, Δ_B, and Δ_C.

The next hinges to form are those at the top of members CD and KL. When these have formed the structure has become a mechanism.

$$\frac{M_R}{M} = \frac{1637}{179.9} = 9.1$$

Collapse will occur when P has increased 9.1 kips during Phase IV. Beyond this point it is no longer necessary to calculate the moment developed.

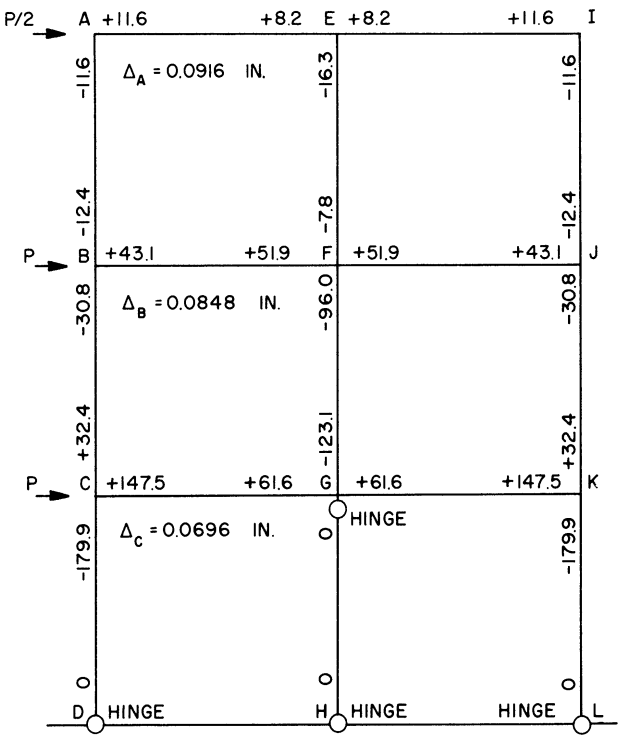

Fig. 6.19 Moments for Phase IV (P = 1 kip).

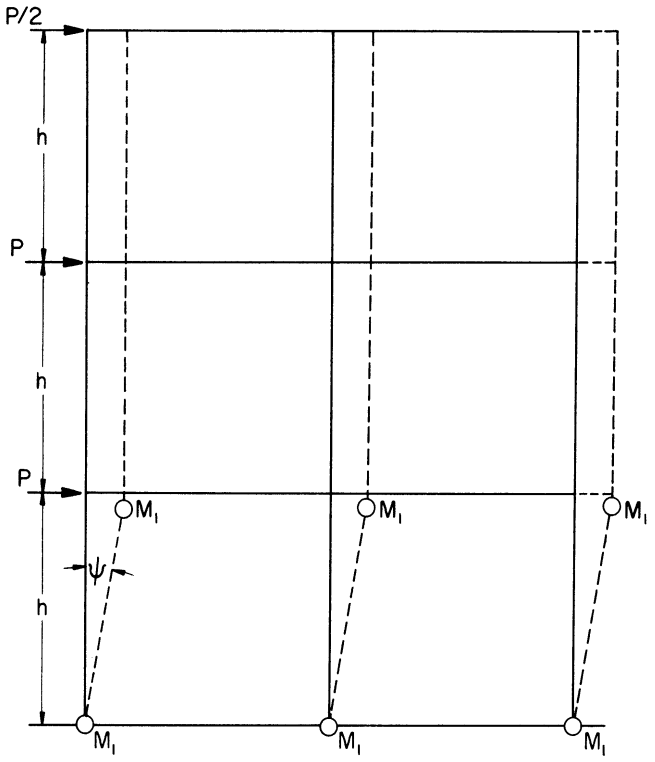

Fig. 6.20 Collapse Mechanism for Rigid Three Story Frame.

e. Calculation of the Upper Bound of Resistance for Rigid Frame Using the Collapse Mechanism Shown in Fig. 6.20

$$2.5\ Ph\ \psi = 6M_1\ \psi$$

$$P = \frac{6M_1}{2.5 \times 144}$$

when $M_1 = M_p$

$$P = \frac{6153 \times 6}{360} = 102.6 \text{ kips.}$$

This is exactly the same as the sum of all the values of P during Phases I to IV. Thus, the two methods check.

The relation between P and Δ_A is shown graphically in Fig. 6.37 (curve 1).

CASE 2. SEMI-RIGID FRAME

The general slope-deflection equations are modified by methods presented by Johnston and Mount (6.2). Moment-rotation curves for each of the semi-rigid joints are obtained by comparison with joints which have been tested (6.3).

a. Moment-Rotation Curve for Joints B,F,J,C,G, and K

It is assumed that the connection at these joints is of a type for which experimental information is available (6.3, p. 108). For the purpose of this analysis the moment-rotation curve is approximated by a number of straight lines (Fig. 6.21).

b. Moment-Rotation Curve for Joints A,E, and I

The M-θ curve for the connection at these joints is assumed to be the same as that on p. 105 of Ref. 6.3. Again it is approximated by straight lines (Fig. 6.22).

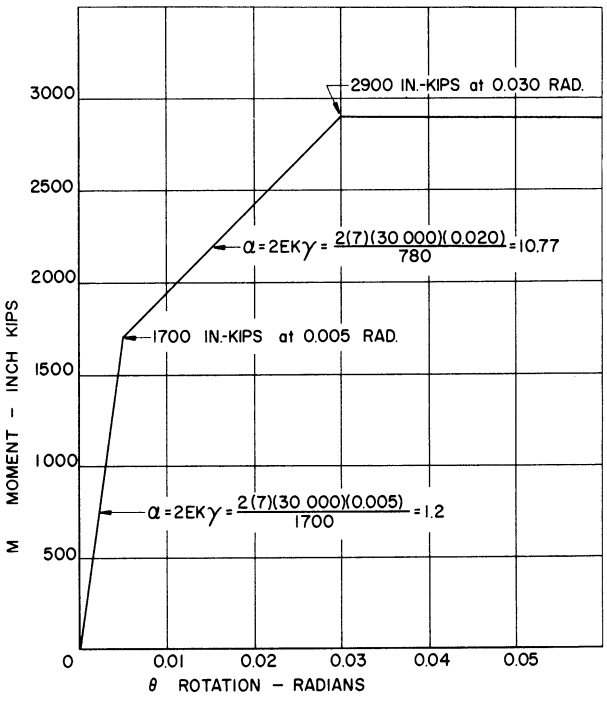

Fig. 6.21 Moment-Rotation Curve for Joints B,F,J,C,G, and K.

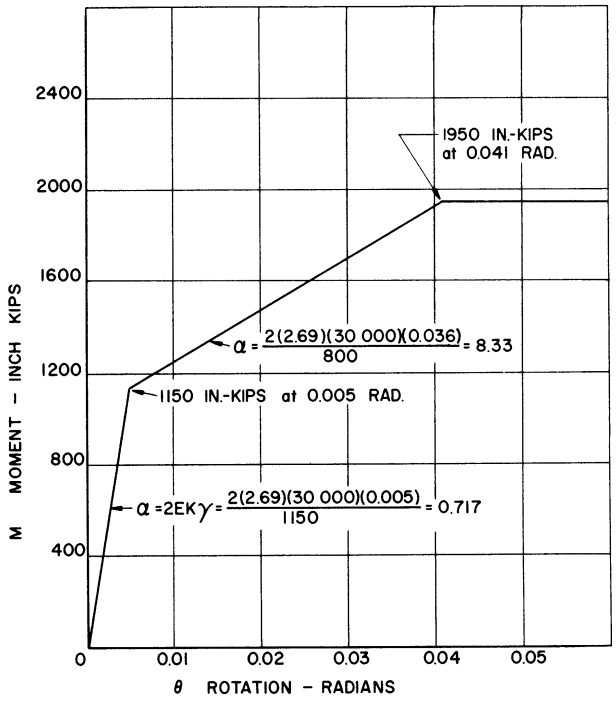

Fig. 6.22 Moment-Rotation Curve for Joints A,E, and I.

c. Moment-Rotation Curve for Anchorage

This curve is calculated using the procedure of Appendix 5.2. The anchorage is typical; designed using AISC Specifications for base plates. Details are shown in Fig. 6.23.

The curve as calculated by the above procedure contains four changes of slope. For the purpose of this analysis it is considered sufficient to approximate this by the three straight lines shown in Fig. 6.24.

d. Summary of Moment-Rotation Characteristics

Joint	Moment in in.-kips	$\alpha = 2EK\frac{d\theta}{dM}$
D,H,L	0 - 3150	0.084
	3150 - 6153	0.791
	6153 -	∞
A,E,I	0 - 1150	0.717
	1150 - 1950	8.33
	1950 -	∞
B,C,F,G,J,K	0 - 1700	1.20
	1700 - 2900	10.77
	2900 -	∞

Plastic moment for members AB, EF, IJ: 4366 in.-kips.
Plastic moment for members BC, FG, JK, CD, GH, KL: 6153 in.-kips.

The same general statical Equations 6.2 are used that were used in the fully rigid case. The slope deflection equations modified for frames with semi-rigid connections (6.2) are

$$M_{AB} = \frac{1}{1 + 2\alpha + 2\beta + 3\alpha\beta}\left[2EK\left(C_{AA}\theta_A + C_{AB}\theta_B - C_{AC}R\right) - F_{AA}M_{RBA} - F_{AB}M_{RBA}\right] - V'_{AB}b_{AB}$$

$$M_{BA} = \frac{1}{1 + 2\alpha + 2\beta + 3\alpha\beta}\left[2EK\left(C_{BB}\theta_B + C_{BA}\theta_A - C_{BC}R\right) + F_{BB}M_{RBA} + F_{BA}M_{RBA}\right] + V'_{BA}b_{BA}$$

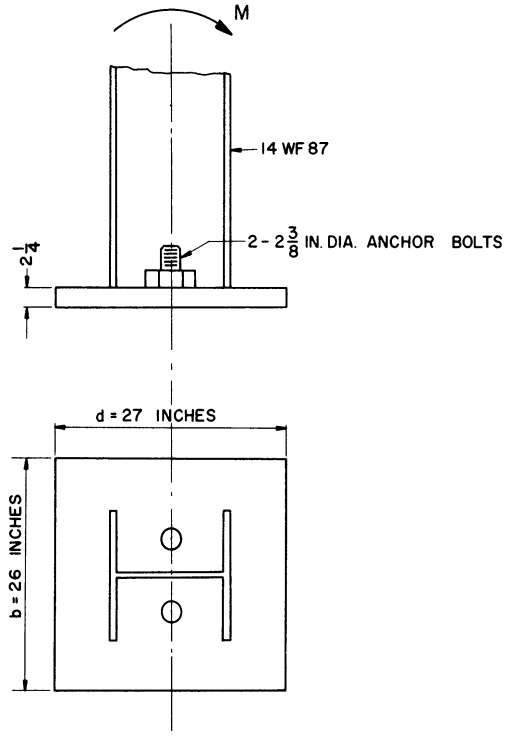

Fig. 6.23

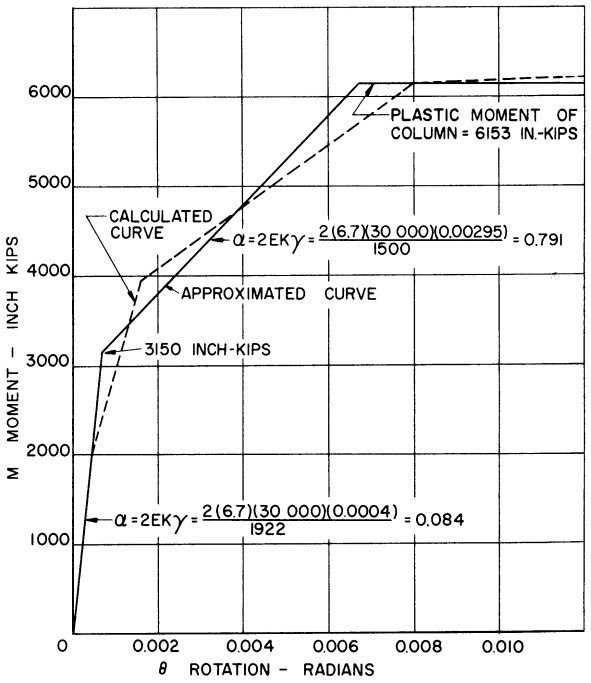

Fig. 6.24 Moment-Rotation Curve for Joints D, H, and L (Anchorage).

where the C and F terms are constants found in Table 1, Johnston and Mount (6.2) and Fig. 4.10 of Chapter IV of this report. The terms M_{RBA} and M_{RAB} are the fixed-end moments for lateral loads acting on a beam with "rigid" connections and without joint rotation. This analysis is performed considering the joint width to be zero ($b_{BA} = b_{AB} = 0$).

The appropriate forms of the two general equations shown above are used for all semi-rigid end moments.

e. Phase I: Initial Slope of Resistance Curve

The end-moment equations are as follows.

$$M_{AB} = 14.8A + 7.4B - 22.2R_1$$

$$M_{BA} = 7.4A + 14.8B - 22.2R_1$$

$$M_{AE} = 4.13A + E$$
$$M_{EA} = A + 4.13E$$

Semi-rigid

$$M_{EF} = 14.8E + 7.4F - 22.2R_1$$

$$M_{FE} = 7.4E + 14.8F - 22.2R_1$$

$$M_{BF} = 7.75B + 1.38F$$
$$M_{FB} = 1.38B + 7.75F$$

Semi-rigid

$$M_{BC} = 26.8B + 13.4C - 40.2R_2$$

$$M_{CB} = 13.4B + 26.8C - 40.2R_2$$

$$M_{FG} = 26.8F + 13.4G - 40.2R_2$$

$$M_{GF} = 13.4F + 26.8G - 40.2R_2$$

$$M_{CG} = 7.75C + 1.38G$$
$$M_{GC} = 1.38C + 7.75G$$
$$M_{GH} = 25.83G - 37.3R_3$$
$$M_{HG} = 11.47G - 34.41R_3$$
$$M_{CD} = 25.83C - 37.3R_3$$
$$M_{DC} = 11.47C - 34.41R_3$$

Semi-rigid

Then, the end-moment equations are solved and the results are as below.

$$A = 0.01941$$
$$B = 0.02958$$
$$C = 0.03629$$
$$E = 0.01603$$
$$F = 0.02621$$

In terms of Ph

$$\left.\begin{aligned} G &= 0.03199 \\ R_1 &= 0.02712 \\ R_2 &= 0.03787 \\ R_3 &= 0.02975 \end{aligned}\right\} \text{ In terms of Ph}$$

The end moments and deflections are calculated in the same manner as for the fully rigid case. Figure 6.25 shows the moments for P = 1 kip. Next, it is necessary to calculate P when the first change of slope is reached. Dividing the moments at which the change takes place at the various joints by the appropriate moment in Fig. 6.25 gives

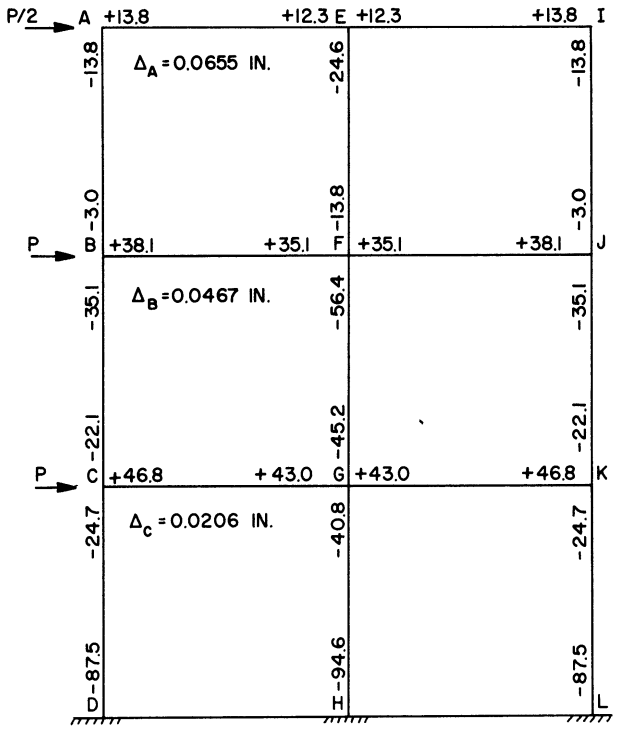

Fig. 6.25 Moments for Phase I (P = 1 kip).

$$\left.\begin{aligned} \text{joint C (CG):}\quad & \frac{1700}{46.8} = 36.3 \\ \text{joint G (CG):}\quad & \frac{1700}{43.0} = 39.5 \\ \text{joint D:}\quad & \frac{3150}{87.5} = 36.0 \\ \text{joint H:}\quad & \frac{3150}{94.6} = 33.3 \end{aligned}\right\} \text{ Average } 36.3$$

All joints reach the second slope of the M-θ curve approximately at an average value of P = 36.3 kips. Figure 6.26 shows the moments of Fig. 6.25 multiplied by 36.3 and the corresponding values of Δ_A, Δ_B, and Δ_C.

Figure 6.27 shows the total moment still available at the ends of each member at the end of Phase I. The values which are circled are the moments remaining until the joint M-θ curve reaches its second slope.

f. Phase II: Semi-Rigid Joints C, G, K, D, H, and L in Second Slope of M-θ Curve

The end-moment equations are given below.

$$M_{AB} = 14.8A + 7.4B - 22.2R_1$$

$$M_{BA} = 7.4A + 14.8B - 22.2R_1$$

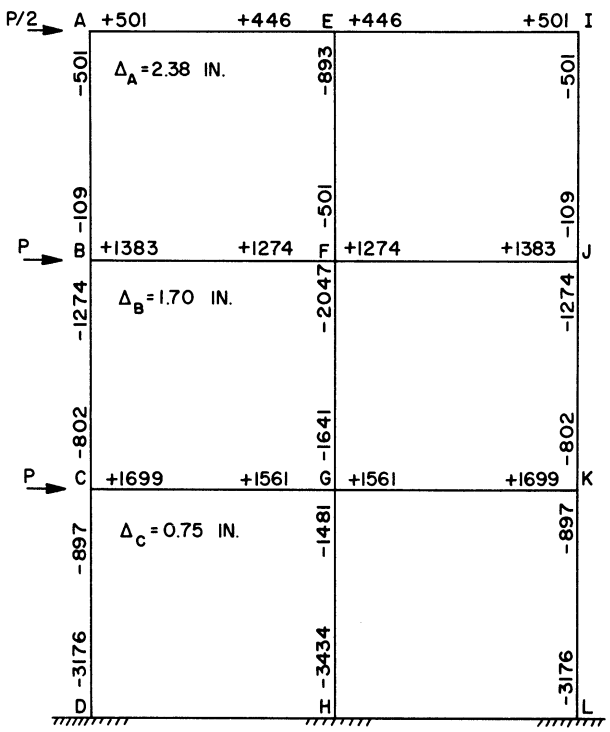

Fig. 6.26 Moments for Phase I (P = 36.3 kips).

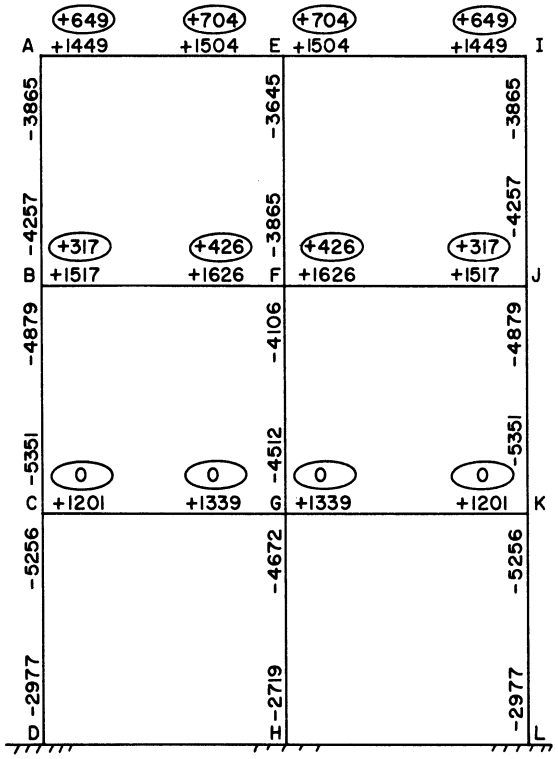

Fig. 6.27 Moments Remaining at the Beginning of Phase II (M_p - M)

$$M_{AE} = 4.13A + E$$

$$M_{EA} = A + 4.13E$$

Semi-rigid

$$M_{EF} = 14.8E + 7.4F - 22.2R_1$$

$$M_{FE} = 7.4E + 14.8F - 22.2R_1$$

$$M_{BF} = 7.75B + 1.38F$$

$$M_{FB} = 1.38B + 7.75F$$

Semi-rigid

$$M_{BC} = 26.8B + 13.4C - 40.2R_2$$

$$M_{CB} = 13.4B + 26.8C - 40.2R_2$$

$$M_{FG} = 26.8F + 13.4G - 40.2R_2$$

$$M_{GF} = 13.4F + 26.8G - 40.2R_2$$

$$\left.\begin{aligned} M_{CG} &= 1.23C + 0.036G \\ M_{GC} &= 0.036C + 1.23G \\ M_{CD} &= 22.7C - 27.89R_3 \\ M_{DC} &= 5.19C - 15.57R_3 \\ M_{GH} &= 22.7G - 27.89R_3 \\ M_{HG} &= 5.19G - 15.57R_3 \end{aligned}\right\} \text{Semi-rigid}$$

Substituting in the general statical Equations 6.2 and solving, the results are given in terms of Ph.

$$\left.\begin{aligned} A &= 0.02455 \\ B &= 0.04564 \\ C &= 0.08141 \\ E &= 0.02119 \\ F &= 0.03862 \\ G &= 0.08133 \\ R_1 &= 0.03712 \\ R_2 &= 0.06856 \\ R_3 &= 0.07142 \end{aligned}\right\} \text{in terms of Ph}$$

The end moments and deflections are calculated as before; for P = 1 kip they are shown in Fig. 6.28. It is now necessary to calculate the force P required during Phase II for certain joints to reach another change of slope on the M-Θ curve. As before,

$$\left.\begin{aligned} \text{joint B (BF)} \quad & \frac{317}{58.7} = 5.4 \\ \text{joint F (BF)} \quad & \frac{426}{52.3} = 8.1 \end{aligned}\right\} \text{average } 6.3$$

$$\text{joint A (AE)} \quad \frac{649}{17.7} = 36.7$$

$$\text{joint E (AE)} \quad \frac{704}{16.2} = 43.5$$

$$\text{joint D} \quad \frac{2977}{99.2} = 30.0$$

$$\text{joint H} \quad \frac{2719}{99.2} = 27.4$$

Thus, the joints B and F connecting member BF will reach the second slope on M-θ curve at an average value of 6.3 kips. Figure 6.29 shows the moments of Fig. 6.28 multiplied by 6.3 along with the corresponding deflections. The moments remaining at the end of Phase II are shown in Fig. 6.30.

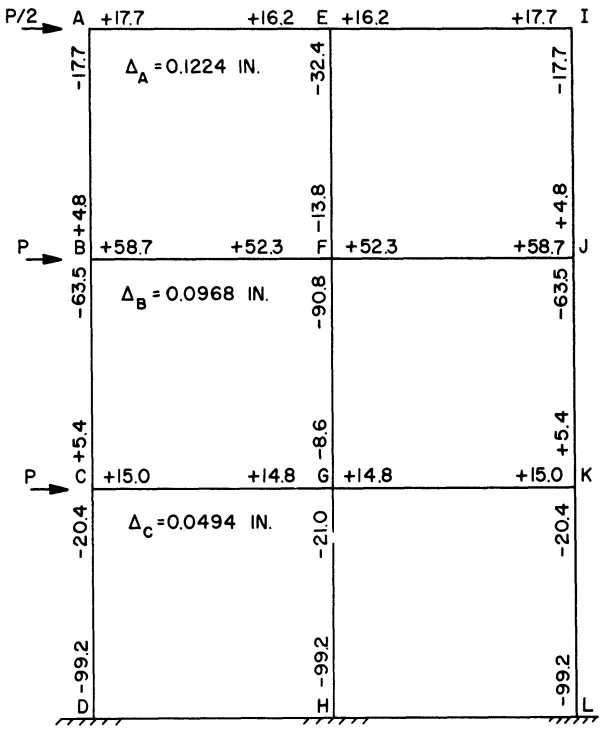

Fig. 6.28 Moments for Phase II (P = 1 kip).

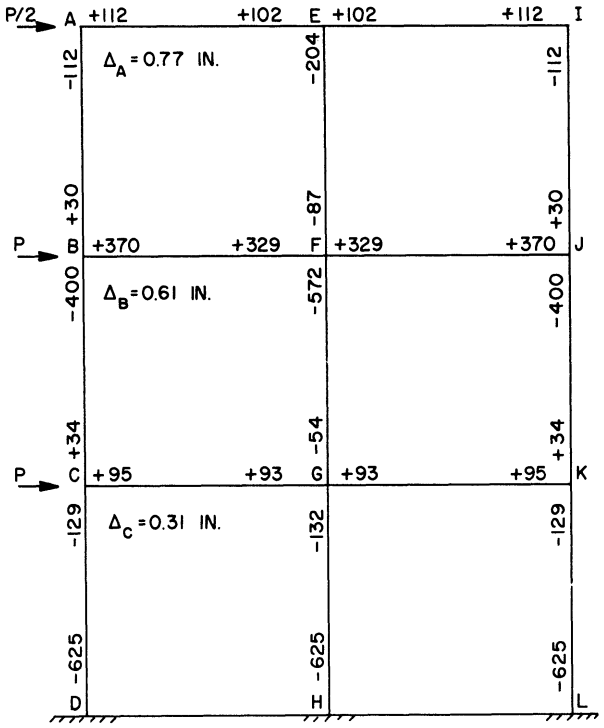

Fig. 6.29 Moments for Phase II (P = 6.3 kips).

g. Phase III: Semi-Rigid Joints C, G, K, D, H, L, B, F, and J in the Second Slope of M-θ Curve

The end-moment equations follow.

$$M_{AB} = 14.8A + 7.4B - 22.2R_1$$

$$M_{BA} = 7.4A + 14.8B - 22.2R_1$$

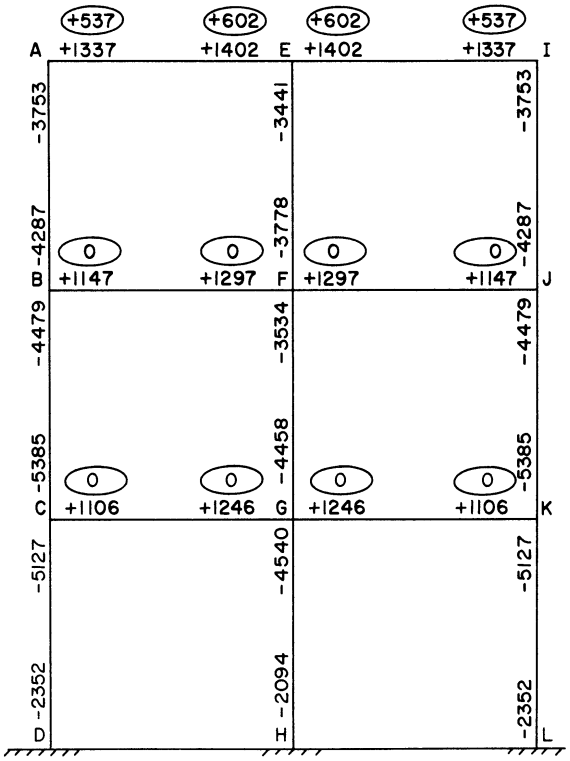

Fig. 6.30 Moments Remaining at Beginning of Phase III ($M_p - \sum M$).

$$M_{AE} = 4.13A + E$$
$$M_{EA} = A + 4.13E$$
} Semi-rigid

$$M_{EF} = 14.8E + 7.4F - 22.2R_1$$

$$M_{FE} = 7.4E + 14.8F - 22.2R_1$$

$$M_{BF} = 1.23B + 0.036F$$
$$M_{FB} = 0.036B + 1.23F$$
} Semi-rigid

$$M_{BC} = 26.8B + 13.4C - 40.2R_2$$

$$M_{CB} = 13.4B + 26.8C - 40.2R_2$$

$$M_{FG} = 26.8F + 13.4G - 40.2R_2$$

$$M_{GF} = 13.4F + 26.8G - 40.2R_2$$

$$M_{CG} = 1.23C + 0.036G$$
$$M_{GC} = 0.036C + 1.23G$$
} Semi-rigid

$$M_{CD} = 22.7C - 27.89R_3$$

$$M_{DC} = 5.19C - 15.57R_3$$

$$M_{GH} = 22.7G - 27.89R_3$$

$$M_{HG} = 5.19G - 15.57R_3$$
} Semi-rigid

Substituting in the general Equation 6.2 and solving, the results are as follows.

$$A = 0.04913$$
$$B = 0.10338$$
$$C = 0.11278$$
$$E = 0.03781$$
$$F = 0.10304$$
} in terms of Ph

$$\left.\begin{aligned} G &= 0.11025 \\ R_1 &= 0.07806 \\ R_2 &= 0.11382 \\ R_3 &= 0.09104 \end{aligned}\right\} \text{ in terms of Ph}$$

The end moments and deflections under the condition of Phase III are calculated as before for P = 1 kip and are shown in Fig. 6.31.

To calculate force P required during Phase III for certain joints to reach another change of slope of M-θ curve

$$\left.\begin{aligned} \text{joint (AE) A:} \quad & \frac{537}{34.7} = 15.5 \\ \text{joint (AE) E:} \quad & \frac{602}{29.6} = 20.3 \\ \text{joint D:} \quad & \frac{2352}{119.8} = 19.6 \\ \text{joint H:} \quad & \frac{2094}{121.7} = 17.2 \end{aligned}\right\} \text{ average } 18.2$$

At this point an average value of 18.2 kips is assumed to be the force added during Phase III. Figure 6.32 shows the moments and deflections due to P = 18.2 kips applied under the conditions of Phase III. Figure 6.33 shows the moments remaining at the end of this phase.

h. Phase IV: Semi-Rigid Joints A, E, I, B, F, J, C, G, and K Are All in the Second Slope of Their M-θ Curves, Base Joints D, H, and L Have Become Plastic Hinges

The end-moment equations are given below.

$$M_{AB} = 14.8A + 7.4B - 22.2R_1$$

$$M_{BA} = 7.4A + 14.8B - 22.2R_1$$

$$\left.\begin{aligned} M_{AE} &= 0.599A + 0.022E \\ M_{EA} &= 0.022A + 0.599E \end{aligned}\right\} \text{ Semi-rigid}$$

$$M_{EF} = 14.8E + 7.4F - 22.2R_1$$

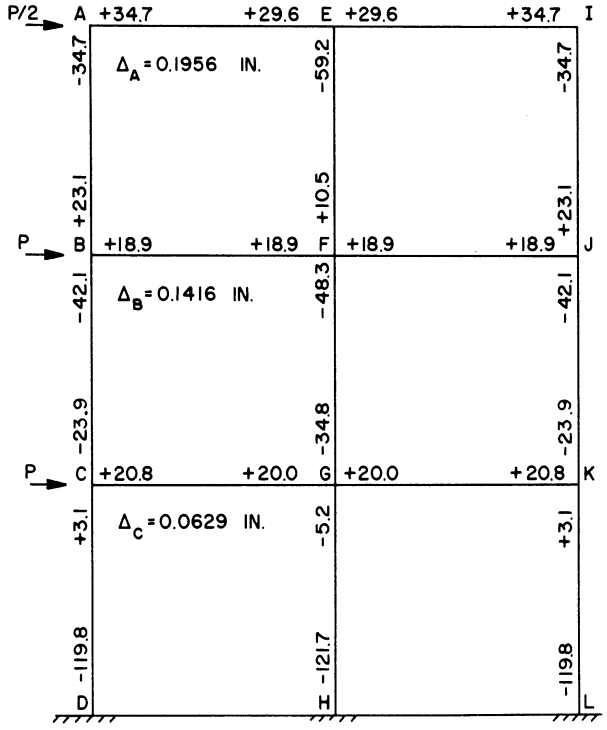

Fig. 6.31 Moments for Phase III (P = 1 kip).

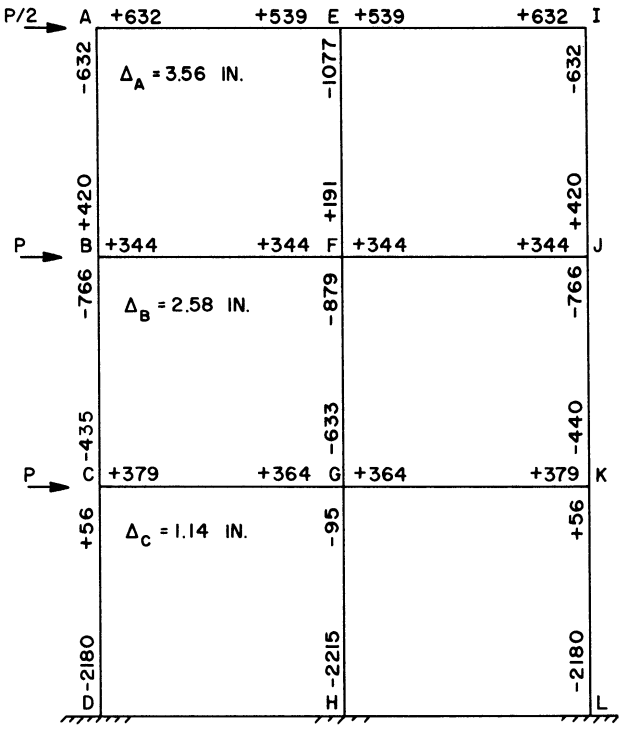

Fig. 6.32 Moments for Phase III (P = 18.2 kips).

$$M_{FE} = 7.4E + 14.8F - 22.2R_1$$

$$M_{BF} = 1.23B + 0.036F$$

$$M_{FB} = 0.036B + 1.23F$$

Semi-rigid

$$M_{BC} = 26.8B + 13.4C - 40.2R_2$$

$$M_{CB} = 13.4B + 26.8C - 40.2R_2$$

$$M_{FG} = 26.8F + 13.4G - 40.2R_2$$

$$M_{GF} = 13.4F + 26.8G - 40.2R_2$$

$$M_{CG} = 1.23C + 0.036G$$

$$M_{GC} = 0.036C + 1.23G$$

Semi-rigid

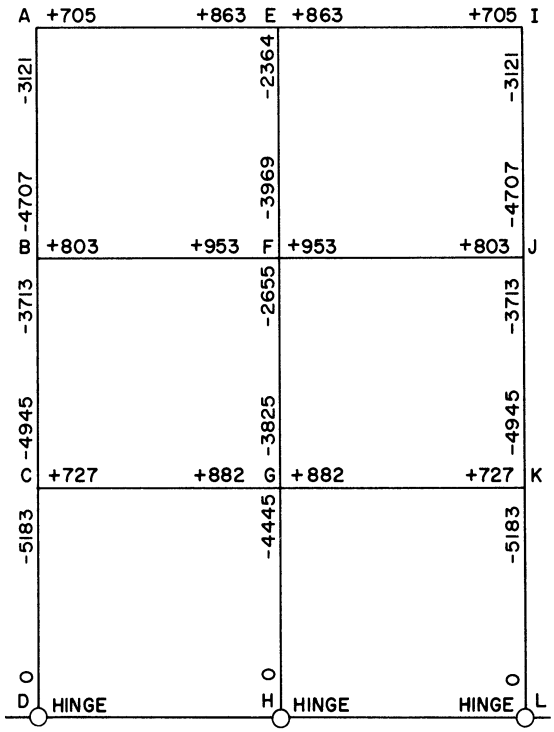

Fig. 6.33 Moments Remaining at Beginning of Phase IV ($M_p - \sum M$).

$$M_{CD} = 20.1C - 20.1R_3$$
$$M_{DC} = 0$$
$$M_{GH} = 20.1G - 20.1R_3$$
$$M_{HG} = 0$$

} Pinned

Substituting in the general Equations 6.2 and solving, the following results are obtained.

$$\begin{aligned} A &= 0.30093 \\ B &= 0.34349 \\ C &= 0.40581 \\ E &= 0.29156 \\ F &= 0.33784 \\ G &= 0.39690 \\ R_1 &= 0.32346 \\ R_2 &= 0.37844 \\ R_3 &= 0.44430 \end{aligned}$$

} in terms of Ph

The end moments and deflections are calculated as before and are shown in Fig. 6.34 for P = 1 kip.

To calculate force P required during Phase IV for any joint to reach a change of slope on its M-θ curve:

$$\text{joint B (BF)}: \quad \frac{803}{62.9} = 12.8$$
$$\text{joint C (CG)}: \quad \frac{727}{73.7} = 9.9$$
$$\text{joint F (BF)}: \quad \frac{953}{61.9} = 15.4$$
$$\text{joint G (CG)}: \quad \frac{882}{72.3} = 12.2$$

} average 12.6

$$\text{joint C (CD)}: \quad \frac{5183}{111.8} = 46.4$$
$$\text{joint G (GH)}: \quad \frac{4445}{137.6} = 32.3$$

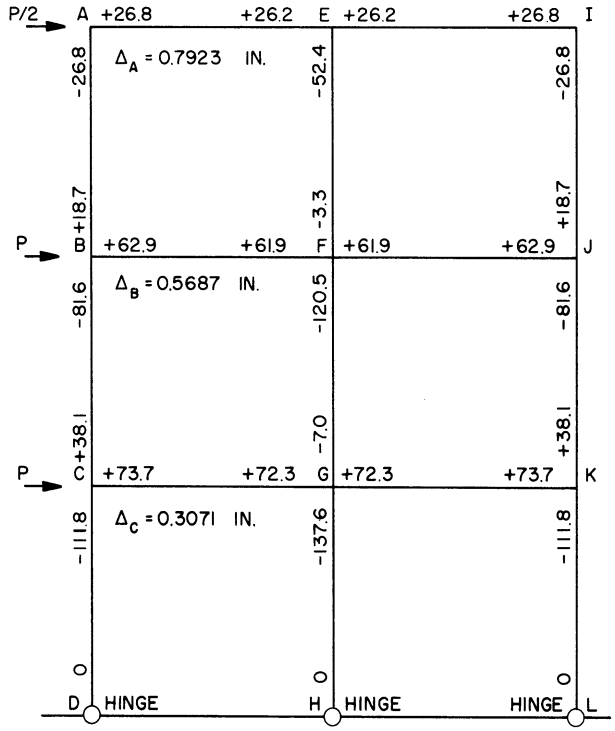

Fig. 6.34 Moments for Phase IV (P = 1 kip).

joint F: (FG) $\frac{2655}{120.5} = 22.0$

joint A: (AE) $\frac{705}{26.8} = 26.3$

joint E: (AE) $\frac{863}{26.2} = 32.9$.

Collapse will occur when all the semi-rigid joints become plastic hinges. The joints B, C, F, and G of members BF and CG will become plastic hinges at the average value, P = 12.6 kips. The deflections resulting from the application of P = 12.6 kips under the conditions of Phase IV are calculated as before,

$$\Delta_A = 9.98 \text{ in.},$$

$$\Delta_B = 7.17 \text{ in.}, \quad \Delta_C = 3.87 \text{ in.}$$

j. Conditions at the End of Phase IV

The following table can now be prepared for the loads and deflections during the various phases.

Phase	Load (kips)	Δ_A (in.)	Total Load	Total Δ_A
I	36.3	2.38	36.3	2.38
II	6.3	0.77	42.6	3.15
III	18.2	3.56	60.8	6.71
IV	12.6	9.98	73.4	16.69

k. Conditions at Collapse

It is clear that collapse will occur as a result of the structure becoming a mechanism, as shown in Fig. 6.35. Therefore, the upper bound of the load can be computed by the method of Greenberg and Prager (6.4),

$$4.5\ Ph\psi = 3M_1\psi + 8M_2\psi + 4M_3\psi$$

$$\therefore \quad P_u = \frac{3(6153) + 8(2900) + 4)1950)}{4.5 \times 144}$$

$$= 76.3 \text{ kips.}$$

The complete load-deflection curve (curve 2) is shown in Fig. 6.36.

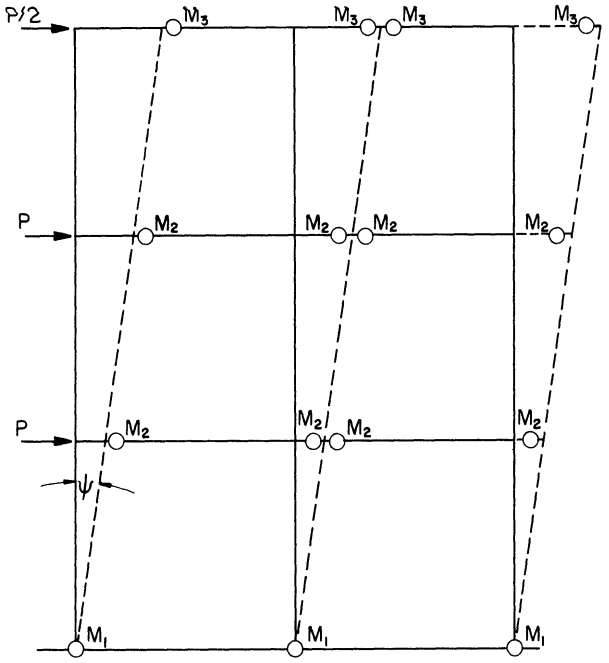

Fig. 6.35 Collapse Mechanism
for Semi-Rigid Three Story Frame.

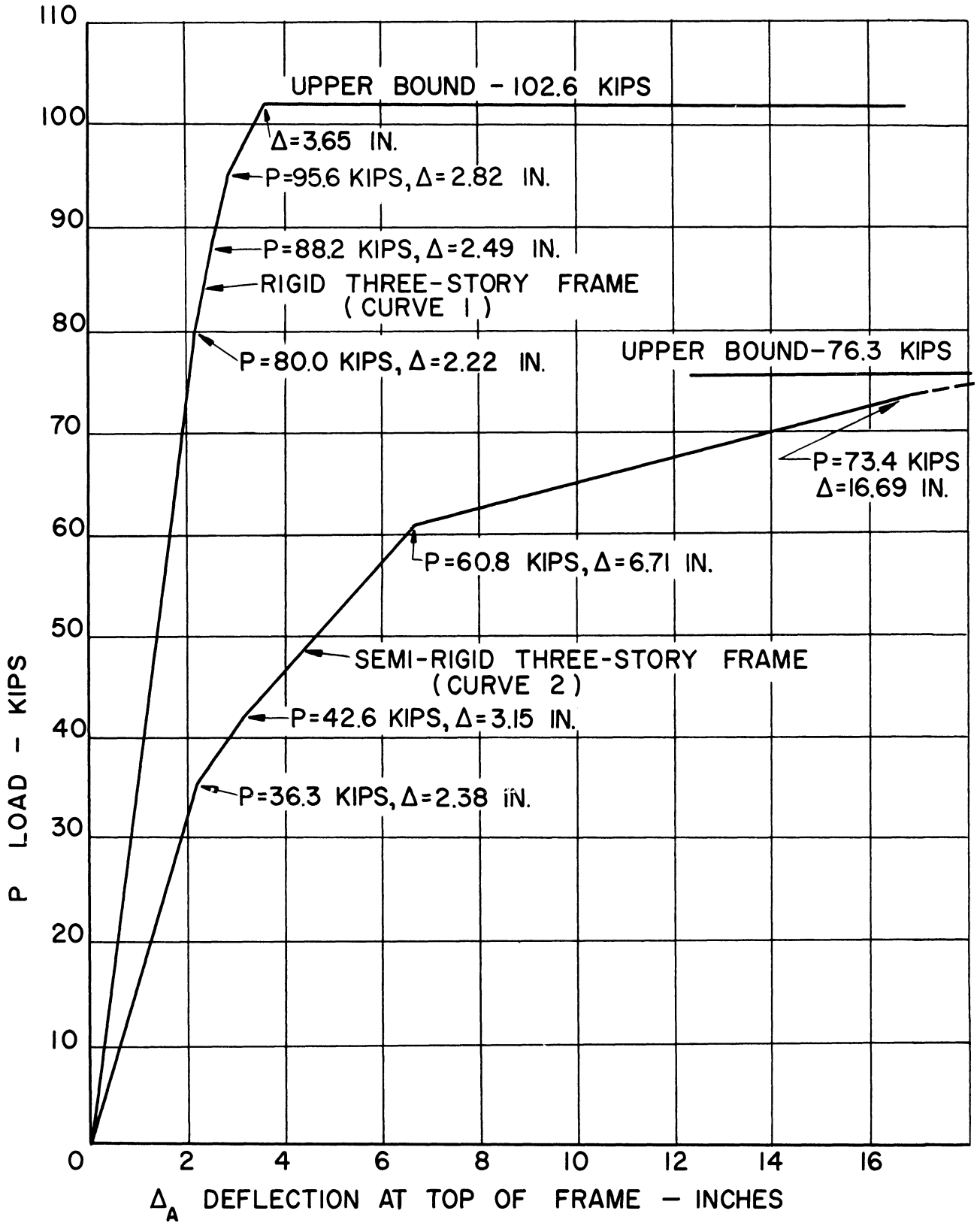

Fig. 6.36 Resistance-Deflection Curves For the Rigid and Semi-Rigid Three Story Frames.

DISTRIBUTION LIST

U. S. NAVY DEPARTMENT
CONTRACT NOY 74521

	No. Copies
Asst Chief of Staff G-3, D/A, Washington 25, D.C. ATTN: Dep Chief of Staff, G-3 (RRand SW)	1
Asst Chief of Staff G-4 Washington 25, D.C.	1
Chief of Ordnance, D/A Washington 25, D.C. ATTN: ORDTX-AR	1
Chief Signal Officer, D/A P and O Div, Washington 25, D.C. ATTN: SIGOP	3
The Surgeon General, D/A Washington, 25, D.C. ATTN: Chairman, Med R and D Bd	1
Chief Chemical Officer, D/A Washington 25, D.C.	2
The Quartermaster General CBR, Liaison Officer, R and D Div, D/A Washington 25, D.C.	1
Chief of Engineers, D/A Washington 25, D.C. ATTN: ENGNB	5
Chief of Transportation Military Planning and Intelligence Division Washington 25, D.C.	1
Chief, Army Field Forces Ft Monroe, Virginia	7
President, Bd No. 1, OCAFF Ft Bragg, N.C.	1
President, Bd No. 4, OCAFF Ft Bliss, Texas	1
Commanding General US Army Carribean Ft Amader, Canal Zone ATTN: Cml Off	1

DISTRIBUTION LIST (CONT)

	No. Copies
Commander-in-Chief EUCOM, APO 128 C/O PM, New York, N.Y.	1
Commander-in-Chief FECOM, APO 500 C/O PM, San Francisco, Calif. ATTN: ACafS, J-3	2
Commanding General US Army, Europe APO 403 C/O PM, New York, N.Y. ATTN: OPOT Div, Combat Dev Br	2
Commandant, Command and General Staff College Ft. Leavenworth, Kansas ATTN: ALLIS (AS)	1
Commandant, The Artillery School Ft. Sill, Okla.	1
Commandant, The AA and GM Branch The Artillery School Ft. Bliss, Texas	1
Commanding General Medical Field Service School Brooke Army Medical Center Ft Sam Houston, Texas	1
Director Special Weapons Development Office OCAFF Ft Bliss, Texas	1
The Superintendant, US Military Academy West Point, N.Y. ATTN: Prof of Ordnance	1
Commandant, Chemical Corps School Chemical Corps Training Command Ft McClellan, Ala	1
Commanding General, Research and Engineering Command Army Chemical Center, Md. ATTN: Deputy for RW and Non-Toxic Material	1
RD Control Officer Aberdeen Proving Grounds, Md. ATTN: Director, Ballistics Research Lab.	2

DISTRIBUTION LIST (CONT)

	No. Copies
Commanding General The Engineer Center Ft Belvoir, Va. ATTN: Asst Cmdnt, Eng School	3
Commanding Officer Engineer Research and Development Laboratory Ft Belvoir, Va. ATTN: Ch. Tech. Int. Br.	1
Commanding Officer Picatinny Arsenal Dover, N.J. ATTN: ORDBB-TK	1
Commanding Officer Chemical Corps Chemical and Rad. Lab. Army Chemical Center, Md. ATTN: Tech Library	2
Commanding Officer Transportation R and D Station Ft Eustis, Va.	1
Director, Technical Documents Center Evans Signal Lab. Belmar, New Jersey	1
Director, Waterways Experiment Station P. O. Box 631 Vicksburg, Miss. ATTN: Library	1
Director, Operations Research Office Johns Hopkins University 6410 Connecticut Ave. Chevy Chase, Md. ATTN: Library	1
Chief of Naval Operations, D/N Washington 25, D.C. ATTN: OP-36	2
Chief of Naval Operations, D/N Washington 25, D.C. ATTN: OP-374 (OEG)	1
Director of Naval Intelligence, D/N Washington 25, D.C. ATTN: OP-322V	1

DISTRIBUTION LIST (CONT)

	No. Copies
Chief, Bureau of Medicine and Surgery, D/N Washington 25, D.C. ATTN: Special Weapons Defense Division	1
Chief, Bureau of Ordnance, D/N Washington 25, D.C.	1
Chief, Bureau of Ships, D/N Washington 25, D.C. ATTN: Code 348	3
Chief, Bureau of Yards and Docks, D/N Washington 25, D.C. ATTN: P-312	3
Chief, Bureau of Supplies and Accounts, D/N Washington 25, D.C.	1
Chief, Bureau of Aeronautics, D/N Washington 25, D.C.	2
Chief of Naval Research, Code 219 Rm 1807, Bldg T-3 Washington 25, D.C. ATTN: RD Control Off	1
Commander-in-Chief US Pacific Fleet FPO San Francisco, Calif.	1
Commander-in-Chief US Atlantic Fleet US Naval Base Norfolk 11, Virginia	1
Commandant, US Marine Corps Washington 25, D.C. ATTN: Code A03H	4
Superintendent US Naval Postgraduate School Monterey, Calif.	1
Commanding Officer, US Naval Schools Command US Naval Station, Treasure Island San Francisco, Calif.	1

DISTRIBUTION LIST (CONT)

	No. Copies
Commanding Officer US Fleet Training Center Naval Base Norfolk 11, Va. ATTN: Special Weapons School	1
Commanding Officer US Fleet Training Center Naval Station San Diego, Calif. ATTN: (SPWP School)	1
Commanding Officer US Naval Damage Control Training Center Naval Base Philadelphia, Pa. ATTB: ABC Defense Course	1
Commanding Officer, US Naval Unit Chemical Corps School Army Chemical Tng Center Ft McClellan, Ala.	1
Joint Landing Force Board Marine Barracks Camp Lejeune, N. C.	1
Commander, US Naval Ordnance Laboratory White Oak Silver Spring 19, Md. ATTN: EH	1
Commander, US Naval Ordnance Laboratory White Oak Silver Spring 19, Md. ATTN: R	1
Commander, US Naval Ordnance Test Station Inyekern China Lake, Calif.	1
Officer-in-Charge US Naval Civil Engineering Research and Evaluation Lab. US Naval Construction Center Port Hueneme, Calif. ATTN: Code 753	1
Director, US Naval Research Laboratory Washington 25, D.C.	1

DISTRIBUTION LIST (CONT)

	No. Copies
Commanding Officer, and Director US Navy Electronics Laboratory San Diego 52, Calif. ATTN: Code 4223	1
Commanding Officer US Naval Radiological Defense Lab. San Francisco, Calif. ATTN: Tech Info Division	2
Commanding Officer and Director David W. Taylor Model Basin Washington 7, D.C. ATTN: Library	1
Commanding Officer and Director US Naval Engineering Experiment Station Annapolis, Md.	1
Commander US Naval Air Development Center Johnsville, Pa.	1
Director Office of Naval Research Branch Office 1000 Geary Street San Francisco, Calif.	2
Asst for Atomic Energy Hqs, USAF Washington 25, D.C. ATTN: DCS/O	1
Director of Operations Hqs, USAF Washington 25, D.C. ATTN: Operations Analysis	1
Director of Plans Hqs, USAF Washington 25, D.C. ATTN: War Plans Division	1
Director of Research and Development, DCS/D Hqs, USAF Washington 25, D.C. ATTN: Combat Components Division	1

DISTRIBUTION LIST (CONT)

	No. Copies
Director of Intelligence Hqs, USAF Washington 25, D.C. ATTN: AFOIN-1B2	2
The Surgeon General Hqs, USAF Washington 25, D.C. ATTN: BIG. Defense Br, Prev. Med. Div.	1
Asst Chief of Staff Intelligence, Hqs, USAFE APO 633 C/O PM, New York, N.Y. ATTN: Air Intelligence Br	1
Commander 497th Reconnasissance Technical Squadron (Augmented) APO 633, C/O PM, New York, N.Y.	1
Commander Far East Air Forces APO 925 C/O PM, San Francisco, Calif.	1
Commander, Strategic Air Command Offutt AFB Omaha, Nebraska ATTN: Operations Analysis	1
Commander, Tactical Air Command Langley AFB, Va. ATTN: Dec Security Br	1
Commander, Air Defense Command Ent AFB, Colorado	1
Commander, Air Materiel Command Wright-Patterson AFB, Dayton, Ohio ATTN: MCAIDS	2
Commander, Air Training Command Scott AFB Belleville, Ill. ATTN: DCS/O GTP	1

DISTRIBUTION LIST (CONT)

	No. Copies
Commander, Air Research and Development Command P. O. Box 1395 Baltimore, Md. ATTN: RDDN	1
Commander Air Proving Ground Command Eglin AFB, Fla. ATTN: AG/TRB	1
Commander Air University Maxwell AFB, Alabama	2
Commander, Flying Training Air Force Waco, Texas ATTN: Director of Observer Training	8
Commander Crew Training Air Force Randolph Field, Texas ATTN: 2GTS,DCS/O	1
Commander, Hqs, Technical Training Air Force Gulfport, Miss. ATTN: TA and D	1
Commandant Air Force School of Aviation Medicine Randolph AFB, Texas	2
Commander Wright Air Development Center Wright-Patterson AFB Dayton, Ohio ATTN: WCOESP	6
Commander, AF Cambridge Research Center 230 Albany Street, Cambridge 39, Mass. ATTN: CRHK, Geophysics Research Directerate	1
Commander, AF Special Weapons Center Kirtland AFB, New Mexico ATTN: Library	3

DISTRIBUTION LIST (CONT)

	No. Copies
Commandant, USAF Institute of Technology Wright-Patterson AFB Dayton, Ohio ATTN: Resident College	1
Commander Lowry AFB Denver, Colorado ATTN: Dept of Armament Training	1
Commander 1009th Special Weapons Squadron, Hqs, USAF Washington 25, D.C.	1
The RAND Corporation 1700 Main Street Santa Monica, California ATTN: Nuclear Energy Division	2
Asst Secretary of Defense Research and Development, DOD Washington 25, D.C. ATTN: Tech Library	1
United States National Military Representative Hqs, SHAPE, APO 55, C/O PM, New York, N.Y. ATTN: Col. J.P. Healy	1
Director, Weapons Evaluation Group OSD, Rm 2E1006, The Pentagon Washington 25, D.C.	1
Commandant, Armed Forces Staff College Norfolk 11, Va. ATTN: Secretary	1
Commanding General, Field Command AFSWP, P. O. Box 5100, Albuquerque, New Mexico	6
Chief, Armed Forces Special Weapons Project P. O. Box 2610 Washington 25, D.C.	9
Chairman, Armed Services Explosives Safety Board DOD, Rm 2403, Barton Hall Washington 25, D.C.	1

DISTRIBUTION LIST (CONT)

	No. Copies
ASTIA, Document Service Center U B Building Dayton 2, Ohio ATTN: DCS-SA	1
Dr. N. M. Newmark Talbot Laboratory University of Illinois Urbana, Illinois	1
Dr. R. J. Hansen Massachusetts Institute of Technology Cambridge 39, Mass.	1
Dr. E. B. Doll Stanford Research Institute Palo Alto, Calif.	1
Professor Harry A. Williams Stanford University Stanford, Calif.	1
Professor R. L. Bisplinghoff Massachusetts Institute of Technology Cambridge 39, Mass.	1
Director, Construction Division U. S. Atomic Energy Commission Washington 25, D.C. ATTN: Mr. C. Beck	1
The Technical Information Service U.S. Atomic Energy Commission 1901 Constitution Ave., N.W., Washington 25, D.C. ATTN: Jean M. O'Leary	1
Director, Department of Applied Mechanics The Johns Hopkins University Baltimore, Maryland	1
Raymond Archibald U.S. Bureau of Public Roads 1261 Flood Building 870 Market Street San Francisco 2, Calif.	1

DISTRIBUTION LIST (CONT)

	No. Copies
Professor L. A. Baier Chairman, Department of Naval Arch. and Marine Engineering 326 West Engineering Building University of Michigan Ann Arbor, Michigan	1
Professor J. F. Baker Engineering Laboratory University of Cambridge Trumpington Street Cambridge, England	1
E. F. Ball Chief Engineer Fabricated Steel Construction Bethlehem Steel Company Bethlehem, Pennsylvania	1
Dr. Frank Baron Director of Structural Research University of California Berkeley, California	1
J. L. Beckel Assistant Engineer New York Central Line East 466 Lexington Avenue New York, New York	1
Dr. L. S. Beedle Assistant Director Fritz Engineering Laboratory Lehigh University Bethlehem, Pennsylvania	1
J. E. Bernhardt Chief Engineer William J. Howard, Inc. 35 East Wacker Drive Chicago, Illinois	1
R. W. Binder Chief Engineer Bethlehem Steel Company Fabricated Steel Construction P. O. Box 58, Watts Station Los Angeles, California	1

	No. Copies
E. S. Birkenwald Engineer of Bridges Southern Railway System 307 East 4th Cincinnati, Ohio	1
Dr. Walker Bleakney Department of Physics Princeton University Princeton, New Jersey	1
Dr. Hans Bleich Columbia University New York, N. Y.	1
E. T. Blix Mississippi Valley Structural Steel Company Melrose Park, Illinois	1
H. C. Boardman Director of Research Chicago Bridge and Iron Company 1305 West 105th Street Chicago 43, Illinois	1
Dr. Harry L. Bowman Drexel Institute of Technology Philadelphia 4, Pennsylvania	1
Harry Brinkman Vice-President and Chief Engineer Phoenix Bridge Company P. O. Box 187 Phoenixville, Pennsylvania	1
R. N. Brodie Engineer of Structures B and M. and M. Central R.R. 150 Causeway Street Boston, Massachusetts	1
W. R. Burrows Assistant Chief Engineer Whiting Refinery Standard Oil Company (Indiana) 2400 New York Avenue A and E Building, Room 236 Whiting, Indiana	1

	No. Copies
B. E. Bushnell Bushnell Steel Companies Tampa, Florida	1
Professor S. T. Carpenter Chairman, Department of Civil Eng. Swarthmore College Swarthmore, Pennsylvania	1
J. W. Carter Structures Design Section The Glenn L. Martin Company Baltimore, Maryland	1
P. R. Cassidy The Babcock and Wilcox Company 80 Federal Street Boston 10, Massachusetts	1
W. E. Chastain, Sr. Engineer of Physical Research 126 East Ash Street Springfield, Illinois	1
E. F. Cox Weapons Effect Department Sandia Corporation Sandia Base Albuquerque, New Mexico	1
J. M. Crowley Office of Naval Research Navy Department Code 438 Washington 25, D.C.	1
J. S. Davey Assistant to the President Russel, Burdsall, and Ward Nut and Bolt Company Port Chester, New York	1
Professor R. E. Davis 202 Engineering Materials Laboratory University of California Berkeley, California	1

	No. Copies
R. P. Davis Dean, College of Engineering West Virginia University Mechanical Hall Morgantown, West Virginia	1
F. H. Dill American Bridge Company Ambridge, Pennsylvania	1
Professor Lloyd Donnell Department of Mechanics Illinois Institute of Technology Technology Center Chicago 16, Illinois	1
W. E. Dowling Bridge Inspector Union Pacific R. R. 5120 Mason Street Omaha, Nebraska	1
Dr. D. C. Drucker Engineering Department Brown University Providence, Rhode Island	1
Professor C. M. Duke Department of Engineering University of California Los Angeles 24, California	1
Professor W. J. Eney Head, Department of Civil Eng. Lehigh University 101 Packer Hall Bethlehem, Pennsylvania	1
West Engineering Library University of Michigan Attn: Mr. F. R. Harrell	1
S. Epstein Metallurgical Department Bethlehem Steel Company Bethlehem, Pennsylvania	1
E. L. Erickson Chief, Bridge Division Bureau of Public Roads Washington 25, D. C.	1

DISTRIBUTION LIST (CONT)

	No. Copies
F. B. Farquharson Director Engineering Experiment Station University of Washington Seattle 5, Washington	1
S. J. Fraenkel Armour Research Foundation Technology Center 221 East Cullert Chicago 16, Illinois	1
Professor J. M. Garrelts Executive Officer, Dept. of Civil Engineering Columbia University New York, New York	1
Department of Civil Engineering University of Michigan	
B. G. Johnston	3
R. H. Sherlock	1
L. C. Maugh	1
L. M. Legatski	1
G. L. Alt	1
R. B. Harris	1
W. S. Rumman	1
A. Mathews	1
Dr. J. N. Goodier School of Engineering Stanford University Stanford, California	1
Professor L. E. Grinter Department of Civil Engineering University of Florida Gainesville, Florida	1
LaMotte Grover Structural Welding Engineer Air Reduction Sales Company 60 East 42nd Street New York, New York	1
H. P. Hall Department of Civil Engineering Technological Institute Northwestern University Evanston, Illinois	1

	No. Copies
S. Hardesty Consulting Engineer Hardesty and Hanover 101 Park Avenue - Room 407 New York, New York	1
E. C. Hartmann Chief Engineer Design Division Aluminum Research Laboratories Box 772 New Kensington, Pennsylvania	1
Dr. R. A. Hechtman Engineering Experiment Station University of Washington Seattle 5, Washington	1
T. R. Higgins Director of Engineering American Institute of Steel Constr. 101 Park Avenue New York 17, New York	1
Harry N. Hill Assistant Chief Engineer Design Div. Aluminum Company of America Box 772 New Kensington, Pennsylvania	1
Dr. N. J. Hoff Head, Dept. of Aeronautical Eng. and Applied Mechanics Polytechnic Institute of Brooklyn 99 Livingston Street Brooklyn 2, New York	1
L. G. Holleran Clarke, Rapuano, and Holleran 145 East 32nd Street New York 16, New York	1
G. W. Housner, Prof. Assistant Professor of Applied Mech. California Institute of Technology Pasadena, California	1
N. E. Hueni Assistant Engineer Missouri Pacific R. R. Union Station, Room 204 Houston, Texas	1

	No. Copies
Professor W. C. Huntington Head, Department of Civil Engineering University of Illinois Urbana, Illinois	1
H. D. Hussey Designing Engineer American Bridge Division United States Steel Company 71 Broadway New York, New York	1
J. O. Jackson Vice-President Engineering and Research Pittsburgh-DeMoines Steel Company Neville Island Pittsburgh 25, Pennsylvania	1
Lydik S. Jacobsen Department of Mechanical Engineering Stanford University Palo Alto, California	1
William H. Jameson Assistant Chief Engineer Bethlehem Steel Company Bethlehem, Pennsylvania	1
C. E. Jackson Union Carbide and Carbon Company Research Laboratory Niagara Falls, New York	1
V. P. Jensen Staff-Consultant C. F. Braun and Company Alhambra, California	1
Professor E. Russell Johnston Department of Civil Engineering Lehigh University Bethlehem, Pennsylvania	1
Finn Jonassen National Research Council 2101 Constitution Avenue Washington, D. C.	1

	No. Copies
Jonathan Jones One Fire Lane R.F.D. No. 3 Wydnor Bethlehem, Pennsylvania	1
O. G. Julian Head, Structural Division Jackson and Moreland 31 St. James Avenue Boston, Massachusetts	1
Professor Thomas C. Kavanagh Chairman, Department of Civil Eng. New York University New York, New York	1
J. J. Kelley District Sales Manager (Detroit) Pittsburgh Screw and Bolt Corp. P. O. Box 1708 Pittsburgh 30, Pennsylvania	1
Jack R. Kelso 4508 North 16th Street Arlington 7, Virginia	1
R. L. Kennedy Assistant Chief Engineer Hazelet and Erdal 53 West Jackson Road Chicago, Illinois	1
R. E. Kolm Assistant Professor of Civil Eng. Lehigh University Bethlehem, Pennsylvania	1
W. J. Krefeld Director Civil Engineering Testing Laboratories Columbia University New York, New York	1
Carl Kreidler Lehigh Structural Steel Company Allentown, Pennsylvania	1

	No. Copies
E. W. Larson, Jr. Research Associate Department of Civil Engineering The Technological Institute Northwestern University Evanston, Illinois	1
Louis J. Lasson Consulting Engineer - Welding Allis-Chalmers Manufacturing Company Milwaukee 1, Wisconsin	1
H. W. Lawson 1677 Rensselaer Road West Englewood, New Jersey	1
K. H. Lenzen Department of Civil Engineering and Eng. Mech. Purdue University Lafayette, Indiana	1
H. H. Lind President Industrial Fasteners Institute 3648 Euclid Avenue Cleveland 15, Ohio	1
C. T. G. Looney Assistant Professor of Civil Engineering Yale University Winchester Hall New Haven, Connecticut	1
E. M. MacCutcheon Naval Architect Bureau of Ships Navy Department Washington 25, D. C.	1
G. W. Magee Association of American Railroads 3140 South Federal Street Chicago 16, Illinois	1
F. M. Masters Consulting Engineer Modjeski and Masters State Street Building Harrisburgh, Pennsylvania	1

DISTRIBUTION LIST (CONT)

	No. Copies
Verne O. McClurg McClurg, Shoemaker, and McClurg 39 S. LaSalle Street Chicago, Illinois	1
A. M. Meyers Kansas City Structural Steel Company Kansas City, Missouri	1
J. Michalos Professor, Department of Civil Engineering Iowa State College Ames, Iowa	1
Professor R. D. Mindlin Department of Civil Engineering Columbia University New York, New York	1
W. D. Moorhead Chief Sales Engineer Truscon Steel Company Youngstown 1, Ohio	1
Professor R. B. B. Moorman Chairman, Department of Civil Eng. Syracuse University Syracuse, New York	1
C. E. Muhlenbruch Associate Professor of Civil Eng. The Technological Institute Northwestern Univessity Evanston, Illinois	1
Professor William Munse 119 Talbot Laboratory University of Illinois Urbana, Illinois	1
R. B. Murphy Assistant Engineer of Bridge and Traffic Structures Bureau of Design Centennial Building State of Illinois Division of Highways Springfield, Illinois	1

DISTRIBUTION LIST (CONT)

	No. Copies
Professor P. M. Naghdi Associate Professor of Engineering Mechanics 201D W. Engineering University of Michigan Ann Arbor, Michigan	1
C. Neufeld Assistant Engineer of Bridges Canadian Pacific Railway Montreal 3, Canada	1
William R. Osgood c/o Department of Mechanics Illinois Institute of Technology Chicago, Illinois	1
Professor J. Ormondroyd Dept. of Engineering Mechanics 201C West Engineering Building University of Michigan Ann Arbor, Michigan	1
J. I. Parcel Sverdrup and Parcel, Inc. Syndicate Trust Building St. Louis 1, Missouri	1
R. E. Peck Bridge Engineer Missouri Pacific R. R. 1211 Missouri Pacific Building St. Louis, Missouri	1
W. R. Penman General Manager, Lebanon Plant Bethlehem Steel Company Lebanon, Pennsylvania	1
F. L. Plummer Director of Engineering Hammond Iron Works P. O. Box 629 Warren, Pennsylvania	1
A. E. Poole The Hallen Company, Inc. 45-24 37th Street Long Island City, New York	1

	No. Copies
V. M. Romine Bureau of Design Bridge Office Centennial Building Springfield, Illinois	1
E. J. Ruble Association of American Railroads Engineering Division Central Research Laboratory 3140 South Federal Street Chicago 16, Illinois	1
Alfred E. Pearson Chief Welding Engineer The Ingalls Company Birmingham, Alabama	1
W. S. Pellini Head, Metal Processing Branch Metallurgical Division Naval Research Laboratory Code 3550 Washington 20, D. C.	1
B. E. Rossi Executive Secretary Pressure Vessel Research Committee of the Welding Research Council 29 West 39th Street New York 18, New York	1
Charles G. Salmon 14335 Forrer Avenue Detroit 27, Michigan	2
Walter Samans Consulting Engineer Room 807 1616 Walnut Street Philadelphia 3, Pennsylvania	1
C. H. Sandberg Assistant Bridge Engineer Atchison, Topeka, and Santa Fe Railway Chicago 4, Illinois	1

DISTRIBUTION LIST (CONT)

	No. Copies
A. L. R. Sanders Partner and Chief Engineer Hazelet and Erdal 63 West Jackson Boulevard Chicago 4, Illinois	1
Leo Schenker 909 Logan Avenue Toronto, Ontario, Canada	2
G. J. Schoessow The Babcock and Wilcox Company Barbertown, Ohio	1
T. C. Shedd Professor of Structural Engineering Civil Engineering Hall University of Illinois Urbana, Illinois	1
Shu-T'ien Li Visiting Professor of Civil Eng. College of Engineering Rutgers University New Brunswick, New Jersey	1
Dr. F. W. Schutz Fritz Engineering Laboratory Lehigh University Bethlehem, Pennsylvania	1
Jack Singleton Chief Engineer American Institute of Steel Construction 101 Park Avenue New York, New York	1
F. T. Sisco Technical Director The Engineering Foundation 29 West 39th Street New York 18, New York	1
C. E. Sloan Engineer of Bridges and Buildings Baltimore and Ohio R. R. 1301 Baltimore and Ohio Building Baltimore, Maryland	1

	No. Copies
Mr. William Spraragen Director Welding Research Council of the Engineering Foundation 29 West 39th Street New York 18, New York	1
D. B. Steinman Consulting Engineer 117 Liberty Street New York, New York	1
W. C. Stewart Industrial Fasteners Institute 3648 Euclid Avenue Cleveland 15, Ohio	1
Robert J. Stoddard American Hoist and Derrick Company St. Paul, Minnesota	1
R. G. Sturm Director Auburn Research Foundation and Engineering Experiment Station Alabama Polytechnic Institute Textile Building Auburn, Alabama	1
R. D. Stout Department of Metallurgical Engineering Lehigh University Bethlehem, Pennsylvania	1
Professor P. S. Symonds Brown University Providence, Rhode Island	1
E. K. Timby Howard, Needles, Tammen and Bergendoff 55 Liberty Street New York 5, New York	1
Professor A. A. Toprac Civil Engineering Department University of Texas Austin 12, Texas	1

	No. Copies
Neil Van Eenam Highway Bridge Engineer U. S. Bureau of Public Roads Washington, D. C.	1
John Vasta Head of Hull Design Scientific Section Bureau of Ships Navy Department Washington 25, D. C.	1
Professor E. T. Vincent Chairman, Dept. of Mech. and Ind. Eng. 223 W. Engineering Building University of Michigan Ann Arbor, Michigan	1
George S. Vincent Principal Highway Bridge Engineer Structural Research Laboratory U. S. Bureau of Public Roads University of Washington Seattle 5, Washington	1
Mr. Eric Wang Chief, Special Studies Office (MCAIDS) Installations Engineering Section Air Installations Division Headquarters, Air Materiel Command Wright-Patterson Air Force Base Dayton, Ohio	1
A. T. Waidelich Research Division The Austin Company 16112 Euclid Avenue Cleveland, Ohio	1
C. Earl Webb Chief Engineer American Bridge Company Room 1820 525 William Penn Place Pittsburgh 30, Pennsylvania	1
W. H. Weiskopf Consulting Engineer Weiskopf and Pickworth 2 West 45th Street New York 36, New York	1

DISTRIBUTION LIST (CONT)

	No. Copies
Edward Wenk, Jr. Head, Structures Division Structural Mechanics Laboratory David Taylor Model Basin Washington, D. C.	1
H. E. Wessman Dean, College of Engineering University of Washington Seattle 5, Washington	1
Dr. Merit P. White Head, Civil Engineering Department University of Massachusetts Amherst, Massachusetts	1
John B. Wilbur Head, Department of Civil and Sanitary Engineering Massachusetts Institute of Tech. Cambridge, Massachusetts	1
J. Lyell Wilson Consulting Naval Architect 145 Clifton Street Westfield, New Jersey	1
Professor George Winter Head, Department of Struct. Eng. College of Engineering Cornell University Ithaca, New York	1
B. L. Wood Consulting Engineer American Iron and Steel Institute 350 Fifth Avenue New York 1, New York	1
Glenn B. Woodruff 101 California Street San Francisco 4, California	1
Professor L. T. Wyly Head, Structural Engineering Department Purdue University Lafayette, Indiana	1
Dr. Dana Young Department of Civil Engineering Yale University New Haven, Connecticut	1